Surface-Atmosphere Trace Gas and Aerosol Exchanges on the Global Scale

Uitwisseling van spore gassen en aerosolen tussen de atmosfeer en het aardoppervlak op de mondiale schaal

Surface-Atmosphere Trace Gas and Aerosol Exchanges on the Global Scale

Uitwisseling van spore gassen en aerosolen tussen de atmosfeer en het aardoppervlak op de mondiale schaal

(met een samenvatting in het Nederlands)

PROEFSCHRIFT

TER VERKRIJGING VAN DE GRAAD VAN DOCTOR AAN DE UNIVERSITEIT VAN UTRECHT OP GEZAG VAN DE RECTOR MAGNIFICUS, PROF. DR. H. O. VOORMA, INVOLGE HET BESLUIT VAN HET COLLEGE VAN PROMOTIES IN HET OPENBAAR TE VERDEDIGEN OP MAANDAG 12 FEBRUARI 2001 DES MIDDAGS TE 16.15 UUR

Door

Laurens Nicolaas Ganzeveld

Geboren op 6 November 1966, te Elburg

Promotoren: **Prof. dr. J. Lelieveld**
Faculteit Natuur- en Sterrenkunde, Universiteit Utrecht

Prof. dr. A. A. M. Holtslag
Meteorologie en Luchtkwaliteit, Wageningen Universiteit

Paranimfen: Ad Jeuken en Mark Ganzeveld

The work presented in this dissertation has been performed within the European Community projects SINDICATE (Study on the Indirect and Direct Climate Influences of Anthropogenic Trace Gas Emissions) and EUSTACH-LBA (European Studies on Trace gases and Atmospheric Chemistry as a contribution to the Large scale Biosphere Atmosphere Experiment in Amazonia).

Drukkerij: Ponsen & Looijen, Wageningen

ISBN: 90-393-2624-X

Preface

The work presented in this dissertation reflects the results of a study focussing on the exchange of trace gases and aerosols between the surface and the global atmosphere. Surface-atmosphere trace gas and aerosol exchanges plays a crucial role in the global atmospheric chemistry since it controls to a large extent the atmospheric burden and surface concentrations of many trace gases and aerosols. It encompasses the antropogenic emissions, e.g., emissions associated with fossil fuel burning, biogenic emissions, which are the natural emissions of gases, e.g., from soils, and the removal of gases and aerosols by precipitation and dry deposition. The main focus of this work has been the dry deposition process, which is the removal of gases and aerosols at the earth's surface, e.g., through uptake by the vegetation. However, since the dry deposition process of some trace gases such as nitrogen oxides, is closely connected to the biogenic emissions, this process is also considered in this work.

The initial motivation to start with the study of the dry deposition process is the relevance of this process for the global atmospheric budgets of trace gases such as ozone and the sulfur oxides. The representation of the dry deposition process in global scale chemistry and climate (or transport) models, which have been used lately to study the atmospheric chemistry and its relationship to the world's climate, was quite simplistic at the moment that we started this work. The common approach was to use constant removal rates, the so-called dry deposition velocities, while measurements have revealed that there are large temporal as well as spatial differences in this parameter. This is related to the surface cover, e.g., vegetation, bare soil, snow or water, and the biological, chemical and physical properties of the surface cover. For instance, a tropical rainforest canopy is a large sink of many trace gases such as ozone during the daytime since these gases are removed through uptake by the leaf stomata, similar to CO_2. However, the uptake of ozone by a wet tropical rainforest due to rainfall can be quite limited due to the low solubility of this trace gas. These subtle differences in the uptake regime due to changes in the surface cover properties indicate the complexity involved with the representation of the dry deposition process, especially in large scale models which generally contain a rather simplified representation of the surface cover and its properties. In addition to the complexity of all the involved processes, most of these processes occur on a typical scale ranging from < 1 m up to > 1 km, which is significantly smaller than the grid resolution of the applied models. Therefore, parameterizations that account for the sub-grid scale processes must be developed and implemented. An advantage of working with global scale models is that we need to distinguish different exchange regimes between very different surface cover types such as tropical forest, tundra, the oceans or the sandy soils of the Sahara. The development and implementation of an explicit representation of the dry deposition process for reactive trace gases and sulfur oxides in a coupled chemistry and climate model is

presented in Chapters 2 and 3.

We also focus in this dissertation on the role of interactions between processes such as dry deposition, emissions, chemistry and turbulence within the vegetation. This work has been motivated by the fact that these interactions are important for the exchange of fast reacting trace gases, e.g., the oxidized nitrogen species (NO_x), over and within dense vegetation. Despite the presence of a significant emission flux of NO_x from the soils there can be a downward or deposition flux of NO_x at the canopy top due to the canopy interactions. These canopy interactions are generally neglected in large scale model studies, which can result in a serious misrepresentation of the surface NO_x fluxes over dense vegetation cover, such as tropical forests. To study the role of the canopy interactions for the atmosphere-biosphere trace gas exchange on a global scale, we have developed a model that explicitly considers the canopy interactions. This work is presented in Chapters 4 and 5.

The study of trace gas and aerosol exchanges on a global scale has been quite fascinating. In addition to a growing understanding of the controlling biological, chemical and micro-meteorological processes, it has given me a quite detailed view of the global distribution of ecosystems with all their specific characteristics. One moment, the work focussed on the snow covered surfaces of Siberia, followed by a detailed study of the surface exchanges over and within the "green slime" (a colleague once referred in such a way to the vegetation) of the Amazon tropical forest. Unfortunately, the exploration of the surface exchange processes over and within these different global ecosystems has been largely restricted to the virtual world of chemistry and climate models. This is hopefully going to change in the near future by joining measurement campaigns to observe the surface exchange processes of the real world. This seems to me a crucial follow-up of the work of last couple of years. The continuous struggle of finding the optimal compromise between the simplicity required for global scale studies, and the complex interpretation of observed surface exchange processes, requires a balanced overview of both disciplines.

First of all, I have to thank Peter Hofschreuder of the department of Air quality (now the department of Meteorology and Air quality) of the Wageningen University since he has given me the opportunity to start working at the department. Just shortly after I started, Jos Lelieveld became the new professor of the department and he asked me to focus on the dry deposition process. Since then I have been working on this topic, first during four years in Wageningen and the remaining three years at the Utrecht University. Jos has given me all the freedom to continue working on this issue and related topics. I remember quite well that Jos has been quite concerned once in a while that I was including too many details in my work but our continuous discussions helped a lot keeping me on the right track and to persuade Jos about the necessity to include these details. Jos, thanks a lot for giving me the opportunity to do this study and for all the support and discussions. I also want to thank my other promotor Bert Holtslag for the discussions.
I greatly appreciate the support of Geert-Jan Roelofs, especially during the first couple of years when I started using the chemistry and climate model. Besides this specific help, I also have learned a lot from the colleques of the Wageningen and Utrecht University and want to thank you all for the good time that we have had together, discussing scientific work but also sharing some social life. I especially want to thank Frank Dentener and Maarten Krol for the

discussions and suggestions concerning the development of the atmosphere-biosphere model and fresh Dr. Jos[2] (De Laat) who has been a great help surviving Word.
Some special words must be devoted to the carpool express. Besides the fact that travelling together between Wageningen en Utrecht has been an initiative to reduce the traffic jams (that obviously never happened), to improve our vocabulary (opzouten…..), and to use a car as responsible environmentalists, spending about one and half hour a day with all the members of the carpool club (Ad, Joël, Frank, and Bert) has been fun and certainly not always a waste of time. Especially the food suggestions of "smulpaap" Bertje (we should be able now to produce the first Carpool Cookbook containing all the suggestions of Bert for a good diner or "snelle hap") are greatly appreciated. Besides the carpooling (including the drinks at Friday night) and the food suggestions, Bert I want to thank you for the good time we spent together as roommates last couple of years.

Writing down these words of appreciation for the support and input I received last couple of years, I realize that I can not explicitly mention everybody. Especially my family, all my good friends, roommates of Heerenstraat 1, y por supesto mi novia Marcela José Quinõnes (MQ, a veces me gusta pronunciar tu nombre completo, porque suena tan bonita), muchas gracias por todo, la viva es muy buena. The best way to thank everybody is to have a good party together with all of you after I have defended this dissertation.

Contents

Chapter 1

Introduction

The exchange of trace gases such as ozone (O_3), sulfur oxides (SO_x) and nitrogen oxides (NO_x), and aerosols between the atmosphere and the surface has a direct impact on human life since it to a large extent controls the trace gas and aerosol concentrations at the surface. Recent studies have addressed the potential risk of the exposure to enhanced trace gas and aerosol concentrations for human health [e.g., *Brunekreef and Hoek*, 2000; *Schwartz*, 2000]. In addition, the observed decline of the forests during the 1970's in regions being exposed to acid deposition, has shown the rather destructive impact of surface trace gas and aerosol deposition on the biosphere. The realization that acid deposition was largely responsible for the observed forest decline initiated many observational campaigns and modeling exercises to improve the understanding of the controlling mechanisms of the surface trace gas and aerosol exchange. Abatement strategies, developed to reduce the emissions of acidifying species such as sulfur dioxide, have been quite successful which actually reduced the interest for this topic in the 1980s [*Erisman and Baldocchi*, 1994]. However, in the last decade an increasing concern has grown about the role of the antropogenic emissions of greenhouse gases and aerosols affecting the earth's climate [*Charlson et al.*, 1992; IPCC, 1995]. Moreover, the concern about the impact of acidification of the environment and direct exposure to high concentrations of air pollutants has partly shifted from west Europe and North America to other fast developing regions such as eastern Europe and Asia.

The enhanced emissions are mainly related to the population growth and the increased use of fossil fuels. The population growth is associated with an intensified demand for exploration of natural areas for urbanization and cultivation, which results in significant changes in the land cover and land use. These changes moderate the surface trace gas and aerosol exchange through changes in the biogeo-physical and -chemical properties of the surface. Moreover, perturbations of the land cover and land use characteristics initiate changes in the micro-meteorological exchange of momentum, heat and moisture and subsequently the meteorology, e.g., cloud formation and turbulent mixing, and the atmospheric chemistry.

Surface trace gas and aerosol exchange involves four different processes; biogenic emissions from soils, vegetation and water surfaces; antropogenic emissions, e.g., from traffic and industrial production processes; dry deposition, which is the removal of gases and aerosol from the atmosphere during non-precipative events by uptake by the surface; and wet deposition, which is the removal of trace gases and aerosols by precipitation. Actually, the distinction between antropogenic and biogenic surface emissions is not always

straightforward since it is quite clear that many of the biogenic emissions are strongly related to human activity by modification of the land cover and land use.
The focus of this work is the dry deposition process and its role on a global scale. However, for several trace gases the dry deposition process is closely connected to the biogenic emissions, as will be shown later in this introduction and chapters 4 and 5. Hence, the biogenic emissions of some trace gases are also considered in this work.

To assess the role of the different processes that control the atmospheric chemical composition and to understand the relation between the atmospheric chemistry and climate, General Circulation Models (GCM) have been extended with chemistry schemes [*Roelofs and Lelieveld*, 1995, 1997, 2000]. The initial representation of the dry deposition of trace gases and aerosols in this first generation on-line chemistry and climate models, but also in global scale off-line chemistry and tracer transport models, was rather simplistic using constant removal rates [*Penner et al.* 1991; *Langner and Rodhe* 1991; *Feichter et al.* [1996]. *Dentener and Crutzen* [1993], *Levy and Moxim* [1989] and *Kasibhatla et al.* [1993] consider the role of turbulent transfer, whereas a study by *Müller* [1992] also takes into account a surface uptake rate dependent on surface characteristics. The removal rate, the so-called dry deposition velocity (V_d), is used to calculate the dry deposition flux (F) from the surface layer concentration (c_z):

$$F = -V_d c_z \qquad (1.1)$$

The validity of using constant or rather basic definitions of the dry deposition velocity is related to the spatial and temporal scale of the interpreted atmospheric chemistry processes. Focussing on the long term (annual) and global scale budgets of trace gases requires a less

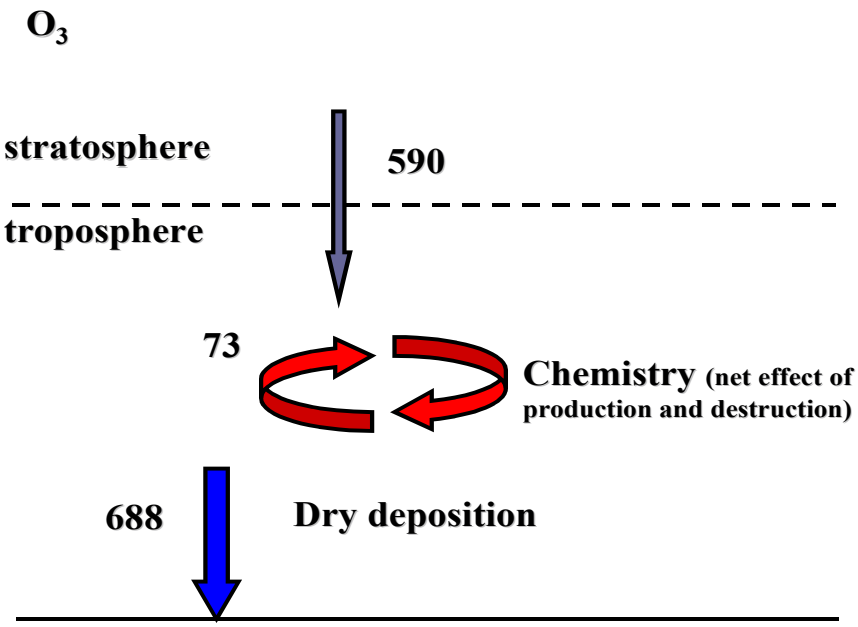

Figure 1.1: The annual mean global tropospheric ozone budget and the controlling processes calculated by a coupled chemistry and climate model [*Roelofs et al..*, 2000]. The numbers are given in Tg

specific representation of the dry deposition velocities compared to a study of the seasonal cycle in the trace gas concentrations close to the surface. Dry deposition measurements over different surfaces show often a distinct seasonal cycle and a spatial variability in the deposition velocities as a function of land cover or land use type. This is related to the large spatial and temporal variability of the controlling processes such as turbulence, the active uptake by vegetation, dissolution in the water films covering the leaves or the biochemical destruction in soils. More details about dry deposition measurements and the mechanisms are presented in section 1.1

There are three major motivations to improve the representation of the trace gas and aerosol dry deposition in global scale models. The first motivation is the contribution of the dry deposition process to the regional and global burden of trace gases and aerosols. Figure 1.1 shows the global and annual mean tropospheric ozone budget and the major controlling processes, calculated with a coupled chemistry and climate model by *Roelofs et al.* [2000]. The model results show that the global tropospheric ozone budget is controlled by the transport of stratospheric ozone, which contributes about 590 Tg, tropospheric photochemistry, which results in a net production of about 73 Tg, and dry deposition of ozone which removes about 688 Tg on an annual basis. The destruction and production terms are not completely balanced since there are some additional processes involved and these numbers do not reflect a long-term steady-state condition. Note that the net chemical photochemical production of 73 Tg ozone consists of large chemical destruction and production terms on the order of about 4000 Tg each.
Another trace gas, of which the atmospheric burden is largely controlled by dry deposition, is sulfur dioxide (SO_2). Figure 1.2 shows the global annual mean sulfur dioxide budget, also calculated by a chemistry and climate model [*Barrie et al.*, 2000]. The annual mean global source is about 92 Tg, comprising of antropogenic emissions of SO_2 and biogenic emissions of Di-Methyl Sulfide (DMS), which is subsequently oxidized to SO_2. About two thirds of the

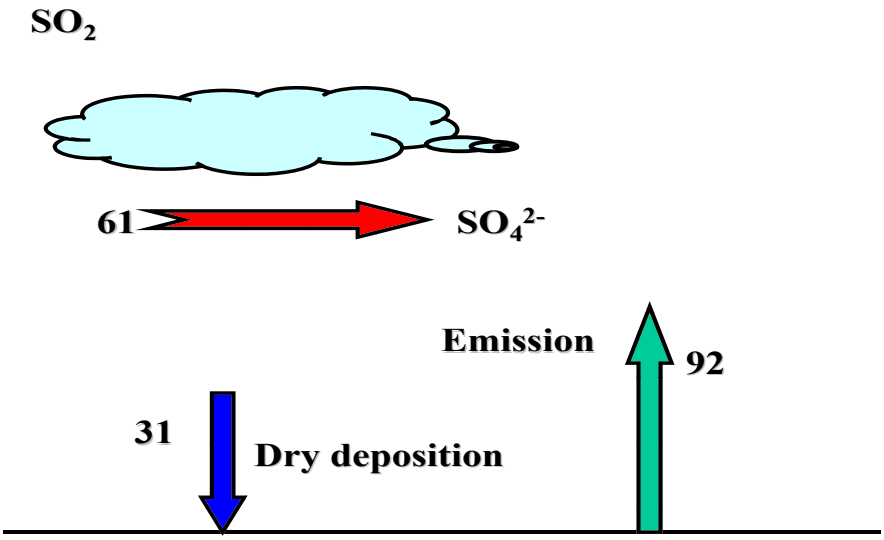

Figure 1.2: The annual mean global tropospheric sulfur dioxide budget and its controlling processes calculated by a coupled chemistry and climate model [*Barrie et al.*, 2000]. The numbers are given in Tg.

emitted SO_2 is transformed to the sulfate aerosol (SO_4^{2-}) by gas- and aqueous-phase chemical oxidation and the 30 % is removed by dry deposition. The largest fraction of the produced sulfate aerosol, about 90 %, is removed by wet deposition, and the remaining 10 % by dry deposition.

A second motivation to introduce a more sophisticated description of surface trace gas and aerosol exchanges in large scale models is the consistency in the representation of the processes that control the atmospheric chemical composition. With the introduction of relative complex chemical schemes that explicitly resolve gas-phase and aqueous-phase chemistry, the transport by advection, convection and turbulence, it seems a rather crude approach to apply a constant deposition velocity. It has been mentioned previously that dry deposition measurements show a large temporal as well as a spatial variability. This introduces concentration fluctuations comparable to those caused by the dynamical and chemical processes. This influence is obviously most pronounced close to the surface and dependent on the magnitude of the surface fluxes and the role of other involved processes. This brings us to a third and crucial motivation. An essential exercise involved with the development of models, such as the chemistry-GCM ECHAM (European Centre model, Hamburg version), is the evaluation of the calculated trace gas and aerosol concentrations by comparison with observed concentrations. Since most of the observations are collected close to the surface within intensive field campaigns or long term measurement programs, the observed concentrations reflect a spatial and temporal variability, which is largely controlled by the site surface fluxes. To ensure a fair comparison between the observed and modeled concentrations, the model must include a realistic representation of the on-site surface exchange processes.

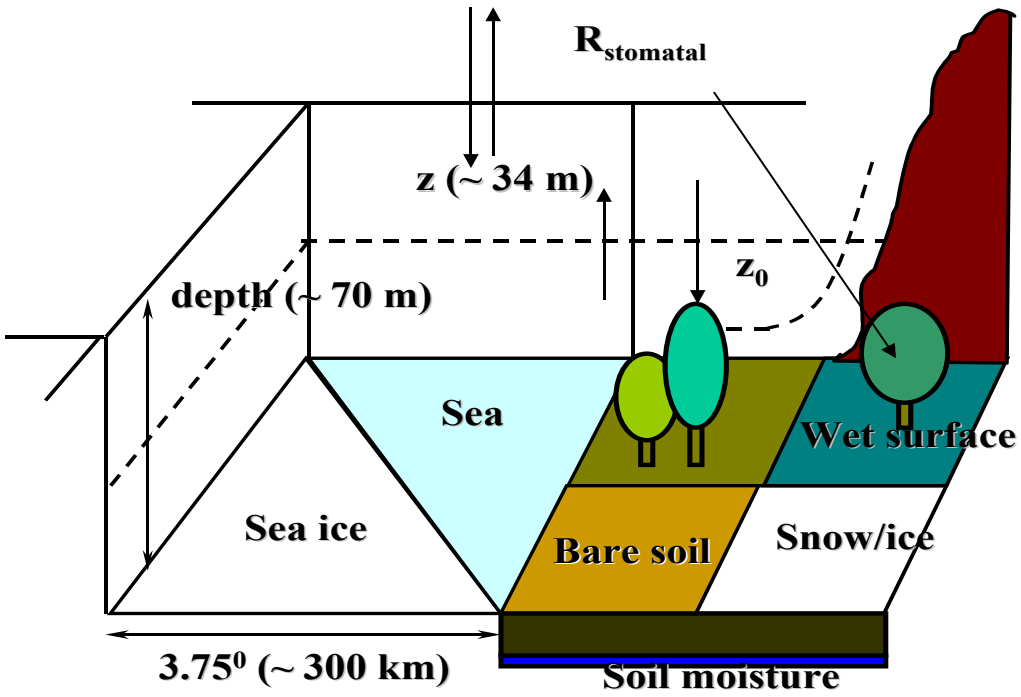

Figure 1.3: ECHAM's atmospheric surface layer and surface characterization

In addition to the aforementioned three motivations to improve the representation of the dry deposition process in large scale models, the description of the surface cover properties in ECHAM is quite detailed for a global scale model. It facilitates the implementation of an explicit representation of the dry deposition process. This is shown in Figure 1.3 in which we present the atmospheric surface layer and the surface cover characterization of ECHAM. The surface layer is about 70 m deep with the prognostic parameters such as temperature and wind speed being calculated for the reference height of about 34 m. Over sea the ice fraction is considered, whereas over land four surface cover fractions are distinguished: a bare soil fraction, a fraction covered by snow and ice, the surface covered by water due to rainfall interception or dew fall, the so-called wet skin fraction, and finally the vegetation fraction. For the vegetation fraction the opening of the stomatal pores, which controls the evapotranspiration and photosynthesis, is considered by the explicit calculation of the stomatal resistance from the Photosynthetic Active Radiation (PAR), soil moisture and amount of biomass according to *Sellers et al.* [1986]. As will be shown later, this stomatal resistance is a crucial parameter for the dry deposition of many trace gases. The amount of biomass is expressed by the Leaf Area Index (LAI), which is the surface area of leaf coverage in m^2 for 1 m^2 soil surface. Closely related to the LAI is the surface roughness (z_0), which indicates the intensity of turbulence that can be generated over that surface. The turbulence intensity, and consequently the turbulent exchange of momentum, heat, moisture and other scalars such as trace gases, increases as the surface roughness increases. ECHAM contains a five-layer soil model that calculates the soil heat fluxes and soil moisture as prognostic variables. For low soil moisture levels there is an increase of the stomatal resistance to reduce evapotranspiration for water stress conditions.

1.1 Measurements of dry deposition fluxes

The main focus of this work is the modeling of the dry deposition process on a global scale. There are no observational activities involved. However, we shortly address this subject since it indicates the availability of observed dry deposition fluxes, which imposes a large constraint on the development of mechanistic models of the dry deposition process.
To develop these models, an understanding of the underlying mechanisms is required. These mechanisms are studied from measurements of the dry deposition flux, relating these observed fluxes to the biogeochemical and bio-geophysical properties of the surface, e.g., the amount of biomass, vegetation type, soil type, soil moisture. The large heterogeneity of the surface and the fact that physical, chemical as well as biological processes control surface trace gas exchange complicates the interpretation of the observed flux in terms of the surface properties. A method to simplify the interpretation is to perform the measurements in a constrained experiment in which the substrate is reduced to only single object, e.g., an enclosed leaf or a soil sample being exposed in an enclosure chamber. An advantage of this method is that the number of interfering processes with an unknown role in the uptake or release process can be minimized such that the controlling mechanism can be identified by changing the properties of the substrate, e.g., the soil moisture in a soil sample. These kind of measurements do certainly benefit the understanding of the controlling mechanism, and representation of surface trace gas and aerosol exchange for relatively "simple" surfaces such as bare soil, snow and ice covered surfaces. However, up-scaling of the observed flux of the specific substrate to the complex vegetation system is not straightforward.

In order to measure the deposition flux for specific land cover such as vegetation, measurement towers are established such that vegetation fluxes can be measured directly or derived from observed concentration profiles. Some of the measurement techniques are discussed shortly further on in this section. The advantage of in-situ measurements is that they reflect the exchange fluxes for the surface as an entity. This facilitates the use of the observed fluxes as a source or sink of trace gases and aerosols in models that consider comparable surface cover types. A disadvantage is that the observed fluxes can not directly be related to all the processes involved such as turbulent transport, chemistry, and the uptake or release by the vegetation. This limits the interpretation of the observed exchange fluxes in terms of the controlling mechanism and thus the use of these kind of data to introduce a mechanistic representation of the deposition or emission process in models. Rather, the observed fluxes are directly applied in model studies over comparable surface cover types or parameterizations are derived.

Observations of the dry deposition process generally use micro-meteorological techniques to infer dry deposition fluxes from the observed wind, temperature and concentration profiles or from the high-frequency fluctuations of the vertical wind speed (w) and concentration (c). The first method is the so-called gradient technique, which yields the observed flux according to:

$$F = K_H \frac{\partial c}{\partial z} \tag{1.2}$$

with K_H being the eddy-diffusivity for heat exchange, which is based on the assumption that trace gas turbulent exchange is similar to the turbulent transfer for heat, and $\partial c/\partial z$ is the trace gas concentration gradient. The latter method is the so-called eddy correlation technique in which the trace gas flux is defined by:

$$F = \overline{w'c'} \tag{1.3}$$

The eddy-correlation method is limited to gases for which fast response (<< 1 sec) measurement instruments exists, which actually limits the application to a small selection of gases. The only gas for which the eddy-correlation technique has been systematically applied is ozone. Recent developments indicate that measurements of surface fluxes of gases such as the oxidized nitrogen species and isoprene using the eddy-correlation technique are already or will be measurable in the near future [e.g., *Munger et al.*, 1996, *Guenther and Hills*, 1998, *Rinne et al.*, 2000].
The gradient method is not limited by the response time of the measurement equipment but rather by the accuracy of the concentration measurements since concentration differences are not likely to exceed 5% of the mean concentration [*Wesely*, 2000]. Moreover, inferring the flux from a measurable gradient requires the estimate of the eddy-diffusivity using relationships that are based on the assumption that the surface is spatially homogenous [*Wesely*, 2000]. This poses a constraint on the selection of the measurement site. Another limitation of the gradient method is related to the occurrence of counter-gradient transport within or over complex vegetation canopies [*Raupach*, 1981; *Denmead and Bradley*, 1985; *Raupach*, 1987]. For daytime conditions, with an efficient turbulent mixing, the local gradient

does not always reflect the true exchange flux since this can largely be controlled by turbulent motions with a spatial scale larger than the separation distance of the concentration measurements. Hence, the flux inferred from an observed gradient within or above a canopy does not always reflect the true flux.
An alternative method is the Relaxed Eddy-Accumulation (REA) technique, in which a system samples separately the concentrations of the down and updrafts. The surface flux is determined according to:

$$F = B\sigma_w (c_{up} - c_{down}) \qquad (1.4)$$

in which B is the Businger constant, which has a value of 0.6, σ_w is the standard deviation of the vertical wind speed and c_{up} and c_{down} are the average concentrations of the up and downdraft samples respectively [e.g., *Sharkey et al.*, 1997]. The advantage of this method is that it can be used to determine the surface fluxes of those trace gases for which there is no fast-response concentration measurement technique, also for those conditions when concentration gradients are too small or when counter-gradient transport controls the surface trace gas exchange.

A disadvantage of aforementioned micrometeorological measurements is the limited spatial representativeness reflecting the footprint of an area with a horizontal scale ranging from 100 m up to some kilometers. The horizontal scale of the footprint depends strongly on the measurement height, the wind speed and the turbulence intensity [e.g., *Schmid*, 1993]. To obtain a measurement that is representative for a larger scale of about 50 km, i.e. the typical grid resolution of regional scale models, aircraft that fly close to the earth's surface within the surface layer can be used. However, aircraft observations can not be performed over longer periods, which limits the temporal interpretation of the observed dry deposition fluxes. The most efficient approach to study the seasonal cycles in dry deposition fluxes, representative for a large footprint area is a combined effort of continuous long term ground based measurements with a selection of aircraft observations to interpret the representativeness of the local flux measurements for the larger area.

For an extensive overview of the observed dry deposition velocities for a selection of trace gases we refer to *Wesely* [2000]. From this and other overviews [*Galbally and Roy*, 1980] it follows that the available (in-situ) observations of dry deposition velocities are strongly biased to the vegetated surfaces of North America and Europe. This is obviously related to the programs on the acidification and air quality research in these regions. The restricted number of available observations for other surface cover types than those being found in the North America and Europe limits the assessment of the role of dry deposition on the global scale.

1.2 Mechanism of the dry deposition process

Only for a small selection of gases, which are very soluble and reactive, e.g., HNO_3, the controlling mechanism of the dry deposition process is fairly well understood. This is basically due to the fact that the uptake by the surface is relative fast compared to the

turbulent transport and diffusion to the surface substrate, which implies that these two processes control the dry deposition process. The turbulent transport and diffusion can be derived rather straightforward from the observed micro-meteorological parameters, e.g., the friction velocity and the temperature profiles. However, for most gases the surface uptake controls the surface exchange fluxes. Characterization of surface uptake processes needs to address the involved processes, e.g., physical, chemical or biological sorption processes, and the selection of different surface substrates, e.g., bare soil, vegetation, and water. Especially for the vegetation canopy with its heterogeneous structure, identification of the controlling processes is complicated due to uptake by the canopy elements as well as the soil surface. Moreover, the turbulent exchange within the canopy and the role of the uptake by wet canopies is not well understood and difficult to quantify. There have been many measurements of the dry deposition process over vegetated surfaces, and of the uptake by enclosed leaves or needles to quantify the role of vegetation. These measurements have revealed that the uptake of many trace gases, e.g., ozone and nitrogen dioxide, by leaves and needles is largely controlled by the opening of stomatal pores, which also controls the evapo-transpiration and photo-synthesis. This is illustrated in Figure 1.4, which shows the observed correlation between the NO_2 dry deposition velocity (V_d) and the stomatal conductance (K_s) observed for an enclosed leaf twig [*Johansson*, 1987]. The good correlation between the deposition velocity and stomatal conductance, especially for the smaller velocities and conductances, suggest that the uptake is controlled by the stomatal conductance. Similar relationships have been found for the uptake of ozone by leaves and needles. Note that the shown correlation between V_d and K_s reflects the measurements for an NO_2 concentration of 41 ppbv, which is a much higher concentration than generally observed in the atmosphere.

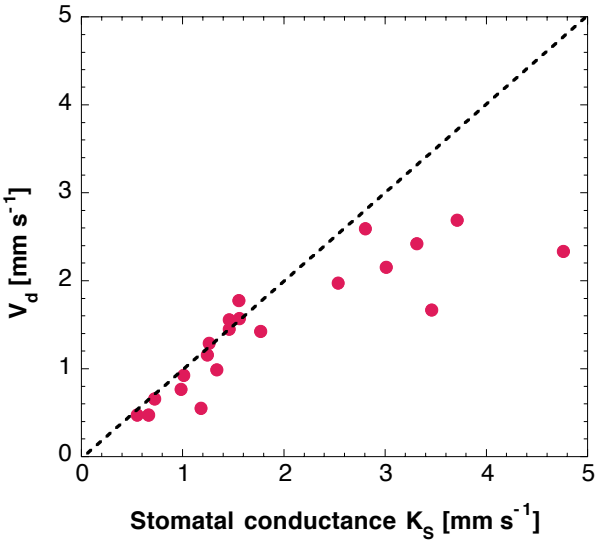

Figure 1.4: NO_2 dry deposition velocity [mm s^{-1}] as a function of the stomatal conductance [mm s^{-1}], C_{NO2} = 41 ppbv.

The uptake mechanisms of other substrates have not been well established due to the limited amount of observations. Observations of the uptake by soils of ozone indicate that the removal is controlled by the organic content and soil water [e.g., *Galbally and Roy*, 1980; *Massman*, 1993]. This suggests that ozone oxidizes the organic material, which is controlled by soil water due to the reduced accessibility of the reaction sites for a high soil moisture content. The reaction of ozone with organic material is also thought to control the uptake of ozone by the oceans [*Schwartz*, 1992]. This has been postulated based on the fact that the solubility of ozone yields a ozone uptake rate by ocean water which is about 40 times smaller

then the observed dry deposition velocities of about 0.05 cm s^{-1} [*Lenshow et al.*, 1982]. Chemical destruction through the oxidation of organic material, present in the thin film layer at the ocean surface, is thought to explain this discrepancy. The uptake of gases by ocean water is different from that of wet surfaces over land such as a wet canopy due to rainfall interception or dew fall. This uptake process has been subject of study due to its significance for the removal of soluble species such as SO_2, nitric acid (HNO_3) and ammonia (NH_3) [e.g., *Baldocchi*, 1992]. The uptake of these gases by wet surfaces is complex since it is controlled by aqueous phase chemical processes, dependent on the water pH and the chemical composition. This chemical composition does not only reflect the contribution of the species dissolved in the water droplets, but also the species that have been deposited previously on the leaf surface or excreted by the plant tissue and which are subsequently dissolved in the water film.
The uptake of soluble trace gases such as SO_2 and HNO_3 by snow or ice covered surfaces also depends on the chemical composition of the snow/ice surface and the physical characteristics such as the presence of a thin water film and surface area [*Conklin et. al.*, 1993]. Observations of SO_2 and HNO_3 uptake by snow often shows a temperature dependency, with relatively large deposition velocities for temperature close the melting point, which suggests that uptake is enhanced due to the presence of a thin water layer [e.g., *Johannson and Granat*, 1986].
Fast chemical transformations of reactive trace gases such as NO and NO_2 complicate the interpretation of observed dry deposition fluxes in terms of the controlling bio-geophysical processes, e.g., stomatal and soil uptake. The fast chemical transformations introduce a flux divergence as a function of the reference height above the surface. This implies that the dry deposition velocity, derived from the observed dry deposition flux and concentration according to equation 1.1, does not only reflect the turbulent transport to the surface and the subsequent removal at the surfac. The dry deposition velocity also reflects the chemical production or destruction, which needs to be accounted for [e.g., *Vilà-Guerau de Arellano and Duynkerke*, 1995; *Galmarini et al.*, 1997]. Moreover, the surface exchange of NO_x ($NO+NO_2$), but also that of NH_3, is complicated due to the presence of a source as well as a sink of these gases at the surface. More details about the occurrence of bi-directional fluxes are given in section 1.4.

The dry deposition process of aerosols is different from the gas dry deposition process since, in addition to the turbulent transport to the surface, the particle size controls the processes involved. Figure 1.5 shows the particle dry deposition velocity and the controlling processes as a function of the particle radius for a 10 m s^{-1} wind speed and a surface roughness of 1 m. The turbulent downward transport of particles is enhanced by sedimentation, which controls the dry deposition velocity of particles in the coarse particle mode > 10 μm. For smaller particles the maximum dry deposition velocity is determined by the turbulent exchange,, indicated in Figure 1.5 by the constant turbulent velocity of about 10 cm s^{-1} for the selected wind speed and surface roughness. For particles larger then 1 μm there is an enhancement of the dry deposition velocity due to the greater inertia, which causes the particle to stay within the airflow around an obstacle, the so-called inertial impaction. Brownian diffusion limits the surface uptake for particles in the accumulation mode, which is the size range from about 0.1 μm up to 1 μm, whereas the dry deposition velocity of particles in the nucleation mode (< 0.1 μm) is controlled by turbulent transport, similar as gases.

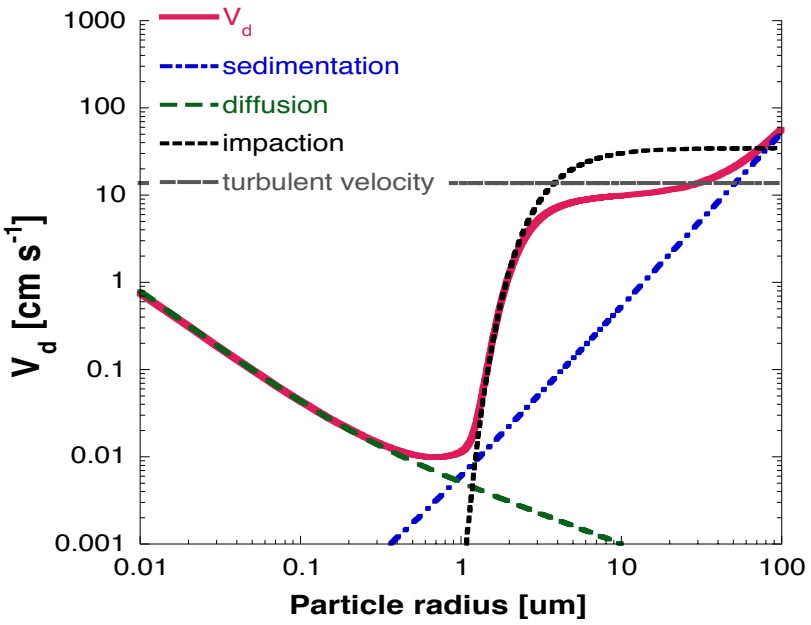

Figure 1.5: Aerosol dry deposition velocity and the controlling processes as a function of particle radius for a wind speed of 10 m s^{-1} and a surface roughness of 1 m.

1.3 Dry deposition modeling

Models for the dry deposition process have been developed for use on different scales, ranging from the site scale to interpret the observed dry deposition fluxes [e.g., *Padro*, 1993; *Matt and Meyers*, 1993], up to the regional scale to study air quality and acidification and to assess the role of the dry deposition process [e.g., *Pleim et. al*, 1984, *Walcek et. al*, 1986, *Erisman and Draaiers*, 1995]. Some aspects of global scale studies of the dry deposition process have been discussed briefly in the introduction.

With regard to global dry deposition modeling, one of the prime challenges is the connection between small and large scale processes. The processes that control dry deposition occur on a typical scale ranging from << 1m to > 1 kilometer, whereas the grid resolution of a regional or global scale model is about 50 km to > 100 km, respectively. This implies that these sub-grid scale processes must be parameterized in terms of available information in these models. Moreover, these parameterizations should also account for the sub-grid scale heterogeneity of the surface cover and its characteristics. Parameterizations are not only required to describe the dry deposition process in large scale models but also for dry deposition models that are used to interpret observed fluxes, especially to represent the processes that control the uptake at the surface. For instance, the complex interactions between emissions, dry deposition, chemistry and turbulence that occur within a forest canopy require a substantial simplification, and often these processes are even ignored. Rather than explicitly describing these detailed processes involved, the vegetation canopy is considered as an entity for which parameterizations of the bulk uptake rate have been developed using the observations. The significance of within-canopy processes for the surface exchange of a selection of trace gases is discussed more extensively in section 1.4.

Dry deposition models generally use selected constant deposition velocities or explicitly calculate dry deposition velocities from site specific surface characteristics such as the vegetation stomatal resistance. The dry deposition velocities are generally calculated using a resistance analog in which the dry deposition velocity is calculated as the reciprocal value of a number of serial and parallel resistances that represent the transfer along the different pathways from the surface layer into the substrate. This is illustrated in Figure 1.6, which

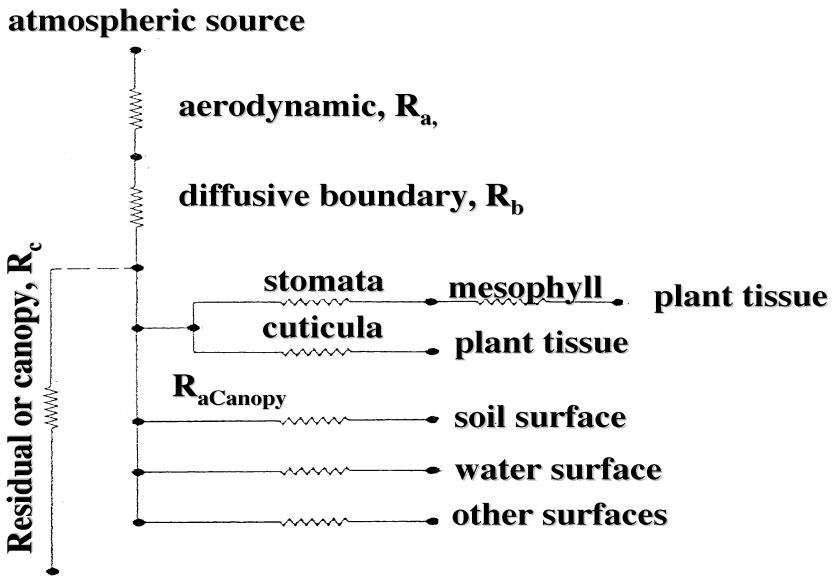

Figure 1.6: Resistance analog for the trace gas dry deposition process [*Hicks et al.*, 1987]

shows the resistance analog according to *Hicks et al.* [1987]. An assumption being made for the application of the resistance analog is that the concentration in the substrate at the end of the transfer pathway is zero. The resistances involved are the aerodynamic resistance, which represents the turbulent transport through the surface layer to the surface, the quasi-laminar boundary layer resistance, which reflects the diffusion through a thin layer close to the surface, and a surface resistance which represents the resistance against uptake by all surface elements:

$$V_d = \frac{1}{R_a + R_b + R_{surf}} \qquad (1.5)$$

For non-vegetative surfaces this basically involves the uptake by water, bare soil or snow and ice covered surfaces, whereas for the vegetation canopies it involves the combined uptake by the vegetation and the bare soil. Moreover, for relative tall canopy structures, the turbulent transport to the substrates within the canopy interior must be considered. The uptake by the vegetation canopy as an entity is calculated from the leaf resistance using the Leaf Area Index (LAI) to arrive at the bulk canopy resistance, which explains the commonly applied name of this "big leaf" approach. The leaf resistance comprises the serial mesophyll and stomatal resistances, which represent the uptake by the stomatal pores and the destruction in the mesophyllic tissue, and the parallel cuticular resistance, which reflects absorption and

destruction at the leaf surface or cuticula. The aerodynamic and quasi-laminar boundary layer resistance can be calculated rather straightforward from the observed or modeled friction velocity and the flux profile relationships according to Monin-Obukhov similarity theory, shown in Chapter 2. The surface resistance can generally not be measured explicitly. However, it can be inferred from observed dry deposition velocities and the inferred aerodynamic and quasi-laminar boundary layer resistance as a residual term, which explains the use of the term residual resistance for the surface resistance in Figure 1.6.

The resistance analog for aerosol particles, considering sedimentation, Brownian diffusion and impaction is shown in Figure 1.7, which yields the dry deposition velocity according to:

$$V_d = \frac{1}{(R_a + R_{cp} + R_a R_{cp} v_g)} + v_g \qquad (1.6)$$

with R_{cp} being the quasi-laminar boundary layer resistance and v_g the sedimentation velocity. There is no surface resistance considered in the particle resistance analog since it is generally assumed that whenever a particle reaches the surface is has been deposited. No further surface destruction mechanisms are involved in contrast to the trace gas dry deposition process. Under specific conditions re-suspension is possible, however, this is assumed to be negligible, and it is not considered in models. For desert dust, for example, this process is captured through the source term.

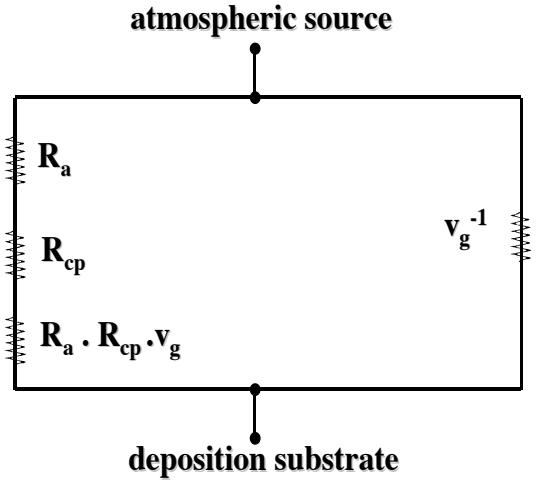

Figure 1.7: resistance analog for aerosol dry deposition.

As has been mentioned previously, the observations of surface exchange fluxes are limited to a small selection of trace gases and surface cover types. To arrive at a first-order estimate of the dry deposition velocity of a trace gas for which observational data are not available, *Wesely* [1989] proposed some simple formulas to estimate the uptake resistances from its solubility relative to SO_2 and its reactivity relative to O_3. Use of this approach is dependent on the availability of observed removal rates of SO_2 and O_3, which have been reasonably well established compared to other trace gases. Actually, applying this first-order estimate can be used to assess the potential importance of the dry deposition process and used in discussions with experimentalists to involve these species in measurement campaigns. *Wesely's* approach has been applied in regional as well as global scale studies. However, since this algorithm is developed for the North American domain, using specific parameters for the surface cover types within this domain, use of this algorithm for other regions or even the globe is questionable. One would prefer to use a model that describes the dry deposition process in a more generalized form,

being less dependent on regionally specific parameters.

In Chapter 2, we present the implementation of the big leaf dry deposition parameterization in the chemistry-GCM ECHAM. This initial version of the dry deposition scheme has been developed for O_3, NO, NO_2, and HNO_3, main gases in atmospheric photochemistry. The dry deposition scheme has subsequently been extended to the sulfur species, SO_2 and SO_4^{2-} aerosol, which is presented in Chapter 3. Moreover, this chapter presents specific details about a more sophisticated representation of the surface cover properties in ECHAM.

1.4 Bi-directional fluxes

Application of the big leaf approach to calculate dry deposition fluxes according to Equation 1.1, using the big leaf resistance analog to calculate the dry deposition velocity as presented in the previous section, is based on the assumption of having a zero concentration within the surface substrate. This assumption is considered to be valid for gases such as ozone and sulfur dioxide, with the selected surface resistances expressing the transfer along the pathway to the location where the destruction of these gases occurs. However, for a selection of gases which are both destroyed and produced by the substrate, the internal concentration is not zero but a function of the balance between the destruction and production processes within the substrate. This implies that alternative formulations of the big leaf approach, that explicitly account for changes in the dry deposition velocity (or exchange velocity) due to a non-zero internal concentration, must be applied. The exchange velocity between the atmosphere and the substrate is related to the concentration gradient and conductances along the transfer pathway. For an internal concentration which is smaller than the ambient concentration, uptake of the trace gas will occur, whereas for internal concentrations larger then the ambient concentrations the trace gas will be released. This threshold concentration above which dry deposition occurs and below which there is an emission is called the "compensation point" [e.g., *Farquhar et. al*, 1980, *Rondon et. al*, 1993]. The existence of such a compensation point is shown in Figure 1.8. It shows the observed NO_2 dry deposition velocity as a function of the stomatal conductance of a leaf twig, similar to that shown in section 1.3, however, this figure refers to an ambient concentration of 1.2 ppbv of NO_2 instead of 41 ppbv. It is clearly seen that, in contrast to the results of Figure 1.4, the dry deposition velocity does not correlate with the stomatal conductance at all and there are actually negative deposition velocities, which reflects the emission of NO_2. These results suggest that for this vegetation type the compensation point of

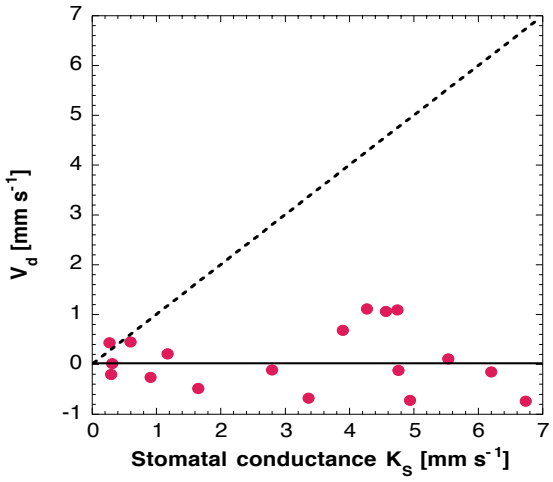

Figure 1.8: NO_2 dry deposition velocity [mm s^{-1}] as a function of the stomatal conductance [mm s^{-1}], similar to Figure 1.4, but for an ambient NO_2 concentration of 1.2 ppbv.

NO_2 for is about 1.2 ppbv.

The definition of a compensation point depends on the scale of interpretation of this phenomenon, e.g., the leaf scale or the canopy scale. This is illustrated in Figure 1.9, which shows the internal cycling of the oxidized nitrogen species within a tropical rainforest, adopted from *Jacob and Bakwin* [1991]. NO is emitted by the soil due to microbial production, and it is subsequently involved in relative fast chemical transformations to NO_2 and peroxyacetylnitrate (PAN), which can be removed through uptake by the vegetation and soils. The extinction of radiation within the canopy and turbulent exchange largely control these canopy interactions since they determine the chemical photodissocation and residence time within the canopy, respectively. The surface trace gas flux, or canopy top flux is controlled by the turbulence and the concentration gradient between the surface layer and the canopy interior. The magnitude and the direction of this gradient are determined by the relative difference between the net sources and sinks within the surface layer and the canopy. Hence, a compensation point at the canopy scale exists as a function of the emissions and dry deposition, the modification of the chemical reaction and photodissociation rates within the canopy relative to the surface layer, and turbulent mixing.
The general approach in large scale models is to ignore the role of these interactions between emissions, chemistry, turbulence and dry deposition within the canopy and to calculate the emissions and dry deposition separately, using the traditional big leaf approach for dry deposition calculations. In addition to the emission of the NO there are also emissions of hydrocarbons by the vegetation, e.g., isoprene (C_5H_8), which are also involved in the chemical transformations. The relative slow chemical transformation rate and the fact that

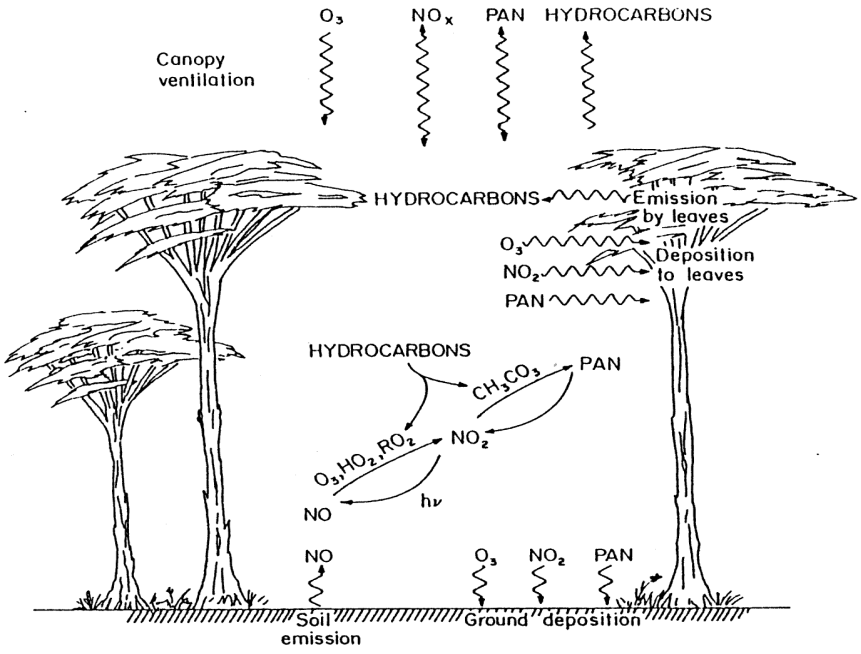

Figure 1.9: Chemical cycling of trace gases within a forest canopy. From: Jacob D. J., and P. S. Bakwin, Cycling of NO_x in tropical forest canopies, In: *Microbial production and consumption of greenhouse gases: methane, nitrogen oxides and halomethanes*, eds. J. E. Rogers and W. B. Whitman, 237-253, American Society of Microbiology, 1991.

there is generally no significant sink by dry deposition implies that for many of these species the role of canopy interactions are likely not relevant for the atmosphere-biosphere trace gas exchange. However, the role of canopy interactions becomes relevant for any trace gas for which there are comparable sources and sinks present within the canopy by dry deposition, emissions and chemical production or destruction, dependent on the turbulent mixing and radiation conditions.

To study the role of the canopy interactions on a global scale, an explicit representation of these interactions has been developed by coupling the biogenic emission and dry deposition formulations and to consider the radiation extinction and the turbulent mixing between the atmosphere and the canopy. To facilitate the development of such an atmosphere-biosphere trace gas exchange model, we have used a single column version of ECHAM, extended with the chemistry scheme of ECHAM. Use of a single column model also facilitates the model evaluation by direct comparison with observations since surface cover properties, which control to a large extent the atmosphere-biosphere trace gas exchange, can rather easily be adjusted to ensure a fair model comparison. More details about the atmosphere-biosphere trace gas exchange model and its evaluation are presented in Chapter 4. In Chapter 5, a more extensive analysis of the role of the canopy interactions for the atmosphere-biosphere trace gas exchange of oxidized nitrogen species on a global scale is presented. Therefore, the atmosphere-biosphere model has been implemented in the chemistry-GCM ECHAM. Details concerning the implementation of the atmosphere-biosphere trace gas model and algorithms for the explicit calculation of the biogenic NO and hydrocarbon emissions are presented in Chapter 5. Moreover, a comparison of the calculated trace gas concentrations and fluxes of the traditional big leaf approach with those of the atmosphere-biosphere trace gas exchange model in ECHAM is shown. Chapter 6 concludes with a summary of the main achievements and recommendations for future research.

Chapter 2

Dry deposition parameterization in a chemistry-General Circulation Model and its influence on the distribution of reactive trace gases[1]

A dry deposition scheme has been developed for the chemistry-general circulation model ECHAM to improve the description of the removal of chemically reactive trace gases at the earth's surface. The chemistry scheme simulates background CH_4-CO-NO_x-HO_x photochemistry and calculates concentrations of, e.g., HNO_3, NO_x and O_3. A resistance analog is used to parameterize the dry deposition velocity for these gases. The aerodynamic resistance is calculated from the model boundary layer stability, wind speed and surface roughness and a quasi-laminar boundary-layer resistance is incorporated. The stomatal resistance is explicitly calculated and combined with representative cuticle and mesophyll resistances for each trace gas. The new scheme contributes to internal consistency in the model, in particular with respect to diurnal and seasonal cycles in both the chemistry and the planetary boundary layer processes, and surface characteristics that control dry deposition. Evaluation of the model indicates satisfactory agreement between calculated and observed deposition velocities. Comparison of the results with model simulations in which the deposition velocity was kept constant indicates significant relative differences in deposition fluxes and surface layer trace gas concentrations up to about ± 35%. Shortcomings are discussed, e.g., violation of the constant flux approach for the surface layer, the lacking canopy description, and effects of surface water layers.

2.1 Introduction

The removal of gases and particles from the atmosphere by turbulent transfer and uptake at the earth's surface is a primary mechanism to cleanse the atmosphere and deliver chemical doses to the surface [*Wesely*, 1989]. This removal of trace gases at the surface by chemical, physical and biological processes, in the absence of precipitation, is defined as dry deposition

[1] Published in the *Journal of Geophysical Research*, **100**, 20,999-21,012, 1995, with J. Lelieveld as co-author.

The dry deposition flux of trace gases is often parameterized in models as the concentration of the trace gas at a specific height multiplied by a deposition velocity (V_d), which depends on atmospheric parameters as well as specific surface parameters. This deposition velocity is usually expressed in terms of an aerodynamic resistance, which is a function of the physical state of the atmosphere and a surface resistance, which is a function of the chemical, physical and biological properties of the surface [*Chameides*, 1987]. Measurement campaigns have confirmed the dependence of the deposition velocity on surface characteristics [*Fuentes et al.*, 1992; *Lenschow et al.*, 1982; *Baldocchi*, 1993; *Massman et al.*, 1994]. Uptake by the vegetation is a major sink for many trace gases and deposition velocities are related to the diurnal and seasonal cycles in plant activity and specific physical properties of the vegetation. Also, for surfaces covered by water layers or sparse vegetation the uptake processes can show a temporal dependence and relations with site specific physical properties, for example, the presence of snow or ice.
A dry deposition model, similar to that presented by *Hicks et al.* [1987], has been incorporated in the chemistry-general circulation model ECHAM [*Roelofs and Lelieveld*, 1995] to improve the description of the removal of chemically reactive trace gases. Different descriptions of the dry deposition process on a global scale have been used in previous studies. *Penner et al.* [1991] use a constant deposition velocity for each trace gas while *Dentener and Crutzen* [1993], *Levy and Moxim* [1989] and *Kasibhatla et al.* [1993] use a constant surface uptake rate, derived from observed deposition velocities, and a parameterization of turbulent transfer calculated from the drag coefficient. An inventory of the global distribution of emission and dry deposition velocities of trace gases by *Müller* [1992] takes into account a surface uptake rate dependent on surface characteristics. However, *Müller* [1992] calculates deposition velocities from assumed surface uptake rates and constant turbulent transport rates. Our scheme calculates deposition velocities according to the 'big-leaf' concept [*Hicks et al.*, 1987] from the turbulent transfer and vegetation activity computed by the ECHAM model, supplemented with representative uptake rates for soil, water and snow/ice on a global scale. The main purpose of the development of this more comprehensive dry deposition scheme for ECHAM is to improve the description of trace gas exchange between the atmosphere and the surface, consistent with temporal and spatial dependencies of the model physics and chemistry. Moreover, the degree of detail of the new dry deposition parameterization should be compatible with that of other process descriptions in ECHAM. We emphasize that the scheme uses all the relevant ECHAM calculated parameters. It is not expected that it reproduces local observed deposition velocities since differences between the spatial and temporal scales of ECHAM and micrometeorological processes may be large. However, the scheme should catch the specific global scale differences between distinct receptor surfaces exposed to very different meteorological conditions, e.g., equatorial tropical forest, desert, high latitude tundra, etc. We will show that the scheme succeeds in simulating deposition velocities which are in reasonable agreement with observations although further improvements must be incorporated in future model versions.

2.2 The ECHAM Model

The GCM used in this study is the ECHAM model (version 3.2) which evolved from the numerical weather prediction model developed at the European Centre for Medium Range

Weather Forecasts (ECMWF) [*Roeckner et al.*, 1992]. We use a T21 horizontal resolution corresponding with grid squares of about 5.6° and a time step of 40 minutes. The model has 19 vertical layers in a hybrid σ-p coordinate system. Prognostic variables are vorticity, divergence, temperature, surface pressure, humidity and cloud water. The model contains parameterizations of radiation, cloud formation and precipitation, convection and horizontal and vertical diffusion. The seasonal cycle of the sea surface temperature is prescribed as a boundary condition. Land surface processes are described by a 5-layer heat conductivity soil model and by a hydrological model to determine evaporation and runoff [*Lohmann et al.*, 1993]. Over land, each grid square is subdivided into 4 fractions to distinguish between snow coverage, bare soil, water in the skin reservoir (water stored within the canopy and on bare soil) and vegetation. Permanent ice cover over land is prescribed by a glacier mask. The vegetation fraction of each grid square is representative for the biological state of the vegetation type assigned to each grid square according to *Wilson and Henderson-Sellers* [1985]. Their classification system discerns 6 major ecotype classes. Over land the roughness length is geographically prescribed while over ice-free sea it is calculated following *Charnock* [1955] [*DKRZ*, 1992, references therein]. Transport of water vapour and trace gases is described by a semi-Lagrangian advection scheme. The ECHAM model is coupled to a chemistry scheme developed by *Roelofs and Lelieveld* [1995]. The scheme calculates the NO_y (NO/NO_2, HNO_3, HNO_4, NO_3 and N_2O_5), OH and O_3 concentrations based on the background CH_4-CO-NO_x-HO_x photochemistry taking into account the role of nighttime chemical reactions of HNO_3 and N_2O_5 on aerosol surfaces and clouds, and the resulting loss of NOx [*Dentener and Crutzen*, 1993]. Emissions of NO_x, CO and CH_4 are considered and the wet deposition calculations use the ECHAM parameterization schemes for large scale and convective clouds [*Roelofs and Lelieveld*, 1995].

2.3 Dry deposition parameterization

2.3.1 Theory

The concentration of a trace gas [c] in the atmosphere, adjacent to the earth's surface, is determined by transport, chemical production or destruction, emission and wet and dry deposition:

$$\frac{dc}{dt} = \left(\frac{\partial c}{\partial t}\right)_{transp} + \left(\frac{\partial c}{\partial t}\right)_{chem} + \left(\frac{\partial c}{\partial t}\right)_{emiss} + \left(\frac{\partial c}{\partial t}\right)_{dep} \qquad (2.1)$$

The contribution of dry deposition is explicitly expressed by a relationship between the deposition flux and deposition velocity according to

$$F_c = c_z V_d \qquad (2.2)$$

where F_c is the deposition flux of the trace gas (molecules m^{-2} s^{-1}), c_z is the concentration of the trace gas (molecules m^{-3}) at a reference height z and V_d is the deposition velocity (m s^{-1}) at the reference height z. The time integrated dry deposition flux is hereafter referred to as "deposition". The deposition velocity is assumed to be independent of the concentration of

the trace gas of interest and to be related to specific characteristics of surfaces and the atmospheric conditions above these surfaces:

$$V_d = \frac{1}{R_a + R_b + R_{surf}} \tag{2.3}$$

where R_a is the aerodynamic resistance, which is a function of the turbulence in the surface layer, R_b is the Quasi-laminar Boundary-layer Resistance (QBR), partially controlled by molecular diffusion, and R_{surf} is the combined resistance of all transfer pathways which play a role in the uptake of trace gases by the surface.

2.3.2 Aerodynamic- and quasi-laminar boundary layer resistance

The aerodynamic resistance is given by

$$R_a = \frac{1}{u_* k}\left[\ln\left(\frac{z-d}{z_0}\right) - \psi\left(\frac{z-d}{L}\right)\right] \tag{2.4}$$

where u* is the friction velocity (m s^{-1}), k is the *Von Karman's* constant (≈ 0.4), z is the reference height which is half the average height of the model's lowest layer (about 70 m, so z ≈ 35 m) and Ψ is a dimensionless stability correction term which is a function of the height and a height independent stability parameter L (m) (*Monin-Obukhov* length); d is the displacement height (m) which is introduced in the calculation of R_a over surfaces with relatively large obstacles (often taken as 2/3 of the canopy height). However, in our scheme the displacement height is assumed to be zero since d is already incorporated in the model's surface level. For the roughness length, z_0, a characteristic length scale of the underlying surface, the surface roughness for momentum z_{0m} as used in the ECHAM model [*DKRZ*, 1992] is used. The stability correction term is calculated from the model's stability in the lowest model layer based on the *Dyer and Hicks* flux-profile relationships for heat [*Brutsaert*, 1973; references therein].

The aerodynamic resistance for a specific trace gas X (R_{aX}) can be expressed as the sum of the aerodynamic resistance, and an additional quasi-laminar boundary layer resistance R_{bX}. This resistance arises in the trace gas flux calculations because of different roughness lengths for momentum (z_{0m}) and trace gases (z_{0X}) [*Fuentes et al.*, 1992; references therein]:

$$R_{aX} = R_a + \ln\left(\frac{z_{0m}}{z_{0X}}\right)\frac{1}{k u_*}(Sc/\mathrm{Pr})^{2/3} \tag{2.5}$$

where the second term on the right hand side represents R_{bX}, *Sc* is the Schmidt number defined as the ratio of the kinematic viscosity for air (0.15 cm^2 s^{-1}) and the molecular

diffusivity of the trace gas (at 1013.25 mbar) and *Pr* is the Prandtl number (0.72) [*Hicks et al.*, 1987]. For vegetated areas a value of 2 has been adopted for ln (z_{0m}/z_{0X}) [*Garrat and Hicks*, 1973]. For snow, ice, water and bare soil, the surface roughness for momentum (z_{om}) ranges from about 0.001 up to 0.1 cm. According to *Brutsaert* [1973] for this range the surface roughness for trace gases is about 3 times larger than for momentum, yielding a logarithmic ratio of ln (z_{0m}/z_{0X}) of about 1. Since R_{bX} is often significantly smaller than R_a and R_{surf}, the computation of the deposition velocity for a specific trace gas, V_{dX}, will not be very sensitive to the chosen definition of R_{bX}. This will also be shown in the presentation of the results (section 2.4).

2.3.3 The surface resistance

In the ECHAM model, each land grid square is divided into 4 subgrids, defined by a snow (ice) covered fraction, one with water in the skin reservoir, one with bare soil and one with vegetation [*DKRZ*, 1992], while over sea the seaice covered fraction is defined. The surface resistance of compound X of the sea and wet skin reservoir, snow, ice and bare soil is defined by

$$R_{surf} = r_{wat/snow/ice/soil} \tag{2.6}$$

and that over vegetation by

$$R_{surf} = \frac{1}{LAI/r_{leaf} + 1/r_{soil}} \tag{2.7}$$

where LAI is the single-side total area of leaves/needles per area surface, r_{leaf} is the leaf/needle resistance which is the resultant resistance of the serial mesophyll and stomatal resistance, r_{mes} and r_{stom}, and a parallel cuticular resistance, r_{cut}. The relative importance of r_{soil} in equation 2.7 increases with a decreasing LAI; locations without vegetation have an LAI of zero. In ECHAM, the r_{stom} of the canopy is calculated as a function of the Photosynthetically Active Radiation (PAR) and the available water in the root zone $F(W_s)$ according to *Sellers et al.* [1986]

$$r_{stom} = \frac{kc}{\left[\frac{b}{dPAR}\ln\left(\frac{de^{kLAI}+1}{d+1}\right) - \ln\left(\frac{d+e^{-kLAI}}{d+1}\right)\right]F(W_s)} \tag{2.8}$$

where d = (a+b*c)/(c*PAR), k = 0.9, a = 5000 J m^{-3}, b = 10 W m^{-2} and c = 100 s m^{-1}. Equation 2.8 is used to determine the r_{stom} for the trace gas of interest for a leaf/needle of any vegetation type, using an LAI of 1, and corrected for differences in molecular diffusivity between H_2O and the trace gas and then combined with r_{cut} and r_{mes} yielding r_{leaf}. The state of the canopy in this ECHAM version is not expressed by the LAI, which has a constant value of 4 for all vegetation types, independent of time and location, but by a seasonally dependent vegetation area fraction, representative for each of the six vegetation classes assigned to each grid square according to *Wilson and Henderson-Sellers* [1985]. This vegetation area fraction

accounts for both the amount of standing biomass and the capacity for uptake of trace gases of the vegetation type in each grid square. The grid-average deposition velocity is computed as the area weighted average of the deposition velocities for each subgrid fraction from R_{aX} and the R_{surf}. The dry deposition parameterization in ECHAM3, as presented in this chapter, is developed for the trace gases O_3, HNO_3 and NO_x (NO and NO_2). Ozone plays a key role in the chemistry of the troposphere and its destruction at the underlying surfaces needs to be realistically represented [*Galbally et al.*, 1980]. Uptake processes of ozone at the surface, especially by vegetation, are relatively straightforward to compute compared to other trace gases, like SO_2 and NO_x. For the latter trace gases R_{surf} is co-determined by a number of complex processes, e.g., uptake of SO_2 and reactions within water layers on the vegetation (dew, rain) and soil emissions (NO_x).
Measurements in different vegetated locations have shown that the dry deposition of O_3 is controlled by rstom and R_{aX} since r_{cut} is relatively large [*Kerstiens and Lendzian*, 1989] and $r_{mes} \approx 0$ [*Wesely*, 1989, *Neubert et al.*, 1993]. The uptake by soil and water surfaces, however, is still uncertain. NO_x is of major importance for the photochemical production of O_3, and HNO_3 serves as a sink for NO_x through the chemical production of HNO_3, e.g., from the reaction between NO_2 and OH, and the subsequent effective wet and dry deposition of HNO_3. Deposition parameterization of additional species, e.g., SO_2, H_2O_2, NO_3, N_2O_5, CH_3O_2H and aerosol particles, will be incorporated in future versions of the scheme. The concentrations of short-lived trace gases like HO_2, OH, CH_3O_2 and CH_2O are largely determined by chemical reactions and not by dry deposition. In the next section, representative resistances of all uptake pathways are presented for O_3, HNO_3, NO and NO_2.

2.3.3.1 Ozone

1) Vegetation
It is generally assumed that the internal leaf concentration of O_3 equals zero, which leads to a zero O_3 mesophyll resistance. The uptake of O_3 by the cuticle is small compared to the uptake through the stomata [*Kerstiens and Lendzian*, 1989], which means that this transfer pathway can be neglected in the parameterization of r_{leaf} [*Baldocchi et al.*, 1987]. Thus, uptake of O_3 by vegetation is solely determined by the stomatal resistance. A large cuticle resistance for O_3 of 10^5 s m^{-1} has been adopted.

2) Soil
Measurements of O_3 uptake by soils show a soil type dependence as well temporal variations in the soil resistance, with typical values ranging from about 50 up to 1000 s m^{-1} [*Galbally and Roy*, 1980; *Stocker*, 1993; *Wesely*, 1981; 1989]. Temporal variations in r_{soil} can be due to variations in soil wetness and temperature. In many experiments a strong dependency of the r_{soil} for O_3 on the soil water content was found [*Galbally and Roy*, 1980 and references therein; *Wesely*, 1981; *Van Pul*, 1992]. In the current version of the model a constant value of r_{soil} of 400 s m^{-1} is used, which is larger than that of *Wesely* [1989], *Leuning et al.* [1979], *Van Pul* [1992], *Galbally and Roy* [1980]. However, most of these values were measured under summer conditions. *Wesely* [1981] observed a considerably higher r_{soil} of about 1000 s m^{-1} for cold bare soil, which is consistent with an observed ozone deposition velocity of about 0.10 cm s^{-1} above a deciduous forest floor [*Hicks et al.*, 1989a, and references therein]. *Stocker et al.* [1993] measured O_3 fluxes over a shortgrass prairie from March to August and derived an

average r_{soil} of about 400 s m^{-1}. This value of 400 s m^{-1} is assumed to be representative throughout the year for all soil types.

3) Water, snow and ice
The deposition of O_3 on water surfaces is small compared to deposition to land surfaces. Measured deposition velocities are of the order of 0.01 cm s^{-1} over fresh water [*Wesely*, 1981] and 0.01 cm s^{-1} [*McKay et al.*, 1992] up to 0.05 cm s^{-1} over sea [*Lenschow et al.*, 1982]. *Galbally and Roy* [1980] presented a summary of results of measurements over sea and fresh water surfaces, indicating that surface resistances range from 1000 to 2000 s m^{-1}. Because of the small surface roughness length, R_{aX} will be larger over water compared to land surfaces. However, the surface resistance is still significantly larger compared to the aerodynamic resistance [*Lenschow et al.*, 1982]. Therefore, introduction of an aerodynamic resistance by application of equation 2.5 will not result in any significant temporal dependence of V_{dO3} over water surfaces. The current dry deposition scheme computes V_{dO3} over water surfaces using a value of r_{wat} of 2000 s m^{-1}. This value is also applied to snow and ice surfaces [*Galbally and Roy*, 1980; *Wesely*, 1981].

2.3.3.2 Nitric acid vapour

Over most surfaces, the deposition velocity for gas phase HNO_3 is solely controlled by the aerodynamic resistance. This suggests that HNO_3 is deposited as rapidly as turbulent transfer allows [*Hanson and Lindberg*, 1991, and references therein]. Observed HNO_3 deposition velocities above crop canopies, deciduous forest, grass and other vegetation range from 0.5 to 26 cm s^{-1}, depending on vegetation type and wind speed. The vegetation resistance of HNO_3 is close to zero due to the high solubility and sticking coefficient, resulting in a small cuticle and mesophyll resistance. In contrast to O_3, the HNO_3 deposition velocity is therefore highly sensitive to the QBR [*Hanson and Lindberg*, 1991, and references therein; *Huebert and Robert*, 1985]. Deposition to water surfaces and soils can also be expected to be large. Parameterization of the surface resistances according to *Wesely* [1989] resulted in very small water and soil resistances. Furthermore, average HNO_3 deposition velocities above water/soil surfaces are rather small because of the small surface roughness. HNO_3 deposition velocities above snow observed by *Johannson and Granat* [1986] show a dependence on the snow temperature with a typical value of about 0.6 cm s^{-1} for a snow temperature of -20° C, decreasing rapidly to about 0 with decreasing snow temperatures [*Hanson and Lindberg*, 1991]. The physical mechanism responsible for this is unclear. In our scheme, the deposition velocity above all surfaces except for snow and ice, is calculated assuming a minimal surface resistance of 10 s m^{-1} in order to avoid unrealistic large deposition velocities over rough surfaces [*Wesely*, 1989]. This threshold deposition velocity is required for the scheme since the large scale model surface roughness is dependent on the orography, resulting in very small aerodynamic resistances above mountainous regions. The HNO_3 surface resistance for snow and ice surfaces is calculated from the model's surface temperature, according to the relationship by *Wesely* [1989], based on the observations by *Johannson and Granat* [1986]. One should bare in mind that only the dry deposition of gaseous HNO_3 is calculated by our scheme. In reality some HNO_3 is removed from the lower troposphere by gas-to-particle conversion of HNO_3 and subsequent removal of aerosol nitrate. However, the latter process has not yet been incorporated in the chemistry scheme. For more information concerning the

calculation of wet deposition of HNO_3 in the chemistry scheme we refer to *Roelofs and Lelieveld* [1995].

2.3.3.3 Nitrogen oxides

The dry deposition description for NO_x is relatively complicated compared to O_3 since the surface can be a sink as well as a source of NO. Results of field experiments have indicated that observed fluxes and concentrations of NO_x are not in agreement with flux-resistance relationship expressed by equation 2.2 and 2.3. Emission of NO is probably one of the causes of the disagreement. Another cause is violation of the constant flux approximation. The time scale of the chemical reactions of NO_x may be small compared to that of diffusive transport, resulting in local sources or sinks of NO_x and possibly flux divergence [*Kramm et al.*, 1993]. The applicability of the aerodynamic resistance using equation 2.4 for calculation of the NO_x deposition velocity seems therefore doubtful for the height of the model's lowest layer (~ 70 m). However, for most surfaces, the aerodynamic resistance is relatively small compared to the surface resistance and thus the error in the calculated deposition velocity will also be small. Concerning the surface resistance, in this work, representative resistances are selected to account for the sources. A more realistic representation of the interaction between emission and deposition has not been applied yet since the NO emission has been calculated in a separate routine of the chemistry model

1) Vegetation
The dry deposition of NO_2 to vegetation is controlled by the stomatal aperture [*Hanson and Lindberg*, 1991; *Neubert et al.*, 1993], suggesting that there is no significant mesophyll resistance. However, deposition of NO_2 to broadleaf plant species appears to exceed that of coniferous species by a factor of 3 - 10 which can not be attributed to a difference of typical LAI values for these plant species alone. It was suggested by *Johansson* [1987] that a mesophyll resistance exists for coniferous trees, which comprises at least 50% of the total resistance to diffusion [*Hicks et al.*, 1989a]. *Johansson* [1987] observed that the relationship between stomatal behaviour and uptake broke down with decreasing concentrations (Scots Pine). This suggests the existence of a 'compensation point', the concentration for which emission balances deposition, and an increasing contribution of the mesophyll resistance into the total leaf resistance. The observed mesophyll resistance ranged from 10 to about 800 s m^{-1} [*Johansson*, 1987]. The existence of a compensation point for NO_2 concentrations of about 1-3 ppbv was also observed for Spruce trees by *Thoene et al.* [1991]. The existence of a mesophyll resistance for NO_2 is a possible explanation for observed differences in O_3 and NO_2 deposition velocities [*Wesely et al.*, 1982; *Delany and Davis*, 1983], the latter being about 2/3 of the O_3 deposition velocities. This difference between deposition velocities of O_3 and NO_2 can not be explained by different O_3 and NO_2 cuticle resistances. The cuticle NO_2 uptake plays a minor role, the cuticular uptake rate for NO_2 being at least 1-2 orders of magnitude less than representative rates to tree foliage through stomata [*Hanson and Lindberg*, 1991; *Kerstiens and Lendzian*, 1989; *Kramm et al.*, 1993]. In our deposition scheme, the mesophyll resistance for NO_2 is assumed to be half the leaf stomatal resistance, in order to calculate a NO_2 deposition velocity of about 2/3 the O_3 deposition velocity above vegetated areas, ignoring the difference of a broadleaf and coniferous plant mesophyll resistance. Calculating the mesophyll resistance from the stomatal resistance indirectly

implies a dependence of the mesophyll resistance on light intensity, in agreement with observations by *Neubert et al.* [1993]. *Kramm et al.* [1993] proposed a correction term, depending on atmospheric and internal concentrations and resistances. This correction term may be accounted for in future versions of our deposition scheme if more detailed information concerning the 'compensation point' of other vegetation types becomes available. As long as this correction has not been made, a representative resistance must be chosen for the co-existence of emission and deposition. The cuticle resistance for O_3 (10^5 s m^{-1}) has also been adopted for NO_2. There is little information available about the uptake of NO by plants. Uptake rates of NO observed by *Neubert et al.* [1993] are about one order of magnitude lower that those for NO_2, consistent with the findings reviewed by *Hanson and Lindberg* [1991]. The main reason for this significantly smaller deposition velocity is the relative large mesophyll resistance for NO [*Neubert et al.*, 1993, *Wesely*, 1989]. *Kisser-Priesack et al.* [1987] concluded, based on measurements with radioactively labelled NO, that cuticular uptake should not be ignored [*Hanson and Lindberg*, 1991; references therein], also because of the relatively small loss by deposition through the stomata. In contrast, *Neubert et al.* [1993] and *Wesely* [1989] find that the uptake of NO by the cuticle does not contribute significantly to the foliage uptake. In our scheme, the mesophyll resistance for NO is assigned a 10 times larger value than that of NO_2, and for the cuticle resistance of NO we assumed the same value as for O_3 and NO_2.

2) Soil
Conductances to different soil types, as presented by *Hanson and Lindberg* [1991], indicate average soil resistances for NO_2 and NO of about 250 s m^{-1} and 950 s m^{-1}, respectively. *Wesely* [1989] derived larger soil resistances for both trace gases. In the dry deposition scheme a value of 600 s m^{-1} is used for NO_2, resulting in NO_2 deposition velocities of 2/3 of the O_3 deposition velocity over vegetated areas (see equation 2.7). This value of 600 s m^{-1} is probably reasonably representative for soils covered by vegetation since all the NO_2 soil conductances in *Hanson and Lindberg* [1991] were determined in enclosure experiments. It can be expected that turbulent transfer in these chambers was optimal, contrary to the conditions in the canopy for which an additional resistance against turbulent transfer through the canopy to the soil surface should be adopted. Furthermore, high exposure concentrations were used in the enclosure experiments. It can be expected that for typical tropospheric surface layer NO_2 concentrations, a representative soil resistance will be larger because of a more significant contribution of NO emission. This effect is more pronounced for NO since emission dominates deposition [*Stocker et al.*, 1993]. Therefore, NO deposition to soils has been neglected.

3) Water, snow and ice
As for O_3, the uptake of NO and NO_2 is limited by uptake into the aqueous phase and/or reaction with dissolved components [*Lee and Schwartz*, 1981; *Schwartz*, 1992]. The Henry's law constants for O_3 and NO_2 are comparable but the difference in reactivity results in a relatively larger uptake resistance for NO_2 for sea and fresh water. The Henry's law constant for NO is smaller than that of O_3, and NO is not significantly reactive in the aqueous phase [*Wesely*, 1989; *Lee and Schwartz*, 1981]. In the dry deposition scheme, a value of 10^5 s m^{-1} is adopted for the sea and fresh water resistance of NO_2 and NO. An exact definition is not required since the dry deposition process to water remains very slow compared to gas phase reactions of NO and NO_2 [*Lee and Schwartz*, 1981]. Observed deposition velocities of NO_x

over snow are less than 0.03 cm s^{-1} [*Granat and Johansson*, 1983]. *Valdez et al.* [1987] observed an average NO_2 deposition velocity to snow of about 0.01 cm s^{-1}. Based on these results and the relatively slow deposition process, a value of 10^5 s m^{-1} has been adopted for the snow and ice resistances for NO_x. Table 2.1 shows all the adopted resistances as used in this study.

Table 2.1: Selected soil, cuticle, mesophyll, water, snow/ice resistances (s m^{-1}) for O_3, HNO_3 and NO/NO_2.

	r_{soil}	r_{cut}	r_{mes}	r_{wat}	$r_{snow/ice}$
O_3	400	10^5	0	2000	2000
HNO_3	10	0	0	10	$\max(10, f(t_{surf})$
NO_2	600	10^5	$0.5 \times r_{stomO3}$	10^5	10^5
NO	10^5	10^5	$5 \times r_{stomO3}$	10^5	10^5

2.4 Results

We present model simulations for the months January and July, for which strong differences in deposition velocities, associated with vegetation activity, chemistry and meteorology, can be expected.

2.4.1 Diurnal cycle and comparison with observations

Evaluation of the model against experimental results is difficult due to the large difference in spatial resolution of measured and model derived deposition velocities. The version of ECHAM model used (T21) has a spatial resolution of 5.6° × 5.6° (500 - 600 km at mid-latitudes), while measured deposition velocities are site specific with typical spatial scales of about 0.1 - 1 km. In ECHAM, surface characteristics, e.g., canopy structure, canopy height, LAI and vegetation type, are only coarsely represented. Therefore, evaluation of V_{dX} is restricted to qualitive comparisons of diurnal and seasonal cycles, which are not very sensitive to the specific surface parameters but which are to a large extent controlled by turbulence and irradiance (e.g., through stomatal uptake). Further, evaluation of calculated NO_x and HNO_3 deposition velocities is limited by the relatively small amount of representative dry deposition data available.

Evaluation of V_{dO3} is most relevant for grid squares covered by vegetation or bare soil. For vegetated grid squares, both the surface and the aerodynamic resistance are computed from ECHAM parameters. Although bare soil surfaces have been assigned a constant surface resistance, the aerodynamic resistance still has a significant influence on V_{dO3} due to the relatively small surface roughness. Evaluation of V_{dO3} over water, snow and ice is of lesser importance because V_{dO3} merely depends on the assigned values of the relatively large surface resistance. Figures 2.1a - h show the calculated monthly average diurnal cycle of V_{dO3} for eight grid squares with typical vegetation classes for January and July. The grid squares are selected based on the distribution of major ecosystems [*Henderson-Sellers et al.*, 1986]

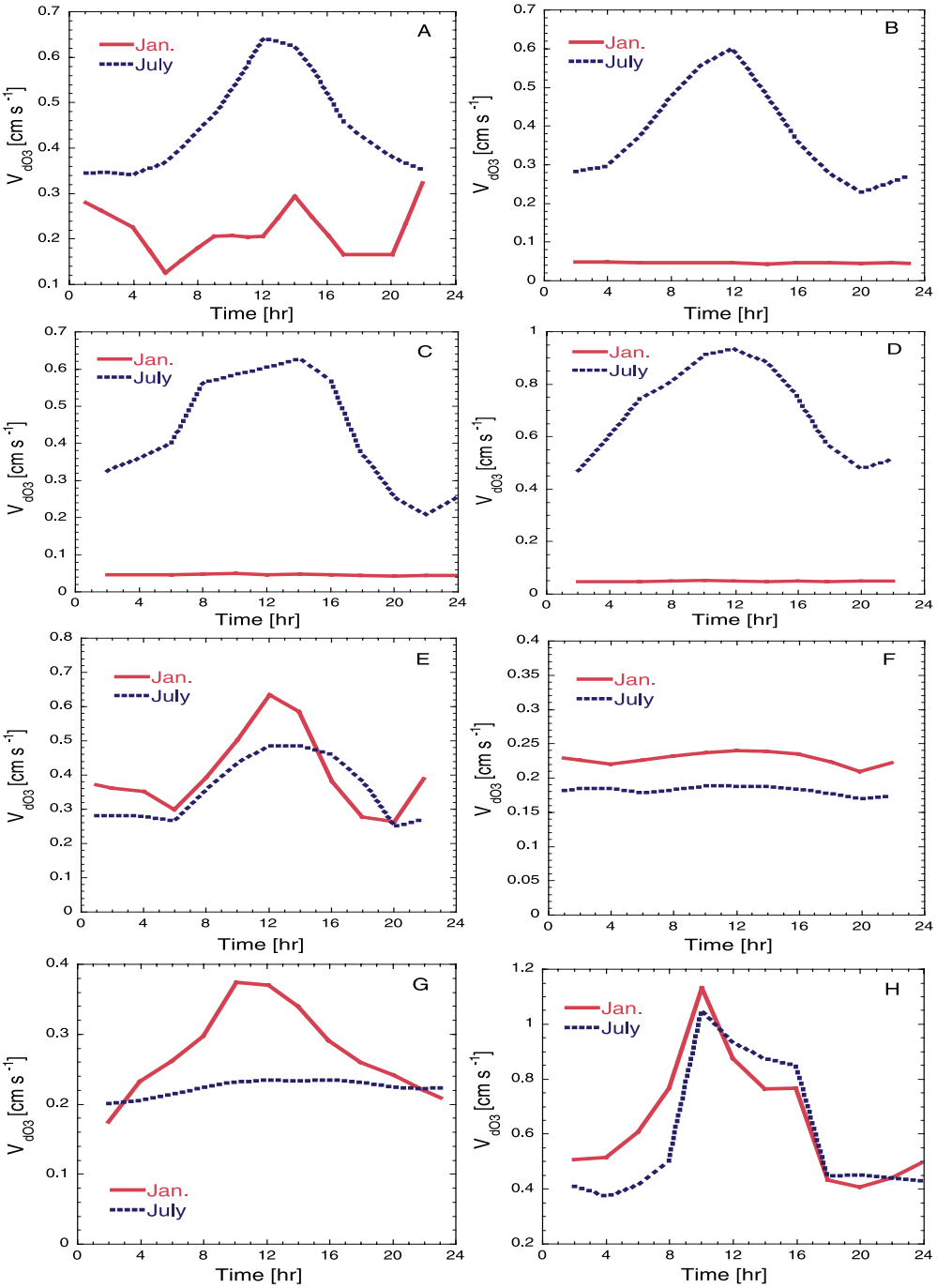

Figure 2.1a-h: Monthly average diurnal cycle of V_{dO3} for January and July, a) north-western Europe, 55° N, 10° E, the vegetation class is crop, b) north-eastern Canada, 55°N, 65° W, vegetation class evergreen tree, in January V_{dO3} has a constant value of 0.05 cm s^{-1} as a result of snow cover, c) east Canada, 45° N, 80° W, vegetation class deciduous tree, snow cover in January, d) Alaska, 60° N, 150° W, vegetation class tundra/desert, snow cover in January, e) western North America, 40° N, 115° W, vegetation class grass and shrub, f) north Africa, 20° N, 15° E, vegetation class tundra/desert, g) Australia, 30° S, 140° E, vegetation class grass and shrub and h) South America, 5° S, 45° W, vegetation class evergreen tree.

vegetation cover). Many available observations could unfortunately not be used because these observations were carried out over very different vegetation compared to the assigned vegetation class of the grid square. Figure 2.1a shows the diurnal cycle of V_{dO3} for north-western Europe. There is a distinct difference between the two months (seasons), resulting from the differences in stomatal and aerodynamic resistances. The January and July average diurnal cycles of r_{stom} and R_a for this grid square are shown in Figures 2.2a and 2.2b. The r_{stom} is large for January ($\approx$ 2000 s m^{-1}) and thus not shown. The deposition velocity is determined

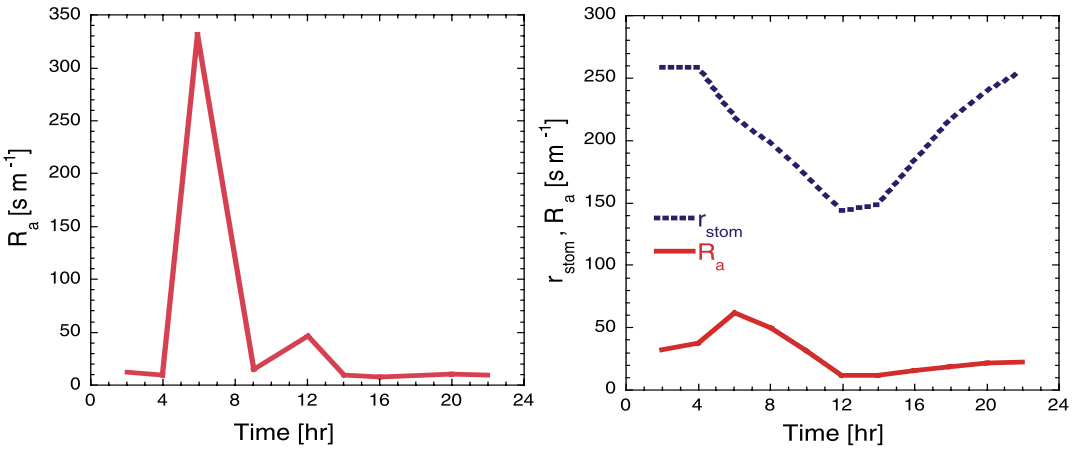

Figure 2.2a-b: Monthly average diurnal cycle of R_a and r_{stom} for O_3 of north-western Europe for (a) January ($r_{stom} \approx$ 2000 s m^{-1}, not shown here) and (b), July.

mostly by the soil resistance and R_a. The January diurnal cycle in V_{dO3} is less pronounced than in July since it is solely determined by R_a, which does not have such a large amplitude in the daily variation as the stomatal resistance. The average V_{dO3} in north-western Europe in January is about 0.25 cm s^{-1}, approximately the inverse value of r_{soil}. In July, r_{stom} is at maximum during nighttime whereas a high R_a additionally limits transfer of O_3 through the atmosphere as a result of the stable stratification. The diurnal cycle of r_{stom} is very similar to the diurnal cycle of V_{dO3}. The inverse value of r_{stom} does not differ much from the absolute level of V_{dO3} which means that V_{dO3} is largely controlled by r_{stom}. R_a has no significant limiting effect on V_{dO3}. The QBR is not presented in Figures 2.2a and b because of its relatively small value. A sensitivity study indicated that the average R_a is about one order of magnitude larger than the QBR, which implies that no elaborate description of the QBR is required for these conditions.

Table 2.2 shows daily average, maximum and minimum calculated O_3 deposition velocities and a selection of observations over comparable surfaces and season. No observed diurnal cycles are presented here, however, the diurnal and seasonal cycles are dependent on the same quantities, which are represented by their average, maximum and minimum values. The agreement between calculated and observed O_3 deposition velocities appears to be satisfactory. The calculated V_{dO3} over all surfaces, except for the deserts of North-Africa and South-American forests, shows a distinct difference between the two months. There is a diurnal cycle in V_{dO3} for all surfaces in the summer and winter except for the snow covered surfaces (a V_{dO3} of about 0.05 cm s^{-1} in January in Figures 2.1b, c and d) and the deserts. The small seasonal and diurnal cycles over deserts are related to the negligible vegetation influence on the deposition process. The average V_{dO3} of 0.25 cm s^{-1} approximates the inverse value of the

Table 2.2: Comparison of Calculated and Observed V_{dO3} Values [cm s^{1}] Above Comparable Surfaces Under Comparable Conditions.

Figure number and deposition surface	**Calc. V_{dO3}, average (maximum, minimum)**	**Reference, obs. V_{dO3}, average (maximum, minimum)**
1a: crop, northwestern Europe	Jan. 0.2 (0.3, 0.15) July 0.5 (0.65, 0.35)	Van Pul [1992] 0.46 (~0.6, 0.35)
1b: evergreen tree, northeastern Canada	Jan. 0.05 (snow) July 0.4 (0.6, 0.25)	Ritter et al. [1994] 0.4 (0.65, 0.25)
1c: deciduous tree, east Canada	Jan. 0.05 (snow) July 0.45 (0.65, 0.25)	Padro et al. [1993] ~ 0.2 (0.3, 0.1) ~0.6 (1.25, 0.25)
1d: tundra, Alaska	Jan. 0.05 (snow) July 0.7 (1.0, 0.4)	Sehmel [1980] 0.7* Jacob et al. [1992] and Ritter et al. [1992], 0. (0.35, 0.1)
1e: grass and shrub, western USA	Jan. 0.4 (0.65, 0.25) July 0.35 (0.5, 0.25)	Massman et al. [1994] 0.3 (0.5, 0.1)
1f: tundra and desert, North Africa	Jan. 0.25 July 0.25	Sehmel [1980] 0.3*
1g: grass and shrub, Australia	Jan. 0.3 (0.4, 0.2) July 0.2	Sehmel [1980] 0.4 (0.6, 0.2)*
1h: evergreen tree, South America	Jan. 0.8 (1.15, 0.4) July 0.8 (1.0, 0.35)	Fan et al. [1990] ~ 1.0 (~2.5, ~0.25)

*Yearly average V_{dO3} and values between parentheses denote maximum and minimum V_{dO3}.

assigned soil resistance since the aerodynamic resistance does not significantly contribute to V_{dO3} despite the relatively small surface roughness. The overestimation of V_{dO3} by the model over tundra in Alaska can probably be attributed to the fact that ECHAM does not contain a representation of inland water while the measurements were carried out over relatively wet tundra terrain [*Jacob et al*., 1992; *Ritter et al., 1992*]. The V_{dO3} over western North-America in July is smaller than in January as a result of the reduced stomatal uptake due to water stress. The daytime V_{dO3} over tropical forest is underestimated by the model which indicates that the scheme does not succeed in simulating the very efficient stomatal uptake by tropical forest.

2.4.2 Global distribution of deposition velocity, deposition and concentrations

1) Ozone

Figures 2.3a and 2.3b show the January and July average global V_{dO3} distribution, indicating a distinct spatial distribution over the continents, which is mostly related to differences in surface characteristics. In July, relatively large values of V_{dO3} occur in the areas with dense vegetation cover, e.g., the temperate forests in the northern hemisphere (NH and forested

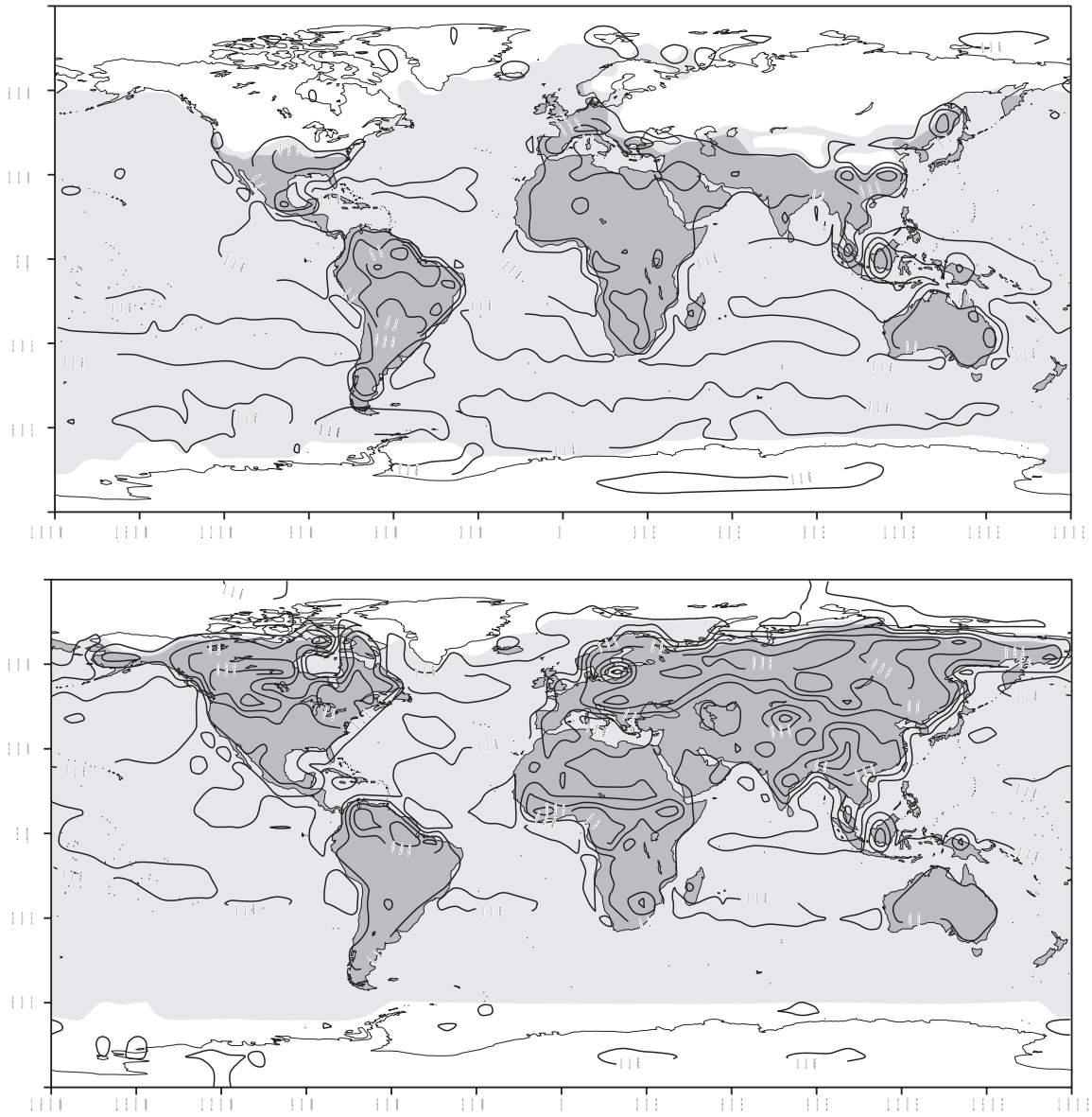

Figure 2.3a-b: Monthly average O_3 deposition velocity (cm s^{-1}), (a) January, (b) July. Ice and snow cover is represented by the white color. The isolines are: 0.045, 0.2, 0.35, 0.5, 0.65.

regions in the tropics. Relatively small deposition velocities of about 0.1 - 0.2 cm s^{-1} are calculated over the deserts of Africa and the Middle-East. In the southern hemisphere (SH), V_{dO3} values are relatively small, with values of about 0.2 cm s^{-1} in Australia, and 0.25 cm s^{-1} in large parts of South-America and Africa. Figures 2.3a and 2.3b also indicate the seasonal differences in V_{dO3} over the continents. The values of V_{dO3} in January are quite different from those in July, being very small over North-America and northern Europe and Siberia in January, caused by the snow cover in these areas. Over sea, V_{dO3} is about 0.05 cm s^{-1}. Relatively low wind speeds and consequently small surface roughnesses in subsidence areas, following the Hadley-cell circulation, result in somewhat increased aerodynamic resistances in the sub-tropics in both hemispheres.
The results of our deposition scheme have been compared with those of a scheme in which V_{dO3} was kept at a constant value (hereafter referred to as "constant V_{dO3}" scheme) of 0.35 cm s^{-1} over land (without snow/ice cover) which was used previously in a global model by *Dentener and Crutzen* [1993], and 0.05 cm s^{-1} over sea and snow/ice surfaces. Figure 2.4a shows the relative differences between O_3 deposition, calculated as (new scheme minus

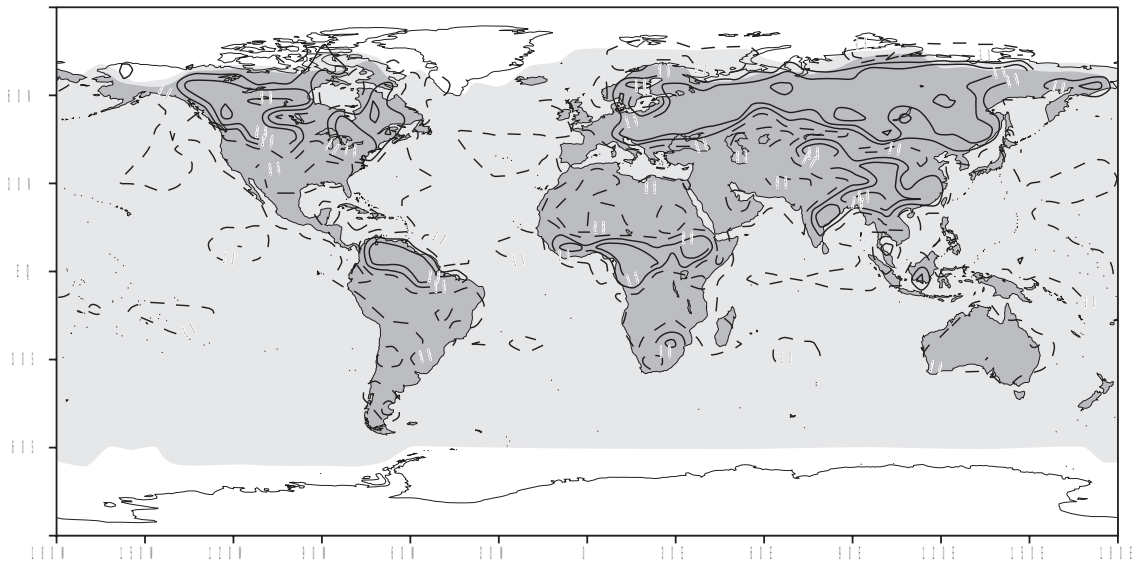

Figure 2.4a: Relative difference (%) of O_3 deposition between the new dry deposition scheme and the "constant V_{dO3}" scheme, July. Dashed and solid lines indicate a decrease and increase, respectively, of deposition calculated by the new scheme compared to the "constant V_{dO3}" scheme. The isolines are: -25, -10, 10, 25, 50.

"constant V_{dX}" scheme) / ("constant V_{dX}" scheme). Especially over vegetated areas, ozone deposition increases by 10 - 50 % over the NH. The new deposition scheme calculates less O_3 deposition over arid regions, e.g., the African and Middle-East deserts and Australia. Reductions of O_3 deposition over the oceans are caused by considering the aerodynamic term, thereby increasing the total resistance with about 200 - 500 s m^{-1}. The relative differences between the monthly average O_3 concentrations in the surface layer by both schemes for July are given in Figure 2.4b. These are generally smaller than the differences in O_3 deposition, associated with negative feedbacks in O_3 concentration changes through dry deposition and chemistry. However, non-negligible O_3 concentration differences occur (~5%) between the two schemes up to an altitude of about 1.5 - 2 km.

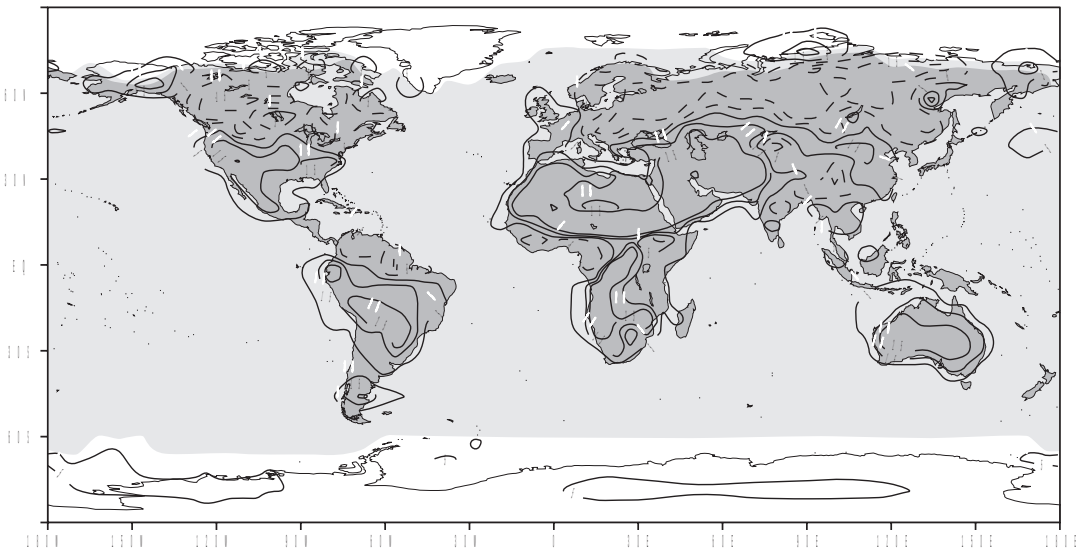

Figure 2.4b: Relative difference (%) of the O_3 surface layer concentration between the new scheme and the "constant V_{dO3}" scheme (see Figure 2.4a), July. The isolines are: -25, -15, -5, 5, 15, 25.

2) Nitric Acid Vapour

Figure 2.5 shows the January average global V_{dHNO3} distribution. The V_{dHNO3} over all surfaces, except snow/ice covered surfaces, is controlled by turbulent transfer. The limiting influence of the surface temperature dependent snow/ice resistance is clearly visible in Canada and Russia. Very large V_{dHNO3} values, up to 7.5 cm s^{-1}, occur in mountainous regions as a result of a large surface roughness. Over land, V_{dHNO3} exceeds 2 cm s^{-1} over large areas, while over sea the calculated V_{dHNO3} ranges between about 0.4 cm s^{-1} in subsidence areas and 0.9 cm s^{-1} in areas with large wind speeds. Figure 2.6 shows the relative differences between the January

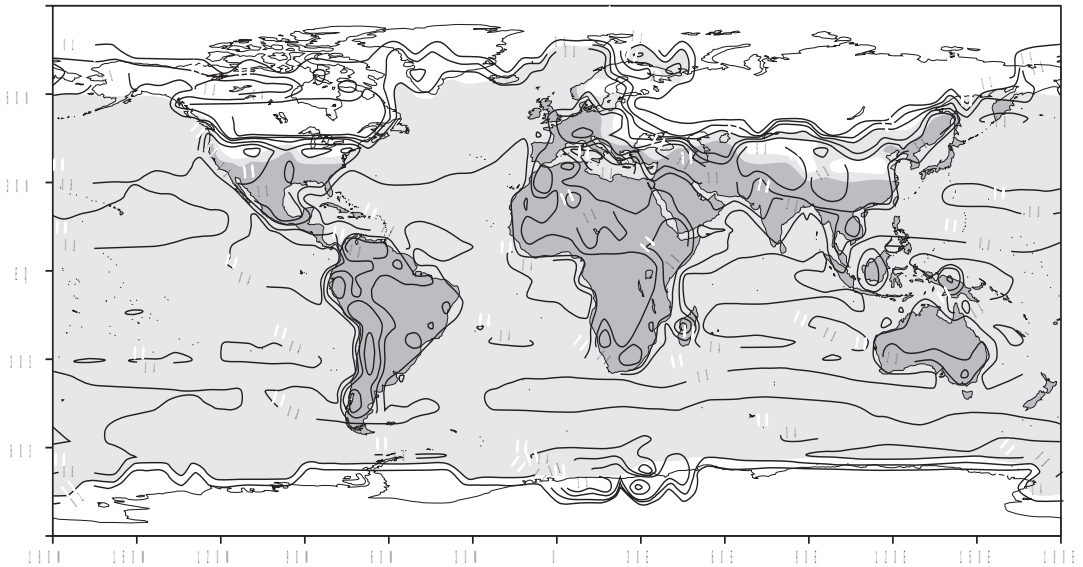

Figure 2.5: Monthly average HNO_3 deposition velocity (cm s^{-1}), January. The isolines are: 0.1, 0.4, 0.8, 2.0, 3.0, 5.0.

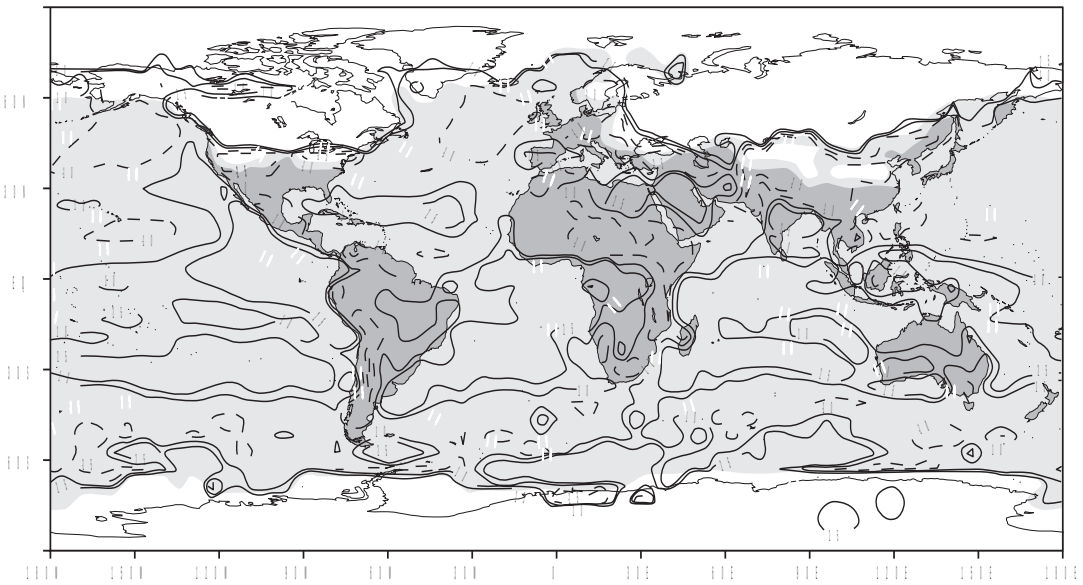

Figure 2.6: Relative difference (%) of HNO_3 surface layer concentration between the new scheme and the "constant V_{dHNO3}" scheme (see Figure 2.4a), January. The isolines are: -25, -10, 10, 25.

average HNO_3 concentrations in the model's surface layer with the "constant V_{dHNO3}" scheme (V_{dHNO3} is 0.8 cm s^{-1} over sea/snow/ice and 2 cm s^{-1} over land, as used by *Dentener and Crutzen* [1993]) and the new scheme. Continental HNO_3 concentrations calculated with the new scheme are significantly smaller while marine concentrations calculated with the new scheme are larger, with relative differences over land up to 45% and in the subsidence areas over sea up to 25%. At higher latitudes, over snow and ice, there is an increase in HNO_3 concentrations due to a relatively small V_{dHNO3} resulting from the large surface resistance. However, HNO_3 concentrations in these areas are relatively small and the contribution of the dry deposition to the global HNO_3 budget is negligible. Changes in HNO_3 dry deposition are counteracted by changes in wet deposition through concentration changes. In general, we calculate only small changes in the O_3 surface layer concentrations as a result of changes in HNO_3, comparing our dynamic and the "constant V_{dHNO3}" scheme.

3) Nitrogen Oxide, Nitrogen Dioxide

The monthly average global $V_{dNO/NO2}$ distributions have similar global distribution patterns as V_{dO3}. The values of V_{dNO2} and V_{dNO} are about 2/3 and 1/10 those of O_3 above vegetation and bare soil, respectively. Over sea, $V_{dNO/NO2}$ is about 10^5 cm s^{-1} and does not show any significant diurnal or seasonal cycles. There are no significant relative differences in NO and NO_2 surface layer concentrations between our scheme and the "constant V_{dNOx}" scheme (V_{dNO} is 0 cm s^{-1} over sea/snow/ice and 0.04 cm s^{-1} over land, and V_{dNO2} is 0.1 cm s^{-1} over sea/snow/ice and 0.25 cm s^{-1} over land [*Dentener and Crutzen*, 1993]) although NO_x deposition fluxes change markedly (see section 2.4.3). These changes are balanced, however, by feedbacks in the chemistry.

2.4.3 Global changes due to the new scheme

Table 2.3 shows the relative differences and the absolute levels of O_3, HNO_3 and NO_x deposition in four approximately equal areas of the globe (0°-30° and 30°-90° N and S), comparing the new scheme and the "constant V_{dX}" scheme for January and July (for the calculation of relative differences, see section 2.4.2). Relative differences of dry deposition in the NH are up to 9% for O_3, 19% for HNO_3 and 29 % for NO_x. The dry deposition of O_3 and NO_x shows a distinct difference between January and July due to a dependency on surface characteristics and vegetation activity. The relative differences integrated over the entire

Table 2.3: Relative differences (%) and absolute levels of O_3, HNO_3 and NO_x dry deposition in four approximately equal areas of the globe, comparing the "constant V_{dX}" scheme and the new dry deposition scheme.

	O_3 (Tg O_3)		**HNO_3 (Tg N)**		**NO_3 (Tg N)**	
	January	**July**	**January**	**July**	**January**	**July**
90°-30° N	0 (6.7)	7 (19.4))	-7 (0.17)	3 (0.74)	-29 (0.46)	15 (0.36)
30°-0° N	-10 (15.1)	-7 (15.8)	0 (0.39)	-2 (0.53)	-8 (0.21)	-2 (0.13)
0°-30° S	3 (8.9)	-10 (10.7)	3 (0.25)	2 (0.37)	3 (0.08)	-10 (0.17)
30°-90° S	-6 (1.3)	-5 (3.5)	0 (0.01)	13 (0.02)	0 (0.0)	-17 (0.01)
Global	-4 (31.9)	-2 (49.5)	-3 (0.82)	1 (1.65)	-20 (0.75)	4 (0.67)

Positive values indicate and increase in the deposition calculated by the new scheme compared to the V_{dX} scheme. The absolute levels are indicated between parentheses.

globe are small for O_3 and HNO_3. Application of our new deposition scheme for NO_x is most significant for the NH, where dry deposition decreases in winter and increases in summer. Although the differences in trace gas deposition and surface layer concentrations on a global scale may not seem dramatic, regional differences can be significant. Moreover, the new scheme contributes to internal consistency of the model, in particular with respect to diurnal and seasonal cycles in the chemistry, turbulent exchange processes and surface characteristics that control dry deposition.

2.5 Discussion

The new model routine presented improves the calculation of deposition velocities at different locations with various coverages. However, there are still shortcomings, which need to be improved in future versions. Some uncertainties involving the calculation of R_{aX}, and R_{surf} are discussed next.

1) Uncertainties in R_{aX}

One possible error in R_{aX} is introduced by the violation of the constant flux layer approach for reactive trace gases. Chemical transformations can modify the local turbulent transfer rates if the time scale for chemical reactions is much smaller than that of turbulent diffusion.

Photochemical reactions between NO/NO_2 and O_3 can be quite rapid, with time scales comparable to those of turbulent transfer at a height of 1 m above the surface. For example, in regions with strong NO emissions, titration of O_3 can be significant. Above ≈ 1 m, the time scale of turbulent transfer increases with height, so that chemical reactions can become increasingly important in the surface layer [*Gao et al.*, 1991]. The aerodynamic resistance, calculated at the model's reference height of 30 m through equation 2.4, might therefore not be representative for the turbulent transfer of these trace gases from this reference height to the surface. If the aerodynamic resistance significantly contributes to the total resistance, ignoring the effects of chemical reactions on deposition velocities of NO and NO_2 may cause errors. However, under most conditions the effects of rapid chemical reactions on the O_3 deposition velocities are expected to be small [*Gao et al.*, 1991]. Violation of the constant flux approach can become significant in regions with relatively small surface roughness, e.g., water, snow, ice, bare soil and vegetated surfaces with low canopies. However, these regions mostly do not have strong NO emissions. Future studies should focus on the relevance and a possible solution of this problem since chemistry and transport calculations are not treated simultaneously in the model.

A second source of errors in calculating R_{aX} is the use of ECHAM's surface roughness for momentum (z_{0m}) as a substitute for that of trace gases. In the current version of the model, z_{0m} also accounts for the large scale orography, in addition to the representation of local surface roughness. This results in extremely large z_{0m} values for some locations (20 m). In this work, a correction for differences between z_{0m} and z_{oX} has been applied by defining a QBR. However, a more representative ratio of z_{om} and z_{0X} may be used in the calculation of the QBR (see equation 2.5), or the definition of a representative local surface roughness to compensate for overestimation of R_{aX} over regions with a large z_{0m}. Changing the surface roughness from its original value of 0.2 m (surface roughness for north-western Europe), to 5 m resulted in average relative difference in V_{dO3} of 11 % with maximum relative differences of about 40 %. In ECHAM, areas in the western part of South-America, Central-America and the Himalaya, have large surface roughnesses of 5 - 15 m, causing very large deposition velocities, especially for HNO_3. In southern South-America the scheme computes relatively large depositions velocities, even though the surface resistance is relatively large, which can be attributed to a large surface roughness and a small R_{aX}. Hence, in future versions of the scheme, the model surface roughness description must be improved for dry deposition calculations.

A possible bias in the model, related to the definition of the surface roughness, is the use of ECHAM's reference height of the lowest layer (≈ 35 m) as reference height for the dry deposition velocity. For small surface roughness and stable conditions the reference height might be higher than the constant flux layer while for very large surface roughnesses, the reference height might be located within the roughness layer; in both cases this results in a violation of the constant flux approach. However, we think that based on the relatively small area with large surface roughness (> 2 m), the small contribution of the deposition during stable events in the total deposition, and a height of the constant flux layer of about 50 m during daytime, using ECHAM's reference height is a good compromise between maintaining consistency in the model and minimizing possible errors.

An additional source of uncertainty is the neglect of a representative local displacement height (see equation 2.4) in our model which would be more appropriate to use for trace gas exchange. Information concerning the canopy structure is restricted to the LAI and the vegetation ratio. The canopy height of each vegetation class, which could be used to estimate

a local displacement height d, is not defined in the model. Sensitivity analysis indicates that V_{dHNO3}, which is largely controlled by R_{aX}, increases about 15% for an (extreme) increase in d of 15 m. The relative errors in the O_3 and NO/NO_2 deposition velocities are small (~ 2%).

2) Uncertainties in R_{surf}

As a consequence of the coarse grid resolution of the model, there are large uncertainties in factors which control the surface resistance. One aspect is the small selection of different vegetation classes. It is shown in the results, based on the comparison of calculated and observed O_3 deposition velocities, that a more sophisticated distinction should be made between different vegetation classes, e.g., tropical forest and evergreen trees. The canopy structure is crudely defined in the ECHAM model, for example the LAI and canopy height for different vegetation classes are not distinguished. The seasonal cycle in the vegetation fraction is only coarsely represented (only winter and summer values), while the LAI is assumed to be constant throughout the year for all vegetation classes. The constant LAI of 4 is used for upscaling the leaf resistance to a foliage resistance in this version of the dry deposition model for internal model consistency. However, due to shade effects and the extinction of turbulence within a canopy, linear scaling with LAI is inaccurate for LAI larger than 2 - 3. Furthermore, the LAI is used to determine the bulk canopy resistance (equation 2.7), resulting in a non-variable contribution of the soil resistance to the bulk resistance for all vegetation classes. Sensitivity analysis, using an LAI of 1 instead of 4, showed a relative difference in the V_{dO3} of 10 - 20 %. Improvement of the LAI representation, e.g., adapting seasonally representative LAI values for a more appropriate selection of different vegetation classes, will be involved in the future. An advancement planned in the representation of the canopy structure, expressed by the LAI, a local displacement height and local surface roughness, will be the use of the Olson vegetation data set [*Olson et al.*, 1983] in which the distribution of 46 global ecosystems and their characteristics are defined.

Further, the compensation point in the NO_2 uptake process by vegetation may be improved in future versions of our scheme. *Johansson* [1987] observed NO_2 emissions from Scots Pine in enclosure experiments at concentrations below the compensation point of 1-3 ppb. In the model, coniferous forests cover large areas of Alaska, Canada, northern Europe and northern Russia, while calculated NO_2 concentrations in the surface layer during July are less than 1 ppb over these areas. If the compensation point as observed by *Johansson* [1987] and *Thoene et al.* [1991] is representative for coniferous forests, more NO_x will remain in the atmosphere over these areas since dry deposition may be negligible whereas emissions of NO are conceivable.

The effect of foliage wetness on the deposition process has been investigated in several recent dry deposition studies [*Baldocchi*, 1993; *Chameides*, 1987; *Fuentes et al.*, 1992; *Wesely*, 1989]. For example, deposition of HNO_3 to a wetted foliage is entirely determined by R_{aX} [*Chameides*, 1987]. Foliage wetness might significantly alter the surface resistances of the less soluble trace gases NO_x and O_3. An enhanced O_3 deposition due to foliage wetness has been measured above a deciduous forest by *Fuentes et al.* [1992]. Their observations indicate that mechanisms, other than stomatal uptake contribute to the O_3 deposition when the foliage is wet. Various assumptions have been made in deposition models regarding the effect of foliage wetness on O_3 uptake. Early models assumed a decrease of the uptake of O_3 under wet conditions. More recent models make a distinction between foliage wetness caused by rain and by dew to account for their different chemical compositions [*Wesely*, 1989]. In our scheme, the effect of foliage wetness on dry deposition due to rain or dew has not be

treated separately since foliage wetness in the ECHAM model (water in skin reservoir) is the net result of both processes. In future, a parameterization by *Chameides* [1987] may be incorporated, especially when the dry deposition scheme is extended to soluble trace gases such as SO_2.

The soil resistance for ozone of 400 s m^{-1} adopted in our scheme, may be relatively large. However, evaluation of the O_3 deposition velocities over vegetated surfaces indicates reasonable agreement between observed and calculated O_3 deposition velocities. Decreasing the soil resistance to about 100 s m^{-1}, a value often used in other schemes, would result in a too large V_{dO3} in absolute terms and in its amplitude in the diurnal cycle. The average V_{dO3} over sand is about 0.3 cm s^{-1} [*Sehmel*, 1980], while the calculated V_{dO3} in the desert areas of North-Africa and the Middle-East ranges from about 0.25 cm s^{-1} up to 0.5 cm s^{-1}, which justifies the choice of r_{soil} = 400 s m^{-1} for ozone. The NO_x soil resistances adopted are debatable since these are based on observed exchange rates of NO_x which may represent the net effect of NO_x uptake and NO emission. NO deposition to soils is ignored and a soil resistance of 600 s m^{-1} has been adopted for NO_2, yielding a deposition velocity of 2/3 the O_3 deposition velocity over vegetation. Considering the uncertainties, the calculated NO_x deposition velocities over surfaces with significant soil uptake should be interpreted with care. It is important to improve the parameterization of the soil uptake process in future because the soil resistance basically determines the dry deposition during nighttime due to the large foliage resistance. Furthermore, introduction of an LAI seasonal cycle will result in an increased contribution of r_{soil} to the surface resistance during winter and for vegetation classes with small LAI values throughout the year. As for the canopy representation, soil data bases will be used to distinguish different soil types and this information will be combined with ECHAM parameters, e.g., soil wetness, to calculate more representative soil resistances for different locations in future versions of the model.

The calculated HNO_3 snow/ice surfaces resistances should be evaluated using additional observations. The O_3 and NO_x deposition are relatively small because of the large water and snow/ice resistances. An exact definition of the NO_x water and snow/ice surface resistance is not required since the deposition process to water and snow/ice surfaces remains very slow compared to the gas phase reactions [*Lee and Schwartz*, 1981]. However, even with relatively low V_{dO3} values over these surfaces, the contribution of O_3 deposition in the overall budget is still significant due to their large areal extent and relatively slow gas phase reactions. For a deposition velocity of about 0.05 cm s^{-1} and an average height of the model's lowest layer of 60 m, the time constant of dry deposition process is 1-2 days, while the average lifetime of ozone in lower troposphere is about 10 days. Thus, deposition to water/snow/ice is very significant for the ozone budget of the lower troposphere. This emphasizes the need for a more sophisticated definition of the dry deposition process to these surfaces in future.

2.6 Conclusions

Even though considerable uncertainties remain, the dry deposition scheme calculates realistic deposition velocities of O_3, HNO_3 and NO_x over most locations for different meteorological conditions, consistent with diurnal and seasonal cycles in both the chemistry and the planetary boundary layer processes and surface characteristics that control dry deposition. This not only improves the overall model performance but also the possibility to compare the

model output with experimental results since most measurements are performed at the surface. In general, we calculate distinct diurnal and seasonal cycles with relatively large deposition velocities during daytime and summer, and lower deposition velocities during nighttime and winter. Incorporation of the scheme in the chemistry-general circulation model ECHAM yielded significant changes in the deposition fluxes and concentrations in the lower troposphere compared to a scheme using constant deposition velocities. For example, the new scheme calculates up to about 25 % lower O_3 concentrations in the surface layer in the summertime continental NH. Dry deposition of HNO_3 is to a large extent controlled by the aerodynamic resistance R_a, while that of O_3 and NO_x is determined mostly by R_{surf}, i.e., r_{soil} and r_{veg}. However, R_a is also strongly influenced by surface characteristics, which emphasizes the great importance of realistic representations of these parameters in future versions of the dry deposition scheme.

Chapter 3

A dry deposition parameterization for sulfur oxides in a chemistry and general circulation model[1]

The dry deposition scheme presented in Chapter 2, is extended to sulfur dioxide (SO_2) and sulfate (SO_4^{2-}). In order to reduce some of the shortcomings of the previous model version, a local surface roughness and a more realistic Leaf Area Index (LAI), derived from a high-resolution ecosystem database, are introduced. The SO_2 deposition velocity over vegetated surfaces is calculated as a function of the vegetation activity, the canopy wetness, turbulent transport through the canopy to the soil and uptake by the soil. The soil resistance is explicitly calculated from the relative humidity and the soil pH, derived from a high-resolution global soil pH database. The snow/ice resistance of SO_2 is a function of temperature. The SO_2 deposition velocity over the oceans is controlled by turbulence. The sulfate deposition velocity is calculated considering diffusion, impaction and sedimentation. Over sea surfaces the effect of bubble bursting, causing the breakdown of the quasi-laminar boundary layer, scavenging of the sulfate aerosol by sea spray and aerosol growth due to high local relative humidities are considered. An integrated sulfate deposition velocity is calculated, applying a unimodal mass size distribution over land and a bimodal mass size distribution over sea. The calculated sulfate deposition velocity is about an order of magnitude larger compared to that based on a monodisperse aerosol, which is often applied in chemistry-transport models. Incorporation of the new dry deposition scheme in the ECHAM model yields significant relative differences (up to ~ 50 %) in mass flux densities and surface layer concentrations compared to those calculated with a simple, constant dry deposition scheme.

3.1 Introduction

Atmospheric sulfur has been studied extensively in relation to deleterious health effects and decline of ecosystems due to antropogenic emissions. The initial interest focussed on the impact of sulfur oxides on plant nutrition [*Chamberlain*, 1980]. In the 1970s, the acidification

[1] Published in the *Journal of Geophysical Research*, **103**, 5679-5694, 1998, with J. Lelieveld and G.-J. Roelofs as co-authors.

of ecosystems through wet and dry deposition of SO_2 and sulfate has been widely investigated. In the 1980s the interest decreased mainly due to successful abatement strategies of sulfur emissions in western Europe, Canada and the United States [*Erisman and Baldocchi*, 1994]. However, in recent years there has been a revival of the interest for atmospheric sulfur due to the strongly increasing emissions in developing countries, particular in Asia [*Arndt et al*, 1997; IPCC, 1995] and the role of sulfate aerosols in climate change [*Charlson et al*., 1992; IPCC, 1995].

In this study we focus on the representation of the dry deposition process of sulfur oxides in the chemistry-general circulation model (GCM) ECHAM. The significance of a realistic sulfur dry deposition representation in global models is illustrated by results of previous studies of the global tropospheric sulfur budget. Roughly 50 % of the emitted gaseous sulfur (about 100 Tg S yr^{-1}), mostly in the form of sulfur dioxide (SO_2) and dimethyl sulfide (DMS), is oxidized to sulfate, while about 10 % is removed by wet deposition. The remaining 40 % is removed through dry deposition. The sulfate formed is mainly removed through wet deposition (about 80 %) while the remaining 20 % is removed through dry deposition [*Langner and Rodhe*, 1991; *Chin et al*., 1996; *Feichter et al*, 1996; *Kasibhatla et al*., 1997]. The importance of dry deposition, in particular SO_2, underscores the need for an accurate description of this process. *Langner and Rodhe* [1991] and *Feichter et al*. [1996] used constant SO_2 and SO_4^{2-} deposition velocities over the ocean, land, and snow/ice. *Chin et al*. [1996] and *Kasibhatla et al*. [1997] calculate the SO_2 deposition velocity using a parameterization of the aerodynamic and surface resistances following *Wesely* [1989]. *Kasibhatla et al*. [1997] prescribe a sulfate deposition velocity of 0.2 cm s^{-1} whereas Chin et al. [1996] explicitly calculate a SO_4^{2-} surface resistance following [*Wesely et al*., 1985; *Hicks et al*., 1989b]. However, the validity of using the *Wesely* [1989] parameterization in a global scale model may be questioned since it was originally developed for regional air quality models. The surface resistances refer to 11 land use types and 5 seasonal categories representative for the North American continent, not for surface covers such as tropical forests and savannas [*Wesely*, 1989]. Moreover, the SO_4^{2-} surface resistance parameterization by *Wesely* [1985] and *Hicks* [1989b] is based on observations of sulfate deposition over vegetation, not for oceans, bare soil and snow and ice.

In Chapter 2 we presented the incorporation of a dry deposition scheme into the chemistry-GCM ECHAM [*Ganzeveld and Lelieveld*, 1995]. The scheme calculates deposition velocities according to the 'big-leaf' concept [e.g., *Hicks et al*., 1987] from the turbulent transfer and vegetation activity computed by the GCM, supplemented with representative uptake rates for soil, water and snow/ice on a global scale. The further development of this scheme, as presented here, aims to improve the description of trace gas exchanges between the atmosphere and surface, consistent with temporal and spatial dependencies of the model physics and chemistry. We will show that the new scheme yields significant relative changes in mass flux densities and concentrations in the atmospheric boundary layer compared to the simpler approaches used in most previous studies.

3.2 ECHAM model and chemistry scheme

In this study we used the T30 horizontal resolution of ECHAM4 corresponding with a grid size of about 3.75° and a timestep of 30 minutes. For more details concerning the description of physical and dynamical processes in ECHAM, we refer to Chapter 2. The main differences between ECHAM4 and the version used in the previous study (ECHAM3), relevant for this

study, are the representation of the vegetation cover and vertical transport. In ECHAM4 the vegetation surface roughness length z_{0v}, leaf area index LAI, vegetation ratio and forest ratio are assigned to each grid cell based on representation of the major ecosystem complexes by - Olson et al. [1983] [*Claussen et al.*, 1994]. This classification discerns 43 ecosystems and their characteristics on a 0.5° × 0.5° resolution [*Olson et. al.*, 1983]. Vertical transport is calculated based on the turbulent kinetic energy closure accounting for transport of generated turbulence through the action of turbulent diffusion, in contrast to the conventional eddy diffusivity model used in ECHAM3 [*Brinkop and Roeckner*, 1993]. ECHAM4 is coupled to a chemistry scheme developed by *Roelofs and Lelieveld* [1995, 1997]. The ECHAM3 chemistry scheme, presented in Chapter 2, has been extended with a sulfur cycle model [*Feichter et al.*, 1996; *Lelieveld et al.*, 1997]. Oxidation of SO_2 and DMS by OH and NO_3 and in-cloud sulfate formation are included explicitly. Emissions of DMS, SO_2 [*Spiro et al.*, 1992], NO_x, CO and CH_4 are considered, and wet deposition calculations use the ECHAM4 parameterization schemes for large scale and convective clouds [*Roelofs and Lelieveld*, 1997]. The latter scheme distinguishes between in-cloud and below-cloud scavenging of aerosol particles and soluble gases, and release of these species to the atmosphere by cloud and precipitation evaporation.

3.3 Surface roughness and leaf area index

In Chapter 2 is has been shown that the dry deposition flux of a trace gas, F_c (molecules m^{-2} s^{-1}), is calculated from its concentration (molecules m^{-3}) at a reference height z, c_z, and the dry deposition velocity (m s^{-1}) at height z, V_d. The dry deposition velocity is related to specific characteristics of surfaces and the atmospheric conditions over these surfaces and calculated from the aerodynamic, quasi-laminar and surface resistance. For a more detailed description of the calculation of the resistances we refer to Chapter 2. Concerning R_a, the major difference with our earlier work is the use of a local (or vegetation) surface roughness for momentum (z_{0mloc}). In the previous model version we used the ECHAM large scale surface roughness [*DKRZ*, 1992]. The problem with this was that extremely high HNO_3 deposition velocities were calculated over mountainous regions due to a small R_a, since the ECHAM z_{0m} can be large as 20 m in these regions. A disadvantage of the introduction of a local surface roughness in the calculation of R_a is loss of consistency with the GCM, since the friction velocity and the stability correction term are still calculated from the large scale surface roughness. In order to remove this inconsistency with the ECHAM friction velocity, it is assumed that the surface drag in each grid square consists of drag generated by the orography and drag by local roughness elements, according to the drag partition theory of *Schlichting* (see *Claussen* [1995]). A local drag coefficient from the reference height z, the local surface roughness and a stability correction term is calculated for the fraction covered with vegetation, bare soil and snow of each grid square. The local drag coefficient is used to calculate a local friction velocity where we assume that the wind speed at the reference height (≈30 m) is unaffected by local shear stress, i.e. the reference height is positioned above the blending height l_b. Also the ECHAM stability is not entirely consistent since the stability correction term is a function of the ECHAM Richardson number which is calculated from the wind and temperature gradient for the large scale surface roughness. However, this inconsistency has been ignored since the sensible heat flux, which reflects the temperature gradient, is mainly determined by surface cover and not by surface roughness [*Claussen*,

1995]. Hence, the Richardson number and the stability correction term will not change significantly due to a change in surface roughness assuming that the wind speed at reference height is unaffected by the local surface roughness.

The local surface roughness for vegetation and bare soil and snow is derived from assigned values of z_{0m} for 13 surface types [*Henderson-Sellers et al.*, 1986] based on the update of the original Davenport classification of roughness by *Wieringa* [1991] [*Claussen et al.*, 1994]. The Olson ecosystem database [*Olson et. al.*, 1983] is reduced to these 13 surface types to estimate the local surface roughness of the ecosystems. The local surface roughness for each ECHAM grid cell is calculated from the 0.5° × 0.5° local surface roughness by averaging the ecosystem neutral drag coefficients [*Claussen et al.*, 1994].

A major difference with the model version presented in Chapter 2 concerning the calculation of the canopy resistance from the leaf resistance and the leaf area index (LAI), is the use of a more realistic LAI. In ECHAM3 the state of the canopy is not expressed by a variable LAI but it has a constant value of 4 for all vegetation types, independent of time and location; the model merely resolved a seasonally dependent vegetation area fraction. Comparison of the calculated monthly average diurnal cycle of the deposition velocity of O_3 with observations indicated that this approach yields realistic O_3 dry deposition velocities of over most locations for different seasons [*Ganzeveld and Lelieveld*, 1995]. However, for some locations, e.g. tropical forests, the poor representation of the local amount of biomass, expressed by the LAI, caused discrepancies between observed and calculated O_3 deposition velocities. Additional explanations for such differences can be related to the parameterization of the stomatal uptake [*Sellers*, 1986], which did not accurately simulate the very efficient stomatal uptake by forests, and misrepresentation of the vegetation fraction at individual grid cells. In ECHAM4, a more realistic LAI is derived for each grid cell from the arithmic mean of a summer and winter LAI for each *Olson et al.* [1983] ecosystem category. These winter and summer LAI values are determined by allocating *Olson et al.* [1983] ecosystem categories to *Lieth and Esser's* vegetation types and their assigned LAI [*Claussen et al.*, 1994]. In the near future, an annual cycle in the LAI, based on a bio-geochemical model will be incorporated in ECHAM4 [*M. Claussen*, personal communication]. However, for this study we have tentatively incorporated a parameterization of the annual cycle in the LAI using a clipped sine function to account for differences between the winter and summer LAI. The length of the growing season is a function of latitude, being 3 months at latitudes higher than 60° N and S, increasing to 6 months for a latitude of about 45° N and S, and up to 12 months for latitudes below 30° N and S. Figure 3.1a and b show the simulated January and July LAI for a 0.5° × 0.5° horizontal grid resolution. A maximum LAI of about 10 occurs in the tropical forests of South America, Central Africa and south-east Asia throughout the year whereas there is a distinct annual cycle in the LAI of non-coniferous forests at higher latitudes, with maximum differences between the January and July LAI of about 6.

Linear upscaling of the leaf resistance to the canopy scale using the LAI, breaks down for an LAI larger than about 3 to 4, since an LAI increase will not yield a proportional increase in uptake due to the extinction of radiation and turbulence within the canopy. However, the canopy resistance in ECHAM4 is calculated using a relationship that accounts for the extinction of the Photosynthetically Active Radiation (PAR) within the canopy [*Sellers*, 1985, 1986]. The impact of turbulence extinction has been ignored since the quasi-laminar boundary layer resistance of the leaves is usually smaller than the stomatal resistance [*Sellers*, 1985]. Improvement of the canopy description has consequences for soil uptake processes since the LAI determines the partitioning of deposition between the soil and vegetation. In sparsely vegetated locations the dry deposition velocity is not only controlled

by the vegetation activity but also by transport through the canopy to the underlying soil and the destruction rate at the soil surface. For trace gases which are removed very efficiently by the soil, e.g. SO_2 to a wet soil with relative high pH (see next section), turbulent transfer to

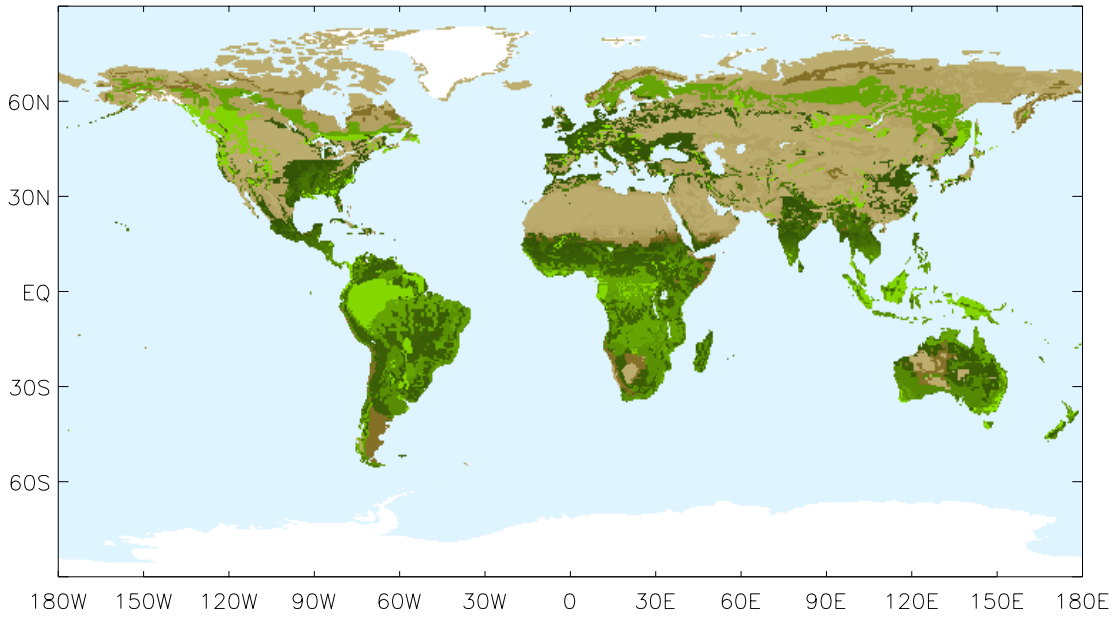

Figure 3.1a: January LAI on a 0.5° × 0.5° horizontal grid resolution, derived from the Olson ecosystem database (*Olson et. al.*, 1983).

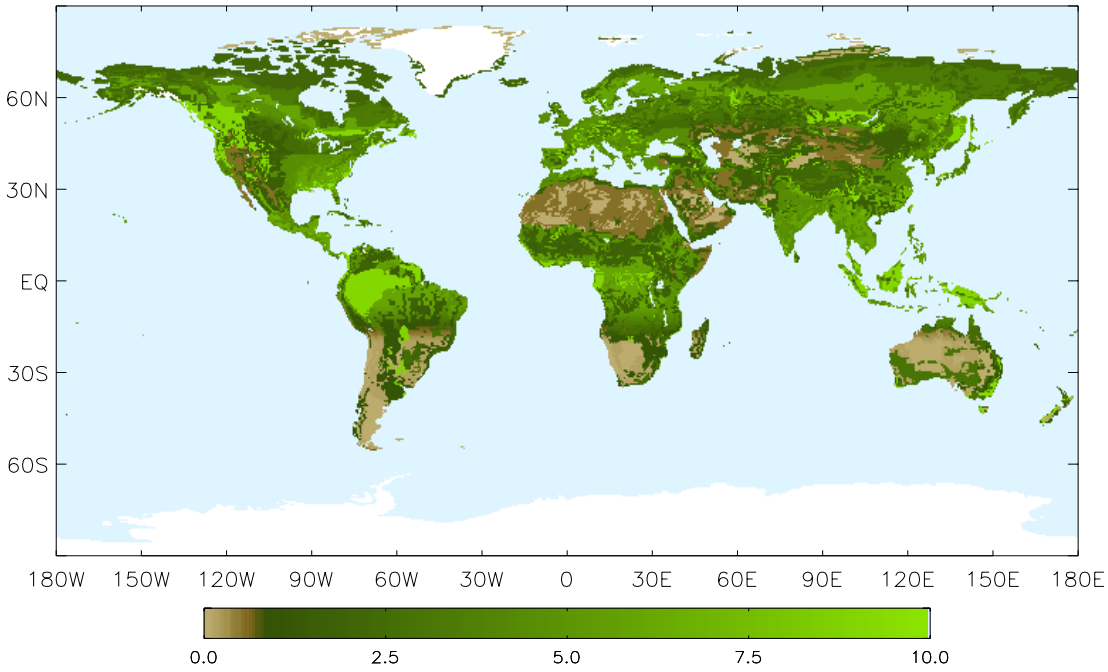

Figure 3.1b: July LAI.

the soil surface can become the controlling factor. To account for this process we have incorporated a parameterization of the aerodynamic resistance within the canopy as a function of canopy height, LAI, the friction velocity u_* and an empirical coeficient [*Erisman*

and Van Pul, 1994]. The results of this parameterization are in reasonable agreement with those of *Wesely* [1989] [*Erisman and Van Pul*, 1994]. The canopy height is not defined in ECHAM4. However, the grid average canopy height can be estimated from the ECHAM4 forest ratio c_F, which is specified from the forest description by Olson et al. [1983] [*Claussen et. al.*, 1994]. It is required that $c_F \leq$ vegetation ratio (c_v), and corrections are applied for different ecosystem categories to account for the canopy spacing of different forest types. For example, for broadleaved evergreen c_F is 0.95, whereas for savanna c_F is 0.4 [*Claussen et al.*, 1994]. For consistency with ECHAM4 we have used this forest ratio to determine an average canopy height for each grid cell by multiplying c_F with an assumed forest canopy height of 20 m.

3.4 Sulfur dioxide surface resistances

Table 3.1 lists the values adopted for the cuticle resistance r_{cut}, the mesophyll resistance r_{mes}, the water resistance r_{wat} and the parameters used for the calculation of the snow/ice resistance $r_{snow/ice}$, and the soil resistance r_{soil}, for SO_2. The cuticle resistance r_{cut} of SO_2 by far exceeds the canopy stomatal resistance [*Baldocchi*, 1993; and references therein], expressed by a large r_{cut}, whereas the mesophyll resistance r_{mes} is negligibly low. A distinction has been made between the water resistance r_{wat} and the wet skin resistance of SO_2, r_{ws}, since SO_2 deposition to wetted surfaces over land is controlled by the aerodynamic and the surface resistance whereas the SO_2 deposition to the oceans is solely controlled by turbulent transfer and diffusion. The surface resistance of oceans is very small due to the high SO_2 solubility associated with an ocean water pH of about 8 [*Spedding*, 1972]. Recent regional scale deposition models distinguish between foliage wetness caused by rain and by dew to account for their different chemical compositions [*Wesely*, 1989]. In our scheme, the effect of foliage wetness on SO_2 dry deposition due to rain or dew has not been treated separately since foliage wetness in ECHAM4 is the net result of both processes. The model results indicate

Table 3.1: Soil, cuticle, mesophyll, water/wet skin, and snow/ice resistance (s m^{-1}) for SO_2.

r_{soil}	r_{cut}	r_{mes}	$r_{wat/ws}$	$r_{snow/ice}$
f(soil pH, rh(2m))	105	0	0/100	max(10,f(T(2m)))

that the monthly average wet skin fraction exceeds 0.25 only for a small area, suggesting that SO_2 uptake through this mechanism does not contribute significantly to dry deposition on a global scale. However, local and transient uptake processes might be affected by foliage wetness. Also the SO_2 snow/ice resistance depends on the chemical composition of the snow/ice surface (i.e. oxidant concentrations and ionic strengths) and the physical characteristics (liquid-like characteristics and surface area) of the surface layer [*Conklin et. al.*, 1993]. A general aspect of studies that consider uptake of SO_2 and the chemical and physical characteristics of snow/ice is the strong dependence of the snow/ice SO_2 uptake on temperature [*Cadle et al.*, 1985; *Dasch and Cadle*, 1986; *Granat and Johansson*, 1983; *Sommerfeld and Lamb*, 1986; *Valdez*, 1987; *Clapsaddle and Lamb*, 1989; *Conklin et al.*, 1993], which manifests itself particularly in the temperature range –10° C to 0° C [*Mitra et al.*, 1990]. In our model the SO_2 snow/ice resistance is calculated from the ECHAM4 surface

temperature, applying a relationship derived from observations of SO_2 uptake by snow [*Dasch and Cadle*, 1986]. This yields a SO_2 snow/ice deposition velocity (for an assumed R_{aH} + R_b of 125 s m^{-1}) which increases exponentially from a minimum value of about 0.01 cm s^{-1} for a temperature of -20° C to a value of about 0.25 cm s^{-1} m for 0° C. SO_2 deposition velocities calculated with a physical-chemical model, which considers gaseous diffusion into the snow pack, air-water partitioning, and aqueous-phase reactions [*Bales et al.*, 1987], also shows an exponential increase with temperature from about 0.01 cm s^{-1} for –20° C, although the increase is slightly less (i.e., a V_{dSO2} of about 0.15 cm s^{-1} for 0° C). The soil resistance of SO_2 is a function of the soil pH and the relative humidity [*Baldocchi*, 1993; and references therein]. Biological activity does not greatly affect SO_2 uptake as indicated by a small decrease of uptake of SO_2 due to soil sterilization [*Murphy and Sigmon*, 1989]. A parameterization of the SO_2 soil resistance, being a function of soil pH and the ECHAM4 relative humidity at 2 m altitude, has been incorporated in the model. The soil pH is derived from a 0.5° × 0.5° global soil pH database, shown in Figure 3.2, which discerns 5 different soil pH classes averaging over the top 30 cm of the soil [*Batjes*, 1995]. The distribution of soil pH reflects the distribution of vegetation; the most acidic soils occur in densely vegetated regions whereas alkaline soils are found in sparsely or non-vegetated regions. For each model cell the fraction of the 5 soil pH classes is determined. The soil resistance is calculated from these fractions and the soil resistances for each class, based on observations of the SO_2 soil resistance for different soil pH and relative humidity by *Payrissat and Beilke* [1975]. A correction of the calculated soil resistance, derived from the observations by *Payrissat and Beilke* [1975], is applied for a calculated relative humidity below 60% at 2 m. Implementation of this parameterization yields deposition velocities as large as 0.8 cm s^{-1} in desert areas, e.g. the Sahara, due to a soil pH of 8. However, for very dry conditions and chemically inert sandy soils, SO_2 uptake is expected to be small. Observations of SO_2 uptake by grass and soil by *Milne et al.* [1979] showed that bare soil, which had thin covering of red quartz gravel, exhibited very little affinity for SO_2. Sensitivity study indicates that a relative humidity of 40% (2m) is a reasonable threshold for arid regions with sandy soils [*Olson et al.*, 1983]. Despite the lack of experimental support to apply this threshold for all soils, the r_{soil} of SO_2 for arid regions is calculated from the soil resistance for a relative humidity of 40%, assuming a linear increase with a decreasing relative humidity to a maximum value of r_{soil}, arbitrarily chosen to be 1000 s m^{-1}. The soil resistance is corrected for a surface temperature less than -2°C [*Wesely*, 1989; *Erisman and Wyers*, 1992].

3.5 Sulfate dry deposition

Dry deposition of sulfate over vegetation is a function of the canopy structure [*Bache*, 1979; *Slinn*, 1982; *Wesely*, 1983], since the deposition velocity is controlled by the turbulent transfer to and through the canopy to the different receptor surfaces, e.g., leafs, branches, tree trunks and the soil. However, we have incorporated the straightforward parameterization of sulfate deposition velocities from the stability and friction velocity by *Wesely* [1985] since the degree of detail of the canopy description required for the mechanistic approach by *Bache* [1979] and *Slinn* [1982] is beyond the capabilities of our GCM. For other surfaces the sulfate surface resistances are assumed to have a minimum value of 1 s m^{-1}, so that the sulfate deposition velocity is controlled by the aerodynamic transfer and diffusion, impaction and gravitational settling, dependent on the particle radius. Figure 3.3 shows the particle

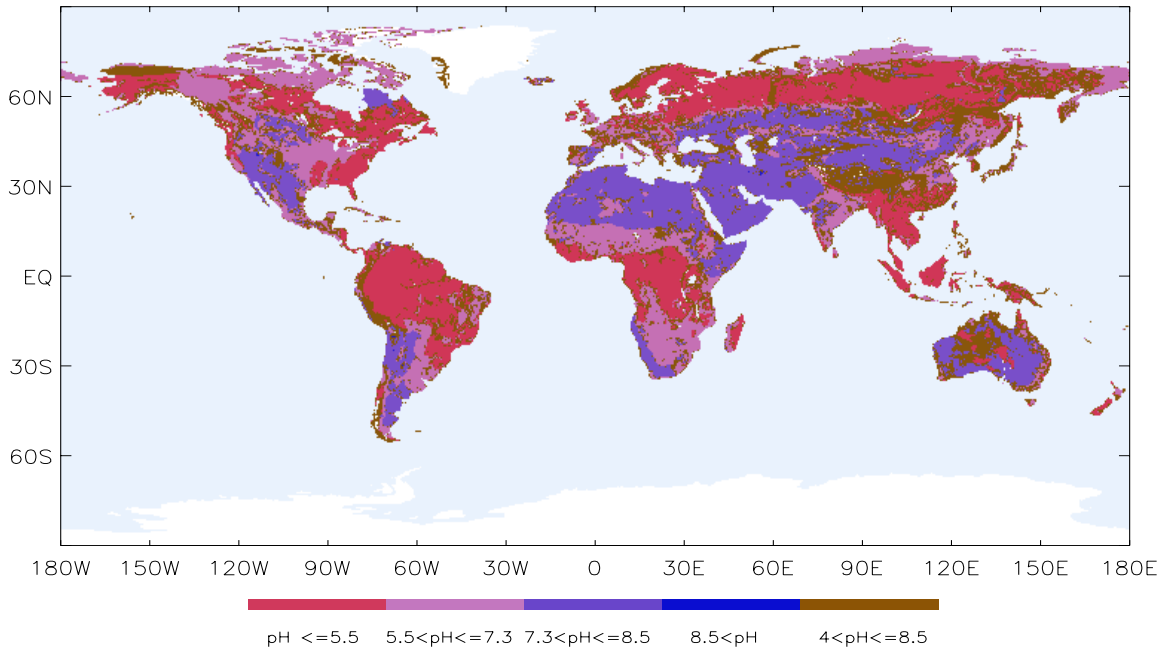

Figure 3.2: Global distribution of soil pH on a 0.5° × 0.5° horizontal grid resolution distinguishing five soil pH classes of the top 30 cm of the soil: pH ≤ 5.5, 5.5 < pH ≤ 7.3, 7.3 < pH ≤ 8.5, 8.5 < pH, 4 < pH ≤ 8.5, indicated by the litmus colors, except of the fifth undefined class [*Batjes*, 1995].

deposition velocity at a reference height of 30 m as a function of particle radius for a wind speed and friction velocity of 10 and 0.5 m s^{-1}, respectively. The deposition velocity is calculated using the parameterization by *Slinn* [1976] for particle dry deposition to smooth surfaces, which we applied to calculate V_{dSO4} over bare soil and snow/ice covered areas. Particles in the accumulation mode (0.1 μm < r < 1 μm) are removed with a relatively small deposition velocity of about 0.01 cm s^{-1} due to diffusion limitation, whereas deposition velocities of particles in the coarse particle range (r > 1 μm) are up to 10 cm s^{-1} due to gravitational settling. Therefore, it is necessary to calculate the deposition velocity from the sulfate mass size distribution and not from a mean mass radius. Over land, most of the sulfate is in the accumulation mode with a mean mass radius of 0.37 μm [*Whitby*, 1978]. Figure 3.3 also shows observed mass size distributions of sulfate associated with rural continental and marine aerosol (data by *Mehlmann* [1986], adopted from *Warneck* [1988]). Integration of the rural continental mass size distribution over the whole size range shows that about 85% of the sulfate mass is in the accumulation mode. This is close to the 95% calculated by Whitby [1978], based on an analysis of continental sulfate observations at different locations. The marine sulfate exhibits a bimodal size distribution with a significant fraction, about 35%, in the coarse particle range. The major source of sulfate in the coarse particle range is sea-salt [*Warneck*, 1988], whereas a relatively small fraction originates from the heterogeneous conversion of SO_2 to non-sea-salt (nss) sulfate. Observations in several clean and antropogenically influenced marine regions indicates that about 30 % of the nss-sulfate occurs in the coarse mode [*Andreae*, 1995]. About 75% of this nss-sulfate in sea-salt particles is found in the 1-5 μm range [*Sievering et al.*, 1992]. We have calculated the sulfate deposition velocity for a mean mass radius of 0.37 μm ($V_{dSO4}(0.37)$) and by integration of the mass size distribution ($V_{dSO4}(msd)$) of the rural continental and the marine aerosol, for different meteorological conditions, to study the sensitivity of V_{dSO4} of the assumed mass size distribution. We also calculated the marine $V_{dSO4}(msd)$ applying the rural continental mass

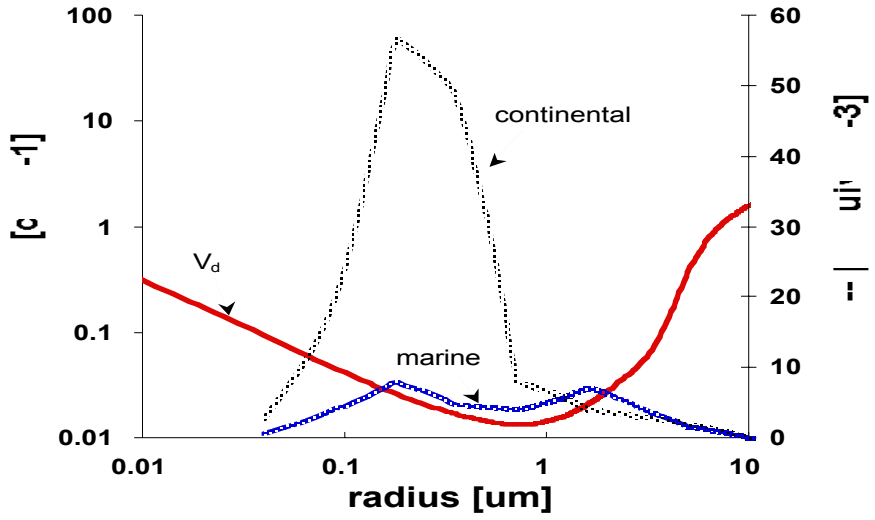

Figure 3.3: Particle dry deposition velocity (cm s^{-1}) as a function of particle radius (μm) for a wind speed of 10 m s^{-1} and a friction velocity of 0.5 m s^{-1}. Also shown are the observed mass size distributions of sulfate (nanoequivalents m^{-3}) associated with rural continental and marine aerosol (data by *Mehlmann* [1986], adopted from *Warneck* [1988]).

size distribution. Since we only consider nss-sulfate in this study, the actual integrated SO_4^{2-} deposition velocity depends on the fraction of nss-sulfate in the coarse particle mode as well as the accumulation mode. However, this information is not directly available from the model since the applied marine mass size distribution represents both the nss-sulfate and sea-salt

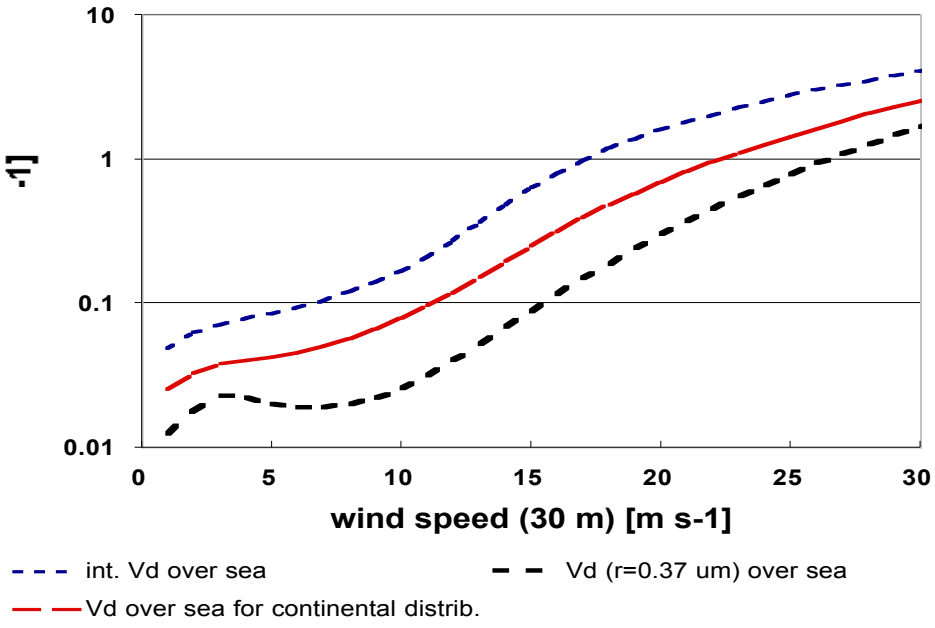

Figure 3.4: Particle dry deposition velocity (cm s^{-1}) over sea as a function of wind speed (m s^{-1}), calculated from a mean mass radius of 0.37 μm, and by integration over the mass size distribution of sulfate associated with rural continental and marine aerosol (see Figure 3.3).

sulfate. Therefore, the calculated V_{dSO4}(msd) for the rural continental and marine sulfate should be interpreted as the lower and upper limit, respectively, of the integrated SO_4^{2-} deposition velocity as a function of the fraction of nss-sulfate in the coarse particle mode.
The deposition velocity of marine sulfate is calculated in this study using a parameterization by *Hummelshøj et al.* [1992]. This is a modification of the parameterization for particle dry deposition to "smooth" natural waters by *Slinn and Slinn* [1980], which accounts for the effect of whitecaps on the dry deposition velocity through the destruction of the quasi-laminar layer and wash out by spray drops [*Hummelshøj et al.*, 1992]. This is an obvious and much discussed physical explanation of the possible enhancement of the particle dry deposition velocity compared to that derived by *Slinn and Slinn* [1980] but, unfortunately, experimental evidence to support this is lacking. The effect of particle growth for a large relative humidity has been accounted for assuming that the water vapor pressure in the quasi-laminar layer is at saturation level. This is expressed by a maximum relative humidity which is limited over salt water to about 98% as a consequence of *Raoult's* law [*Williams*, 1982]. The wet particle radius, which is calculated according to *Fitzgerald* [1975], is about twice the dry particle radius with a consequent increase of the dry deposition velocity by an order of magnitude. Figure 3.4 shows the integrated marine SO_4^{2-} deposition velocity for different mass size distributions and the marine SO_4^{2-} deposition velocity for a mean mass radius of 0.37 μm, calculated as a function of wind speed. The V_{dSO4}(0.37) over the ocean is about an order of magnitude smaller than the V_{dSO4}(msd) over the whole wind speed range. The calculated marine V_{dSO4}(msd) for the marine mass size distribution is a factor of 5 larger than the V_{dSO4}(msd) for the rural continental aerosol due to the larger dry deposition velocity of the sulfate mass in the coarse particle range. The V_{dSO4}(msd) for the rural continental mass size distribution, which is not shown here, is more than an order of magnitude larger compared to the V_{dSO4}(0.37). These results confirm the importance of calculating the SO_4^{2-} deposition velocity based on a mass size distribution rather than a mean mass radius, since the latter method significantly underestimates the dry removal. Moreover, the partitioning of the sulfate between the accumulation and coarse particle mode must be accounted for explicitly.

3.6 Results

First we present the effects of the model improvements from incorporating the local surface roughness and a more realistic LAI. We also show a comparison between simulated and observed diurnally and annually varying SO_2 and SO_4^{2-} deposition velocities. Further, we show the global distribution of V_{dSO2} and V_{dSO4} for the months January and July, for which strong differences in deposition velocities, associated with vegetation activity, chemistry and meteorology, are expected. The calculated SO_4^{2-} deposition velocities account for the rural continental and marine sulfate mass size distributions as presented in Figure 3.3.

3.6.1 Impact of introduction of local surface roughness and LAI

In Chapter 2 it has been shown that the first version of the dry deposition model, which used the ECHAM3 surface roughness and a constant LAI of 4, reproduces observed deposition velocities over several surfaces. However, some discrepancies remained which could partly be explained by the limited representation of the surface cover and roughness. Observed

diurnal ozone deposition velocities over tropical forests are about 2.5 cm s^{-1} [*Fan et. al.*, 1990], whereas the previous model version calculated a maximum V_{dO3} of 1.2 cm s^{-1}. However, the current model calculates a maximum January V_{dO3} over the tropical forests of South America of about 2.4 cm s^{-1}. This increase can largely be explained by the increase in LAI from 4 to 10. Our previous study indicated a large overestimation of the ozone deposition velocity during July in Alaska with a calculated maximum, average and minimum V_{dO3} of 1.0, 0.7 and 0.4 cm s^{-1}, respectively. The new model version calculates ozone deposition velocities which agree well with observations over tundra [*Jacob et. al.*, 1992; and *Ritter et. al.*, 1992]. Calculated maximum, average and minimum V_{dO3} are 0.45, 0.15 and 0.05 cm s^{-1}, respectively, compared to the observed maximum, average and minimum V_{dO3} of 0.35, 0.2 and 0.1 cm s^{-1}, respectively. The previous model version yielded HNO_3 deposition velocities in mountainous regions up to 10 cm s^{-1} due to the high ECHAM surface roughness in these regions (about 20 m). The introduction of the local surface roughness yields a January average V_{dHNO3} of about 1 cm s^{-1} compared to 5 cm s^{-1} in the previous model version. Despite the lack of observations to validate the model HNO_3 deposition velocities over these locations, we feel that the current model calculates more realistic HNO_3 deposition velocities.

3.6.2 Diurnal and annual cycles of $V_{dSO2/SO4}$: Comparison with observations

It should be emphasized that evaluation of the model by comparing with experimental results is difficult due to the large difference in spatial resolution of measured and model derived deposition velocities. The currently applied ECHAM model version (T30) has a spatial resolution of 3.75° × 3.75° (300 - 400 km at mid-latitudes), while measured deposition velocities are site specific, with typical spatial scales of several kilometers (assuming homogeneous terrain).

Therefore, evaluation of $V_{dSO2/SO}$mainly focuses on qualitative comparisons of diurnal and seasonal cycles, which are not very sensitive to the specific surface parameters but which are to a large extent controlled by turbulence and irradiance (e.g., through stomatal uptake). Table 3.2 shows the calculated monthly average diurnal dry deposition velocities, represented by the average, maximum and minimum $V_{dSO2/SO4}$ for several grid cells, and available observations for SO_2 and SO_4^{2-} under comparable conditions (season, surface and surface cover). Instead of presenting the average, maximum and minimum $V_{dSO2/SO4}$ per grid, we show those calculated over the (four) subgrid fractions, in line with the surface cover pertaining to the observations. For evaluation of deposition velocities over vegetation we have considered both the vegetation deposition velocity and the wet skin deposition velocity, despite that the wet skin fraction also represents the wet bare soil fraction. The grid cells are selected based on the distribution of major ecosystems according to *Olson et al.* [1983]. The SO_2 and SO_4^{2-} deposition velocities over the Atlantic Ocean, north of the UK, in February, have not been measured directly but are derived by *Prahm et al.* [1975], using an air trajectory model and aerosol measurements at the Faroer Islands and the British Isles. Comparison of the calculated and derived average V_{dSO2} shows that the model simulates the very efficient removal of SO_2 in winter over the North Atlantic Ocean with a maximum SO_2 deposition velocity of 3.4 cm s^{-1}. On the other hand, the sulfate deposition velocity seems to be overestimated in this location. Calculating the SO_4^{2-} deposition velocity from the rural continental mass size distribution yields a smaller average SO_4^{2-} deposition velocity of about

Table 3.2: Calculated and observed $V_{dSO2/SO4}$ [cm s-1] values, comparing similar surfaces conditions (values between parentheses denote maximum and minimum $V_{dSO2/SO4}$ and * denotes daytime values)

Deposition surface	**Calc. V_d, average (maximum, minimum)**	**Reference, obs. V_d, average (maximum, minimum)**
Water, north Atlantic Ocean	Feb., SO_2 1.6 (3.4, 0.1), SO_4^{2-} 1.2 (3.1, 0.1)	*Prahm et al.* [1976] SO_2 2.0 (±50%), SO_4^{2-} 0.4 (± 50%)
Snow, Greenland	June, SO_4^{2-} 0.04 (0.07, 0.02)	*Bergin et al.* [1995] 0.04 (0.06, 0.02)
Snow, exact location unknown	Feb., SO_4^{2-}, 0.07 (0.3, 0.04)	*Ibrahim et al.* [1983] 0.07
Snow, Arizona	Dec., Jan., Feb., Mar., SO_2 0.13	*Valdez et al.* [1987] 0.06
Snow, Canada	Mar., SO_2 0.18 (0.34,0)	*Barrie and Walmsley* [1978] 0.25 (± 0.20)
Snow, Norway	Feb., SO_2, 0.12 (0.26,0.08)	*Dovland and Eliassen* [1976] 0.1 (0.33, 0.04)
Crop, northwestern Europe	June, SO_2 0.6 (1.0, 0.1)	*Fowler and Unsworth* [1979] 0.6 (1.1, 0.2)
Crop, East USA	June, SO_4^{2-}, 0.2 (0.7,0)	*Wesely et al.* [1985] 0.2 (0.8, 0)
	Sept., SO_2, 0.7*(1.1*,0.3*), SO_4^{2-} , 0.3*(0.9*,0.05)	*Hicks et al.* [1986] SO_2, 0.6*(1.1*, 0.2*), SO_4^{2-}, 0.3* (0.7*, 0*)
Deciduous forest, South-eastern USA	May, SO_4^{2-}, 0.2 (0.8, 0)	*Hicks et al.* [1989b] 0.6 (1.0,0)
Deciduous forest, East Canada	Mar., Apr., SO_2 0.5 (0.8, 0.05)	*Padro et al.* [1992] 0.3 (0.8, 0)

0.7 cm s^{-1}, which is, however, still too large by almost a factor of 2. There is good agreement between the observed and calculated SO_4^{2-} deposition velocity over snow/ice. For the comparison with the observed ammonium sulfate deposition velocities over snow by *Ibrahim et al.* [1983], the average V_{dSO4} of the two experiments for the sub-micrometer particles with a diameter of 0.7 μm are presented. The average SO_4^{2-} dry deposition velocity over snow is significantly smaller than the constant value of 0.2 cm s^{-1} used previously by *Langner and Rodhe* [1991], *Feichter et al.* [1996] and *Kasibhatla et al.* [1997] over snow/ice covered surfaces. The SO_2 deposition velocity over snow/ice in Arizona is overestimated by about a factor two. This is likely due to differences in temperature, which largely controls the deposition velocity through the surface resistance, as a result of the difference between the local elevation of the measurement site and the mean surface altitude of the ECHAM model

grid cell, 2200 versus 700 m, respectively. There is generally good agreement between calculated and observed vegetation deposition velocities, except for the 35° N 85° W grid where the model underestimates the May average SO_4^{2-} deposition velocity. However, this underestimation can be explained by the difference between the typical surface roughness of deciduous forest and the derived local surface roughness in the model, about 1 m [*Dolman*, 1986] and 0.1 m, respectively. For the comparison between the observed and calculated SO_2 deposition velocities over deciduous forest in March and April, the grid square at 45°N and 90°W has been selected, since the LAI of the grid cell resembles that of the location of the observations. Figure 3.5a shows the simulated annual cycle of the monthly average SO_2 deposition velocity for 35°N, 85°W with an LAI and local surface roughness representative for deciduous trees. The annual cycle of V_{dSO2} has also been inferred by *Matt and Meyers* [1993], using the Dry Deposition Inferential Measurement (DDIM) technique. The inferred annual cycle of V_{dSO2} indicates a minimum value of about 0.2 cm s^{-1} during winter, increasing to a maximum value of 0.6 cm s^{-1} in May and then decreasing again in summer to a value of about 0.4 cm s^{-1} in August and September, and further decreasing in October to a value of 0.2 cm s^{-1} due to leaf fall. Our model reproduces this cycle reasonably well except during winter for which our model calculates a V_{dSO2} up to about 0.5 cm s^{-1} due to a smaller calculated SO_2 soil resistance relative to the constant value of 300 s m^{-1} in DDIM. Figure 3.5b shows the annual cycle of V_{dSO2} over Great Britain, 50°N 0°W, and the observed summer and winter mean SO_2 deposition velocity of 1.0 and 0.8 cm s^{-1}, respectively, over a site covered with rough pasture, short grass and ploughed soil [*Nicholson and Davies*, 1988]. The lack of a distinct annual cycle in the observations indicates that other processes besides stomatal uptake contribute to the SO_2 deposition process. For many observations, the fetch contained sparse vegetation or exposed

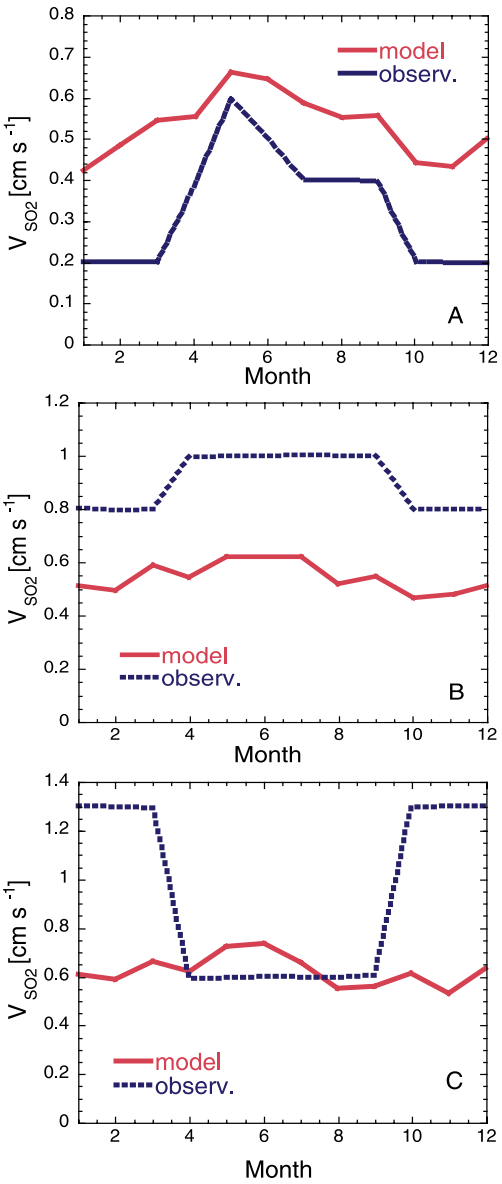

Figure 3.5a,b, c: Annual cycle of calculated monthly mean V_{dSO2} (cm s-1) for three grid cells (solid lines) and the estimated annual cycle from an inferential model (a) and observed annual cycles (b and c) over comparable surface cover (dashed-dotted lines): (a) deciduous forest in south-east United States, 35°N, 85°W, (b) grass/bare soil, England, 50°N, 0°, (c) coniferous forest, western Europe, 45°N, 0°.

soil and direct uptake by the soil with a pH of 8 could have been a major influence on V_{dSO2} [*Nicholson and Davies*, 1988]. Observations by *Davies and Mitchell* [1983] at the same site, two years earlier, yielded an annual mean SO_2 deposition velocity which is about 0.2 cm s^{-1} smaller compared to the annual mean V_{dSO2} of 0.9 cm s^{-1} by *Nicholson and Davies* [1988]. This was explained by the differences in the density of the surface cover [*Nicholson and Davies*, 1988]. The model reproduces a small annual cycle in V_{dSO2} but underpredicts the SO_2 deposition velocities. This can be explained by the relatively large calculated aerodynamic resistance compared to the observed aerodynamic resistance. The model calculates a relatively small surface resistance of 25 s m^{-1}, which is in good agreement with the observed surface resistance. During winter, the calculated surface resistance is largely controlled by soil uptake associated with a soil pH of about 8 and an LAI of 0.5, whereas the summer surface resistance is controlled by both the soil uptake and of vegetation. The impact of canopy wetness on the SO_2 deposition velocity is more clearly shown in Figure 3.5c, which presents the simulated annual cycle of the monthly mean SO_2 deposition velocity for 45°N 0°. The January average wet skin fraction for this location is 0.6, much higher than the June average wet skin fraction of 0.1. Also shown are SO_2 deposition velocities observed by *Vermetten et al.* [1991], the wintertime average being as high as 1.3 cm s^{-1}, with a maximum of 2.0 cm s^{-1}, over Douglas Fir in the Netherlands during the autumn and winter whereas the V_{dSO2} during the summer was much smaller, i.e. 0.2 cm s^{-1}. We have not selected the grid cell of the latitude and longitude of the measurement site in the Netherlands since this grid has a winter LAI of only 0.25 compared to the LAI of the Douglas Fir of 10 [*Vermetten et al.*, 1992]. The selected grid square has a January average SO_2 soil resistance of ± 75 s m^{-1} and an in-canopy transfer resistance of ± 125 s m^{-1} so that the deposition velocity is largely controlled by stomatal uptake and the wet cuticle. The model does not simulate the large deposition velocities during the winter and autumn, which can be explained by the smaller LAI of about 3.5 and the assumed wet skin resistance of 100 s m^{-1} compared to the observed canopy resistance of ± 25 s m^{-1} for wet conditions [*Vermetten et al.*, 1992]. However, the model seems to reproduce the impact of the wet winter on the annual cycle of the SO_2 deposition velocity, characteristic for the north-western European climate, with wintertime deposition velocities comparable to those in summer, despite the small vegetation activity in the winter.

3.6.3 Global deposition and concentration calculations

Sulfur dioxide: Figures 3.6a and 3.6b show the January and July average global V_{dSO2} distribution. Distinct spatial gradients occur over the continents, mostly related to variable surface characteristics, whereas over sea the spatial distribution of V_{dSO2} reflects the wind speed distribution. In July, relatively large values of V_{dSO2} occur in dense vegetated areas, e.g., the temperate forests in the northern hemisphere (NH). In January, the deposition velocity in north western Europe is still relatively large due to canopy wetness through dew formation and precipitation interception. Over the deserts of Africa and the Middle-East the deposition velocity is very small for a relative humidity as low as 10%. Large areas with deposition velocities less than 0.025 cm s^{-1} in winter occur over snow and ice covered surfaces. The July V_{dSO2} is about 0.15 cm s^{-1} over the Arctic snow/ice surfaces. In the southern hemisphere (SH), the January and July V_{dSO2} values are relatively small in Australia, with values of about 0.2 cm s^{-1}, whereas the average January and July average V_{dSO2} over the tropical forest in South America is as high as 0.8 cm s^{-1}. A striking feature is the large

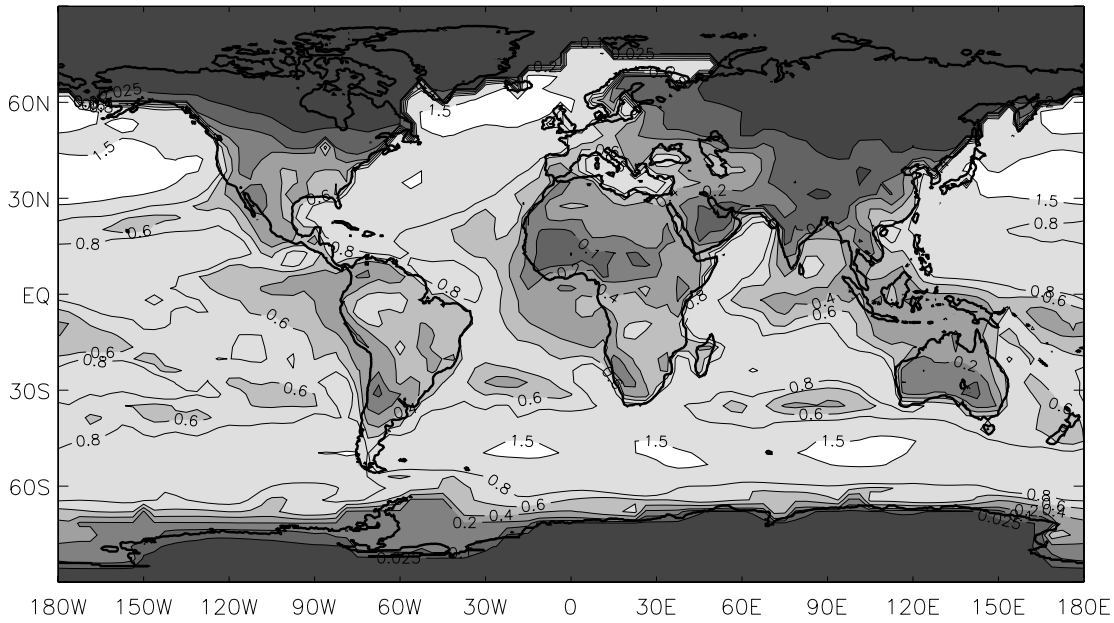

Figure 3.6a: Monthly average SO_2 deposition velocity (cm s^{-1}), January. The isolines are: 0.025, 0.1, 0.2, 0.4, 0.6, 0.8, 1.5.

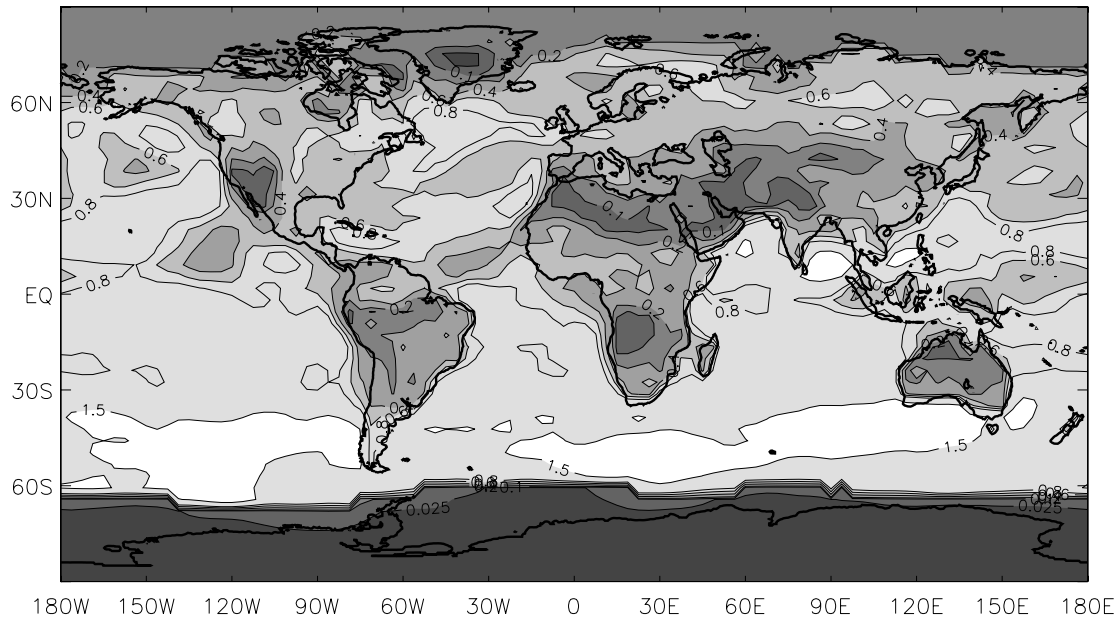

Figure 3.6b: July

difference between the January and July average V_{dSO2} over southern Africa and south of the tropical forest in South America, 0.6 and 0.05 cm s^{-1}, respectively. Over the oceans, the SO_2 deposition velocity is relatively high, i.e. up to 2.0 cm s^{-1} over the North Atlantic in January,

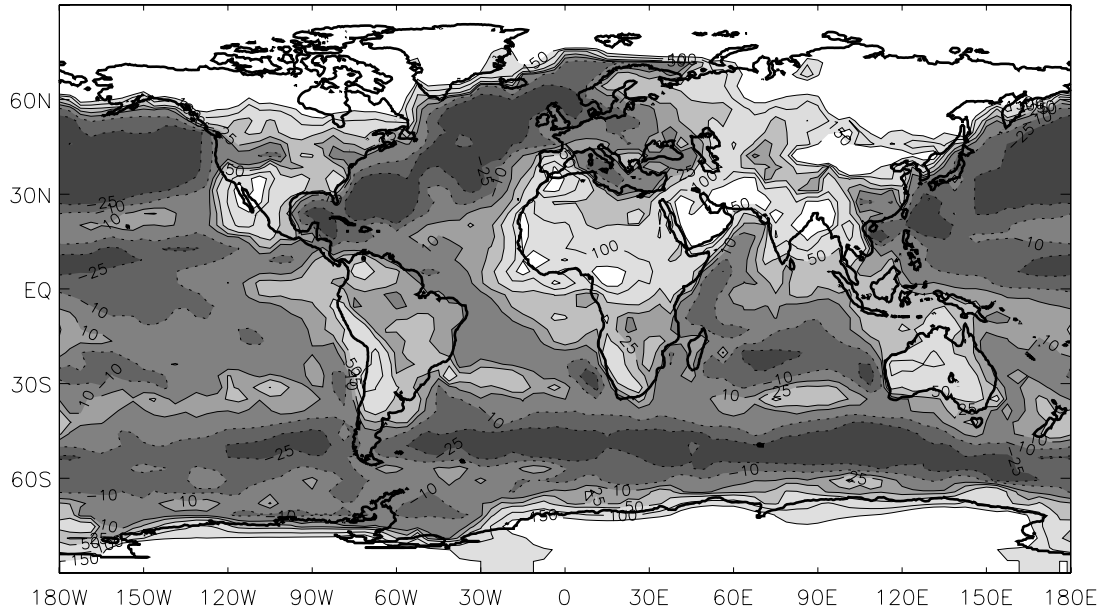

Figure 3.7: Relative differences (percent) of the SO_2 surface layer concentration between the new scheme and the "constant V_{dSO2}" scheme, January. Dashed and solid lines indicate a decrease and increase, respectively, of the concentrations calculated by the new scheme compared to the "constant V_{dSO2}" scheme. The isolines are: -25, -10, 10, 25, 50, 100, 150.

and it has a minimum of about 0.3 cm s^{-1} in subsidence (low wind speed) regions. The SO_2 deposition calculated with the new scheme has been compared to a "constant V_{dSO2}" scheme (V_{dSO2} is 0.6 cm s^{-1} over land without snow/ice cover, 0.1 cm s^{-1} over snow/ice surfaces and 0.8 cm s^{-1} over sea; see *Feichter et al.* [1996]). The relative differences are calculated as (new scheme minus "constant V_{dX}" scheme)/("constant V_{dX}" scheme). Over land, the SO_2 deposition calculated with the new scheme is generally smaller compared to the "constant V_{dSO2}", with relative decreases up to 100% over snow covered surfaces. The new scheme calculates SO_2 deposition velocities over snow/ice less than 0.01 cm s^{-1}. Over sea, the SO_2 deposition calculated with the new scheme shows relative increases compared to the "constant V_{dSO2}" scheme up to 75% in the regions with high wind speeds. This can have significant consequences for SO_2 concentrations in the marine boundary layer which, in turn, affects the calculated amount of precursor gases available for new particle formation. Figure 3.7 shows the relative differences between the January average SO_2 concentrations in the model surface layer (~ 30 m) by both schemes. Although these are generally smaller than the differences in SO_2 deposition, associated with negative feedbacks in SO_2 concentration changes through dry deposition and chemistry, relative differences between the new and "constant V_{dSO2}" scheme of about 25% occur up to an altitude of 5 km.

Sulfate: Figure 3.8a and b show the January and July average SO_4^{2-} deposition velocities by applying the rural continental and marine mass size distribution shown in Figure 3.3. Over land, V_{dSO4} is relatively small with minimum deposition velocities of about 0.05 cm s^{-1} over even surfaces, e.g. the snow and ice areas and over the deserts. Over vegetated surfaces with a large surface roughness, e.g. the tropical forests, SO_4^{2-} deposition velocities are as high as 0.25 cm s^{-1}. Over sea, V_{dSO4} ranges between about 0.1 cm s^{-1} in the subsidence regions and up to 1.0 cm s^{-1} over the North Atlantic in January. Figure 3.9 shows the relative differences

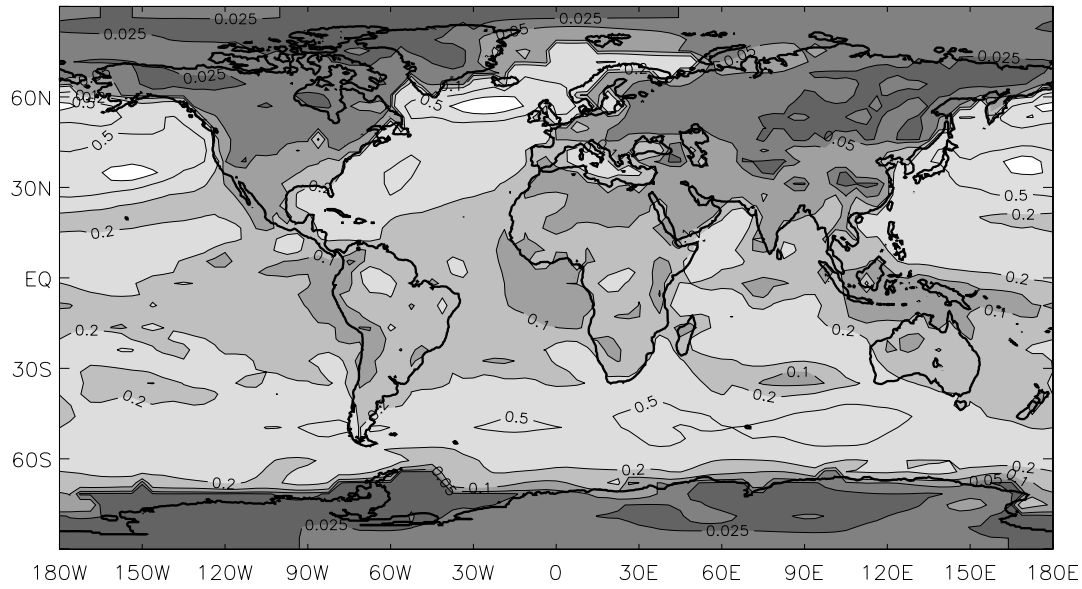

Figure 3.8a: Monthly average SO_4^{2-} deposition velocity (cm s^{-1}) for January. The isolines are: 0.01, 0.025, 0.05, 0.1, 0.2, 0.5, 0.75.

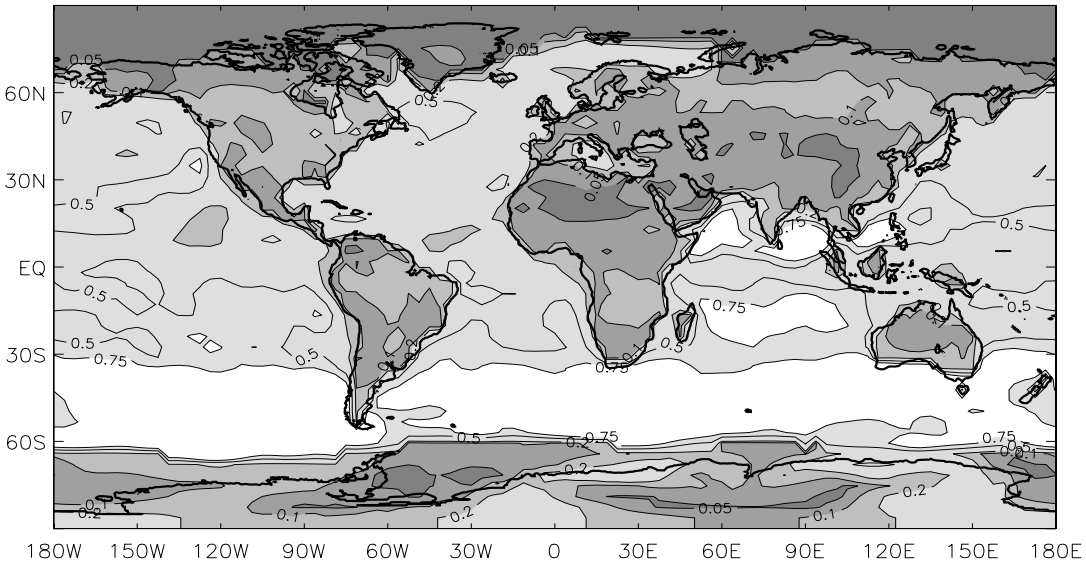

Figure 3.8b: July.

between the January average SO_4^{2-} concentrations in the model surface layer calculated with the new scheme and the "constant V_{dSO4}" scheme (V_{dSO4} is 0.2 cm s^{-1} over all surfaces; see *Feichter et al.* [1996]). Over land, the SO_4^{2-} surface layer concentrations calculated with the new scheme are generally higher compared to those of the "constant V_{dSO4}" scheme, with relative increases of more than a factor 2. Over marine regions with high wind speeds, the SO_4^{2-} concentrations calculated with the new scheme are up to about 50% lower compared to the "constant V_{dSO4}" scheme.

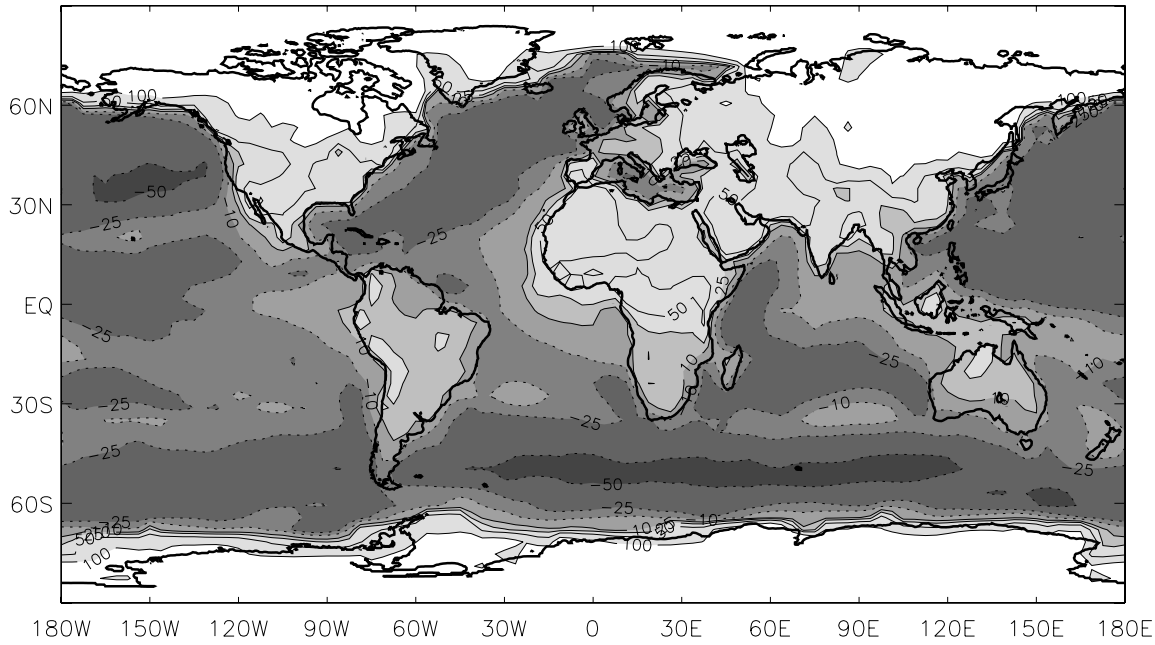

Figure 3.9: Relative difference (percent) of SO_4^{2-} surface layer concentration between the new scheme and the "constant V_{sSO4}" scheme (see Figure 3.7), January. The isolines are: -50, -25, -10, 10, 25, 50, 100.

3.6.4 Global budget differences by the new scheme

Table 3.3 shows the relative differences in column SO_2 and SO_4^{2-} burdens in four approximately equal areas of the globe (0°-30° and 30°-90° N and S), comparing the new scheme and the "constant V_{dX}" scheme for January and July (for the calculation of the relative differences, see section 3.6.3). The total S-columns, calculated with the new scheme,

Table 3.3: Relative differences (%) of SO_2 and SO_4^{2-} columns over four approximately equal areas of the globe, comparing the "constant V_{dX}" scheme and the new dry deposition scheme. Positive values indicate an increase in the budget calculated by the new scheme

	SO_2, Tg S		**SO_4^{2-}, Tg S**	
	January	**July**	**January**	**July**
90°-30° N	20 (0.49)	17 (0.11)	1 (0.19)	7 (0.45)
30°-0° N	23 (0.09)	21 (0.05)	0 (0.23)	7 (0.33)
0°-30° S	12 (0.04)	18 (0.06)	0 (0.20)	1 (0.18)
30°-90° S	6 (0.03)	8 (0.03)	-1 (0.11)	-2 (0.06)
Global	20 (0.65)	18 (0.24)	0 (0.72)	5 (1.02)

Positive values indicate and increase in the budget calculated by the new scheme compared to the V_{dX} scheme. The total column SO_2 and SO_4^{2-} burdens for these areas are indicated between parentheses.

are shown as well. The new scheme yields larger SO_2 burdens in all areas for January and July, with a relative increase of about 20% for the 30°N-90°N area which contains 75% of the global SO_2 burden in January and 45% in July. This also reflects the global relative increase of about 20%. The January and July global SO_4^{2-} burdens increase with 9% and 15%,

respectively, due to the larger SO_2 burden.
This increase through SO_2 is more pronounced compared to changes in the SO_4^{2-} burden due the improved SO_4^{2-} dry deposition formulation. The new scheme does not yield a significant change in the January global SO_4^{2-} burden, whereas there is a relative increase of 7% in July in the 30°N-90°N area. These results indicate that a realistic simulation of the global sulfate burden requires, in particular, a realistic SO_2 dry deposition representation. In addition, regional differences in boundary layer SO_4^{2-} concentrations related to dry deposition parameterizations are significant as well.

3.7 Discussion

The new dry deposition routine improves the model calculated deposition velocities at different locations with various surface covers. The introduction of a local surface roughness and a more realistic LAI representation has reduced several shortcomings of the model. Calculation of the aerodynamic resistance R_a in the new model version has improved significantly. Further improvement will rely on the ECHAM turbulent exchange representation and the description of ecosystems and their characteristics in global vegetation databases. The amount of standing biomass is more realistically represented through the LAI as a function of vegetation cover and season. However, there appears to be some misrepresentatrion of the LAI at some locations, e.g., a too large January LAI in the central United States, due to a misrepresentation of the vegetation cover for that location or the assigned LAI. Therefore, it needs further validation based on observations, especially concerning the seasonal cycle. We intend to use the NDVI (Normalized Difference Vegetation Index) data by *Kidwell* [1990] for validation and introduction of a realistic seasonally dependent LAI, following *Gao and Wesely* [1995] who have used satellite data for the modeling of dry deposition on a regional scale.
A dry deposition formulation for a global scale model requires an adequate representation of uptake processes by sparsely or non-vegetated surfaces, since deserts, grass and tundra cover large areas. Most continents have a bare soil fraction exceeding 0.25, up to almost 1, e.g. in North Africa and the Middle East. This implies that soil uptake plays an important role in the deposition process over these continents. The current SO_2 soil resistance parameterization accounts for the influences of soil pH and the relative humidity on the SO_2 uptake. It is possible that other soil properties also affect the SO_2 uptake, e.g. the organic soil composition, but quantitative information about additional important parameters is not available. Nevertheless, *Murphy and Sigmon* [1989] showed that a layer of partially decomposed organic matter covering the soil can influence the SO_2 uptake. This is probably only relevant for forest soils but will not significantly influence the SO_2 deposition velocity since deposition is mainly controlled by the vegetation.

A large part of the wintertime northern hemisphere is covered with snow and ice, for which we calculate an SO_2 dry deposition velocity close to zero, except for some regions with surface temperatures between 263 and 273 K. Although differences between the calculated V_{dSO2} and the fixed value of 0.1 cm s^{-1} used in the "constant V_{dSO2}" scheme are not very large, differences in total deposition are significant since the SO_2 concentrations are relatively high as a result of large SO_2 emissions, a low SO_2 oxidation rate, and suppressed vertical exchange in the stable stratified boundary layer. The negligible low SO_2 dry deposition velocity over

snow and ice in the NH winter yields surface concentrations of SO_2 which are significantly larger than observed surface concentrations in this region [*Lelieveld et al.*, 1997]. One possible explanation of this discrepancy, which is a common feature in global sulfur models, is that we underestimate SO_2 deposition. However, the SO_2 snow/ice resistance parameterization has been derived from observations, while the results are consistent which a large number of additional observations. Other explanations for the overestimation are the strong horizontal and vertical concentration gradients at some locations, which are not reproduced by the model due to the coarse horizontal grid resolution, and possible misrepresentation of vertical mixing. Another possible explanation is the potential importance of an additional SO_2 oxidation pathway(s) which is not considered in the model [*Lelieveld et al.*, 1997].

Validation of our scheme suggests that we calculate realistic SO_4^{2-} deposition velocities over vegetation and snow covered surfaces. As far as we know, there are no observations available over bare soil, but it may be expected that the SO_4^{2-} dry deposition velocities over bare soil are comparable to those over snow and ice (similar surface roughness), neglecting possible resuspension of particles. The relatively largest uncertainties are associated with the calculation of SO_4^{2-} dry deposition velocities over sea surfaces. In fact, removal processes over the ocean are still not well understood [*Williams*, 1982; *Hummelshøj et. al.*, 1992]. A main problem is the lack of observations of particle dry deposition to the sea surface. The difference between the particle dry deposition velocity calculated by the parameterization of *Hummelshøj et al.* [1992] and the parameterization by *Slinn et al.* [1980], which does not consider the effect of whitecaps on the dry deposition process, is relatively small for wind speeds less than about 10 m s^{-1}. The January average wind speed at 10 m in ECHAM4 is less than 10 m s^{-1} except for a few small regions over the North Atlantic and the Pacific Ocean. However, differences in calculated SO_4^{2-} deposition velocities between the two parameterizations are very large, i.e. more than one order of magnitude, for a wind speed of 30 m s^{-1} over the North Atlantic Ocean in January. It has been shown in section 3.6.3 that SO_4^{2-} surface layer concentrations decrease by about 50%, associated with a factor of 10 increase of the SO_4^{2-} deposition velocity. Sensitivity analysis also shows that transfer of a small fraction of marine sulfate to the coarse particle mode can significantly enhance the deposition velocity due to sedimentation. Therefore, the representation of the sulfate aerosol size distributions needs further study based on additional observations. Future efforts will focus on the explicit calculation of sulfate mass size distributions as a function of the controlling processes, e.g., nucleation, condensation and coagulation [*J. Wilson,* 1996, personal communication] providing a basis for further improvements.

3.8 Conclusions

Our dry deposition scheme calculates SO_2 and SO_4^{2-} removal rates of over many locations for different meteorological conditions, consistent with surface characteristics that control dry deposition. Dry deposition of SO_2 over sea is to a large extent controlled by the aerodynamic resistance while over land it is determined mostly by the surface resistance (i.e., r_{soil}, r_{veg}, r_{ws} and $r_{snow/ice}$). The SO_2 soil resistance is explicitly calculated from the soil pH and relative humidity whereas the SO_2 snow/ice resistance is a function of temperature. Incorporation of the scheme in the chemistry-general circulation model ECHAM4 yields significant changes in SO_2 mass flux densities, SO_2 and SO_4^{2-} concentrations in the lower troposphere and in their column burdens, compared to a previous scheme using constant deposition velocities

[*Feichter et al.*, 1996]. For example, the new scheme calculates up to about 50% larger SO_2 concentrations near the surface in the continental NH in January whereas there is a relative decrease in SO_2 concentrations over the North Atlantic Ocean of about 50% in January. The global SO_2 burden calculated with the new scheme is about 20% larger compared to the "constant V_{dSO2}" scheme. The consequent SO_4^{2-} burden increase is relatively large compared to the SO_4^{2-} increase resulting from the new SO_4^{2-} dry deposition parameterization. This emphasizes the need for a realistic representation of the SO_2 dry deposition process. In addition, significant differences in SO_4^{2-} mass flux densities and surface layer concentrations are calculated between the new and the "constant V_{dSO4}" scheme.

Chapter 4

Atmosphere-biosphere trace gas exchanges simulated with a single column model[1]

When considering surface exchange of reactive trace gases such as the oxidized nitrogen species (NO_x) in atmospheric models, fast chemical transformations result in a flux divergence, which is not accounted for when the traditional aerodynamic resistance formulas for turbulent transport are applied. Moreover, the atmosphere-biosphere exchange flux of NO_x at the canopy top is bi-directional, depending on the surface layer concentrations and interactions between the controlling processes within the canopy, e.g., emissions, dry deposition, chemistry, and turbulence. We have developed a multi-layer atmosphere-biosphere trace gas exchange model to study the role of the canopy interactions for the NO_x canopy flux divergence on a global scale. We evaluate the atmosphere-biosphere model, implemented in a single column chemistry and meteorological model, for a selection of ecosystems by comparison with observations. The modeled and observed ozone and oxidized nitrogen concentrations and fluxes are generally in reasonable agreement if we constrain our model with site specific surface and meteorological parameters. The sensitivity of atmosphere-biosphere trace gas exchange to nocturnal turbulent exchange appears to be large. A comparison of the NO_x fluxes calculated by the traditional big leaf approach and the atmosphere-biosphere model is presented. For sites that are exposed to relatively large antropogenic emission fluxes, the big leaf approach and biosphere model calculate similar NO_x fluxes, which confirms the applicability of the big leaf approach for polluted regions. However, for relatively pristine sites, differences between the NO_x fluxes of the biosphere model and the big leaf approach are significant. This underscores the importance of an explicit representation of the biosphere processes for those locations where the NO soil emissions flux is comparable to or exceeds the antropogenic emissions.

[1] Submitted to the *Journal of Geophysical Research*, with J. Lelieveld, F. Dentener, M. Krol, and G.-J. Roelofs as co-authors

4.1 Introduction

In Chapter 2 and 3, the implementation of an explicit representation of the dry deposition processes of trace gases and aerosols, and the impact on the calculated concentrations and fluxes on a global scale have been presented. The dry deposition flux is calculated from the surface layer concentrations and the dry deposition velocity, which reflects the turbulent transport to the earth's surface, molecular diffusion through the quasi-laminary boundary layer, and the surface absorption efficiency. The uptake of trace gases, such as ozone (O_3) and sulfur dioxide (SO_2), by the vegetation is largely controlled by plant physiological processes and the canopy structure. The dry deposition velocity over vegetated surfaces is calculated in the coupled chemistry and general circulation model (GCM) ECHAM (European Centre model, Hamburg version) applying the "big leaf" approach [e.g., *Hicks et al.*, 1987]. Since this approach is based on a large number of observations of dry deposition velocities of trace gases such as ozone and sulfur dioxide, it is expected to yield realistic deposition velocities for these trace gases for many locations and different seasons. This is confirmed by the agreement between the calculated and observed O_3 and SO_2 dry deposition velocities, shown in Chapter 2 and 3.
The dry deposition scheme has also been applied to calculate the dry deposition flux of nitric acid (HNO_3), nitrogen oxide (NO) and -dioxide (NO_2). However, for the latter two trace gases, as well as for other reactive trace gases with comparable short chemical lifetimes, it can be questioned if the big leaf approach is valid. For a trace gas with a typical chemical lifetime smaller than or comparable to the turbulent timescale, fast chemical transformations result in a flux divergence, which is not accounted for by applying the traditional aerodynamic resistance formulas for turbulent transport. Moreover, the atmosphere-biosphere exchange flux of NO and NO_2 at the canopy top is bi-directional, dependent on the surface layer concentrations and interactions between the controlling processes within the canopy, e.g., emissions, dry deposition, chemistry, and turbulence. NO emitted from the soil, reacts with O_3, producing NO_2, which is removed by dry deposition. NO_2 also reacts with the oxidation products of the emitted hydrocarbons, e.g., isoprene, forming organic nitrates (e.g, peroxyacetylnitrate (PAN)) which can be removed by dry deposition and by thermal decomposition. The effectiveness of this internal cycling of NO_x ($NO+NO_2$) within the canopy further depends on radiation flux densities within the canopy and the turbulent exchange between the canopy and the atmosphere. The chemical conversion of reactive trace gases changes with height within the canopy due to decreasing photodissociation rates through the interception of radiation. Moreover, the residence time of the trace gases within the chemical regime of the canopy strongly depends on the turbulent mixing.

The flux divergence of reactive trace gases within the canopy has been addressed in previous studies using observations and model simulations [*Jacob and Wofsy*, 1990, hereafter *JW90*; *Gao and Wesely*, 1993; *Duyzer et al*, 1995; *Joss and Graber*, 1996; *Walton et al.*, 1997]. Common among these studies is the use of multi-layer trace gas exchange models being constrained by observations. We have developed an atmosphere-biosphere trace gas exchange model, which is similar to the multi-layer trace gas exchange models, but which can be used to study the role of the biosphere interactions for trace gas exchanges on a global scale. We have implemented the biosphere model in the single column version of the Regional Atmospheric Climate Model (RACMO) [*Christensen et al.*, 1996], coupled to a

non-methane hydrocarbon chemistry scheme. This allows evaluation of the biosphere model by comparison of the calculated canopy top fluxes with observations. The atmosphere-biosphere trace gas exchange model considers the dry deposition process, biogenic emissions of oxidized nitrogen and hydrocarbons and the extinction of radiation and turbulence within the canopy. However, the model must be applicable for global scale studies, imposing rather strong constraints on the model structure. Hence, the process description is highly parameterized and a coarse vertical and temporal resolution is applied. Another important limitation is related to the applied micro-meteorological, biophysical and biogeochemical input parameters to the vegetation model. The aforementioned case specific studies generally used observed site specific biophysical parameters, such as the Leaf Area Index (LAI), or biogeochemical parameters, such as the soil biogenic NO flux, to constrain the models [*JW90*; *Walton et al.,* 1997]. However, this detailed information is not available for many ecosystems on a global scale, which implies that we must rely on the available information in global databases.

The implementation of the atmosphere-biosphere trace gas exchange model in RACMO is described in section 4.2. Numerical issues relevant to the application of atmosphere-biosphere models are discussed in section 4.3. In section 4.4 we evaluate the atmosphere-biosphere trace gas exchange model by comparison with observations and showing the differences between the NO_x fluxes calculated by the big leaf approach and the biosphere model, followed by a discussion in section 4.5 and conclusions in section 4.6. In Chapter 5 we present an assessment of the role of biosphere interactions for the effective emissions of NO_x on a global scale.

4.2 Atmosphere-biosphere trace gas exchanges in a single column model

For the development and evaluation of the atmosphere-biosphere trace gas exchange model we apply the single column version of RACMO. The description of the physical processes within RACMO resembles that of the general circulation model ECHAM4 [*Roeckner et al.*, 1996], the model being used for global scale studies presented in Chapters 2, 3 and 5. Hence, RACMO offers the opportunity to perform process studies, e.g., of the sensitivity to the spatial and temporal resolution, and the development of parameterizations with an optimal consistency for application in ECHAM. Moreover, specific surface cover characteristics such as soil moisture and canopy structure can be prescribed for a consistent evaluation of modeled and observed parameters. The horizontal grid resolution of a global scale chemistry-GCM like ECHAM is typically 100 km or more, which implies that the surface characteristics of the model grid cells with a heterogeneous coverage can be very different from the specific site characteristics.

The chemistry scheme used in ECHAM [*Roelofs and Lelieveld*, 1995, 1997, and 2000], including specific modifications required for the study of atmosphere-biosphere trace gas exchange, has also been implemented into RACMO. The chemistry scheme used in this study, calculates the concentrations of CH_4, CO, NO_y (NO, NO_2, HNO_4, NO_3, N_2O_5, PAN, methylperoxyacetylnitrate (MPAN) and HNO_3), OH, O_3, and non-methane hydrocarbons including isoprene (C_5H_8), and a selection of the resulting hydrocarbon oxidation products such as formaldehyde (CH_2O), higher aldehydes and acetone (CH_3COCH_3). Antropogenic

and biogenic emissions of NO_x, CO, CH_4 and higher hydrocarbons, including acetone, are considered using monthly mean global emission fluxes. Dry deposition processes are described using the big leaf resistance approach [*Ganzeveld and Lelieveld*, 1995; *Ganzeveld et al.*, 1998]. With the implementation of the atmosphere-biosphere trace gas exchange model, the calculation of the dry deposition and biogenic emission fluxes for the vegetated areas has been modified as described in the next section.
The single column model needs to be initialized with vertical profiles of temperature, moisture, wind speed, trace gas concentrations and surface boundary conditions, e.g., surface temperature, soil moisture and the surface cover characteristics. For the initialization of the physical and dynamical parameters we apply the vertical profiles and surface properties of the grid cell of the ECHAM model most closely resembling the location of the single column model. The trace gas concentrations are initialized using monthly mean vertical profiles of trace gas concentrations from the tracer transport model TM3 [*Houweling et al.*, 1998; *Lelieveld and Dentener*, 2000]. At the time of the development of the single column model, the corresponding calculated ECHAM concentrations where not yet available. In this study the model integrations with RACMO have been performed using the default ECHAM vertical coordinate system of 19 atmospheric levels, with approximately 5 layers in the Planetary Boundary Layer, 10 in the free troposphere, and 5 in the stratosphere.

4.2.1 Atmosphere-biosphere trace gas exchange model

The concentration tendency in the surface layer (SL) is calculated from the tendencies over the vegetation, wet skin (ws), bare soil and snow/ice cover fractions:

$$\left(\frac{dc}{dt}\right)_{SL} = \left(\frac{\partial c}{\partial t}\right)_{veg} + \left(\frac{\partial c}{\partial t}\right)_{ws} + \left(\frac{\partial c}{\partial t}\right)_{soil} + \left(\frac{\partial c}{\partial t}\right)_{snow/ice} \tag{4.1}$$

The concentration tendency in the surface layer over the bare soil and snow/ice fraction is calculated according to

$$\left(\frac{\partial c}{\partial t}\right)_{soil/snow/ice} = \left(\frac{\partial c}{\partial t}\right)_{turb} + \left(\frac{\partial c}{\partial t}\right)_{emiss} + \left(\frac{\partial c}{\partial t}\right)_{dep} + \left(\frac{\partial c}{\partial t}\right)_{chem} \tag{4.2}$$

which reflects the contribution by turbulent transport between the surface layer and the layer aloft, biogenic as well as antropogenic emissions, dry deposition, and chemical transformations. Note that the convection is ignored here whereas the advection tendency is obviously not calculated in a single column model. To calculate the concentration tendency in the surface layer over the vegetated surface, Equation 4.2 reduces to

$$\left(\frac{\partial c}{\partial t}\right)_{veg/ws} = \left(\frac{\partial c}{\partial t}\right)_{turb} + \left(\frac{\partial c}{\partial t}\right)_{chem} \tag{4.3}$$

with the turbulent tendency reflecting the change in the concentrations due the turbulent exchange between the surface layer and the layer aloft as well as the turbulent exchange between the surface layer and the canopy-top layer of the vegetation model. The

concentration tendency within the canopy is calculated according to Equation 4.2, considering only the biogenic emissions in the emission tendency. Concentration tendencies due to the turbulent exchange, emissions and dry deposition are calculated according to

$$\left(\frac{\partial c}{\partial t}\right)_{turb/emiss/dep} = \frac{\partial F_{turb/emiss/dep}}{\partial z} \tag{4.4}$$

The calculation of the dry deposition and biogenic emission flux, F_{dep} and F_{emiss}, respectively, is discussed more extensively in the next section. The turbulent flux is calculated based on local closure theory:

$$F_{turb} = -K_H \frac{\partial c}{\partial z} \tag{4.5}$$

where K_H is eddy-diffusivity for heat and $\partial c/\partial z$ is the concentration gradient between the reference height of the surface and canopy layers. The eddy-diffusivity profile in the canopy is estimated by scaling the surface layer K_H with the calculated wind speed for each layer relative to the calculated surface layer wind speed. The wind speed profile within the canopy is represented by an exponential function so that the wind speed is a function of the canopy height and an attenuation coefficient dependent on the canopy characteristics [*Cionco*, 1978].

Dry deposition, biogenic emissions, and photochemistry within the canopy

The original formulation of the dry deposition calculations is described in Chapters 2 and 3. The algorithm calculates the dry deposition flux F_{dep} from the surface layer concentration and the dry deposition velocity V_d. The latter is calculated from the aerodynamic and quasi-laminar boundary layer resistance and the stomatal resistance [*Sellers et al.*, 1986] and ocean water, bare soil, cuticle, mesophyll and wet surface resistances. The dry deposition scheme has originally been developed for O_3, NO, NO_2, HNO_3, SO_2 and SO_4^{2-} aerosol. Additional resistances of the trace gases of the hydrocarbon chemistry scheme, for which the dry deposition process is expected to be a significant sink, have been estimated using the approach by *Wesely* [1989]. Based on the Henry's law coefficient and an estimated reactivity constant, the different uptake resistances are calculated by scaling these with the SO_2 uptake resistances for soluble non-reactive trace gases, and with O_3 for non-soluble reactive trace gases. The dry deposition calculations have been modified for the atmosphere-biosphere model calculating a "vegetation" dry deposition velocity for each canopy layer as the reciprocal value of the vegetation resistance. This resistance is calculated from the stomatal, mesophyll, cuticle resistance, a leaf boundary layer resistance and the amount of biomass in each layer. The leaf boundary layer resistance, which represents the diffusion through a thin layer adjacent the leaf surface, is calculated from the wind speed profile according to *Meyers* [1987]. The selected uptake resistances of the original big leaf dry deposition scheme result in a small dry deposition velocity of NO, and an NO_2 dry deposition velocity which is about 2/3 of the ozone dry deposition velocity over vegetation [*Ganzeveld and Lelieveld*, 1995]. In contrast to the ozone and sulfur dioxide dry deposition velocities, the NO and NO_2 big leaf deposition velocities do not only reflect a biological sink but also sources from chemical transformations and biogenic emissions within the canopy. The presence of NO_2 and NO

sources due to chemical production and the biogenic emissions, respectively, results in a decrease of the NO and NO_2 dry deposition velocity compared to the ozone dry deposition velocity for the big leaf approach. However, since these processes are explicitly resolved in the biosphere model, a zero NO_2 mesophyll resistance is applied whereas we assume zero uptake of NO by the leaves, corresponding to an infinite mesophyll resistance.
The soil biogenic NO emission flux is calculated according to *Yienger and Levy* [1995] (hereafter referred to as *YL95*), however, without applying their canopy reduction factor (see section 4.4.2). The emissions of isoprene by the vegetation are calculated according to *Guenther et al.* [1995]. For more details concerning the calculation of the biogenic emissions we refer to Chapter 5.
As has been mentioned in the introduction, the extinction of radiation in the canopy due to the interception by biomass needs to be considered since it controls the photochemistry within the canopy. Moreover, the biogenic emissions of hydrocarbons strongly depend on the radiation regime within the canopy. The vertical profiles of radiation within the canopy are calculated according to *Norman* [1979] and *Weiss and Norman* [1985]. The algorithm calculates the profiles of the direct and diffusive irradiance in both the visible (Photosynthetically Active Radiation, PAR) and near infrared spectral region from the net solar radiation [*Weiss and Norman*, 1985], the canopy structure and soil albedo**.** These radiation profiles are used to estimate the photodissociation rates within the canopy from the above canopy PAR flux and the surface layer photodissociation rate. This approach implies that it has been assumed that the spectral leaf transmission of the photodissociation rates (e.g., $NO_2 + h\upsilon \rightarrow NO + O$, $\lambda \leq 410$ nm) in our model is similar to that of PAR (400-750 nm).

Canopy structure

The atmosphere-biosphere trace gas exchange model is initialized by biogeophysical parameters, e.g., the Leaf Area Index (LAI), canopy height, surface roughness and the vertical distribution of biomass expressed by the Leaf Area Density (LAD) profile, and biogeochemical parameters such as emission factors. Since a part of this study entails the evaluation of the model performance by comparison with observations, the model is initialized with the available site specific canopy characteristics to ensure a realistic comparison. However, the required input parameters are often unavailable and therefore the biosphere characterization partly relies on the parameter values derived from the global scale data sources that we apply to define the canopy structure in ECHAM. For more details concerning the surface cover characterization in ECHAM we refer to Chapter 5.

4.3 Spatial and temporal resolution

4.3.1 Vertical grid spacing

To determine the number of vertical layers that need to be distinguished within the canopy to resolve the effect of the biosphere interactions on the flux divergence, simulations with the single column model with 1, 2 and 10 equidistant layers have been performed for a tropical rainforest canopy. For more specific details concerning the defined canopy structure we refer to section 4.4.1. The maximum number of 10 layers is selected based on an analysis showing

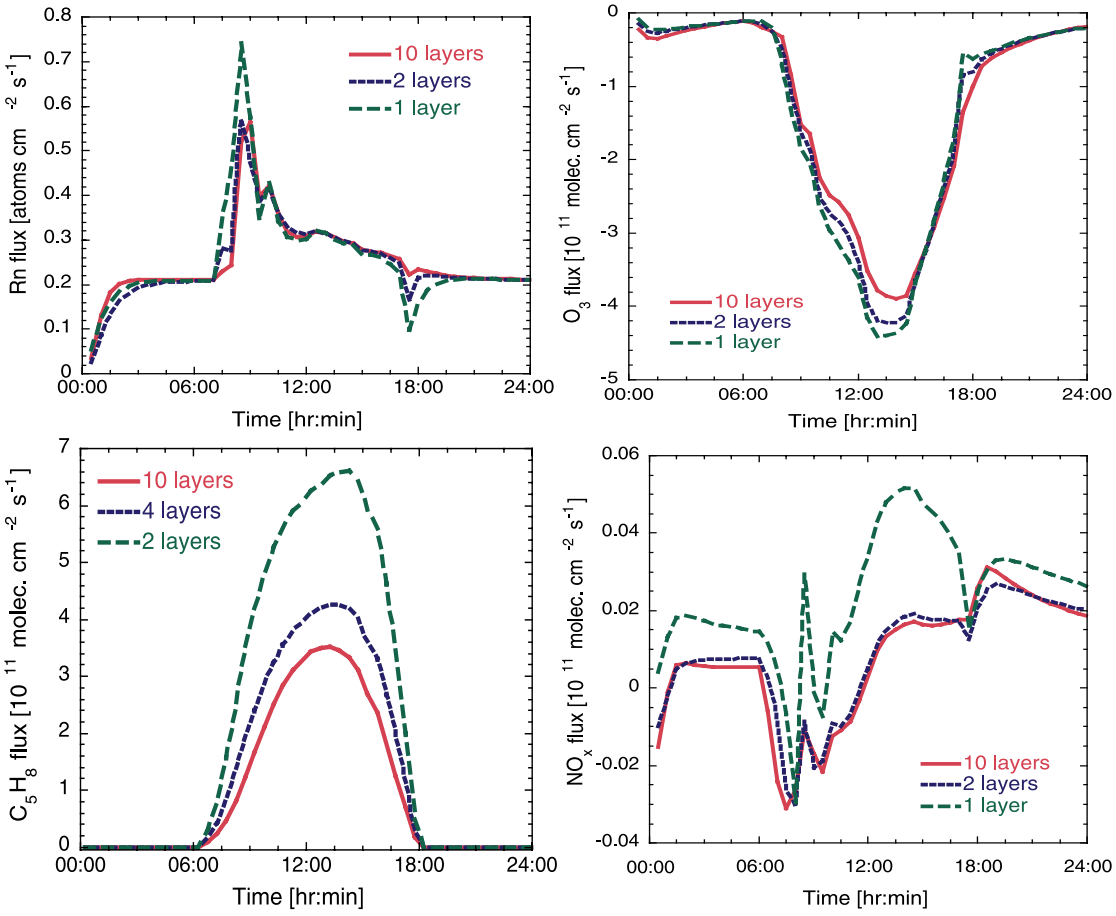

Figure 4.1a-d: Modeled diurnal cycle of the canopy top flux for tropical rainforest with a canopy height of 30 m and an LAI of 7, for three different vertical resolutions: 10 layers (solid line), 2 layers (dashed) and 1 layer (long-dashed), a) radon canopy flux (atoms cm^{-2} s^{-1}), b) ozone (10^{11} molecules cm^{-2} s^{-1}), c) isoprene (10^{11} molecules cm^{-2} s^{-1}) with the dashed line referring to 4 layers and the long-dashed line referring to 2 layers, and d) NO_x (10^{11} molecules cm^{-2} s^{-1}).

that there is no significant change in the modeled fluxes and concentrations when more layers are added. This maximum number of 10 canopy layers would be unpractical for a global model. However, the results can be used to develop parameterizations for a one or two-layer canopy model. Model integrations have been performed for one day using a timestep of 10 seconds. Figures 4.1a, b, c and d show the model resolved diurnal cycle in the radon, ozone, isoprene and the NO_x canopy top (30 m) fluxes for the three vertical resolutions. These four trace gases are selected based on their distinctly different chemical behavior and lifetime, and the location and magnitude of the sources and sinks within the canopy. Figure 4.1a shows the modeled diurnal cycle of the canopy top flux of radon, for which we assume a constant soil emission flux of 0.3 atoms cm^{-2} s^{-1} [*Trumbore et al.*, 1990]. At night radon accumulates within the canopy, which results in an early morning peak flux after the breakdown of the surface layer inversion. The three vertical resolutions yield similar diurnal cycles. However, in the 1-layer model version the sunrise peak flux is larger than the 2- and 10-layer model

because the 1-layer version does not account for turbulent transport between the soil and canopy crown. Figure 4.1b shows that the calculated canopy top fluxes of O_3, using the 1- and 2-layer grid resolution version, are comparable to that of the 10-layer version. The canopy top flux of O_3 for tropical rainforest is controlled by downward turbulent transport of ozone from the Planetary Boundary Layer (PBL) and surface layer into the canopy and subsequent dry deposition. Maximum daytime dry deposition velocities are about 2 cm s^{-1}. The similarity of the modeled canopy top fluxes for the three model versions suggests that dry deposition and turbulent transport are quite insensitive for the selected vertical resolution. Hence, it is expected that the big leaf approach calculates similar deposition fluxes as the biosphere model (see section 4.4.2). Figure 4.1c shows that the calculated canopy top fluxes of isoprene are highly sensitive for the vertical grid resolution with a > 50% larger isoprene canopy top flux for the 2-layer model version compared to the 10-layer model. The 1-layer isoprene canopy top flux is not shown here since it is very similar to that calculated with the 2-layer model version. The large sensitivity for the vertical resolution is mainly due to impact of the discretization of the vertical radiation profiles on the simulated emission strength. There is a strong radiation gradient close to the canopy top, which requires a relative high vertical resolution in the canopy crown. Figure 4.1c also shows the isoprene canopy flux distinguishing 4 layers and a subsequent interpolation of the calculated emission flux to 2 layers, which yields an isoprene emission flux that deviates less than 20% from the emission flux in the 10 layer model version. Figure 4.1d shows the modeled diurnal cycle of NO_x, which is controlled by biogenic emissions, dry deposition, chemistry and turbulent transport. The complexity of the interactions between these processes results in a bi-directional canopy top flux. It is shown that representing the canopy by one single layer results in an overestimation of the canopy top NO_x flux throughout the day compared to that calculated by the 10-layer resolution. It is also shown that by distinguishing two layers the canopy top NO_x flux is very similar to that calculated by the high-resolution vegetation model.
In conclusion, the sensitivity of the four trace gases for the selected vertical resolution suggests that we need to distinguish at least two canopy layers to resolve the atmosphere-biosphere trace gas exchange adequately. These two layers are hereafter referred to as the crown and canopy-soil layer.

4.3.2 Temporal resolution

The model integrations shown in the previous section were performed using a timestep of 10 seconds. However, since the atmosphere-biosphere model will be implemented in a global model, trace gas exchange processes will be resolved at a timestep of 15-30 minutes. However, it is not legitimate to consider the turbulent (and convective) transport of NO, NO_2, NO_3, N_2O_5, and HNO_4 separately in a model with a timestep larger than 15 minutes, since there is a large flux divergence at the “sub" timestep scale due to rapid chemical transformations. Therefore the flux-gradient relationships, developed to describe the turbulent transport of inert trace gases, can not be used to calculate the vertical turbulent fluxes of these reactive species [*Fitzjarrald and Lenshow*, 1983; *Kramm*, 1989; *Gao et al.*, 1991; *Vilà-Guerau de Arellano and Duynkerke*, 1995; *Galmarini et al.*, 1997]. However, the commonly applied approach in models with a timestep larger than the chemical timescale is to consider the transport of the so-called NO_x family (in this work defined as NO, NO_2, NO_3, $2 \bullet N_2O_5$, and HNO_4). This is based on the assumption that the NO_x family is a conserved chemical

species at a timescale of about 30 minutes. In addition to the chemical flux divergence, the timescale of emissions and dry deposition may be of the same order as the turbulence timescale, thereby also causing a flux divergence. For a tropical rainforest canopy of 30 m height and a daytime O_3 deposition velocity of 2.5 cm s^{-1} [*Fan et al.*, 1990] and assuming that dry deposition occurs mostly in the canopy crown, the deposition timescale is about 10 minutes. Therefore, such processes can not be modeled accurately with a timestep as large as 30 minutes. To remove potential numerical inaccuracies, the turbulent and dry deposition timescales are calculated separately from the thickness of the canopy layers and the eddy-diffusivity and dry deposition velocity, respectively. The length of the required "sub" timestep is taken as 10% of the smallest timescale. Consequently, the dry deposition, emissions and the turbulent exchange between the two canopy layers and the surface layer are resolved for the number of "sub" timesteps within each timestep. Note that the applied criterion to derive the "sub" timestep has been selected rather arbitrary from trial and error analysis. In the original version of the implemented chemistry scheme, emissions, dry

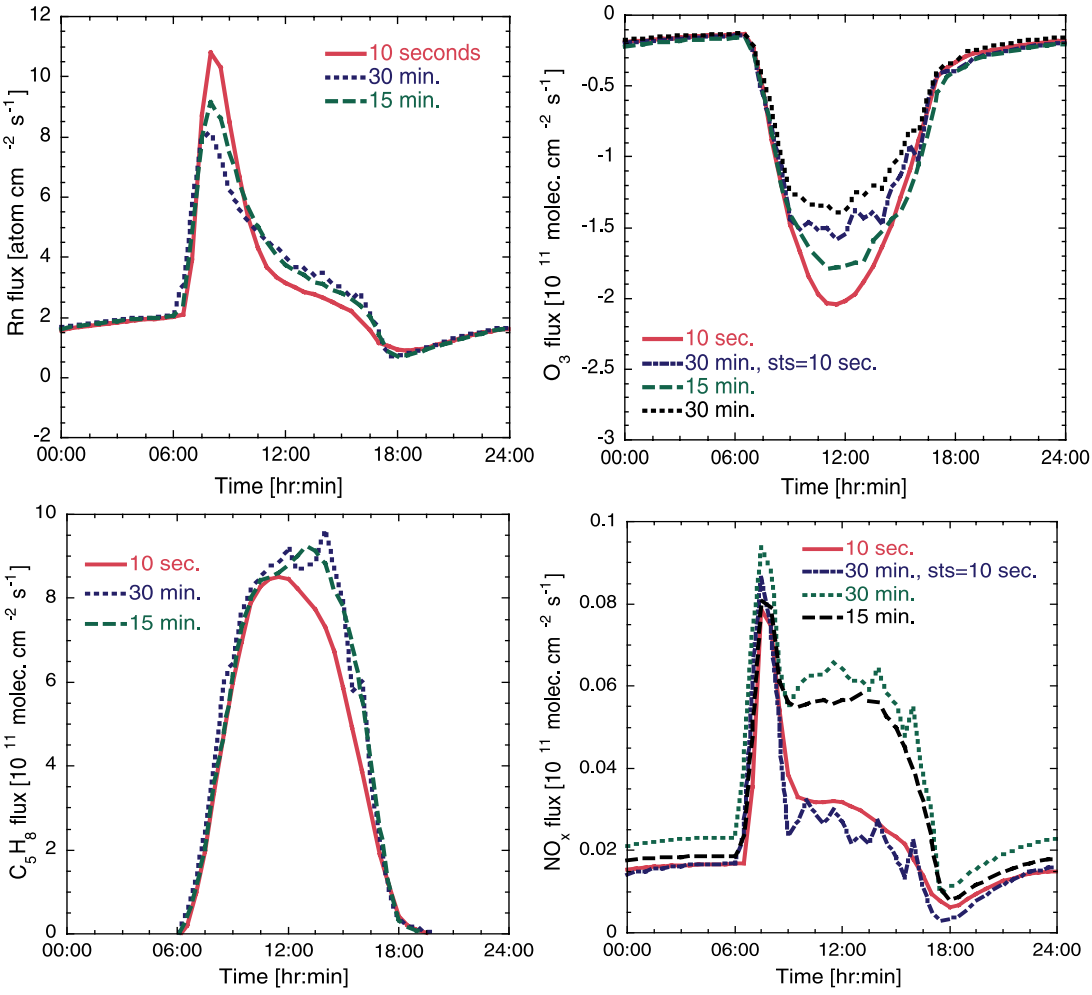

Figure 4.2a-d: Modeled diurnal cycle of the canopy top flux for a tropical rain forest with a canopy height of 30 m and an LAI of 7, distinguishing two equidistant canopy layers, for three different temporal resolutions: 10 seconds (solid line), 15 minutes (dashed) and 30 minutes (dotted), a) radon canopy flux (atoms cm^{-2} s^{-1}), b) ozone (10^{11} molecules cm^{-2} s^{-1}), c) isoprene (10^{11} molecules cm^{-2} s^{-1}), and d) NO_x family (10^{11} molecules cm^{-2} s^{-1}).

deposition, and turbulence are resolved using an operator splitting procedure. However, because of the controlling role of dry deposition, emissions and turbulence for a selection of trace gases under specific conditions we have removed the operator splitting and resolve the coupled differential equations of the vegetation model with a non-iterative implicit Eulerian Backward Integration solver.

Since we are particularly interested in studying the sensitivity of the chemistry calculations for the timestep we have only considered turbulent transport, dry deposition, emissions and gas phase chemistry. Convective transport and aqueous phase chemistry have been ignored due to the sensitivity of cloud processes to the timestep and we use fixed nocturnal and daytime vertical profiles of the eddy-diffusivity. Figures 4.2a, b, c and d show the calculated Rn, O_3, C_5H_8 and NO_x canopy top flux for a tropical rainforest for one day, distinguishing the crown and canopy-soil layer, and using a timestep of 10 seconds, 15 and 30 minutes. For Rn, largest differences in the canopy top flux occur shortly after sunrise at the onset of turbulent mixing. This can largely be explained by the representation of the transition of the stable nocturnal to the unstable daytime mixing regime by the semi-implicit algorithm for turbulent exchange of RACMO and ECHAM [*DKRZ*, 1992]. Figure 4.2b shows a significant reduction of the canopy top flux of O_3 of about 40% for the 30-minute model integration compared to the 10-second model integration. Applying the sub-timestep (hereafter referred to as STS) increases the downward flux but does not remove the bias. The underestimation of the canopy top flux is due to a limited downward transport of O_3 from the PBL to the surface layer. Reducing the timestep of RACMO from 30 to 15 minutes shows a significant increase of the O_3 canopy top flux with a maximum noon deposition flux which deviates less than

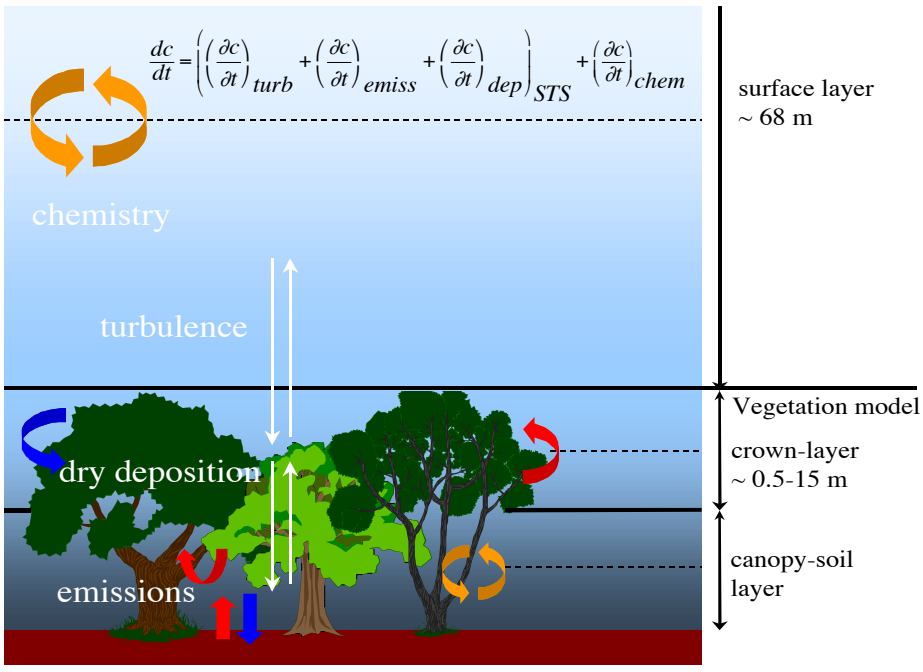

Figure 4.3: Implementation of the 2-layer vegetation model in RACMO (and ECHAM), with a typical surface layer height of ~ 68 m. The contribution of biogenic emissions, dry deposition, and turbulence to the concentration changes at the reference height of the canopy layers and surface layer (dotted lines), are calculated using the STS, whereas chemistry calculations use the timestep of RACMO (or ECHAM).

15% from the 10 second maximum flux of $3 \cdot 10^{11}$ molecules cm^{-2} s^{-1}. Figure 4.2c shows that the calculated isoprene canopy top fluxes are not very sensitive to the applied timestep. The afternoon C_5H_8 canopy top flux of the 30-minute timestep integration is about 15% larger compared to the 10-second model integration. Finally, in Figure 4.2d the comparison between the model resolved NO_x canopy top flux for the 10 second integration and the 30 minute integration is shown. For the 30-minute integration the NO_x canopy top fluxes with and without applying the STS are shown. There is good agreement between the model resolved NO_x canopy top flux for the 10-second integration and the 30-minute STS integration, whereas the NO_x canopy top flux for the non-STS integration is overestimated throughout the day. This is explained by an underestimation of the NO_2 dry deposition for the non-STS calculations. In addition, there is also good agreement between the modeled NO_x concentrations for the 10 second and 30 minute STS integration.
We conclude that a 2-layer version and a 30 minute timestep, considering sub timesteps in the coupled differential equations for turbulent transport, dry deposition and emissions of the EBI solver, is sufficient to resolve the canopy top fluxes for a selection of trace gases. This has been implemented in the single column model for a model evaluation that is presented in the next section. The implementation is shown in Figure 4.3, with the 2-layer vegetation model being used to calculate the canopy top fluxes for the vegetation and wet skin fraction. We emphasize that we only calculate trace gas concentrations and fluxes and do no consider the transfer of momentum, heat and moisture within the canopy. The thickness of the equidistant crown and canopy-soil layer ranges from 0.5 to about 15 m, dependent on the canopy height. We only consider canopy interactions for a canopy height larger than 1 m.

4.4 Model evaluation

4.4.1 Comparison between model and observations

We have evaluated the modeled trace gas fluxes and concentrations of the 2-layer vegetation model for three surface cover types; tropical rainforest in Brazil, deciduous forest in the northeastern USA and sub-arctic taiga woodland in Canada, for which detailed observations are available. Moreover, the sites reflect a rather wide range of meteorological and biogeochemical conditions which indicates the capability of the model to calculate the trace gas exchanges on a global scale. We largely focus on NO_x since we use the vegetation model to study the effect of the surface cover on NO_x emission fluxes on a global scale, as presented in Chapter 5. We have also compared the ozone fluxes since it provides valuable information concerning dry deposition, chemistry and vertical turbulent transport processes. Moreover, we have included the surface net radiation, energy partitioning and turbulence in our analysis since the representation of these processes will help explaining any disagreement between the calculated and observed concentrations and fluxes. The single column model has been initialized using ECHAM4 vertical profiles of wind speed, temperature, and moisture and surface properties for the grid cell that resemble the location of the measurement sites. Any adjustment of the modeled physical and dynamical processes, e.g., prescribing the surface net radiation or temperature, is minimized since it introduces inconsistencies between modeled processes. Adjustments that have been made in this work, to ensure a fair comparison between the model and the observations, are the optimization of the surface cover properties

and initial vertical profiles. Simulations have been performed for five days, which requires the use of a fixed geostrophic wind speed in the free troposphere.
The observations over the deciduous forest and taiga woodland indicate that the trace gas concentrations are influenced by the advection of polluted air from nearby antropogenic sources. Monthly average antropogenic emissions are considered in the model but these may differ substantially from the local influence of antropogenic emissions during the observations. In addition to the contribution of primary antropogenic emissions of NO_x, the O_3 surface layer concentrations are also controlled by advection of photochemically produced O_3 over the source regions. Therefore, we do not use the monthly mean antropogenic NO_x emission but have forced the model calculated O_3 and NO_2 surface layer concentrations towards the observed concentrations for the deciduous forest and taiga woodland sites. Actually, constraining the surface layer concentrations using observed concentrations can be interpreted as adding an advection term to the model. The observed O_3 and NO_2 concentrations show rather large fluctuations on a timescale of less than an hour. A sensitivity analysis indicates that in order to reproduce the observed concentration fluctuations a relaxation coefficient of $\sim 10^{-2}$ s^{-1} is required, which implies the use of a timestep shorter than 100 seconds. Moreover, since NO_2 or NO_y fluxes have been observed, and not of NO_x, the explicit calculation of the fluxes of individual species of the NO_x family is required, which can only be done for a timestep on the order of seconds. Therefore, we use a timestep of 10 seconds for the model evaluation instead of the 30 minute timestep of ECHAM, also since it is expected that the 10 second and 30 minute integrations yield rather similar calculated trace gas fluxes and concentrations, as has been shown in the previous section. To allow a model spin-up for the trace gases, the modeled concentrations starting at the second day are used for the evaluation.

Tropical rainforest, Brazil

For a comparison of the observed and modeled O_3 and NO_x canopy top fluxes and surface layer concentrations over tropical rainforest we have used observations collected during the ABLE-2B campaign, April and May 1987, near Manaus, Brazil [*Harriss et al*, 1990]. The observations at this site reflect a pristine atmospheric composition indicated by NO, O_3 and CO surface layer concentrations as low as 10 pptv, 6 ppbv and 80 ppbv respectively [*JW90*; and references therein]. Here we show a comparison of modeled fluxes and concentrations for a 5-day model integration starting at the 1st of May. Unfortunately, direct flux measurements are restricted to ozone. Fluxes of oxidized nitrogen have been derived using observed concentration gradients and prescribed vertical exchange velocities in a one-dimensional photochemical model [*JW90*]. These vertical exchange velocities have been derived from observed vertical concentration profiles and fluxes of O_3, Rn and CO_2 throughout the PBL and within the canopy. The canopy structure is defined by a complete vegetation cover expressed by a vegetation fraction of 1, an LAI of 7 and a canopy height of 30 m. The LAD profile reflects a vertical biomass distribution with the maximum amount of biomass in the canopy crown [*Fan et al.*, 1990]. A surface roughness of 2.35 m has been derived from the canopy characteristics according to *Raupach* [1994]. Modeled and observed micro-meteorological parameters for this site are presented in Table 4.1. The maximum model calculated net radiation (R_n) of about 450 W m^{-2} is smaller then the observed net radiation [*Fan et al.*, 1990, *Roberts et al.*, 1990]. This underestimation of net radiation is associated with a somewhat larger calculated cloud cover (CC) of about 0.9 compared to an observed CC of 0.7. The model reproduces the observed strong extinction of radiation within

Table 4.1: Comparison between modeled and observed micrometeorological parameters above and within tropical rainforest, Manaus, Brazil. The superscript (1) indicates a 5-day average maximum value for the simulation whereas (2) indicates a 5-day average value. Also indicated are the 5-day average ranges between the minimum nocturnal and maximum daytime values. For the modeled air temperature, wind speed and specific humidity the reference height within the surface layer is given between brackets.

	Model	**Measurements**
R_n [W m^{-2}]	450 (1)	~ 600
CC [0-1]	0.9 (2)	~0.7
H [W m^{-2}]	20 (1)	~200
T_{air} [K]	297 – 300 (32 m)	~296-301 (~39 m)
u [m s^{-1}]	0.5 – 2 (~39 m)	~1.5 – 2.5 (~39 m)
q [g kg^{-1}]	19 (~53 m)	15 (~39 m)

the canopy [*Shuttleworth et al.*, 1984], indicated by a fraction of leaves exposed to sunlight near the soil surface < 2%. According to the model nearly all the available energy at the surface is used for evapotranspiration, which results in the underestimation of the sensible heat flux (H) compared to observations [*Fitzjarrald and Moore*, 1990a]. It is beyond the scope of this study to address this misrepresentation of the energy partitioning of the tropical rainforest and we refer to a study by *Sellers et al.* [1989] for a more extensive discussion about this issue. Despite the misrepresentation of the surface energy balance, the model reproduces the observed diurnal cycle in the temperature above the canopy with a nocturnal minimum 2 meter temperature (T_{air}) of about 297 K and a maximum 2 meter temperature of about 300 K [*Fan et al.*, 1990, *Roberts et al.*, 1990]. The modeled wind speed (u) at the reference height of the observations, which is derived from the modeled surface layer wind speed using the logarithmic wind profile, is smaller than observed. The overestimation of the latent heat flux by the model is consistent with an overestimation of the surface layer specific humidity (q) of about 19 g kg^{-1} compared to an observed specific humidity of about 15 g kg^{-1} [*Fitzjarrald and Moore*, 1990a]. In summary, comparison of the calculated and observed micro-

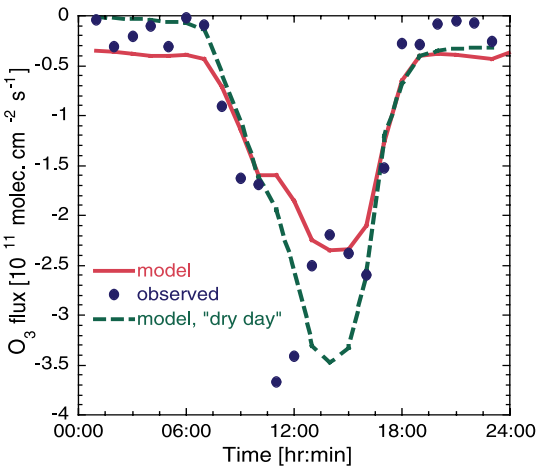

Figure 4.4: Comparison between the modeled 5-day average diurnal cycle in the canopy top O_3 flux (solid line) (10^{11} molecules cm^{-2} s^{-1}) and the average diurnal cycle in the observed O_3 canopy flux (dots) over tropical rain forest near Manaus, Brazil, during the ABLE-2B measurement campaign in April and May, 1987. The dashed line shows the modeled diurnal cycle in the O_3 canopy flux for the 1st of May.

meteorology for tropical rainforest suggests that there are significant discrepancies, which likely imposes a serious constraint on the interpretation of the trace gas exchanges.
Figure 4.4 shows the 5-day average diurnal cycle in the modeled and observed O_3 canopy top flux. The maximum modeled O_3 flux is smaller than the observed maximum flux of about $3.5 \cdot 10^{11}$ molecules cm^{-2} s^{-1} [*Fan et al.*, 1990]. The modeled nocturnal fluxes are about $0.4 \cdot 10^{11}$ molecules cm^{-2} s^{-1} and the maximum daytime downward (deposition) flux is about $2.5 \cdot 10^{11}$ molecules cm^{-2} s^{-1}. The underestimation of the O_3 canopy top flux reflects the overestimation of the modeled ozone surface layer concentrations of ~ 10 ppbv compared to the observed maximum daytime concentrations of about 7 ppbv. Further analysis shows that the underestimate of the O_3 canopy top flux is caused by a too small calculated O_3 dry deposition velocity compared to the observations [*Fan et al.*, 1990]. This is mainly due to a significant fraction of wet vegetation in the model (the so-called wet skin fraction) from convective rainfall interception. It is assumed in our dry deposition model that uptake by a wet canopy is relatively small due to a small removal rate by the wet cuticle whereas stomatal exchange stops due to the covering of leaf stomata [*Wesely,* 1989]. The observed diurnal cycle in the ozone dry deposition flux and velocity reflects the exchange regime for dry conditions [*Fan et al.*, 1990]. The modeled fraction of wet vegetation increases throughout the five days from a daytime average of about 0.2 during the first two days to more than 0.6 at the 5th of May. The modeled O_3 canopy top flux for the 1thof May, shown in Figure 4.4 by the dashed line, agrees better with the observations. The maximum modeled O_3 dry deposition velocity for the 1st of May of about 2 cm s^{-1} compares well with the observed maximum O_3 dry deposition velocity [*Fan et al.*, 1990]. Despite the relatively large canopy top fluxes for the dry compared to the wet days, the difference in the daily average surface layer concentrations during the 5-day integration is small. The modeled daytime concentration of about 10 ppbv in the surface layer is also controlled by the downward convective transport of about 1 ppbv/hr of ozone to the surface layer. Simulations without considering the convective transport yield surface layer concentrations low as 6 ppbv in the afternoon, which agrees well with the observed surface layer concentrations. This suggests that the downward convective transport of O_3 is overestimated by the model. The nocturnal decrease in the O_3 surface layer concentrations is reproduced by the model. However, the observations show a rapid decrease shortly after sunset from 6 ppbv down to about 3 ppbv, whereas a slower but continuous depletion of the modeled nocturnal O_3 concentration takes place throughout the night. Observations of nocturnal O_3 dry deposition velocities by *Fan et al.* [1990] are as large as 0.5 cm s^{-1}. These relatively large removal rates are likely related to the observed nocturnal exchange events between the surface layer and the canopy [*Fitzjarrald and Moore*, 1990b]. Moreover, the nocturnal O_3 flux is

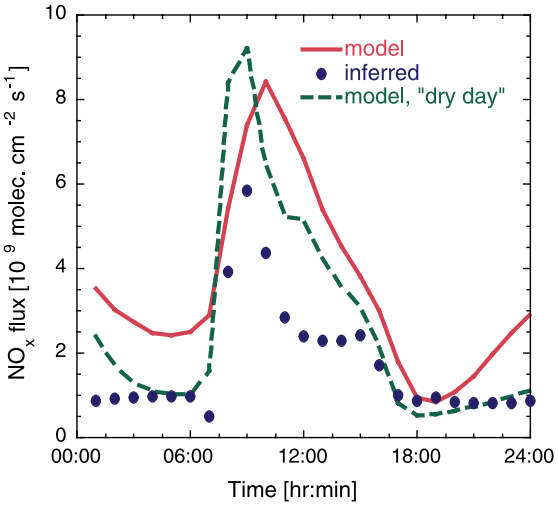

Figure 4.5: As Figure 4.4 but then for NO_x (10^9 molecules cm^{-2} s^{-1}). The NO_x flux has been derived from the observed concentration profiles and estimated eddy-diffusivities.

expected to be modified by reactions with NO emitted by the soil [*Bakwin et al.*, 1990]. It remains an open question if the intermittent nocturnal turbulent exchange or other mechanisms, e.g., chemical destruction by NO, are responsible for the observed rapid decrease after sunset. Since the soil emission algorithm is constrained by the observed NO emission flux of $8.9 \cdot 10^9$ molecules cm^{-2} s^{-1} [*Bakwin et al.*, 1990], we only show in Figure 4.5 the modeled diurnal cycle of the canopy top NO_x fluxes and the inferred flux by *JW90*. The presence of a wet canopy also leads to a large overestimation of the canopy top NO_x fluxes compared to the estimate by the *JW90* model. There is reasonable agreement between the inferred and modeled NO_x fluxes for the 1st of May, although the modeled afternoon fluxes are still larger compared to the derived NO_x fluxes. The modeled nocturnal canopy top flux of about $1 \cdot 10^9$ molecules cm^{-2} s^{-1} on the 1st of May is similar to the inferred flux, whereas the 5-day average modeled nocturnal flux is $3 \cdot 10^9$ molecules cm^{-2} s^{-1}. Differences in the nocturnal exchange fluxes determine the early morning burst of NO_x into the surface layer due to its accumulation within the canopy during the night. The observations show a nocturnal NO accumulation within the canopy from about 200 up to 500 pptv, and the maximum concentration exceeds 1 ppbv close to the soil surface in the early morning at the onset of turbulent exchange between the canopy and the surface layer [*Bakwin et al.*, 1990]. In Figure 4.6 the 5-day average modeled diurnal cycle in the NO concentration of the canopy-soil layer (7.5 m) is shown versus the observed concentrations at 6 m. The modeled average nocturnal NO concentrations are significantly higher compared to the observations of about 400 pptv. This is partly explained by an underestimation of the nocturnal turbulent exchange between the canopy-soil and the crown layer, indicated by an underestimation of the modeled nocturnal NO concentration in the crown layer of about 100 pptv. Unfortunately there are no observations of NO_2, which would provide information about the chemical conversion of NO to NO_2. The average modeled nocturnal O_3 concentrations of the canopy-soil layer are similar to the observed concentrations at 6 m, about 500 pptv, which indicates that in addition to chemical destruction of NO another sink of NO may be present in the lower canopy, e.g., dry deposition of NO. However, the 5-day modeled O_3 concentration shows that during the first two days the nocturnal concentrations of the canopy-soil layer are nearly zero, so that NO accumulates up to 2 ppbv. For the last three days the nocturnal O_3 concentrations are larger, resulting in modeled NO concentrations of about 500 pptv, in good agreement with the observed concentrations. The differences in the modeled nocturnal O_3 concentrations are related to a decrease in the nocturnal dry deposition velocity as a result of an increase in the wet skin

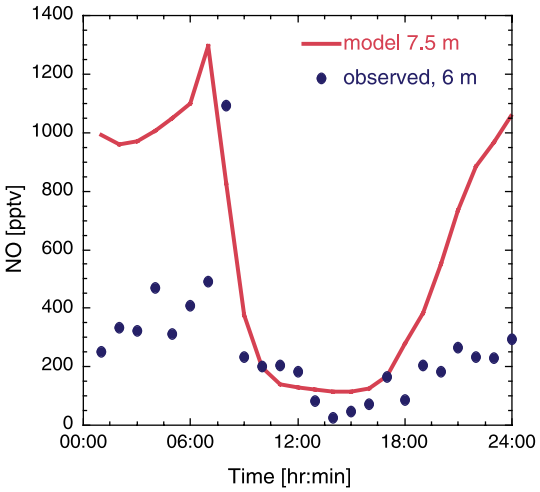

Figure 4.6: Comparison between the modeled 5-day average diurnal cycle in the canopy-soil NO concentration at 7.5 m (solid line) (pptv) and the average diurnal cycle in the observed NO concentration (dots) at 6 m within a tropical rain forest.

fraction. This underscores the sensitivity of nocturnal NO_x concentrations and fluxes to dry deposition associated with small vertical turbulent exchange between the canopy layers during the night.

Deciduous forest, northeastern USA

Munger et al. [1996, hereafter *M96*] present micro-meteorological and trace gas exchange measurements from 8-13 September 1992 over a mixed deciduous forest. During the first three days the wind was from the south-west, bringing in warm, moist and polluted air, indicated by observed NO_x and O_3 surface layer concentrations high as 6 and 70 ppbv, respectively. During the last two days a significant decrease in temperature, humidity and O_3 and NO_x concentrations occurs, related to a change to a northerly wind direction. The LAI is about 3.4 and the canopy height is 24 m. A vegetation fraction of 1 has been applied and the surface roughness, calculated from the LAI and canopy height, according to *Raupach* [1994], is 2.6 m.

The modeled stomatal resistances are relatively large, applying the initial ECHAM soil wetness since the soil moisture level is close to the permanent wilting point. Unfortunately, no soil moisture measurements have been reported by *M96*. However, it was concluded that the trees at the measurement site were able to access deep soil moisture and not dependent on local rainfall [*J. W. Munger*, personal communication, 1999]. This is confirmed by the observed maximum latent heat flux of about 500 W m^{-2} for a maximum net radiation of about 625 W m^{-2} [*M96*]. Because of the sensitivity of the modeled dry deposition to the soil moisture through the stomatal resistance, we have increased the initial soil moisture content to the field capacity. One additional model constraint is that we have nudged the O_3 and NO_2 surface layer concentrations using the observed concentrations to mimic advection from nearby sources during the 8^{th} and 9^{th} of September. Comparison between the observed and modeled parameters is presented here by showing the average diurnal cycles for the entire period.

Table 4.2: Comparison between modeled and observed micrometeorological parameters above and within a deciduous forest, central Massachusetts, USA. See Table 4.1 for the explanation of footnotes.

	Model	**Measurements**
R_n [W m^{-2}]	500 (1)	~ 550
LE [W m^{-2}]	440 (1)	~ 300
H [W m^{-2}]	25 (1)	~125
PAR 11 m/top [-]	~0.15	~0.25
T_{air} [K]	289 – 294 (26 m)	~287 - 294 (~28 m)
u [m s^{-1}]	1 – 2.5 (~28 m)	~1.8 – 2.7 (~28 m)
u_* [m s^{-1}]	0.2 - 0.6 (~58 m)	0.4 - 0.8 (~28 m)
q [g kg^{-1}]	11 - 13 (~ 58 m)	9 - 12 (~28 m)

Table 4.2 shows that the calculated maximum net surface radiation is somewhat smaller than that observed. The modeled latent heat flux (LE) is overestimated whereas the sensible heat flux (H) is underestimated. Comparison of the modeled and observed fraction of PAR at 11 m to surface layer PAR indicates reasonable agreement with a modeled fraction of about 0.15 versus an observed fraction of about 0.25 [*Moore et al.*, 1996]. The modeled 5-day average

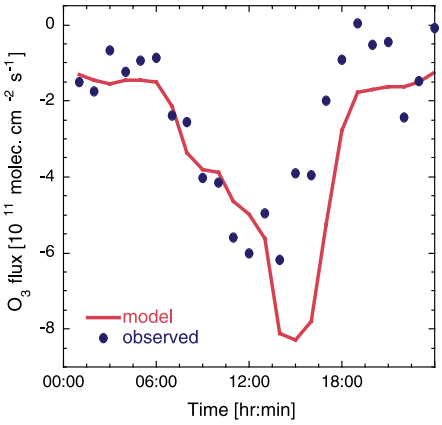

Figure 4.7: Comparison between the modeled 5-day average diurnal cycle of the canopy top O_3 flux (solid line) (10^{11} molecules cm^{-2} s^{-1}) and the average diurnal cycle in the observed O_3 canopy flux (dots) over a deciduous forest in Massachusetts, USA, from 8-13 September 1992.

air temperature agrees well with the observed temperature, both in absolute magnitude and the diurnal cycle. The modeled daytime friction velocity is somewhat smaller compared to the observations despite the good agreement for the daytime wind speed. During the night the modeled wind speed is smaller than observed, also reflected in a smaller modeled friction velocity. Finally, there is reasonable agreement between the modeled and observed specific humidity with a 5-day average of about 12 g kg^{-1}. It is concluded that the site micro-meteorology is fairly well reproduced by the model.

The comparison between the 5-day average modeled canopy top and observed O_3 flux at about 29 m is shown in Figure 4.7. The model agrees reasonably well with the observations, indicating nocturnal O_3 fluxes of about -1.5·10^{11} molecules cm^{-2} s^{-1}and maximum deposition fluxes in the afternoon of about -6·10^{11} molecules cm^{-2} s^{-1}. The model calculates a maximum deposition flux in the afternoon whereas the observed peak flux occurs around noon. The 5-day average diurnal cycle of the modeled dry deposition velocity shows an initial rapid increase in the early morning after sunrise to about 0.5 cm s^{-1}, followed by a small decrease before noon due to an increase in the wet skin fraction as a result of convective rainfall. In the afternoon the wet skin fraction decreases, reflected in an increase of the dry deposition velocity to a maximum of about 0.8 cm s^{-1}. This maximum modeled dry deposition velocity is about 0.2 cm s^{-1} larger than that reported by *M96*, which explains the overestimation of the maximum modeled O_3 canopy top flux. There are no observations of the NO soil emission flux. However, the calculated flux by the *YL95* algorithm is compared to the estimate by *M96*, who used a mass balance method and the observed vertical profiles of ozone and NO within the canopy. Their estimate of 15·10^{9} molecules cm^{-2} s^{-1}, representative of midsummer, is twice as large as our model average flux, based on an emission factor of 1.16·10^{9} molecules cm^{-2} s^{-1} for a wet soil for a woodland ecosystem according to *YL95*.

The comparison between the 5-day average diurnal cycle in the observed and the modeled

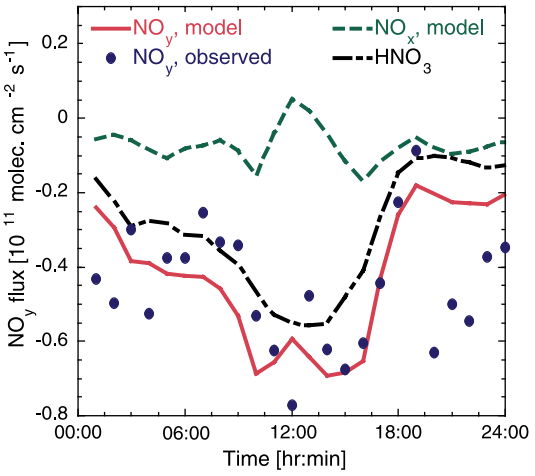

Figure 4.8: The modeled 5-day average diurnal cycle of the canopy top NO_y flux (solid line) (10^{11} molecules cm^{-2} s^{-1}) and the the observed canopy flux (dots) over a deciduous forest. Also shown are the modeled NO_x (dashed line) and HNO_3 flux (dot-dashed line).

NO_y (NO_x family + HNO_3 + PAN + MPAN + organic nitrate) flux is shown in Figure 4.8. The modeled daytime NO_y fluxes compare well to the observed fluxes of about $-0.6 \cdot 10^{11}$ molecules cm^{-2} s^{-1}. However, especially in the evening the modeled NO_y fluxes are significantly smaller compared to the observations. Figure 4.8 also shows the contribution of the NO_x and HNO_3 fluxes to the NO_y flux, indicating that it is largely controlled by the HNO_3 flux, whereas the NO_x flux is smaller then $-0.15 \cdot 10^{11}$ molecules cm^{-2} s^{-1}. The modeled average nocturnal NO_x canopy top flux is downward, being comparable to the soil biogenic emission flux whereas there is an upward daytime NO_x canopy top flux of about half the soil emission flux. The nocturnal NO_x canopy top flux is controlled by dry deposition of NO_2, whereas during daytime there is an upward NO_2 and NO_x flux due the chemical production of NO_2 within the canopy. The fact that the NO_y flux is controlled by the HNO_3 flux explains the large variability in the 5-day average observed NO_y fluxes, since the HNO_3 canopy top flux is controlled by turbulent exchange. The explanation for the underestimation of the nocturnal NO_y flux is therefore related to a misrepresentation of the nocturnal turbulent exchange. The 5-day average modeled and observed friction velocity agree reasonable well for the late night and daytime. However, the modeled friction velocity in the evening and early night is significantly smaller than observed, which suggests that the modeled growth of the nocturnal inversion is too fast. The underestimation of the turbulent exchange in the evening is also reflected in the comparison of the modeled and observed NO concentrations of the canopy-soil layer, shown in Figure 4.9. The modeled nocturnal NO concentrations at 6 m are about 100 pptv compared to observed concentrations at 6 m (derived from 4.5 and 7.5 m concentrations) of about 20 pptv. In addition to a too small nocturnal turbulent exchange, the fact that we do not consider dry deposition of NO may explain the overestimation. Underestimation of the chemical destruction is not likely the cause of the overestimation since nocturnal O_3 concentrations are as large as 10 ppbv. There is reasonable agreement between the modeled and observed surface layer concentrations with maximum concentrations up to about 500 pptv in the early morning due to the photo-dissociation of NO_2. The modeled NO_2 concentrations in the canopy, not shown here, are in good agreement with the observations. The maximum concentration is about 3 ppbv around midnight, after which there is a decrease to about 2 ppbv in the early morning, reaching minimum concentrations of about 700 pptv around noon.

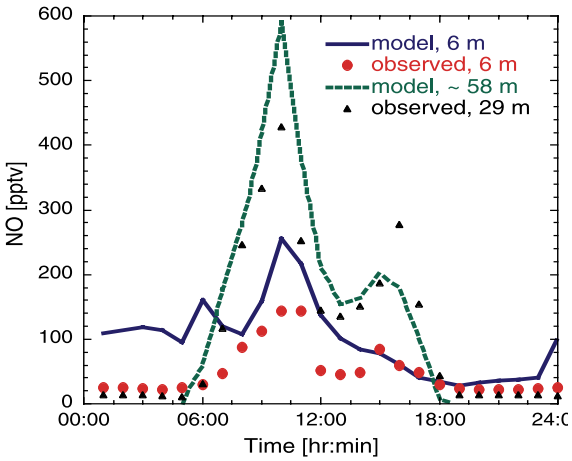

Figure 4.9: Comparison of the modeled 5-day average diurnal cycle of NO concentrations (pptv) of the canopy-soil layer (6 m) (solid line) and the surface layer (58 m) (dashed line) with the average diurnal cycle of the observed NO concentrations at 6 m within the canopy (dots), and 29 m above (triangles) a deciduous forest.

The comparison between the modeled and observed O_3 concentrations within the canopy, shown in Figure 4.10, again underscores the role of nocturnal turbulent exchange within the canopy. There is good agreement between the modeled and observed O_3 concentrations in the crown layer. However, especially during the night the modeled concentrations in the canopy-soil layer are about 10 ppbv smaller than observed. A striking feature is that largest

differences between the modeled and observed concentrations occur in the evening after which there is actually an increase in the modeled concentrations at night due to downward turbulent transport. Further analysis shows that relatively large destruction of ozone by dry deposition takes place after sunset, which is not balanced by turbulent transport. Maximum destruction rates up to 5 ppbv hr^{-1} are calculated, which explains the rather large decrease in the modeled O_3 canopy-soil concentrations. This highlights, in addition to the results for tropical rainforest, the sensitivity of the atmosphere-biosphere trace gas exchange to the nocturnal turbulent exchange. Moreover, it shows the sensitivity to the transition from day to night conditions by the timing of the de-coupling between the surface layer and the canopy, and significant changes in the other canopy processes such as dry deposition.

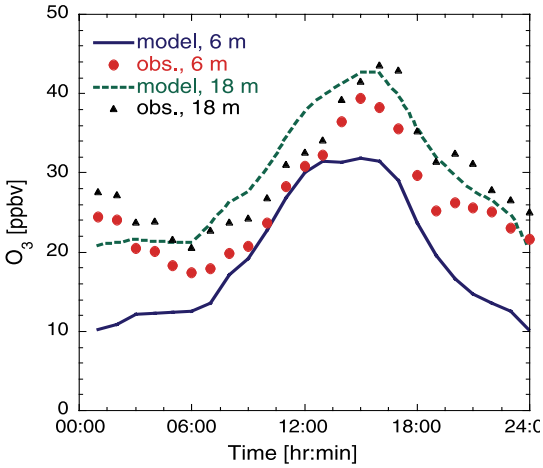

Figure 4.10: Comparison of the modeled 5-day average diurnal O_3 cycle (ppbv) of the canopy-soil layer (6 m) (solid line) and the crown layer (58 m) (dashed line) with the average diurnal cycle of the observed NO concentrations at 6 m (dots) and 18 m (triangles) within a deciduous forest.

Taiga, Canada

Observations of NO_y and O_3 concentrations and fluxes over a woodland in Canada have been made during June-August, 1990, as part of the Arctic Boundary Layer Expedition (ABLE-3B) [*Bakwin et. al.*, 1994; *M96*]. The vegetation type was a lichen woodland with an average canopy height of 6.5 m. The inferred LAI for this site in August is 3.3. We have applied a surface roughness of 0.45 m based on a inferred daytime surface roughness of 0.7 m and a nocturnal surface roughness of 0.2 m [*Fitzjarrald and Moore*, 1994]. The vegetation fraction of ECHAM of about 30% for this site is comparable to the canopy coverage calculated from the observed tree density of 616 stems/ha and an average crown basal diameter of 2 m [*Fitzjarrald and Moore*, 1994]. The remaining 70% of bare soil surface in the model is assumed to represent the surface cover properties of the lichen mat at the measurement site. Using the initial vertical profiles and surface properties derived from the ECHAM model yields a Bowen ratio (ratio of sensible to latent heat flux, β) of about 0.5 compared to an observed one of 2.5-3 [*Fitzjarrald and Moore,* 1994]. This underestimation of the modeled sensible heat flux is also clearly reflected in an underestimation of the calculated PBL height and surface layer temperature. The observed PBL height was about 2 km whereas the model resolved PBL reaches a maximum height of 750 m. Reducing the soil moisture by a factor of two (the initial soil moisture level is about 7 cm), improves the agreement between the calculated and observed evaporation, which is only 10% of the potential evaporation. *Fitzjarrald and Moore* [1994] hypothesize that a possible explanation for the relatively small evaporation is a soil water deficit. However, there are no observations of soil moisture to confirm this.

We have selected a 5-day period of observations starting at the 20th of July. The observed daily average air temperature for this 5-day period shows a steady increase from less then 278^0 K for the 20th of July up to about 289^0 K at the 24th of July. This transition can be

explained by changes in wind direction and wind speed. Since there is a large difference between the observed and our initial temperature and moisture profiles, we have modified the initial temperature profile such that the initial surface layer temperature resembles the observed air temperature and moisture at the start of the integration.
The comparison between modeled and observed micro-meteorological parameters using the modified initial vertical profiles and soil moisture for this site, and a derived July LAI of 3.8, is shown in Table 4.3. The 5-day average calculated maximum net surface radiation is about 50 W m^{-2} smaller than observed. The maximum modeled and observed sensible heat fluxes

Table 4.3: Comparison between modeled and observed micrometeorological parameters above and within a lichen woodland, Schefferville, Canada. See Table 4.1 for the explanation of footnotes. The Bowen ratio is the 5-day average daytime value**.**

	Model	**Measurements**
R_n [W m^{-2}]	400 (1)	450
H [W m^{-2}]	200 (1)	200
β [-]	2.9	2.5 - 3
T_{air} [K]	279 – 285 (~ 39 m)	280 - 286 (~ 30 m)
u [m s^{-1}]	3.3 – 5.3 (~ 30 m)	2.1 – 4.8 (~ 30 m)
u_* [m s^{-1}]	0.25 - 0.55 (~ 39 m)	0.1 - 0.45 (~ 30 m)

are about 200 W m^{-2}. The improved representation of the energy partitioning using the modified soil moisture is supported by the agreement between the calculated and observed average daytime Bowen ratio. The modeled 5-day average air temperature agrees well with the observations both in absolute magnitude and the diurnal cycle. The daily average increases from about 278 K on the 20th of July to 286° K on the 25th of July. The calculated and observed daytime wind speed and friction velocity agree reasonable well. However, the modeled nocturnal turbulent mixing is significantly larger compared to the observed turbulence, indicated by a modeled nocturnal friction velocity which is about 0.15 m s^{-1} larger than observed due to an overestimation of the nocturnal wind speed. In conclusion, similar to that over deciduous forest, the model reproduces the micro-meteorology over the taiga woodland fairly well, using the modified soil moisture, air temperature and moisture profiles.
A striking feature of the observed oxidized nitrogen concentrations is the small NO_x to NO_y ratio, which has been explained by a large production of PAN due to the presence of oxidation products of isoprene [*Bakwin et al.*, 1994, hereafter *B94*]. However, model calculations indicate that the maximum PAN concentrations do not exceed 125 pptv, whereas the observed NO_y concentrations reach 400 pptv. This suggests that NO_y mostly consists of other NO_y species such as HNO_3, reaching the site by advection and subsidence [*B94*]. Hence, the model surface layer NO_y and O_3 concentrations have been forced towards the observed concentrations. To distribute the additional NO_y over the contributing species, the observed ratio between NO_x and NO_y of about 0.2 [*B94*] has been used to adjust the NO_2 and HNO_3 surface layer concentrations.
Figure 4.11 shows the comparison between the 5-day average modeled and observed O_3 flux at about 30 m. Actually, since the surface of this site is not completely covered by vegetation, we show both the modeled canopy top flux and the surface flux. The latter reflects the contribution of the vegetation as well as the bare soil fraction in the trace gas flux and is

calculated from the vegetation and bare soil fraction of 30 % and 70 %, respectively, and the canopy top flux and bare soil dry deposition flux. There is good agreement between the calculated and observed daytime surface fluxes of O_3 with maximum values of about $-2 \cdot 10^{11}$ molecules cm^{-2} s^{-1}. The modeled nocturnal O_3 surface flux, however, is significantly larger than observed, which can be explained by the differences between the modeled and observed nocturnal turbulence intensity. The calculated canopy top flux reflects the exchange fluxes for a complete vegetation cover with the selected canopy characteristics. Hence, the differences between the canopy top flux and surface flux underscores the sensitivity of the resolved O_3 exchange flux to the selected initial fractions of surface cover. The calculated maximum O_3 dry deposition velocity of about 0.3 cm s^{-1} is comparable to that reported by *M96*.

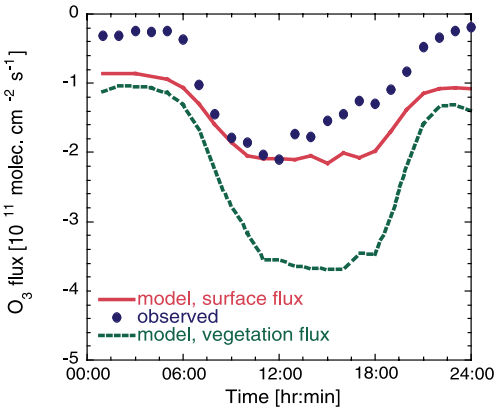

Figure 4.11: Comparison between the modeled 5-day average diurnal cycle of the O_3 surface flux (solid line) and the canopy top flux (dotted line) (10^{11} molecules cm^{-2} s^{-1}) and the average diurnal cycle of the observed O_3 flux (dots) over a taiga woodland, Schefferville, Canada, from the 20th until the 25th of July, 1992.

There are no observations of the NO soil emission flux, but it has been inferred using a similar approach as used for the Harvard forest site. The 5-day average modeled NO soil emission flux of about $0.4 \cdot 10^9$ molecules cm^{-2} s^{-1} is similar to the inferred flux for the woodland site between 0 and $1 \cdot 10^9$ molecules cm^{-2} s^{-1} [*M96*]. The comparison between the 5-day average diurnal cycle in the modeled and the observed NO_y flux is shown in Figure 4.12. The modeled daytime NO_y surface fluxes agree well with the observations of $-8 \cdot 10^9$ molecules cm^{-2} s^{-1}, whereas the modeled nocturnal NO_y fluxes are larger than observed due to the too strong turbulence intensity. The contribution of the NO_x and HNO_3 fluxes to NO_y is not shown here since NO_x fluxes are as small as $-0.1 \cdot 10^9$ molecules cm^{-2} s^{-1}, which indicates that also for this site the NO_y fluxes are controlled by HNO_3. Since there are distinct differences in the deposition velocities of the different species of NO_y, e.g., HNO_3 and PAN, the agreement between the modeled and observed NO_y fluxes supports the assumption that the advected NO_y basically consists of HNO_3. The daily average downward NO_x canopy top flux of about half the soil biogenic emission flux reflects the NO_2 deposition flux, whereas the daily average NO surface flux is negligible.

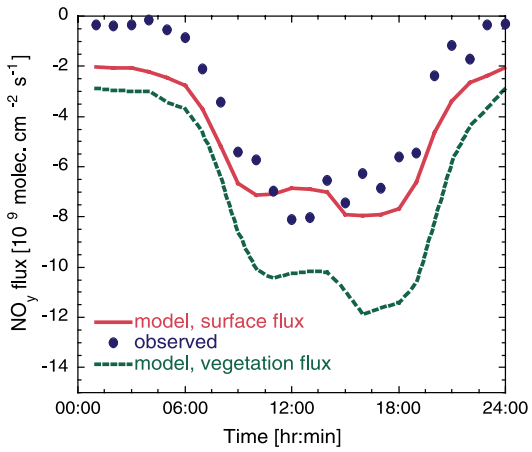

Figure 4.12: As Figure 4.11 but for NO_y.

Evaluation of the modeled concentrations within the canopy is not straightforward since the modeled within-canopy concentrations reflect a fully covered woodland canopy, whereas the observations reflect the concentrations of the canopy environment and the open space between the trees dependent on the mixing conditions. Therefore, we have performed one

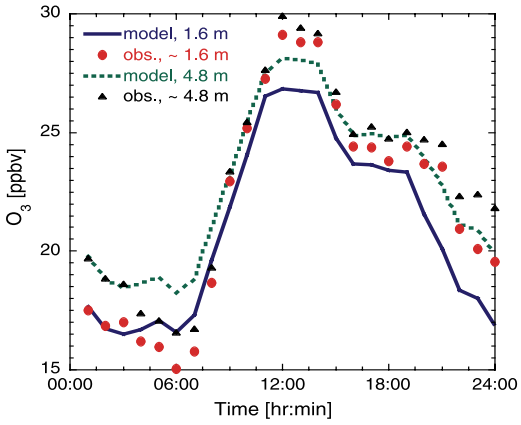

Figure 4.13: Comparison of the modeled 5-day average diurnal O_3 cycle (ppbv) of the canopy-soil layer (1.6 m) (solid line) and the crown layer (4.8 m) (dashed line) with the average diurnal cycle of observed O_3 at ~ 1.6 m (dots) and ~ 4.8 m (triangles) within taiga woodland.

the observed surface ozone concentrations). Turbulent transport also controls the NO_2 concentrations within the canopy since these are comparable to the surface layer concentrations. Figure 4.14 shows reasonable agreement between the modeled and observed NO_2 concentrations with minimum calculated concentrations before sunrise of about 35 pptv, with a subsequent continuous increase to a maximum of about 65 pptv after sunset. The modeled daytime NO_2 concentrations are about 55 pptv, whereas the observed daytime NO_2 concentrations are about 40 pptv. This overestimation of the calculated vegetation and surface layer NO_2 concentrations is also reflected in the NO concentrations. The modeled maximum daytime NO concentrations is about 22 pptv compared to an observed concentration of about 8 pptv. Nocturnal NO concentrations are negligible, as reproduced by the model.

additional model integration using a vegetation fraction of 1 and a reduced LAI of 1.2 (derived from the 30 % vegetation fraction with an LAI of 3.8). The comparison of the modeled and observed concentrations of the canopy-soil and crown layer is shown in Figure 4.13. There is good agreement between modeled and observed nocturnal concentrations. Note that the 5-day hourly average observed concentrations in the afternoon are biased due to missing data for three of the five days. Therefore we have only sampled the calculated concentrations for those hours for which observations were available. The good agreement indicates that the vegetation concentrations are controlled by the downward turbulent transport of surface layer ozone (which has been adjusted using

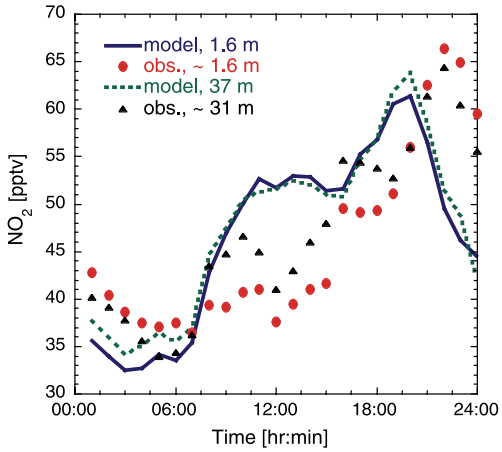

Figure 4.14: Comparison of the modeled 5-day average diurnal cycle of NO_2 concentrations (pptv) of the canopy-soil layer (1.6 m) (line) and the surface layer (~37 m) (dashed line) with the average diurnal cycle of observed NO_2 at ~ 1.6 m within the canopy (dots), and ~31 m above (triangles) a taiga woodland.

4.4.2 Biosphere model versus big leaf approach

The model evaluation has shown the ability of the biosphere model to reproduce the observed fluxes and concentrations for three different surface cover types. In this section, we compare

the modeled NO_x canopy top fluxes of the biosphere model with the net flux of the separate representation of emissions and dry deposition of the big leaf approach, for the same three sites and time of year. *YL95* introduced a first-order estimate of the decrease in the NO soil emission flux due to within-canopy chemical transformations and dry deposition, expressed by the daily averaged flux escape efficiency, or Canopy Reduction Factor (CRF). Their CRF is an ecosystem dependent parameter calculated from the LAI reflecting the uptake by the cuticle and the Stomatal Area Index (SAI) which represents the active absorption of NO_2 by the leaf stomata. To show the influence of using the CRF on the net fluxes of NO_x, the calculations for the big leaf approach have been done with and without the CRF. The simulations have been performed using the ECHAM timestep of 30 minutes and a monthly mean antropogenic NO_x emission flux, representative for the considered site. Soil emissions are explicitly calculated using the *YL95* algorithm. Figure 4.15 shows the modeled 5-day average diurnal cycle of the canopy top NO_x flux and the net emission and dry deposition flux by the big leaf approach (hereafter referred to as big leaf surface flux) for tropical rainforest. The *YL95* canopy reduction factor for tropical rainforest is about 0.25. The relatively small value of the CRF is reflected in the difference between the daily average NO_x flux calculated with the big leaf approach with and without this CRF of 1 and $5 \cdot 10^9$ molecules cm^{-2} s^{-1}, respectively. Clearly, using the CRF improves the description of NO_x exchange fluxes within the canopy compared to the uncorrected big leaf approach, however, discrepancies remain especially concerning the calculated diurnal cycle. The daytime NO_x flux calculated with the big leaf approach with the CRF is comparable to the NO_x flux of the biosphere model with an early morning dry deposition flux and an afternoon emission flux of about $1.5 \cdot 10^9$ molecules cm^{-2} s^{-1}. However, the nocturnal NO_x fluxes are very different with an emission flux of about $1 \cdot 10^9$ molecules cm^{-2} s^{-1} calculated with the big leaf approach, whereas the biosphere model calculates a small NO_x deposition flux. Further analysis indicates that the differences between the nocturnal big leaf and biosphere NO_x fluxes are basically due to relatively small differences between the modeled big leaf and biosphere dry deposition velocities. This shows again the sensitivity of the nocturnal trace gas exchange to the dry deposition process for suppressed turbulent exchange. There is a significant difference in the daily average fluxes of both approaches, indicated by a negligible daily average NO_x flux calculated with the biosphere model, whereas the daily average NO_x flux of the big leaf approach, using the CRF, is about $0.7 \cdot 10^9$ molecules cm^{-2} s^{-1}. However, the smaller canopy top flux of the biosphere model does not result in a smaller surface layer NO_x concentration. The calculated 5-day average NO_x surface layer concentration of the biosphere model of about 250 pptv is generally larger compared to the big leaf approach with maximum

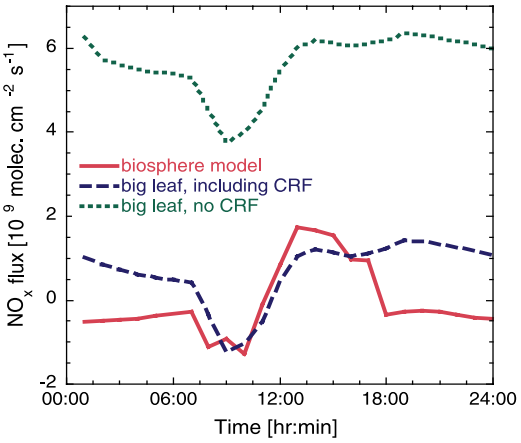

Figure 4.15: The modeled 5-day average diurnal cycle in the canopy top NO_x flux (solid line) (10^9 molecules cm^{-2} s^{-1}) and the net emission and dry deposition NO_x flux by the big leaf approach, with the CRF (dashed line) and without the CRF (dotted line), for tropical rain forest.

differences of about 200 pptv toward the end of the night. This can largely be explained by the decrease in the surface layer concentrations due to dry deposition for the big leaf approach, whereas in the biosphere model the removal by dry deposition occurs within the canopy. These results show that by explicitly considering the processes in the canopy, the canopy top NO_x flux from tropical rainforest is reduced. However, this does not necessarily imply that the surface layer concentrations are reduced as well. Figure 4.16 shows the modeled 5-day average diurnal cycle of the canopy top and big leaf surface NO_x flux for deciduous forest with an inferred canopy reduction factor of about 0.6. The NO_x flux for the big leaf approach, without the CRF, is not shown here since it is very similar to the flux calculated by the big leaf approach using the CRF. The canopy top NO_x flux is largely controlled by dry deposition of surface layer NO_x being supplied by an antropogenic NO_x emission flux in the surface layer of $1.9 \cdot 10^{11}$ molecules cm^{-2} s^{-1}, which is about a factor of 20 larger than the average biogenic NO emission flux. There is a small emission flux in early afternoon, with maximum fluxes of $-0.4 \cdot 10^{11}$ molecules cm^{-2} s^{-1} occurring in the early morning due to the dry deposition of NO_x that has accumulated in the surface layer during the night. The negligible early afternoon NO_x flux is related to a reduced dry deposition velocity due to the presence of a significant fraction of wet vegetation. Again, small differences between the big leaf and biosphere dry deposition velocities largely explain the differences between nocturnal NO_x deposition fluxes of the biosphere model and big leaf approach.

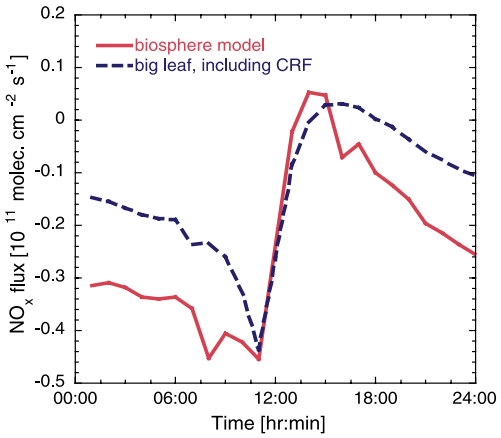

Figure 4.16: The modeled 5-day average diurnal cycle of the canopy top NO_x flux (solid line) (10^{11} molecules cm^{-2} s^{-1}) and the net emission and dry deposition NO_x flux of the big leaf approach with the CRF (dashed line) for deciduous forest.

Figure 4.17 shows the calculated 5-day average diurnal cycle of the vegetation model and big leaf surface flux of NO_x, with and without the CRF, for taiga woodland. The inferred CRF for this site is about 0.6 and the antropogenic NO_x emission flux for this site is $1.3 \cdot 10^9$ molecules cm^{-2} s^{-1} compared to a 5-day average soil biogenic emission flux of about $0.3 \cdot 10^9$ molecules cm^{-2} s^{-1}. The big

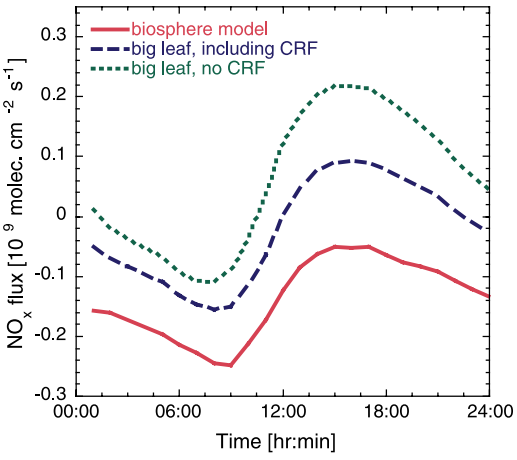

Figure 4.17: The modeled 5-day average diurnal cycle of the canopy top NO_x flux (solid line) (10^9 molecules cm^{-2} s^{-1}) and the net emission and dry deposition NO_x flux by the big leaf approach, with CRF (dashed line) and without the CRF (dotted line), for a taiga woodland.

leaf and biosphere surface flux show a similar diurnal cycle, but the big leaf surface flux is larger than the biosphere surface flux. This is also reflected in the daily average surface fluxes of both approaches with an average deposition flux of $-0.15 \cdot 10^9$ molecules cm^{-2} s^{-1} for the biosphere model and a negligible NO_x flux for the big leaf approach, with and without using the CRF.

It is concluded that for the deciduous forest, with NO_x concentrations being controlled by the continuous supply of NO_x by advection, the big leaf approach provides a reasonable estimate of the NO_x surface fluxes. Differences between calculated NO_x fluxes by the big leaf approach and the biosphere model are largely explained by differences in the dry deposition velocities and not by the canopy interactions. For the tropical rainforest and taiga woodland, where the NO_x burden is controlled by the biogenic emission, there are large differences in the calculated NO_x fluxes with the big leaf approach without using the CRF, and the biosphere model, both concerning the diurnal cycle and the daily average magnitude. The CRF by *YL95* provides a first-order estimate of the NO_x canopy flux divergence for the separate description of the emissions and dry deposition of the big leaf approach, which seems to be a realistic estimate for the tropical rainforest but it underestimates the flux divergence for the taiga woodland. However, the multi-layer vegetation model provides a mechanistic representation of canopy interactions between emissions and dry deposition and is preferred over the big leaf approach, including the CRF, to assess the role of these interactions for the NO_x flux divergence as an explicit function of the involved processes.

4.5 Discussion

The model comparison of the micro-meteorology and atmosphere-biosphere trace gas exchanges has provided important indications about the capability of the 2-layer vegetation and single column model to reproduce the site specific physical and chemical properties. The selected vertical grid resolution, distinguishing two equidistant layers has been based on a sensitivity study for the tropical rainforest. It has been shown that for this ecosystem the subdivision into a crown layer and a canopy-soil layer is sufficient to resolve the main features of atmosphere-biosphere trace gas exchanges of NO_x and O_3. However, this limited vertical resolution is strongly related to the relevant trace gases, the canopy structure and the degree of detail of the description of the processes involved. *JW90* distinguish three layers within the tropical rainforest canopy, the additional third one being a thin layer close to the soil surface. Their vertical grid spacing has been adjusted to resolve the observed vertical gradients of Rn, NO and O_3 and vertical distributions of biomass and stomatal resistances [*JW90*]. However, this specific information of the vertical distribution of bio-geophysical properties is generally not available for most of the ecosystems represented in large scale models.

The model evaluation indicates that the modeled canopy concentrations and canopy top fluxes are sensitive to turbulent transport. In our model, turbulent exchange between the canopy layers and surface layer is calculated using simple ‘K-theory’, and an improved representation should clearly have a high priority for further model development. The turbulent exchange between the canopy and the surface layer determines the residence time of the trace gases in the canopy with its profoundly different biogeochemical environment

compared to that of the surface layer. Any improvement in the description of the emissions, dry deposition and chemistry within the canopy is limited by the ability of the model to resolve the atmosphere-biosphere turbulent exchange. Using 'K-theory', or first-order closure, to calculate turbulent exchange from the eddy-diffusivity and concentration gradient implies that the turbulent exchange is considered to be a down-gradient diffusion process. However, it has been shown that counter-gradient transport occurs regularly, a phenomenon that can not be reproduced by 'K-theory'. This occurrence of counter-gradient transport is related to the fact that the turbulent exchange within the canopy is largely controlled by large scale intermittent down-sweeps originating in the overlying PBL [*Raupach and Thom*, 1981]. Thus the within canopy turbulent exchange is controlled by non-locally generated turbulent kinetic energy and, consequently, the local gradient does not necessarily reflect the magnitude and direction of the exchange fluxes. In addition to counter-gradient transfer, the intermittent character of canopy turbulence, associated with the occurrence of a small number of short exchange events that control the average turbulent exchange, is important for atmosphere-biosphere trace gas exchange. Intermittent turbulent exchange may lead to a vertical segregation of reactive trace gases within the canopy and the PBL during quiescent periods. Such periods are followed by bursts into the surface layer of canopy air containing gases from biogenic emissions or chemical production, e.g., NO and NO_2, and mixing into the canopy of trace gases that can subsequently be removed by dry deposition. The penetration depth of the down-sweeps into the canopy and the frequency at which these disturbances occur depend on the turbulent characteristics of the PBL. The intermittent turbulent exchange does not only occur during the daytime when convective conditions prevail but also during the nighttime. Observations *by Fitzjarrald and Moore* [1990b] underscore the role of nocturnal intermittent turbulent exchange for the CO_2, heat and moisture budgets above and within a tropical rainforest canopy.

It is expected that the temporal and spatial average trace gas concentrations and fluxes, considering the intermittent turbulent exchange, are different compared to that for conditions of continuous mixing between the atmosphere and the biosphere. This is caused by the spatial segregation of the reactive species which reduces the efficiency of second-order chemical reactions, which is expressed by the so-called intensity of segregation (I_s) [*Brodkey*, 1981]. *Patton et al.* [2000] have used a Large Eddy Simulation (LES) model to study the significance of the interactions between turbulence and chemistry within the canopy and surface layer by including multiple scalars that are emitted by the canopy and subjected to varying chemical destruction rates. The scalar source distribution and chemical destruction rates are selected to mimic the atmosphere-biosphere trace gas exchange of isoprene and the hydroxyl radical (OH). The study indicates that a maximum intensity of segregation of about 17% occurs at the canopy top, which decreases to about 5% at three times the canopy height. Based on the work by *Verver* [1999], *Petersen* [1999] and *Krol et al.* [2000], it is expected that by inclusion of the NO_x chemistry to the idealized second-order chemistry considered in the LES model the intensity of segregation for the isoprene-OH system will reduce [*Patton*, 2000].

It is beyond the capability of our model to present the turbulent exchange with the degree of detail compared to models that are specifically developed to study counter-gradient and intermittent turbulent exchange, such as higher-order closure models [*Meyers and Paw U*, 1987; *Meyers and Baldocchi*, 1991], Lagrangian models [*Raupach*, 1987; *Baldocchi*, 1992] or LES models [*Patton et al.*, 2000]. Rather, parameterizations that account for the non-local

and intermittent character of the turbulent exchange should be developed from the studies in which these models have been applied.
Besides ignoring the non-local and intermittent character of the turbulent exchange, an additional simplification in the representation of turbulent trace gas exchange is that stability effects within the canopy are not considered. The canopy stability often shows a different diurnal cycle compared to the surface layer stability. At night longwave radiative cooling results in a relatively colder canopy top compared to the soil surface, which induces unstable mixing conditions within the canopy. During daytime there is a canopy inversion due to the relatively warmer canopy compared to the soil. Observations of turbulence in a maize crop by *Jacobs et al.* [1992] indicate that during daytime, when the turbulent exchange is controlled by large scale motions, buoyancy effects within the canopy have little or no influence on canopy turbulence. However, the role of the canopy stability becomes relevant for that part of the canopy in which the exchange is not controlled by the large scale turbulent motions but rather by small scale diffusion. Observations by *Kruijt et al.* [2000] of the turbulent exchange of CO_2, heat and moisture in a tropical rainforest canopy indicate that especially the lower part of the canopy can be de-coupled from the crown layer and the atmosphere. Observed temperature gradients between the crown layer and the soil surface can be as large as 4 K. This thermal stratification suppresses turbulence in the lower part of the canopy since the large scale turbulent motions are unable to penetrate deeply into the canopy [*Kruijt et al.*, 2000]. During nights with low wind speeds and shear stress, the stability regime expressed by an unstable temperature profile in the canopy controls the nocturnal turbulent exchange, with an inversion layer at the canopy top isolating the canopy interior from the surface layer and PBL. The occurrence of these free convection conditions in the canopy have been observed for different vegetation types [*Jacobs et al.*, 1994; *Bosveld et al.*, 1999]. This is relevant for trace gas exchange in the canopy interior since it increases the efficiency of the nocturnal chemical conversion of gases such as NO and O_3 to NO_2, which can subsequently be removed by dry deposition. It is desirable to include an explicit calculation of the canopy temperature to consider the stability effect within the canopy on turbulent mixing for those conditions for which it is expected that the canopy turbulence is controlled by small scale motions. Introduction of a canopy temperature is also relevant for other processes. For the calculation of hydrocarbon emissions and the chemical transformations within the canopy we have applied the skin temperature of the single column model. This skin temperature reflects the average temperature of the soil and the vegetation. It has been mentioned previously that substantial temperature differences within the canopy can exist, which are significant for hydrocarbon emissions and chemical transformations. Since the hydrocarbon emissions are concentrated in the canopy top due to the optimal conditions in terms of biomass and radiation intensity, the temperature for this reference height should be used.

The model evaluation for the tropical rainforest and deciduous forest sites shows the relevance of changes in surface cover properties due to rainfall and the consequent increase in the wet skin fraction. The surface can also become wet due the formation of dew. Since in our model it is assumed that the dry deposition velocities to wet and dry surfaces are generally different, dependent on the solubility of the trace gas, a sudden increase in the wet skin fraction induces significant changes in the modeled canopy top fluxes. This complicates the model evaluation by comparison with measurements. The uptake or release of trace gases by wet canopies is a process which is not well understood, basically due to the limited number of observations and the complex mechanism that controls the uptake. Several studies

have focussed on the role of canopy wetness for the "dry" deposition of sulfur dioxide indicating that the deposition strongly depends on whether the surface is wetted by rain or dew [*Baldocchi*, 1992; and references therein]. This is related to a different acidity and chemical composition of rain and dew water. This is actually also relevant for other species since the uptake of gases that are not very soluble, e.g., ozone, can be enhanced due to aqueous phase chemistry such as the oxidation of SO_2 by O_3 [*Wesely*, 1990]. Observations of ozone dry deposition fluxes over a deciduous forest by *Fuentes et al.* [1992] show that there is still significant uptake of ozone by a wet canopy due to the formation of dew or rainfall. This is at variance with the assumptions made in many deposition models [*Fuentes et al.*, 1992; and references therein] and also our model. In future, the significance of the uptake by wet foliage will be studied more extensively. Nevertheless, the complexity of the uptake mechanism by a wet foliage requires the development of parameterizations that account for this process, which relies on additional measurements of the uptake by wet canopies.

4.6 Conclusions

We have developed a two-layer vegetation model to describe atmosphere-biosphere trace gas exchanges in large scale models. The main focus has been the exchange of O_3, NO_x, and NO_y for relative pristine as well as polluted conditions. Our model evaluation indicates that a two-layer representation of the biosphere can reproduce the main features of atmosphere-biosphere trace gas exchanges for different canopy structures exposed to different climatological conditions and trace gas concentrations. The results are very sensitive to the selected initial vertical profiles and surface cover properties. By adjustment of the initial vertical profiles and surface properties, the agreement between the modeled and observed meteorology is significantly improved although discrepancies remain, especially concerning the surface energy partitioning. To ensure a realistic representation of the local micro-meteorology, future model evaluations could be performed using high-resolution weather prediction models to constrain the single column model.

We generally obtain good agreement between the modeled and observed daytime canopy top ozone fluxes, which suggests that dry deposition and turbulent exchange are realistically described. However, the evaluation of the nocturnal canopy trace gas concentrations and fluxes emphasizes the sensitivity of atmosphere-biosphere trace gas exchange to the nocturnal turbulent exchange. Therefore, future research should address the role of nocturnal free convection conditions within the canopy interior and intermittent exchange for atmosphere-biosphere trace gas exchange. We generally obtain reasonable agreement between the modeled and observed oxidized nitrogen concentrations and canopy top fluxes. At the deciduous forest and taiga woodland site, the canopy top fluxes of oxidized nitrogen are controlled by the deposition of NO_y due to the significantly larger source of NO_y by advection from source regions compared to the soil biogenic source. Even for a relatively high NO_x to NO_y ratio, the NO_y fluxes are largely controlled by the HNO_3 deposition fluxes due to its large deposition velocity relative to NO_x.

For sites that are exposed to relatively large antropogenic emission fluxes compared to the soil biogenic emission flux, the big leaf approach and biosphere model calculate similar NO_x fluxes, which confirms the validity of using the big leaf approach for polluted regions. However, for relative pristine sites such as the tropical rainforest, there are distinct differences between the NO_x canopy top flux of the biosphere model and surface flux by the

big leaf approach, both in terms of the diurnal cycle and the daily average absolute magnitude. The canopy reduction factor by *YL95* provides a first-order estimate of the reduction of the soil emissions of NO_x due to the canopy interactions. We have compared the applicability of the CRF by comparison of the NO_x fluxes calculated by the big leaf approach, using the CRF and the biosphere model for three ecosystems. Using the CRF does not change the calculated surface flux of NO_x over deciduous forest due to the aforementioned controlling role of the antropogenic emission fluxes. For the tropical rainforest and taiga woodland, where the NO_x concentrations are largely controlled by the biogenic emission, there are significant differences between NO_x fluxes calculated with the big leaf approach and the biosphere model, both concerning the diurnal cycle and the daily average magnitude. However, firm conclusions about the applicability of the CRF on a larger spatial and temporal scale can not be drawn from this analysis. Therefore, our analysis is extended to a larger selection of ecosystems by performing this comparison on a global scale using the chemistry-GCM ECHAM, presented in Chapter 5.

Chapter 5

Global soil-biogenic NO_x emissions and the role of canopy processes[1]

Soils are an important source of oxidized nitrogen to the atmosphere. Global inventories of the soil biogenic NO_x emissions show a large range between 4 and 21 Tg N/yr. One of the uncertainties in the emission inventories is the role of the canopy interactions between emissions, dry deposition, turbulence and chemistry. Previous studies, that only consider the role of dry deposition in terms of a Canopy Reduction Factor (CRF), indicate a reduction of about 50% of the globally emitted NO_x by soils. We have implemented a multi-layer trace gas exchange model in the chemistry-GCM ECHAM, to explicitly calculate the role of canopy interactions in regulating the effective NO_x emissions into the atmosphere. Moreover, algorithms for the on-line calculations of soil-biogenic NO_x emissions and isoprene emissions by the vegetation have been implemented. Our new NO_x emission algorithm calculates a global soil emission flux of about 12 Tg/yr, which is comparable to previous estimates. For comparison, we have also included a global soil NO_x emissions inventory of about 21 Tg/yr. The sensitivity of the calculated surface layer NO_x and O_3 concentrations to the soil emission flux has diminished due to the compensating effect of enhanced dry deposition. For sites that are exposed to relatively large emission fluxes, the multi-layer and the previously used big leaf model, which does not consider canopy interactions, calculate similar surface NO_x fluxes. This confirms the validity of the big leaf approach for polluted regions. However, for relatively pristine sites in the subtropics and tropics, there are distinct differences between the multi-layer and big leaf NO_x surface fluxes. Use of the CRF to account for the reduction of the annual soil NO emission flux on a global scale seems feasible. However, comparison of the NO_x surface fluxes calculated with the multi-layer and the big leaf model, including the CRF, shows that there are distinct differences between the surface fluxes for specific ecosystems, e.g., tropical forest. Despite the many uncertainties involved, the implementation of the multi-layer model in ECHAM provides a mechanistic representation of the canopy interactions, which can used to further explore the role of flux divergence of reactive trace gases on a global scale.

[1] Submitted to the *Journal of Geophysical Research*, with J. Lelieveld, F. Dentener, M. Krol, L. Bouwman, and G.-J. Roelofs as co-authors

5.1 Introduction

The oxidized nitrogen species nitric oxide (NO) and nitrogen dioxide (NO_2) play an important role in tropospheric chemistry. They regulate the photochemical production of ozone and the abundance of the hydroxyl radical (OH), which is the main oxidant of the atmosphere. Another crucial role of reactive nitrogen is related to the biogeochemical cycling of nutrients due to its potential role in regulating the Net Primary Production (NPP) in a future enhanced carbon dioxide climate [*Holland et al.*, 1997]. On the other hand, a too large loading of the soils with oxidized nitrogen (and other acids) due to dry and wet deposition fluxes of species such as nitric acid (HNO_3), has resulted in the acidification of ecosystems located within or nearby densely populated areas [*Bouwman and Van Vuuren*, 1999; *Erisman and de Vries*, 2000].

Soils are an important source of atmospheric oxidized nitrogen due to the microbial production of nitric oxide, depending on biogeophysical and chemical properties of the soil, e.g., soil porosity, soil water content, temperature and the nutrient status. The emitted NO is rapidly oxidized to NO_2 (within minutes), resulting in an net upward or emission flux of NO_x ($NO+NO_2$). Previous studies of the global NO_x budget indicate that soil-biogenic NO_x emissions play a crucial role in the tropospheric chemistry in remote and rural areas. The estimated global annual fossil fuel source of > 20 Tg N/yr [*Logan*, 1983; *Hamied and Dignon*, 1988; *Levy and Moxim*, 1989] dominates the NO_x budget in industrialized areas. The inventories of the soil biogenic NO_x emissions show a large range between 4 and 21 Tg N/yr [*Yienger and Levy*, 1995; *Potter et al., 1996*; *Davidson and Kingerlee*, 1997; and references therein]. *Davidson and Kingerlee* [1997] (hereafter referred to as *DK97*) estimate the uncertainty of the global source estimate to be at least ± 4 Tg N/yr and perhaps as large as ± 10 Tg N/yr. Their review of a large selection of measurements of biogenic NO emissions, shows a large range in observed soil fluxes for different ecosystems. Due to the large heterogeneity of the soil-plant system, observations of the soil-biogenic NO_x emission fluxes are difficult to extrapolate to the horizontal resolution of global scale databases, which only crudely represent the controlling parameters for the soil biogenic emissions. This extrapolation is nevertheless required to assess the role of the different processes in the global NO_x budget and tropospheric photochemistry. One major constraint of the interpretation of the observed NO_x soil emission fluxes is the reference height at which the NO_x fluxes have been observed. Closed chamber techniques are considered to be representative for the “true” soil emission flux, whereas observations over the canopy do not only reflect the soil emission fluxes but also the role of within-canopy processes, e.g., the local removal by dry deposition and chemical transformations. Actually, above canopy flux measurements represent the canopy top flux which can be interpreted as the effective NO_x emission flux and surface boundary condition for large scale models that do not consider the biogeochemical canopy interactions.

Yienger and Levy [1995] (hereafter referred to as *YL95*) used a rather pragmatic approach to arrive at a global biogenic NO_x soil emission inventory. They used an empirical model, which accounts for temperature and precipitation effects and the application of nitrogen containing fertilizers. They introduced a first-order estimate of within-canopy interactions expressed by the Canopy Reduction Factor (CRF). The *YL95* CRF is an ecosystem dependent parameter calculated from the amount of biomass, expressed by the Leaf Area Index (LAI) and the Stomatal Area Index (SAI) to represent the uptake by the leaf cuticle and stomata,

respectively. *YL95* state that the CRF is not entirely physically based since the modification of the soil emission flux is not only a function of the stomatal uptake and cuticular absorption, but also controlled by vertical turbulent exchange and chemical transformations. However, the applied CRF contains an implicit dependency on vertical turbulent exchange since this exchange is partly controlled by the amount of biomass. The study by *YL95* indicates use of the CRF results in reduction of about 50% of the globally emitted NO_x by soils. Despite the large uncertainty associated with their approach, it clearly shows the importance of a realistic representation of the within-canopy interactions in global NO_x emission inventories. The CRF of YL95 is based on a study of the exchange of reactive nitrogen over the Amazon tropical rainforest during the wet season by *Jacob and Wofsy* [1990]. This study indicated that the canopy top flux of tropical rainforest is only about 20% of the soil emission flux. A study by *Gao and Wesely* [1993] of the atmosphere-biosphere exchange of reactive trace gases over and within a deciduous forest canopy even shows a downward canopy top flux, despite the presence of a significant soil emission flux. This large flux divergence within the canopy (applying a constant NO_x concentration at the top of the Planetary Boundary Layer (PBL) of 0.5 ppbv) could largely be explained by the combined effect of the dry deposition and chemical transformations within the canopy [*Gao and Wesely*, 1993]

In this study we assess the impact of a realistic representation of the flux divergence of NO_x within the canopy on the global distribution of reactive trace gases. We have implemented an atmosphere-biosphere trace gas exchange model, described and evaluated in Chapter 4, in the global chemistry and General Circulation Model (GCM) ECHAM (European Centre Hamburg model). The atmosphere-biosphere trace gas exchange model distinguishes two equidistant canopy layers, a crown and canopy-soil layer, and calculates the contribution of biogenic emissions, dry deposition, and turbulence to the concentration changes within the canopy and surface layer. Calculations of emissions, dry deposition, and turbulence are performed using a sub-timestep, which is determined from the turbulent and dry deposition timescale, to account for the short timescales of the processes involved for relative thin canopy layers. Chemistry calculations are performed using the ECHAM timestep and consider the extinction of radiation within the canopy for the photodissociation calculations. The grid square surface flux consists of the canopy-top fluxes calculated for the vegetation and wet skin fraction, and the net emission and dry deposition flux of the other surface cover fractions

An important element of the photochemistry is the role of non-methane hydrocarbons (NMHC), e.g., isoprene, in the production/destruction of ozone. ECHAM has therefore been extended with a higher hydrocarbon chemistry scheme, which is presented in more detail in section 5.2. In addition to the multi-layer vegetation model, we have implemented the *YL95* algorithm and the isoprene emission algorithm described by *Guenther et al.* [1995] in ECHAM to perform on-line calculations of the NO_x and isoprene emission fluxes, consistent with the model meteorology and surface cover properties. Details of the biogenic nitrogen and isoprene emission algorithms are presented in section 5.3. The importance of the NO_x canopy flux divergence, both in terms of its absolute long-term average magnitude and the short-term trace gas concentrations and budgets on the global scale, is discussed in section 5.4. A discussion of the uncertainties involved in the calculations of canopy interactions is presented in section 5.5, while section 5.6 presents the conclusions.

5.2 The chemistry-GCM ECHAM

We used the T30 horizontal resolution of the general circulation model ECHAM4 [*Roeckner et al.*, 1996], corresponding with a grid size of about 3.75 degrees and a timestep of 30 minutes. For more details concerning the used ECHAM version we refer to Chapter 3. The chemistry-GCM ECHAM [*Roelofs and Lelieveld*, 1995, 1997], as presented in Chapter 2 and 3, has been extended to consider the role of the NMHC chemistry for the ozone production/destruction [*Roelofs and Lelieveld*, 2000]. The chemistry scheme calculates the concentrations of CH_4, CO, NO_y (NO, NO_2, HNO_4, NO_3, N_2O_5, peroxyacetylnitrate (PAN), methylperoxyacetylnitrate (MPAN) and HNO_3), OH, O_3, C_5H_8 and a selection of NMHC oxidation products such as formaldehyde (CH_2O), higher aldehydes and acetone. Emissions of antropogenically produced NO_x, CO, CH_4 and hydrocarbons are considered using mean monthly global emission fluxes whereas the biogenic NO_x and isoprene emissions are calculated on-line applying a modified versions of the *YL95* and *Guenther et al.* [1995] algorithms, respectively (see section 5.3). Dry deposition processes are described using the "big leaf" resistance approach considering turbulent transport to the surface, stomatal uptake, and different uptake rates for the ocean, snow, bare soil and wet surfaces, expressed by selected or explicitly resolved uptake resistances [*Ganzeveld and Lelieveld*, 1995; *Ganzeveld et al.*, 1998]. With the implementation of the multi-layer vegetation model, dry deposition calculations for the vegetated areas have been modified. The dry deposition velocity for the two canopy layers is calculated from the stomatal, mesophyll, cuticle resistance, a leaf boundary layer resistance, and the amount of biomass in each layer [*Ganzeveld et al.*, 2000a]. Moreover, the uptake of NO and NO_2 by vegetation is different from the "big leaf" dry deposition scheme by using a zero NO_2 an infinite NO mesophyll resistance. The dry deposition scheme is extended to the NMHC oxidation products, for which the dry deposition process is expected to be a significant sink based on their solubility or reactivity, e.g., PAN and CH_2O. Their resistances have been estimated using the method of *Wesely* [1989].

Biosphere characterization

One major improvement of the dry deposition scheme presented by *Ganzeveld et al.* [1998] is the implementation of a spatially and temporally resolved LAI, as compared to the constant LAI of 4 used in the original version of the dry deposition scheme [*Ganzeveld and Lelieveld*, 1995]. As mentioned in the discussion of the study by *Ganzeveld et al.* [1998], further development of the representation of the biosphere should rely on the use of satellite data. Although we realize that the use of NDVI for retrieval of biomass amounts is very uncertain, in this study a 5-year climatology of monthly NDVI satellite data [*Gutman et al.,* 1995] has been used to derive LAI. This is based on the assignment of vegetation characteristic, e.g., NPP, to the 72 ecosystem types of an ecosystems database [*Olson*, 1992] according to *Guenther et al.* [1995]. The representation of LAI is consistent with the description of other vegetation parameters, e.g., foliar density, that are required to calculate the emissions, dry deposition, turbulence and chemistry in the multi-layer vegetation model. These calculations also require the definition of the vertical distribution of biomass, expressed by the Leaf Area Density (LAD) profile. We have assigned two different LAD profiles to the 72 ecosystems of the ecosystem database [*Olson*, 1992] to distinguish between forest and non-forest canopies. Figure 5.1 shows the adopted LAD profile for forest, with a concentration of biomass in the

top, and the LAD profile used for non-forest canopies with an LAD profile that reflects a more evenly vertical distribution of biomass. The grid average canopy height is calculated using an assumed canopy height of 0.01, 1, 15 or 30 m for each of the 72 ecosystems, their fractional coverage and an estimated forest fraction within an ECHAM grid square. For a forest fraction of 1, the grid box canopy height is used whereas for a grid box without forest, the canopy height is calculated from the monthly LAI and the maximum LAI. To introduce an optimal consistency between the applied canopy characteristics in ECHAM, the surface roughness of the ecosystems of the Olson database is calculated from the LAI and canopy height according to *Raupach* [1994]. The surface roughness of each ECHAM grid square is calculated from the high-resolution surface roughness global distribution by averaging the ecosystem neutral drag coefficients [*Claussen et al.*, 1994].

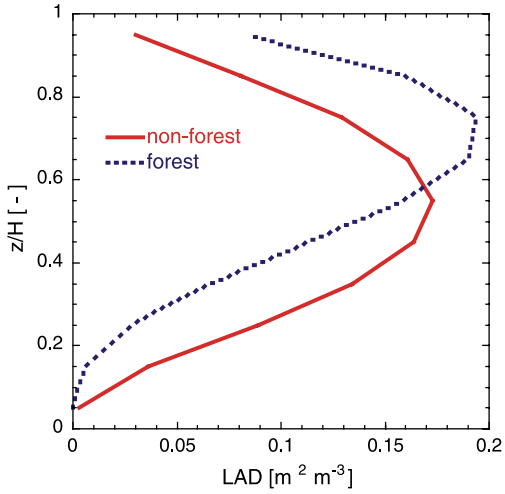

Figure 5.1: Assumed LAD profiles for forest and other canopies as a function of the height z normalized with the canopy height H.

5.3 Biogenic emissions of nitrogen oxides and isoprene

Nitrogen oxides

The *YL95* algorithm calculates soil-biogenic NO_x emissions as a function of ecosystem specific emission factors, soil wetness and temperature, and the cultivation intensity. It also accounts for the effect of "pulsing", which are the enhanced emissions of NO_x after a rainfall event, preceded by a period of drought. The algorithm discerns twelve different biomes: water, ice, desert, tundra, grassland, scrubland, woodland, deciduous forest, coniferous forest, drought-deciduous forest, rain forests and agricultural lands. In the original algorithm the *Matthews* [1983] ecosystem database has been applied to derive the global distribution of twelve ecosystems. However, we have alternatively applied the *Olson* [1992] database, reducing its 72 ecosystems to the twelve ecosystems of the *YL95* algorithm to achieve a maximum consistency with the global biomass distribution in ECHAM. The temperature effect on the emissions is calculated using the calculated soil temperature for the models soil top layer (6.5 cm deep) [*DKRZ*, 1992], different from *YL95* who applied lowest model layer temperature. Moreover, we have used the models soil moisture to distinguish between dry and wet soils. The agricultural soil emission flux is a function of a cultivation index, representing the intensity of the agricultural activity, and the application of fertilizers, which enhances NO_x emissions [*YL95*]. In contrast to the study by YL95, who used the *Matthews* [1983] database, we have used the more recent *Bouwman et al.* [1995] database for the global

distribution of the cultivation intensity and fertilizer application. Following *YL95*, we consider the effect of pulsing using a 2-week history record of the ECHAM resolved large scale and convective precipitation to determine the extent of the dry period. Our modified NO_x emission algorithm is hereafter referred to as G-YL95.

Isoprene

The emissions of isoprene are calculated according to *Guenther et al.* [1995] as a function of ecosystem specific emission factors, surface radiation, temperature, the foliar density and its vertical distribution. Different from the original *Guenther* algorithm, in which the extinction of radiation is calculated considering one single layer, in this study the vertical profiles of radiation within the canopy are calculated according to *Norman* [1979] and *Weiss and Norman* [1985]. The algorithm calculates the profiles of direct and diffusive irradiance in both the visible (Photosynthetically Active Radiation, PAR) and near infrared spectral bands from the net solar radiation [*Weiss and Norman,* 1985], the canopy structure and soil albedo. The direct and diffusive PAR profiles and the fraction of sunlit and shaded leaves are used to calculate the isoprene emission fluxes by the different vegetation layers.

5.4 Results

In this section we present the calculated impact of within-canopy processes on the effective NO_x emission fluxes. Rather than calculating the fluxes of the individual NO_x species, the fluxes of the NO_x-family (in this work defined as NO, NO_2, NO_3, $2{\cdot}N_2O_5$, and HNO_4, hereafter referred to as NO_x) are calculated, related to the ECHAM model timestep of 30 minutes [*Ganzeveld et al.*, 2000a]. We compare the surface fluxes and concentrations of NO_x and O_3 of model integrations with and without considering the canopy interactions and using the method of *YL95*. Moreover, differences in the tropospheric budgets of NO_x and O_3 are compared. This comparison is preceded by an analysis of the on-line calculated soil NO emission fluxes using the G-YL95 algorithm in ECHAM. To study the sensitivity of the calculated NO_x concentrations and surface fluxes for the soil-biogenic NO emission fluxes, the inventory by *DK97* is also included. Unless stated differently, we present model simulations for the months January and July, for which strong differences in the atmosphere-biosphere trace gas exchanges, associated with vegetation cover and activity, chemistry and meteorology, can be expected.

5.4.1 Soil-biogenic NO emission fluxes

Figure 5.2 shows the monthly mean soil-biogenic NO emission fluxes calculated by the G-YL95 algorithm, without the CRF, in ECHAM for July. Largest emission fluxes exceeding $1{\cdot}10^{11}$ molecules cm^{-2} s^{-1} are calculated in the agricultural regions of Asia, Europe and North America, related to the application of fertilizers. NO emission fluxes for tundra and the boreal forests are less than $1{\cdot}10^{9}$ molecules cm^{-2} s^{-1} whereas the emission fluxes of the tropical forest regions are between 2.5 and $5{\cdot}10^{10}$ molecules cm^{-2} s^{-1}. The calculated global NO soil emission flux of about 12 Tg N/yr (without CRF) is about 1.5 Tg larger than that originally calculated by *YL95*. The global agricultural NO emission flux of about 3.8 Tg N/yr is slightly

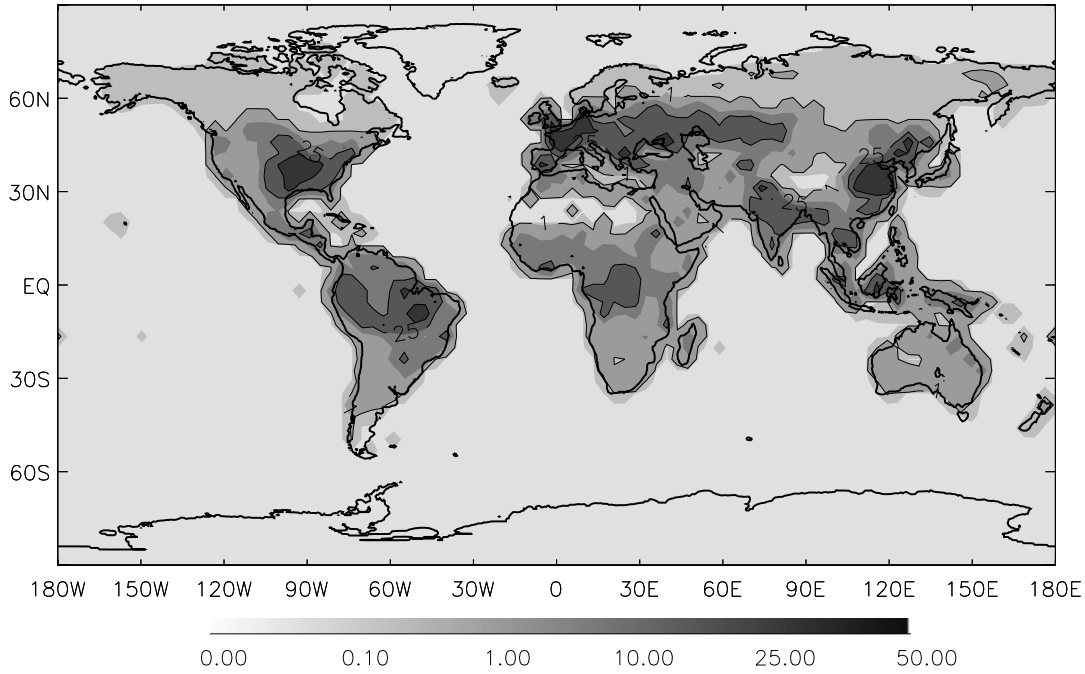

Figure 5.2: Monthly mean soil-biogenic NO emission flux (10^9 molecules cm^{-2} s^{-1}) calculated with the G-YL95 inventory for July.

larger than the estimate of 3 Tg N/yr by YL95 (we applied the *Bouwman et al.* [1995] dataset for cultivation intensity and fertilizer application whereas *YL95* applied the *Matthews* [1983] database).

For comparison with *DK97*, we have also included their emission inventory; the 17 NO emission classes of the *DK97* inventory have been assigned to the 72 classes of the *Olson* ecosystem database [*Lex Bouwman*, personal communication, 2000]. The *DK97* inventory using the *Olson* ecosystems is hereafter referred to as B-DK97. The global NO emission inventory by *DK97* is determined by the geographical distribution of the emission classes and does not contain any temporally resolved cycle like *YL95*. The *YL95* attenuation functions for temperature, moisture, and fertilizer application are not used for the B-DK97 inventory since these are already implicitly considered in the selected emission factors. However, an annual cycle in the B-DK97 NO emission fluxes is introduced in ECHAM by only considering the emission fluxes for the bare soil and vegetation fraction, which are explicitly calculated in ECHAM as a function of season. Figure 5.3 shows the absolute difference between the annual mean G-YL95 and B-DK97 NO soil emission flux, calculated as (B-DK97 minus G-YL95 flux). For the tropical forests of South-America, central Africa and south-eastern Asia the B-DK97 calculated emission fluxes are generally smaller than those of the G-YL95 inventory. The significantly larger G-YL95 emission flux compared to the B-DK97 flux in south-eastern China reflects the large contribution from fertilizer application to the emission flux for that region in the G-YL95 inventory. For the savannas and grasslands in the tropics as well as the temperate regions, the B-DK97 inventory gives significantly larger emission fluxes compared to those of the G-YL95 inventory, with maximum differences of exceeding $0.5 \cdot 10^{11}$ molecules cm^{-2} s^{-1}. This is also reflected in the calculated global annual NO soil emission flux of about 21 Tg N/yr, which is similar to the flux calculated by *DK97*. This agreement supports the assignment of the emission classes to the ecosystems of the *Olson*

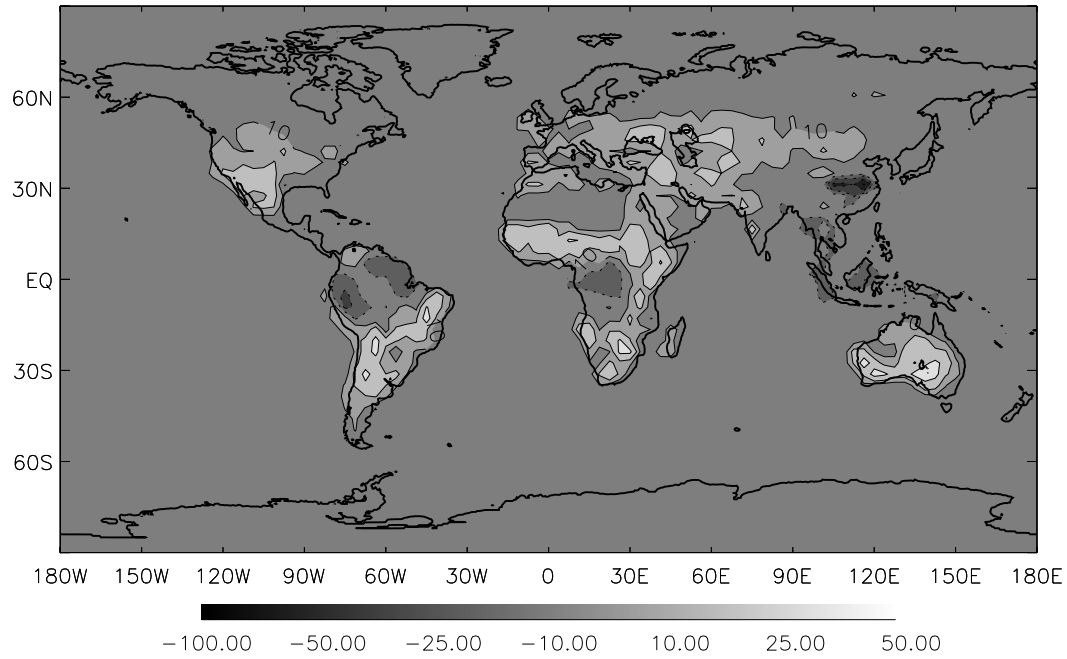

Figure 5.3: Annual mean absolute difference in soil-biogenic NO emission flux (10^9 molecules cm^{-2} s^{-1}) between the B-DK97 and G-YL95 inventories. The isolines are: -50, -25, -10, 10, 25, 50.

database. This is not a trivial exercise since a different assignment of the emission classes with large emission fluxes according to *DK97*, e.g., tropical savanna and woodland, to the ecosystems of the *Olson* database that do not clearly represent one specific emission class, can introduce large differences in the calculated NO emission fluxes.

5.4.2 Surface fluxes of NO_x and O_3

The previous section showed that we calculate global and annual NO soil emission fluxes with the G-YL95 and B-DK97 algorithms which are similar to the original emission inventories. The distinct differences concerning the absolute magnitude and distribution of the calculated fluxes offer the opportunity to assess the sensitivity of the calculated NO_x and O_3 concentrations to the soil biogenic emissions of NO. In this section, we present an assessment of the role of the canopy in modulating the soil emission flux and the subsequent effective emissions of NO_x into the PBL. Unless stated differently, soil NO emission fluxes are calculated using the G-YL95 algorithm.

Multi-layer canopy-top fluxes

Figures 5.4a and b show the monthly mean surface NO_x fluxes of the multi-layer vegetation model (hereafter referred to as ML model) for July and January, respectively. This surface flux consists of the canopy-top flux of the vegetation fraction and the net emission and dry deposition fluxes of the other surface fractions. Antropogenic NO_x emissions are assumed to occur in the surface layer or higher up in the PBL, dependent on the effective emission height, hence they are not considered in the surface flux.

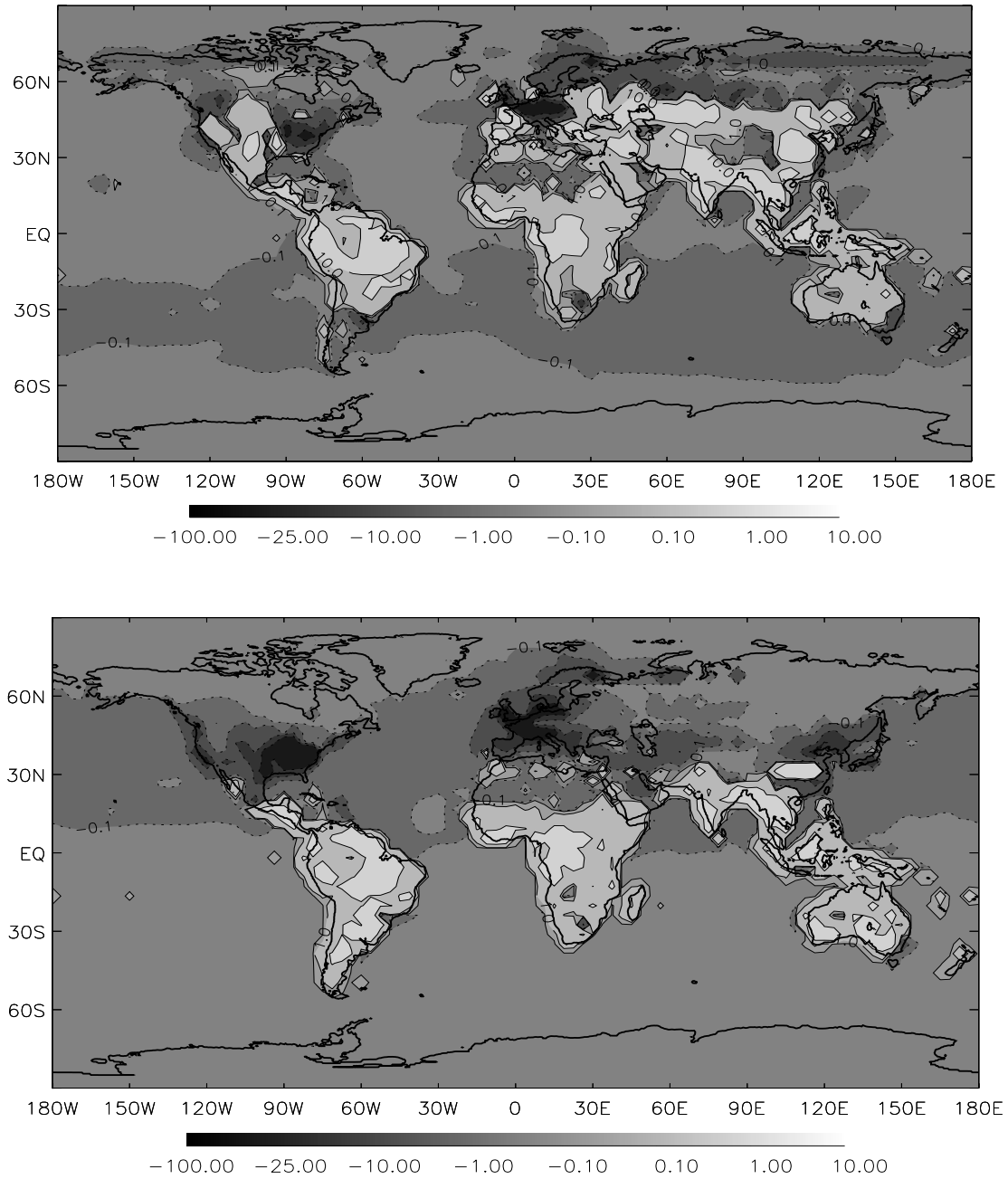

Figure 5.4a-b: Monthly mean NO_x surface flux (10^9 molecules cm^{-2} s^{-1}) calculated by the multi-layer vegetation model for a) July and b) January. Dotted and solid isolines indicate a net deposition and emission flux, respectively.

The global distribution of the surface NO_x flux largely reflects the distribution of the soil NO emissions except for regions where dry deposition of NO_x, supplied by antropogenic emissions, prevails, e.g., over western Europe and eastern North-America. In the NH winter, dry deposition of NO_x occurs over most of the continents associated with negligible soil emission fluxes due to snow cover and relatively low temperatures, and the accumulation of antropogenically produced NO_x in a stable stratified PBL. Maximum emission fluxes > $25 \cdot 10^9$ molecules cm^{-2} s^{-1} are found over the savanna of South-America and agricultural areas in

China, whereas the maximum NO_x deposition fluxes in Europe and North-America are as large as $75 \cdot 10^9$ molecules cm^{-2} s^{-1}.

Multi-layer versus big leaf model

Figure 5.5 shows the July average ratio of the ML canopy-top NO_x flux to the soil NO emission flux. This ratio indicates the contribution of soil emissions to the surface flux of NO_x, with positive values indicating an emission flux of NO_x into the surface layer, whereas

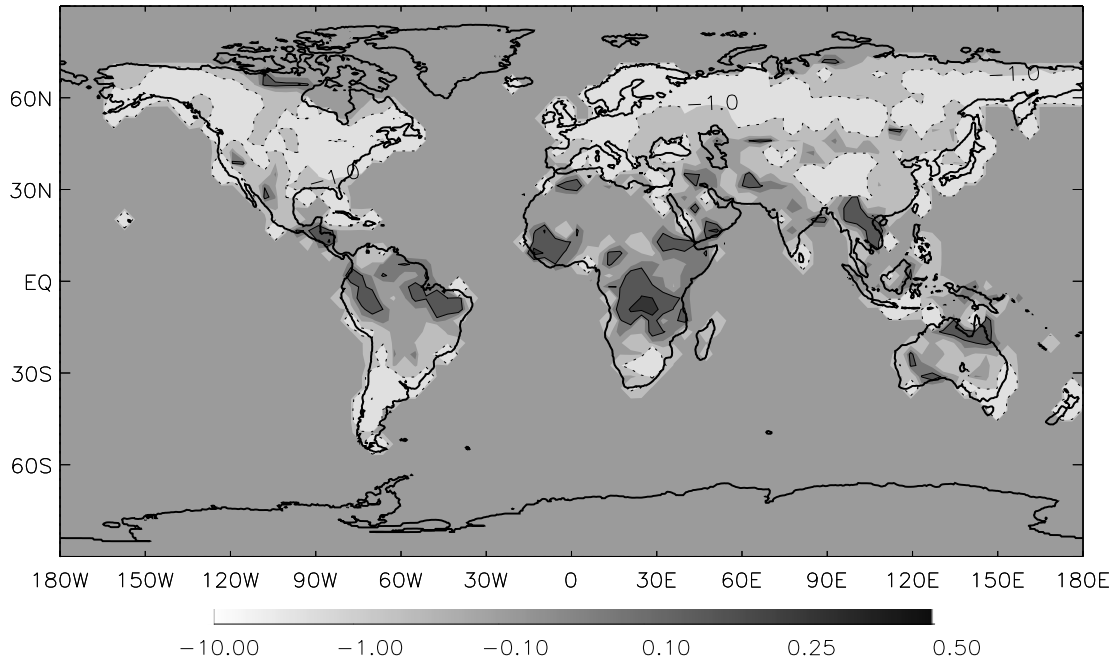

Figure 5.5: Monthly mean ratio of canopy-top to soil-biogenic NO_x emission flux for July. The isolines are: -10, -1, -0.1, 0.1, 0.25, 0.5. Dotted and solid isolines indicate a negative and positive ratio, respectively.

negative values indicate net dry deposition of NO_x. Over the forests of the northern hemisphere (NH), values significantly smaller than -1 indicate that dry deposition of NO_x prevails. In western Europe and eastern North-America, dry deposition fluxes of NO_x are at least two times larger than the soil emission flux. A more significant contribution of soil emissions into the surface flux is found over the grasslands and agricultural areas in North-America, eastern Europe and central Asia. Biogenic emissions dominate the surface NO_x flux over the vegetated regions of the tropics and sub-tropics with a ratio of about 0.4 for dense forest, e.g. tropical rainforest in the Amazon basin. This implies that only 40% of the biogenic NO_x flux is released into the atmosphere over these forests.

As discussed in Chapter 4, it is expected that only for those regions where the canopy-top NO_x flux and the soil NO emission flux are of a comparable magnitude, interactions between emissions, dry deposition, chemistry and turbulence within the canopy must be considered. For other regions, the surface flux of NO_x can fairly well be represented using the big leaf approach, while differences between the ML and big leaf approaches are mainly due to differences in the calculated NO_x dry deposition velocities. Figure 5.6 shows the relative difference between the monthly mean surface NO_x fluxes calculated by the ML model and

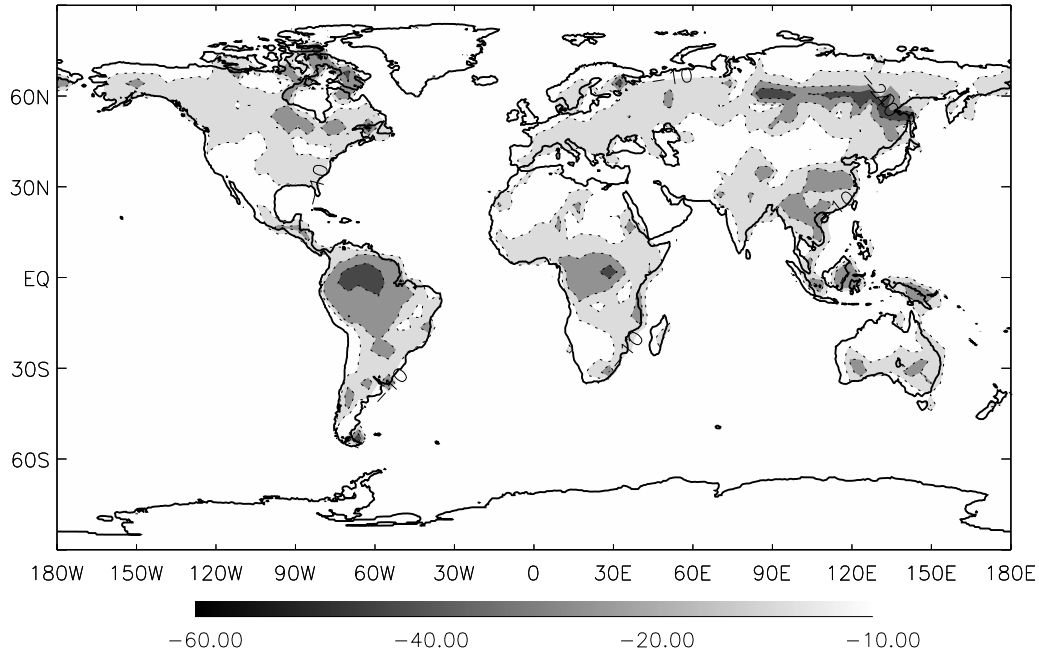

Figure 5.6: Monthly mean relative difference (%) between the surface NO_x flux calculated by the ML and BL model for July. The isolines are: -60, -40, -20, -10.

big leaf model (hereafter referred to as BL model) for July. The BL surface flux consists of the biogenic emission flux and dry deposition flux of all surface fractions. To highlight the relative contribution of the surface flux to the total flux, consisting of the surface and antropogenic flux, relative differences are calculated as (ML- minus BL surface flux)/(average surface flux plus antropogenic flux). Differences are most pronounced for the vegetated regions of the sub-tropics and tropics with upward (emission) surface fluxes calculated by the ML model over tropical forest being about 25% smaller than those calculated by the BL model. Differences over the vegetated regions of the NH are generally less than 10% except for some locations with a significant contribution of the soil-biogenic NO_x flux to the surface flux, e.g., north-eastern Asia. Differences for January, which are not shown here, are comparable and show a similar spatial distribution in the tropics and subtropics, whereas the NH differences are generally smaller than 10% and restricted to the regions without snow cover.

Multi-layer versus big leaf model, including the CRF

To study the applicability of the CRF, as proposed by *YL95* as a first-order estimate to account for reduction of the soil emission flux of NO_x due to dry deposition, we have performed model simulations with the big leaf approach using their CRF. The CRF is calculated from the global distribution of LAI, and the Stomatal Area Index of the twelve ecosystems of the *YL95* inventory. The CRF is as small as 0.2 for tropical rainforest, which implies that only 20% of the NO_x being emitted by the soil is actually released into the atmosphere, whereas for temperate and boreal forests the CRF is about 0.6. Figures 5.7a and b show the relative difference in the monthly mean surface NO_x flux calculated by the ML model and the BL model, including the CRF (hereafter referred to as BL+CRF model) for

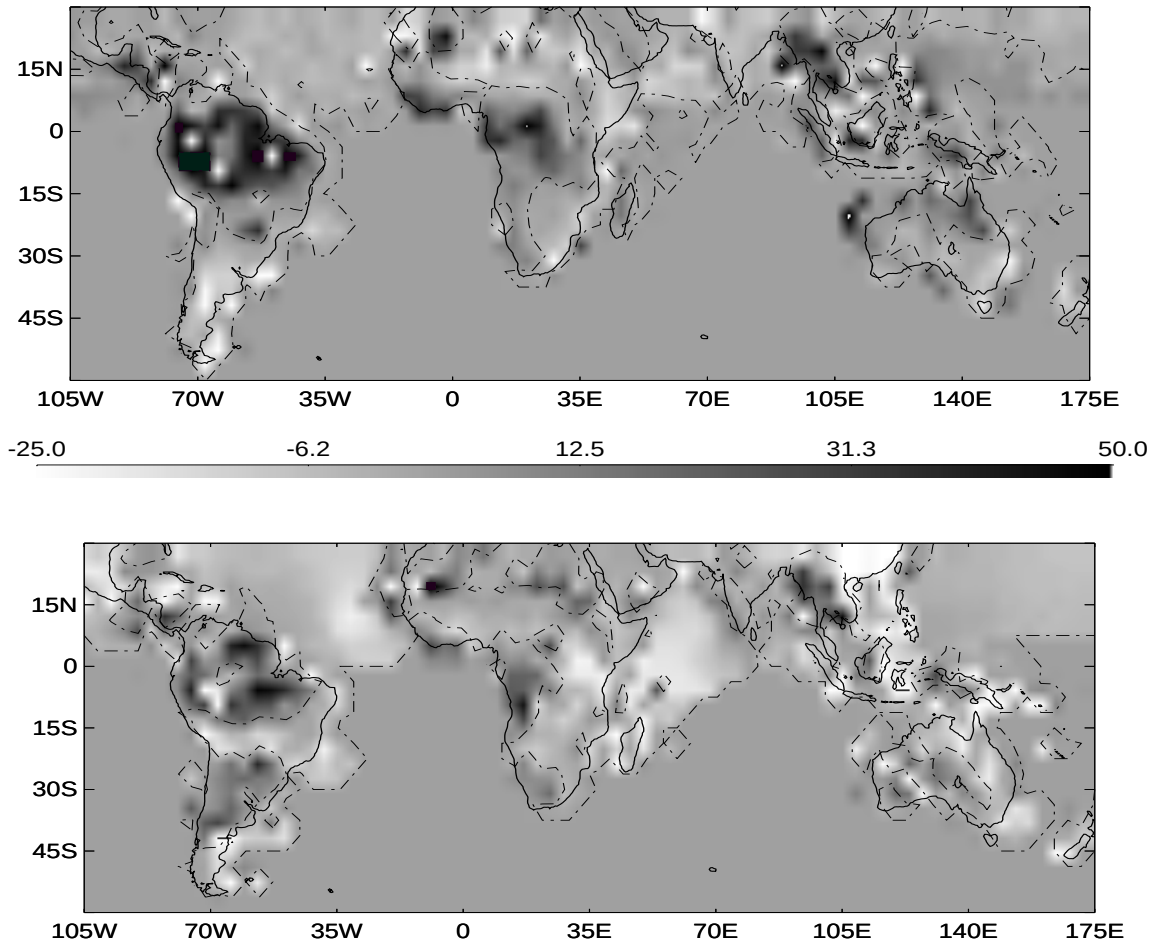

Figure 5.7a-b: Monthly mean relative difference (%) between the surface NO_x flux calculated by the ML and BL+CRF model for a) July and b) January. Black indicates an increase whereas white ndicates a decrease in the calculated flux by the ML model, respectively. The dashed-dotted line indicates the zero contour line. Relative differences are only shown for those locations where the absolute NO_x flux of the ML model is larger than 0.05 10^9 molecules cm^{-2} s^{-1}.

July and January, respectively. The relative difference is calculated as (ML minus BL+CRF surface flux)/(average surface flux plus antropogenic flux).

Since relative differences in the NH extratropics, where NO_x surface layer concentrations are controlled by antropogenic emissions, are negligible we focus on the NH sub-tropics and tropics and the southern hemisphere (SH). The July NO_x surface fluxes of the ML model in the tropics and subtropics are generally larger than those calculated by the BL+CRF model, with differences as large as 75% for the tropical forests of South-America, central Africa and south-eastern Asia. Figure 5.7b shows that the January ML surface NO_x flux over tropical forest is also larger than that of the BL+CRF model, although differences are generally smaller than 50%. These results suggest that the CRF for this ecosystem is too small (a small CRF implies a large reduction of the soil emission flux). The relative decrease in the surface NO_x fluxes in the winter at mid- and high latitudes, e.g., south-eastern Asia in January, generally reflects a decrease in dry deposition flux. The ML surface NO_x fluxes over the non-forest canopies during wintertime at mid- and high-latitude locations of the SH, e.g., southern

South-America, Africa and Australia are smaller than those calculated by the BL+CRF model. A more thorough analysis of the calculated fluxes in South-America reveals that the BL+CRF model calculates a surface emission flux comparable to the NO soil emission flux associated with a CRF of about 0.9 and a negligible dry deposition flux, whereas the ML surface flux is negligible. The difference between the January and July ML and BL+CRF surface fluxes suggests that the NO_x canopy flux divergence for these mid- and high-latitude canopies is controlled to a large extent by chemistry and turbulence since emissions and dry deposition of both models are similar. One explanation for the distinctly different fluxes is the limited turbulent exchange during stable winter conditions, which is explicitly considered by the ML model but not by the BL+CRF model. Moreover, subtle differences in the calculated dry deposition velocities by the BL+CRF and ML model can result in significant differences in calculated fluxes and concentrations for suppressed turbulent mixing [*Ganzeveld et al.*, 2000a]. This justifies the use of the ML model, also for relatively sparse canopies in locations with a distinct seasonality in the chemistry, dry deposition and turbulence. However, for a more explicit assessment of the role of the processes involved and the sensitivity to the defined canopy structure, a more extensive analysis is required for which we will apply the single column model.

5.4.3 NO_x and O_3 concentrations

To indicate the differences in the calculated NO_x concentrations by the ML and BL+CRF model, Figure 5.8 shows the relative difference between the July NO_x concentrations in the surface layer over the NH sub-tropics and tropics and the SH by both approaches. Over tropical forest, relatively larger emission fluxes by the ML model result in a relative increase

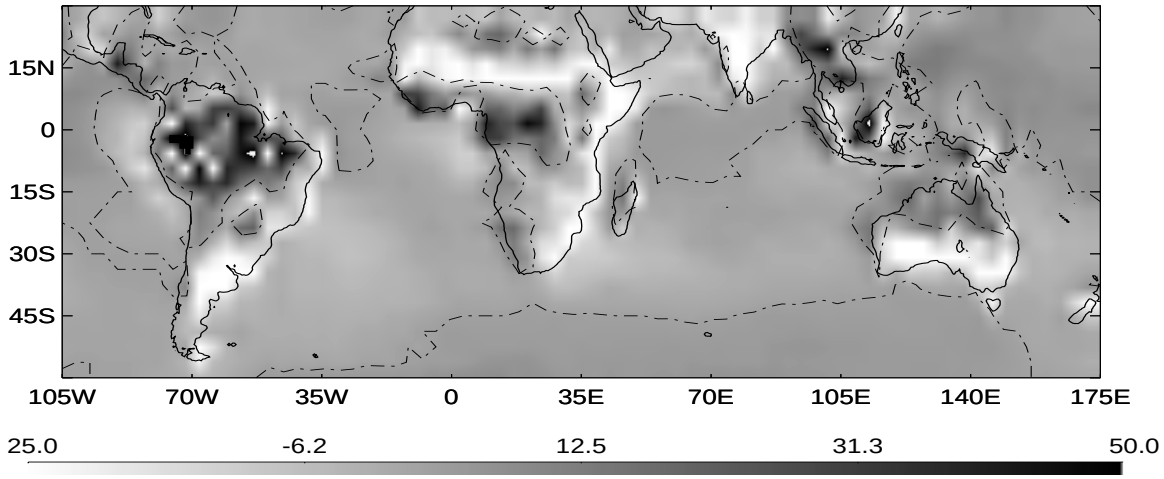

Figure 5.8: Monthly mean relative difference (%) between the surface layer NO_x concentrations calculated by the ML and BL+CRF model for July. Black indicates an increase whereas white indicates a decrease in the calculated concentrations by the ML model, respectively.

in surface layer NO_x concentrations as large as 50%, whereas for less dense vegetation cover, e.g., African savanna and grasslands, we calculate a relative decrease of about 25%. Relative changes in the NH extra-tropics are generally less than 10%. There are also distinct differences in the calculated NO_x concentrations higher up in the PBL and free troposphere.

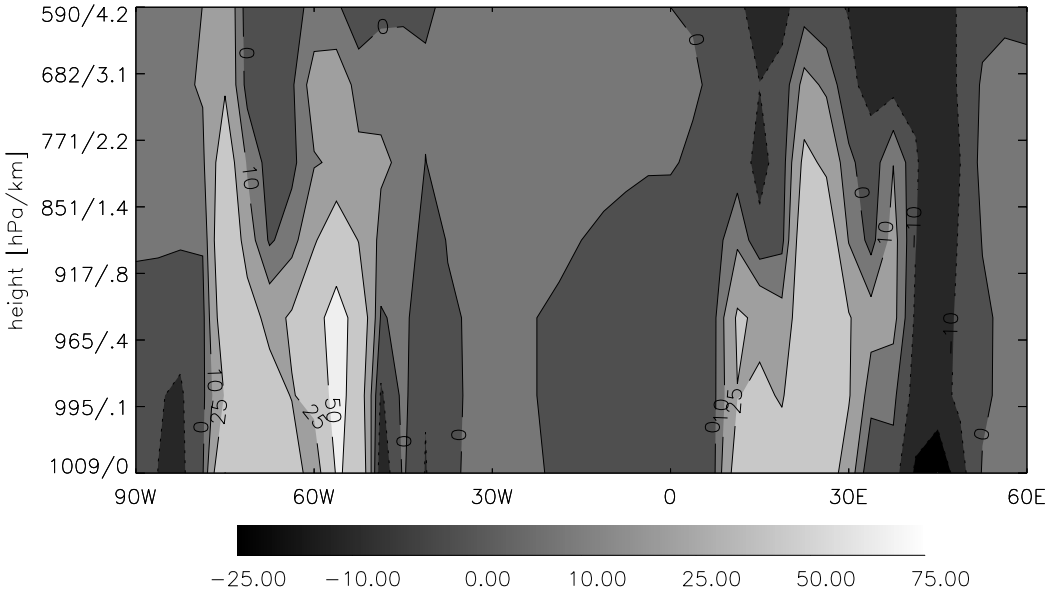

Figure 5.9: Zonal distribution of the relative difference (%) between the NO_x concentrations calculated by the ML and BL+CRF model, from 90°W to 60°E at the equator as a function of height for July. The isolines are: -50, -25, -10, -5, 5, 10. Dotted and solid isolines indicate a decrease and increase in the calculated concentration by the ML model, respectively.

This is shown in Figure 5.9, in which the longitudinal distribution of the relative differences in the NO_x concentrations from 90° W to 60° E at the equator is presented as a function of height. There are non-negligible relative differences up to an altitude of about 3 km due to the upward transport of surface layer NO_x by turbulence and convection over the Amazon basin and central African forest. However, absolute differences larger than 100 pptv, associated with surface layer concentrations of about 250-500 pptv, extend to an altitude of about 400 m. The increase in the NO_x concentrations over tropical forest, calculated by the ML model compared to the BL+CRF model, is not reflected in an increase in O_3 surface layer concentrations. The ML model calculates smaller O_3 concentrations compared to the BL+CRF approach with a maximum relative decrease > 25% for boreal forest. This is largely explained by larger O_3 dry deposition velocities calculated with the ML model, which results in a maximum relative increase in the O_3 dry deposition flux up to 25%.

Comparison of the calculated NO_x and O_3 concentrations with the ML model, using the G-YL95 and B-DK97 inventories, reflects solely the sensitivity to NO emissions fluxes since the dry deposition, chemistry, and turbulence formulations are similar. In section 5.4.1, the absolute differences in the calculated NO emission fluxes have been presented, indicating a global annual absolute difference of about 9 Tg N/yr between the B-DK97 and G-YL95 inventory. However, the relative differences in the calculated annual mean NO_x and O_3 surface layer concentrations by both inventories are generally smaller than 7.5%. The limited sensitivity is partly explained by an increase of uptake within the canopy, which removes an additional 30% of the enhanced soil emission flux. Hence, the effective emission flux using the B-DK97 inventory is 6 Tg N yr^{-1} larger than that calculated for the G-YL95 inventory. Furthermore, chemical transformations and transport processes also reduce the impact on the global NO_x and O_3 burdens, as will be shown in the next section.

5.4.4 Global budget differences between ML and BL model

Figure 5.10a shows the absolute differences in the budgets of the processes that control the tropospheric NO_x burden in four approximately equal areas of the globe (0°-30° and 30°-90° N and S), comparing the ML and the BL model, including the CRF, for July (ML – BL+CRF model). The absolute differences in the NO_x burden are not shown since these are about two

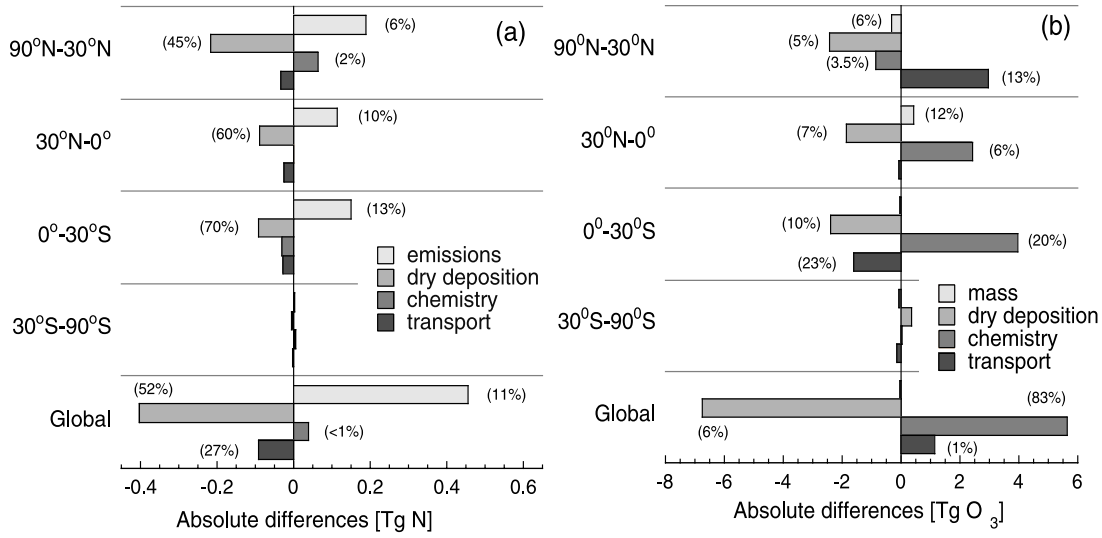

Figure 5.10a-b: Absolute differences (and relative differences between parentheses) of the tropospheric NO_x and O_3 mass, emissions, dry deposition, chemistry and transport for July over four approximately equal areas of the globe, comparing simulations with the BL+CRF and the ML model, a) NO_x with absolute differences in Tg N, differences in mass not shown here, b) O_3, in Tg O_3. Positive values indicate an increase in mass or a larger production whereas negative values indicate a decrease in mass or an increased destruction.

orders of magnitude smaller than the process budgets. Negative values indicate a net removal whereas positive values indicate a net source of NO_x. Also shown are the relative differences (between parentheses) to indicate the impact of the canopy interactions on the individual processes. The absolute differences in the NO_x emissions show the reduction in the soil-biogenic emissions due to the CRF, which is not considered in the emission flux of the ML model. The maximum absolute differences are about 0.2 Tg N/month for the NH 90°-30° compartment and 0.45 Tg N/month on a global scale. Relative differences are most significant in the tropics and subtropics due to the relative larger contribution of the soil-biogenic flux in the total emission flux. On a global scale, we calculate a relative reduction in the emissions of 11% when considering the CRF. The ML model calculates a significantly larger removal by dry deposition compared to the BL+CRF model. Absolute differences in the dry deposition are similar to those of the emissions suggesting that the increase in the emissions is largely compensated by an increase in the dry deposition, whereas minor differences are obtained for chemical transformations and transport. The comparable magnitude of the dry deposition flux, which is explicitly calculated with the ML model, and the reduction of the emissions through the CRF, supports the approach by *YL95*, who obviously introduced the CRF to represent the reduction of the soil NO_x emission flux by dry

deposition. Figure 5.10b shows the absolute and relative differences in the July tropospheric burden and process budgets for O_3, calculated by the ML and BL+CRF models. Relative differences in process budgets for the four compartments are significant, with maximum values for dry deposition, chemistry, and transport of 10%, 20%, and 23%, respectively. However, the differences are mutually compensating, resulting in a small difference in the

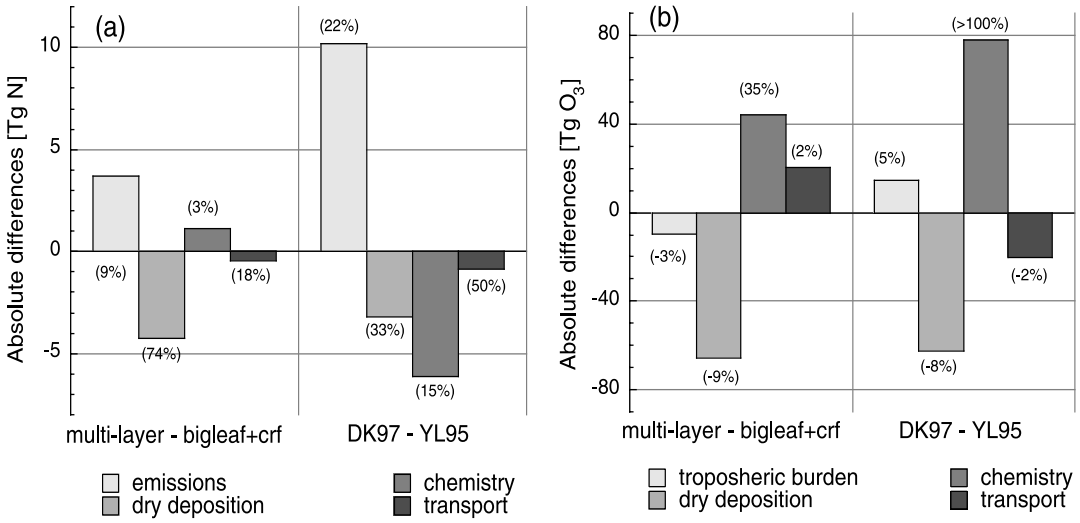

Figure 5.11a-b: Absolute differences (relative differences between parentheses) of the annual tropospheric mass, emissions, dry deposition, chemistry and transport on a global scale, comparing simulations with the BL+CRF and ML model, and comparing simulations with the the ML model with the G-YL95 and B-DK97 emission inventories, a) NO_x with absolute differences in Tg N, differences in mass not shown here, b) O_3, in Tg O_3. Positive values indicate an increase in mass or a larger production, whereas negative values indicate a decrease in mass or a larger destruction.

global O_3 burden. Note that the large relative differences for chemistry reflect the net effect of chemical production and destruction terms of about 460 Tg N/month. The global relative increase in the O_3 dry deposition flux for the ML model is largely explained by an increase in the dry deposition velocities. The absolute and relative differences in the annual global tropospheric burden and process budgets of NO_x and O_3, calculated with the ML and BL+CRF model, are shown in Figures 5.11a and b, respectively. To indicate the sensitivity of the NO_x and O_3 burden and process budgets for the soil-biogenic NO emission flux, we also show differences between the simulations using the G-YL95 and the B-DK97 emission inventories. The annual global absolute differences in the NO_x emissions, dry deposition, chemistry and transport are similar to those shown in Figure 5.10a. Using the CRF yields a global reduction of soil-biogenic NO_x emissions of about 4 Tg N/yr. This is somewhat less than an estimated reduction of 50% of the global soil emission flux of ~ 10 Tg N/yr by *YL95*. The absolute difference in the soil emission flux is more than compensated by a significantly larger dry deposition flux of about 4.5 Tg N/yr calculated by the ML model. Comparison of the NO_x process budgets for the ML model using the G-YL95 and B-DK97 emission inventories shows an absolute difference in the total NO_x emission flux of about 10 Tg N/yr, as discussed in section 5.4.1. Despite the significantly larger emission flux for the B-DK97 inventory, there is no significant increase in the NO_x burden due to the compensating effect of the aforementioned dry deposition increase, and chemical destruction and transport into

the stratosphere, which remove about 3, 6, and 1 Tg N/yr, respectively. Figure 5.11b shows that a relative increase in the annual global O_3 tropospheric burden of about 5% accompanies the 10 Tg N/yr increase in the NO_x emission flux, which is mainly caused by an increase in the chemical production of O_3. Differences in the annual global burden of O_3 between the simulations with the ML and model, including the CRF, are small due to the compensating effect by the increased dry deposition, chemical production, and transport by the ML model compared to the BL model.

5.5 Discussion

The calculated NO_x canopy flux divergence is associated with many uncertainties due to the complexity of the involved processes, being controlled by bio-geophysical as well as bio-geochemical properties of the canopy-soil system. This is reflected in the range of global annual soil-biogenic NO_x emission inventories with numbers ranging < 6 Tg N/yr [*YL95*], and > 20 Tg N/yr [*DK97*] (without CRF). A major uncertainty in these inventories is the definition of the ecosystem or soil type emission factors since this involves the upscaling of observed NO emission fluxes, representative for a spatial scale of perhaps tens of meters, to the spatial resolution of the ecosystem or soil type database. A study of the spatial and temporal variability of NO emission fluxes from a tree plantation by *Weitz et al.* [1999] shows that observed fluxes are spatially independent at scales exceeding one meter. Moreover, the high temporal variability in the observed NO emission fluxes and soil moisture content also limits the calculation of long-term emission fluxes from the relative small number of observations for each site [*Weitz et al.*, 1999]. For a more extensive discussion of the uncertainties in the soil-biogenic NO_x emission inventories, we refer to *DK97*. Here, we limit ourselves to a discussion of some of the uncertainties involved in the calculations of the canopy interactions.

One of the uncertainties in the calculation of the NO_x canopy flux divergence is associated with the uptake of NO_x by the vegetation. In our model it is assumed that NO_2 is removed by dry deposition as efficient as O_3, whereas NO uptake is assumed to be negligible. However, the validity of these assumptions is not supported by a number of observations. Observations of NO_x fluxes above the canopy do not only reflect the dry deposition process but also the emissions and chemical transformations. Therefore, the role of uptake by the vegetation can only be derived from enclosure studies. These indicate the existence of so-called compensation points for trace gas exchanges, defined as the ambient concentration above which a net uptake occurs whereas for lower concentrations the trace gas is released [e.g., *Farquhar et al.*, 1980]. A study by *Johansson* [1987] in which leaf twigs have been exposed to a wide range of NO_2 concentrations, indicates the existence of an NO_2 compensation point of about 1.2 ppbv. Observations of NO_2 and NO exchange over coniferous forest by *Rondon et al.* [1993] showed a decrease in the dry deposition velocity NO_2 relative to the stomatal conductance for ambient NO_2 concentrations less than 1 ppbv. This decreasing correlation between the NO_2 dry deposition velocity and the stomatal conductance indicates the increasing significance of the internal NO_2 concentration in determining the concentration gradient between the atmosphere and the leaf tissue. For ambient concentrations of about 0.5 ppbv *Rondon et al.* [1993] actually observed an emission of NO_2. *Lerdau et al.* [2000] discuss the potential importance of an NO_2 compensation point for the NO_x surface exchange and

burden. They hypothesize that there might be a significant source of NO_x in the form of NO_2, being released by the vegetation in areas where the ambient NO_2 concentrations are less than about 1 ppbv. Their estimated vegetation emission flux of NO_2 of about $2 \cdot 10^{10}$ molecules cm^{-2} s^{-1} is comparable to the soil-biogenic NO emission flux, which ranges between 10^8 and 10^{11} molecules cm^{-2} s^{-1} [*Lerdau et al.*, 2000]. To test if the existence of a compensation point would have a large effect on our results, we have performed one additional model simulation in which we use an NO_2 leaf uptake resistance as a function of the canopy NO_2 concentrations and an assumed NO_2 compensation point of 1 ppbv. The calculated leaf uptake resistance resembles the NO_2 stomatal resistance for surface layer concentrations smaller than 0.5 and larger than 1.5 ppbv, whereas for concentrations between 0.5-1.5 ppbv there is an exponential increase in the leaf resistance to a value of 10^5 for an ambient concentration of 1 ppbv. For concentrations larger than 1 ppbv the contribution of NO_2 dry deposition to the NO_x deposition flux is calculated, whereas for a concentration smaller than 1 ppbv, there is no NO_2 dry deposition but an emission flux of NO_2. This emission flux is calculated from the concentration gradient and the exchange velocity, which resembles the reciprocal value of the quasi-laminar boundary layer and leaf resistance. To account for the surface area where emissions occur, we have used a SAI of 0.12 [*YL95*, and references therein] and the LAI of the crown- and the canopy-soil layer, which implies that we assume that the emissions occur through the leaf stomata.

Figure 5.13 shows the global distribution of the monthly mean relative difference in the NO_2 dry deposition velocity with and without considering an NO_2 compensation point of 1 ppbv, $V_{dNO2\text{-}Cno2}$ and V_{dNO2} respectively for July (relative difference calculated as (V_{dNO2} minus $V_{dNO2\text{-}CNO2}$)/V_{dNO2}). The differences reflect the global distribution of the NO_2 concentrations within the canopy with relative differences smaller than 40% for locations in the vicinity of antropogenic sources or with relatively large soil emission fluxes, e.g., western Europe, and

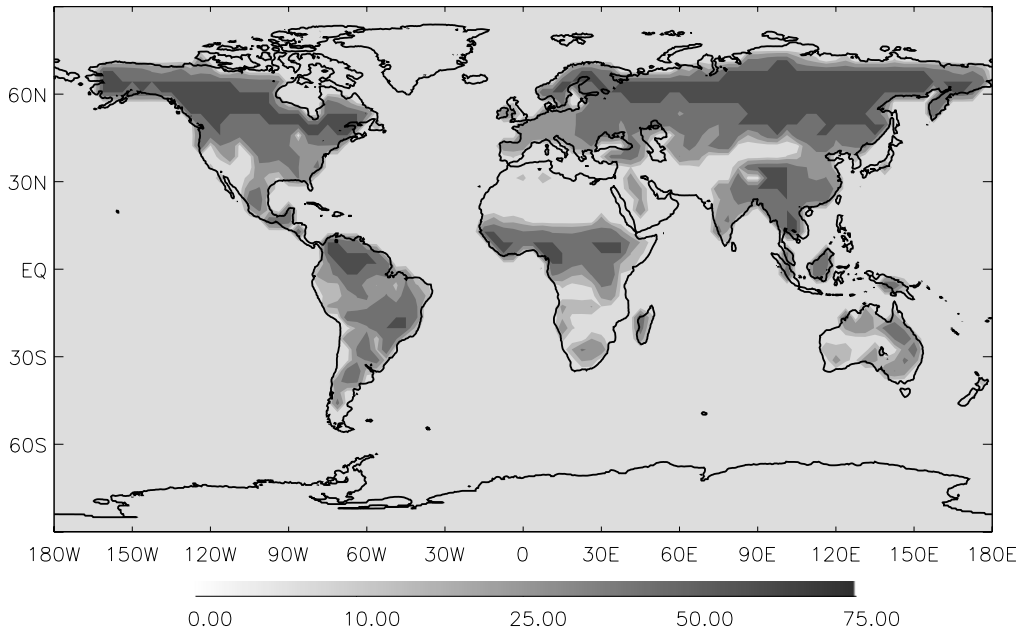

Figure 5.13: Monthly mean relative difference between V_{dNO2} and $V_{dNO2\text{-}Cno2}$ for July (relative difference calculated as (V_{dNO2} minus $V_{dNO2\text{-}CNO2}$)/V_{dNO2}) The isolines are: 10, 25, 50, 75.

some forested areas in South America and Africa. Most pronounced differences are calculated over the African savanna, tropical and boreal forest with maximum values > 80 % over Alaska. However, further analysis reveals that the relative difference in the NO_x fluxes and surface layer trace gases concentrations, considering the NO_2 compensation point, is small due to a relative small decrease in the NO_x dry deposition velocity. Rather than calculating the dry deposition fluxes of the individual NO_x species, we calculate the dry deposition flux of NO_x from the relative contribution of the individual species to the NO_x concentration and their deposition velocities. This significantly reduces the sensitivity of the NO_x canopy-top flux to the NO_2 deposition velocity. Over the NH boreal forests and tundra relative differences in the calculated NO_x canopy-top fluxes with and without considering the compensation point can be as large as 50%. For these ecosystems we actually calculate a vegetation emission flux of NO_2. Relative differences in the canopy-top flux over tropical forest are generally smaller than 10%. We emphasize that this analysis is much affected by uncertainties in the definition of the compensation point, e.g., as a function of vegetation type, the presence of a temporal dependence related to the plant-metabolism. Moreover, it is important to assess the sensitivity to the calculation of the dry deposition flux of the NO_x-family rather than of the individual species. In future, we will further explore the significance of compensation points for atmosphere-biosphere NO_x exchange.

An additional uncertainty is the uptake of NO_x by the soil due to the microbial production of NO in the soil. Hence, uptake of NO is not very likely. Observations of NO_2 uptake by soils using enclosure chambers showed NO_2 uptake resistances small as 200 s m^{-1} [*Hanson and Lindberg*, 1991]. However, high exposure concentrations were used in these experiments. For typical within-canopy NO_2 concentrations it is expected that the uptake rate by the soils is relatively inefficient due to the chemical production of NO_2 from NO and O_3 close to the soil surface. Additional mechanisms that can be a potential significant sink of NO_x include uptake by the undergrowth, litter at the soil surface or the chemical interaction with organic compounds, e.g. producing PAN, which can subsequently be removed by dry deposition. Unfortunately, understanding of these mechanisms is strongly limited by the availability of observations, e.g., of the dry deposition of PAN.
The internal cycling of the individual oxidized nitrogen species within the canopy is related to the penetration of radiation and turbulence deep into the canopy interior since it controls the photodissociation and the residence time of the trace gases within the canopy. For a more extensive discussion of the role of turbulent exchange between the canopy and the atmosphere for atmosphere-biosphere trace gas exchanges, e.g., intermittent exchange, stability effects and nocturnal exchange, we refer to Chapter 4. In that study we also show the ability of the model to calculate a realistic radiation regime within the canopy by comparison of the observed and calculated extinction of radiation within a tropical rainforest and a deciduous forest. For the model comparison, the characterization of the canopy structure, which controls the extinction of radiation, has been prescribed using the observed canopy characteristics. However, in this work we have derived the canopy characteristics from the ecosystem database and satellite data as presented in section 5.2. Large uncertainties are involved with the definition of LAI, canopy height, surface roughness and a representative vertical biomass distribution. Additional surface cover characteristics such as the foliage clumping, which is the nonrandom distribution of foliage [*Gower et al.*, 1999], are not considered in this study. Foliage clumping is relevant for the atmosphere-biosphere exchange of reactive trace gases since it enhances the beam penetration compared to a canopy with a

random distribution of biomass. It is expected that significant errors are introduced in the assessment of non-linear, energy dependent processes, e.g., photodissociation of reactive trace gases, by using algorithms for radiative transfer in canopies that neglect foliage clumping [*Baldocchi and Harley*, 1995]. This issue needs further analysis for which we plan to use the single column model extended with more sophisticated algorithms for radiative transfer within the canopy, which explicitly consider foliage clumping.

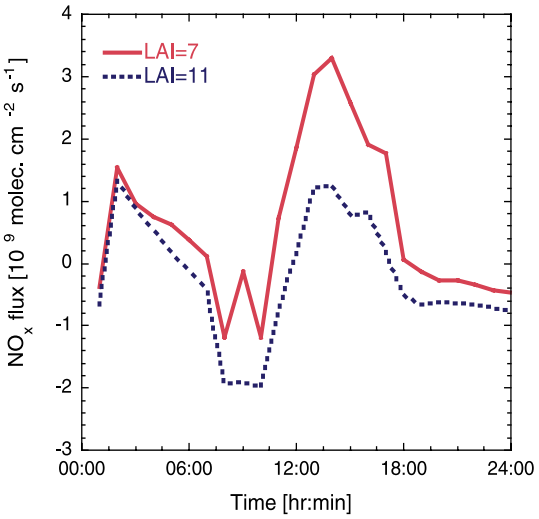

Figure 5.14: The modeled 5-day average diurnal cycle in the canopy top NO_x flux (10^9 molecules cm^{-2} s^{-1}) for tropical forest with an LAI of 7 (solid line) and an LAI of 11 (dotted line)

Inferring the surface cover characteristics from the ecosystem database and satellite data is a follow-up of our continuous effort to improve the surface cover properties, relevant to atmosphere-biosphere trace gas exchanges, in ECHAM. Use of a 5-year climatology of monthly mean NDVI satellite data implies that the seasonal changes in biomass are fairly well represented in ECHAM. However, a major concern is the absolute estimate of biomass for some ecosystems, consistent with the findings of *Wang et al.* [1998]. The inferred LAI for tropical rainforest is about 10, which seems a too large estimate based on in-situ measurements of the LAI of tropical rainforest which range from about 5 to 7 [e.g., *Fan et al.*, 1990, *Kruijt et al.*, 2000]. *Wang et al.* [1998] have used the maximum LAI values reported by *Lieth* [1975] and *Box* [1981] to correct the inferred LAI distribution. This reduces their inferred tropical rainforest LAI of 11 and savanna LAI of 6.3 to 8 and 4, respectively [*Wang et al.*, 1998]. Figure 5.14 shows the NO_x canopy top flux for tropical rainforest with an LAI of 7 and 11, calculated with the atmosphere-biosphere trace gas exchange model in the single column model. For more details concerning model simulations for this ecosystem we refer to Chapter 4. Differences in ozone canopy top fluxes are not shown here since the differences for the LAI of 7 and 11 are negligible. The NO_x canopy top fluxes for and LAI of 11 are smaller compared to that calculated for an LAI of 7 due to a more efficient removal of NO_x by dry deposition, which results in a maximum relative decrease of about 50% in the afternoon. These results indicate the sensitivity of the calculated NO_x canopy fluxes for one specific ecosystem. We will continue the evaluation of the atmosphere-biosphere model by comparison of calculated and observed trace gas fluxes and concentrations, as presented in Chapter 4, for a larger selection of ecosystems. A major focus of these evaluations will be the sensitivity of the calculations to the canopy structure. Despite the sensitivity of the calculated canopy top fluxes for the used LAI, we have not corrected the inferred LAI in this work, also since the focus of this work has been a relative comparison of biogenic NO_x fluxes, with or without considering the role of canopy interactions. However, in future work we will apply the atmosphere-biosphere trace gas exchange model to assess the role of canopy processes to simulate absolute trace gas concentrations and fluxes. It will be necessary to pursue further development of algorithms to translate remote sensing observations to surface cover properties, recognizing that the uncertain representation of

surface cover properties limits the accuracy of calculated atmosphere-biosphere trace gas exchanges.

5.6 Conclusions

A two-layer vegetation model to describe atmosphere-biosphere trace gas exchanges has been implemented in the chemistry-GCM ECHAM to study the effects of the canopy interactions between dry deposition, emissions, chemistry and turbulence on the NO_x canopy flux divergence on a global scale. To calculate soil-biogenic emission fluxes of NO, consistent with the meteorology and surface characteristics of ECHAM, we have implemented the emission algorithm by *YL95* in ECHAM. Moreover, to assess the sensitivity of the calculated fluxes and concentrations of NO_x and O_3 to the soil biogenic emissions, an inventory by *DK97*, which yields a substantially larger soil NO emission flux compared to *YL95*, has been implemented as well. We calculate global soil emission fluxes similar to those reported by *YL95* and *DK97* of about 12 and 21 Tg N/yr, respectively. The sensitivity of the calculated NO_x surface fluxes and concentrations to the soil emission flux is largely compensated by dry deposition, chemistry and transport processes, as indicated by the relative differences in the NO_x flux and concentrations calculated with the G-YL95 and B-DK97 inventory. The sensitivity of the O_3 surface concentrations to the NO soil emission fluxes is smaller than the sensitivity to the dry deposition formulations of the BL and ML model.

For sites that are exposed to relatively large emission fluxes, the ML and BL model calculate similar surface deposition NO_x fluxes, which confirms the validity of the big leaf approach for polluted regions. However, for relatively pristine sites in the sub-tropics and tropics, there are distinct differences between the ML and BL NO_x surface fluxes since the fluxes are controlled by the within-canopy interactions between soil emissions, dry deposition, chemistry and turbulence. Interpretation of the global annual NO_x budgets resulting from the ML and BL model including the CRF by *YL95*, confirms the applicability of the CRF approach to account for the reduction of soil NO emission flux due to dry deposition within the canopy on a global scale. However, comparison of the NO_x surface fluxes calculated with the multi-layer and the big leaf model, including the CRF, shows that there are distinct differences between the surface fluxes for specific ecosystems. For example, the BL model calculates an upward NO_x surface flux over tropical forest of about 0.2 times the soil emission flux, whereas we calculate an average ratio of about 0.4-0.5. Relatively large differences between the BL and ML surface fluxes are found over relatively sparse canopies at mid- or high latitude locations. These differences are due to explicit representation of chemical transformations within the canopy and turbulent exchange between the atmosphere and the canopy, which are not considered in the BL model. Moreover, due to a large sensitivity of the calculated fluxes and concentrations to dry deposition for suppressed turbulent mixing, subtle changes in the calculated dry deposition velocities by the BL and ML models are quite relevant. The sensitivity of the NO_x flux to the dry deposition process has been studied by considering a compensation point of 1 ppbv for NO_2. Relative differences in the NO_x surface fluxes are only significant over a relatively small area over the NH tundra and boreal forests, despite a significant reduction of the NO_2 dry deposition velocities for canopy NO_2 concentrations smaller than about 1.5 ppbv or even emissions for concentrations smaller than 1 ppbv.

In addition to the uncertainty in the definition of the compensation point, there are many uncertainties involved in our analysis, inherently related to the complexity of the soil-canopy system in controlling atmosphere-biosphere trace gas exchanges. However, the implementation of the multi-layer model in ECHAM provides a mechanistic representation of the canopy interactions between emissions, dry deposition, chemistry and turbulence, which can used to further explore the role of flux divergence of reactive trace gases on a global scale. As a starting point for the global assessment studies, the single column model will be used to reduce some of uncertainties in the processes involved, and further to evaluate the representativeness of the ML model by comparison with observations.

Chapter 6

Summary and discussion

The initial aim of the work, as presented in Chapter 2 of this thesis, has been the implementation of an improved description of the dry deposition of the reactive trace gases O_3, NO_x, and HNO_3, in the chemistry-GCM ECHAM. This was motivated by the fact that the common approach at that moment was to use constant dry deposition velocities despite the fact that observations had revealed that the dry deposition velocity often shows a distinct temporal cycle as well as spatial distribution as a function of surface cover. Moreover, a realistic representation of the dry deposition process is essential since it controls to a large extent the burden of many trace gases, e.g., O_3, and SO_2. It also ensures a fair model evaluation using surface observations, which are often largely controlled by dry deposition.
Our scheme calculates dry deposition velocities according to the big-leaf concept from the turbulent transport, surface cover fractions and vegetation activity calculated by ECHAM. Use of ECHAM parameters assures the calculation of dry deposition velocities consistent with temporal and spatial dependencies of the model physics and chemistry. Moreover, the degree of detail of the improved dry deposition parameterization is compatible with that of other surface and boundary layer process descriptions in ECHAM. This is the first time that such a high level of detail has been considered in the representation of the dry deposition process in a global model.
In Chapter 3, the extension of the dry deposition parameterization to the oxidized sulfur species SO_2 and the sulfate aerosol has been described. A further extension has been shortly described in Chapter 5, in which a first-order estimate of the surface uptake resistances of the dry deposition scheme for a selection of trace gases, which are involved in non-methane hydrocarbon chemistry, has been introduced. The use of estimated uptake resistances is required since for most of the involved trace gases such as PAN, CH_2O, and higher aldehydes and ketones, the understanding of the uptake mechanism is limited by the availability of observations. Actually, for most of the trace gases of the dry deposition scheme, the small number of observations over surface cover types such as oceans, bare soil and snow covered surfaces, imposes a serious constraint on a more sophisticated representation of the dry deposition process over these surfaces. However, using the first-order estimate to study the role of the dry deposition process for the burden of various trace gases will be helpful in discussions with experimentalist to consider these species in measurement campaigns. Future work would greatly benefit from additional observations of the dry deposition process over oceans, bare soil surface and snow and ice covered surfaces. In addition, observations of uptake by these substrates in experiments using enclosure chambers will help identify the

controlling mechanism, e.g., the relationship between O_3 soil uptake and the organic content and soil moisture. An explicit representation of these mechanisms, or inferred parameterizations, can subsequently be implemented in models like ECHAM. Obviously, this also depends on the availability of global scale databases of the controlling parameters. An example has been presented in Chapter 3, in which a global soil pH database has been used for an improved representation of the soil uptake of SO_2.

The initial representation of the dry deposition process also considered the dry deposition of NO_x, despite the fact that application of the big leaf approach for these species is questionable due to the occurrence of fast chemical transformations and bi-directional surface exchanges. However, at that moment we decided that a more realistic representation of the dry deposition process compared to the "constant V_d" approach would introduce at least a more realistic estimate of the removal of NO_x by dry deposition. The validity of this approach has been assessed in Chapters 4 and 5, which discusses the role of the canopy interactions for NO_x surface exchanges by coupling the biogenic emissions and dry deposition calculations, and by considering the chemistry and turbulence regime within the canopy. For those regions where the surface layer NO_x concentrations are controlled by antropogenic emissions, e.g. much of the northern hemispheric continents, the surface exchange is controlled by dry deposition. For these conditions, differences between the NO_x surface exchange calculated with the big leaf approach, in which the biogenic emissions and dry deposition are considered separately, and the coupled approach, are negligible. However, in subtropical and tropical regions, with a more significant role for soil-biogenic emission of NO_x, relative differences in NO_x surface fluxes and concentrations by both approaches are significant. Note that in these regions NO_x is often a rate limiting species in O_3 chemistry. This underscores the importance of the use of the coupled representation of atmosphere-biosphere NO_x exchange for those regions.

A major uncertainty involved with the description of aerosol dry deposition, in addition to the potential role of processes such as re-suspension and uptake by the canopy, is the mass size distribution of the aerosol. The sensitivity of the dry deposition velocity of sulfate aerosol for the mass size distribution, as presented in Chapter 3, has indicated the significance of considering the large differences in the dry deposition velocity as a function of the particle radius. We have applied representative continental (polluted) and marine (clean) sulfate mass size distributions. However, using these fixed mass size distributions implies that it has been assumed that there is an equilibrium between the sources of aerosols, e.g., production by coagulation and nucleation, and the removal by dry deposition over the whole particle radius range. Ideally, the mass size distribution is explicitly resolved as a function of the involved processes such as dry deposition.
In Chapter 2 we mention that dry deposition of the nitrate aerosol, which is relevant for the removal of HNO_3, is not considered in this work due to the fact that nitrate aerosol concentrations are not calculated by the chemistry scheme. However, model results of an off-line chemistry and transport model have shown that HNO_3 was predicted to partition almost completely into the aerosol phase if neutralized by ammonium for European winter time conditions [*Metzger*, 2000]. Consequently, for these conditions the contribution of the ammonium nitrate aerosol deposition should be considered in addition to the gas phase dry deposition of HNO_3. Future work on these issues on aerosol dry deposition relies on the progress made in the explicit representation of other processes involved.

The initial representation of the dry deposition scheme used the constant LAI of four of the applied ECHAM version, which was the main cause for the discrepancy between calculated and observed dry deposition velocities for sites with significantly larger or smaller LAI values than 4, e.g., tropical rainforest. Therefore, an initial modification of the surface cover representation has been introduced using a high-resolution ecosystem database [*Olson*, 1983], whereas maximum and minimum LAI values were scaled with an assumed seasonal cycle as a function of latitude. In Chapter 5, an additional modification of the representation of the surface cover properties using satellite data to describe observed seasonal cycles in the biomass has been described. However, as has been discussed in that chapter, use of satellite data to characterize the biomass does not always result in realistic absolute estimates of biomass for some ecosystems, e.g., tropical rainforest. This is likely related to a misrepresentation of the adopted values for parameters such as net primary production (NPP) and peak foliar density, which are used to translate the satellite data to an absolute amount of biomass expressed by the LAI. Moreover, the use of NDVI data to infer the amount of biomass is likely limited to canopies with an LAI smaller than about 6-7 due to a reduced sensitivity of the observed signal for larger amounts of biomass. In future, we will continue to improve the representation of surface cover by continuous evaluation with observations and introducing modifications of the applied algorithms. A clear example of the potential differences, introduced in the estimates of biomass using field observations, is presented in a study by *Guenther et al*. [1999]. They estimated the isoprene emission fluxes from Central Africa using an isoprene emission model for the global scale [*Guenther et al.,* 1995], which we also applied in our work presented in Chapter 4 and 5, and a modified model version using observations within the Central African domain. They report a relative difference in the peak foliar density of savanna of 41 % between the 1995 global emission inventory model and the modified model [*Guenther et. al.,* 1999]. The subsequent changes in the calculated isoprene emission fluxes are less dramatic, however, it indicates about the uncertainties involved in the definition of surface cover properties.

An essential issue of the characterization of surface cover is the assignment of discrete ecosystem classes to the grid cells of the global scale ecosystem databases. In our work we initially used the 1983 Olson ecosystem database, which contains 46 ecosystem classes, after which we introduced the 1992 version in which 72 ecosystem are distinguished on a 1/6° × 1/6° grid resolution. The detail in surface cover properties using the high-resolution databases is illustrated in Chapter 3 by showing the inferred July and January LAI distribution. However, this detail is somewhat misleading since it suggests a high accuracy of the global distribution of surface cover and its properties. A comparison of three different global ecosystem databases by *DeFries et al*. [1995] reveals that only for 26% of the land surface the three databases agree, whereas for 28% of the land surface the three databases do not agree at all. This indicates the potential errors that can be introduced by using different ecosystem databases to infer surface cover properties for models like ECHAM. Since many of the involved processes in the trace gas and aerosol exchanges are quite sensitive to the surface cover properties such as LAI, a continuous effort is needed to improve the representation of surface cover properties relevant to surface trace gas and aerosol exchanges in ECHAM.

The implementation of an explicit representation of the dry deposition and biogenic emission process, as a function of surface cover and land use, provides the opportunity to assess the

potential role of changes in surface cover and land use for the climate system through changes in the atmospheric chemical composition. In addition, surface cover and land use changes modify the micro-meteorological exchange of momentum, heat, and moisture and consequently the local, regional or even global scale meteorology [e.g., *Chase and Pielke*, 1996]. An example of the potential role of these interactions between the model dynamics, physics, chemistry and land cover and land use properties, is the sensitivity of the isoprene emissions to the surface roughness. Simulations with the single column model, presented in Chapter 4, show a significant change in the isoprene emissions for a small decrease in surface roughness due to a change in evaporation, moisture and the cloud cover and consequently the surface radiation, which largely controls the isoprene emissions. In future, ECHAM will be applied to study these complex interactions between dynamical, physical and chemical processes, considering possible future changes in land cover and land use on a global scale. Obviously, a large uncertainty is involved in the characterization of the future status of the land surface due to the role of complex social-economical factors. However, use of an ensemble of future land cover and land use scenarios will provide indications about the potential impact of land cover and land use changes for the global atmospheric chemistry and the climate system.

So far, the discussion is basically restricted to the uncertainties involved in the modeling of the atmosphere-biosphere trace gas and aerosol exchanges. Some of these uncertainties have been derived from model evaluation by comparison of calculated and observed parameters. In Chapters 2 and 3 we have performed an evaluation of the calculated O_3, and SO_2 and SO_4^{2-} dry deposition velocities, respectively. We did not include a comparison of the calculated and observed concentrations in these evaluations. However, a comparison of calculated and observed SO_2 and SO_4^{2-} concentrations by *Lelieveld et al.* [1997] showed that the explicit calculation of the SO_2 dry deposition velocity over snow and ice covered surfaces, presented in Chapter 3, actually reduced the agreement between calculated and observed SO_2 concentrations. Possible explanations for this misrepresentation have been discussed more extensively in Chapter 3. This example clearly shows that introduction of a more sophisticated representation of processes such as dry deposition does not necessarily imply that the overall model performance is improved. This underscores the need for a continuous evaluation of the representation of surface trace gas and aerosol exchanges in large scale models such as ECHAM. Therefore, a major focus of future work should be the collaboration with scientists involved in measurements campaigns, which will hopefully be performed over the various surface cover types of the world, and help reducing the uncertainties involved in global scale modeling of surface trace gas and aerosol exchanges.

Appendix A

Abbreviations

Abbreviations

GCM	general circulation model
ECHAM	European Centre model, Hamburg version
PAR	photosynthetic active radiation
LAI	leaf area index
REA	relaxed eddy-accumulation
ECMWF	European Centre for Medium Range Weather Forecasts
QBR	quasi-laminar boundary-layer resistance
NH	northern hemisphere
SH	southern hemisphere
NSS	non-sea-salt
DDIM	Dry Deposition Inferential Measurement
NDVI	Normalized Difference Vegetation Index
RACMO	Regional Atmospheric Climate Model
SL	surface layer
LAD	leaf area density
PBL	planetary boundary layer
STS	sub-timestep
ABLE-3B	Arctic Boundary Layer Expedition
CRF	canopy reduction factor
SAI	stomatal area index
LES	large eddy simulation
NPP	net primary production
NMHC	non-methane hydrocarbons
G-YL95	modified version of the soil-biogenic NO_x emission algorithm by Yienger Levy [1995]
B-DK97	modified version of the soil-biogenic NO_x emission inventory by Davidson and Kingerlee [1997]
BL	Big Leaf
ML	multi-layer

Bibliography

Andreae, M. O., W. Elbert, and S. J. de Mora, Biogenic sulfur emissions and aerosols over the tropical South Atlanctic, 3. Atmospheric dimethylsulfide, aerosols and cloud condensation, *J. Geophys. Res., 100*, 11,335-11,355, 1995.

Arndt, R. L., G. R. Carmichael, D. G. Streets, and N. Bhatti, Sulfur dioxide emissions and sectoral contributions to sulfur deposition in Asia, *Atmos. Environ., 31*, 1553-1573, 1997.

Bache, D. H., Particulate transport within plant canopies, 2, Predictions of deposition velocities, *Atmos. Environ., 13*, 1681-1687, 1979.

Bakwin, P S., S. C. Wofsy, S.-M. Fan, M. Keller, S. E. Trumbore, and J. M. Da Costa, Emission of nitric oxide (NO) from tropical forest soils and exchange of NO between the forest canopy and atmospheric boundary layers, *J. Geophys. Res., 95,* 16,755-16,764, 1990.

Bakwin, P. S., D. J. Jacob, S. C. Wofsy, J. M. Munger, B. C. Daube, J. D. Bradshaw, S. T. Sandholm, R. W. Talbot, H. B. Singh, G. L. Gregory, and D. J. Blake, Reactive nitrogen oxides and ozone above a taiga woodland, *J. Geophys. Res., 99,* 1927-1936, 1994.

Baldocchi, D. D., B. B. Hicks, and P. Camara, A canopy stomatal resistance model for gaseous deposition to vegetated surfaces, *Atmos. Environ.*, *21*, 91-101, 1987.

Baldocchi, D. D., A lagrangian random-walk model for simulating water vapor, CO_2 and sensible heat flux densities and scalar profiles over and within a Soybean canopy, *Boundary Layer Meteorol., 61,* 113-144, 1992.

Baldocchi, D. D., Deposition of gaseous sulfur compounds to vegetation, in *Sulfur nutrition and assimilation and higher plants*, edited by L. J. De Kok et al., 271-293, SPB Academic Publishing bv, The Hague, The Netherlands, 1993.

Baldocchi, D. D., and P. C. Harley, Scaling carbon dioxide and water vapour exchange from leaf to canopy in a deciduous forest. 2. Model testing and application, *Plant. Cell and Environ., 18,* 1157-1173, 1995.

Bales, R. C., M. P. Valdez, and G. A. Dawson, Gaseous deposition to snow, 2. Physical-chemical model for SO_2 deposition, *J. Geophys. Res., 92*, 9789-9799, 1987. Barrie, L.A., and J. L. Walmsley, A study of sulphur dioxide deposition velocities to snow in Northern Canada, *Atmos. Environ., 12*, 2321-2332, 1978.

Barrie, L., Y. Yi, W.R. Leaitch, U. Lohmann, P. Kasibhatla, G.J. Roelofs, J.Wilson, F. McGovern, C. Benkovitz, M.A. Melieres, K. Law, J. Prospero, M. Kritz, D. Bergmann, C. Bridgemann, M. Chin, J. Christensen, R. Easter, J. Feichter, C. Land, A. Jeuken, E. Kjellström, D. Koch and P. Rasch, A comparison of large scale atmospheric sulphate aerosol models (COSAM): Overview and highlights, *Tellus*, in press.

Batjes, N. H., A global data set of soil pH properties, *Tech. Paper 27*, International Soil Reference and Information Centre, Wageningen, 1995.

Bergin, M. H., J.-L. Jaffrezo, C. I. , J. E. Dibb, S. N. Pandis, R. Hillamo, W. Maenhaut, H. D. Kuhns, and T. Makela, The contributions of snow, fog, and dry deposition to the summer flux of anions and cations at summit, Greenland, *J. Geophys. Res., 100*, 16,275-16,288, 1995.

Bosveld, F. C., A. A. M. Holtslag, and B. J. J. M. van den Hurk, Nighttime convection in the interior of a dense Douglas Fir forest, *Boundary Layer Meteorol., 93,* 171-195, 1999.

Bouwman, A. F., K. W. van der Hoek, and J. G. J. Olivier, Uncertainties in the global source distribution of nitrous oxide, *J. Geophys. Res., 100,* 2785-2800, 1995.

Bouwman, A. F., and D. P. Van Vuuren, Global assessment of acidification and eutrophication of natural ecosystems, *UNEP/DEAI&EW/TR.99-6* and *RIVM 4020001012,* 1999.

Box, E., Foliar biomass: Data base of the international biological program and other sources, in *Atmospheric Biogenic Hydrocarbons,* edited by J. Bufalini and R. Arnts, Butterworth-Heinemannm, Newton, Mass., 1981.

Brinkop, S., and E. Roeckner, Cloud-turbulence interactions: Sensitivity of a general circulation model to closure assumptions, *Rep. 17*, Max-Planck-Institut für Meteorologie, Hamburg, 1993.

Brodkey, R. S., Fundamentals of turbulent motion, mixing and kinetics, *Chem. Eng. Commun., 8*, 1-23, 1981

Brunekreef , B. , and G. Hoek, Beyond the body count: air pollution and death, *Am. J. Epidemiol., 151*, 449-451, 2000

Brutsaert, W., Evaporation into the atmosphere, Kluwer, Dordrecht, The Netherlands, 1973.

Cadle, S. H., J. Muhlbaier Dasch, and P. A. Mulawa, Atmospheric concentrations and the deposition velocity to snow of nitric acid, sulfur dioxide and various particulate species., *Atmos. Environ., 11*, 1819-1827, 1985.

Chamberlain, A. C., Dry deposition of sulfur dioxide, in: *Atmospheric sulfur deposition*, edited by D. S. Shriner et al., Ann Harbor Science, Michigan, 185-197, 1980.

Chameides, W. L., Acid dew and the role of chemistry in the dry deposition of reactive gases to wetted surfaces, *J. Geophys. Res.*, 92, 11,895-11,908, 1987.

Charlson, R. J., S. E. Schwartz, J. M. Hales, R. D. Cess, J. A. Coakley, J. E. Hansen, and D. J. Hofmann, Climate forcing by anthropogenic aerosols, *Science, 255,* 423-430, 1992.

Charnock, M., Wind stress on a water surface, *Q. J. R. Meterol. Soc., 81*, 639-640, 1955.

Chase, T. N., R. A. Pielke, T. G. F. Kittel, R. Nemani, and S. W. Running, Sensitivity of a general circulation model to global changes in leaf area index, *J. Geophys. Res., 101,* 7393-7408, 1996.

Chin, M., D. J. Jacob, G. M. Gardner, M. Foreman-Fowler, and P. A. Spiro, A global three-dimensional model of tropospheric sulfate, *J. Geophys. Res., 101*, 18,667-18,690, 1996.

Chin, M., and D. J. Jacob, Anthropogenic and natural contributions to tropospheric sulfate: A global model analysis, *J. Geophys. Res., 101*, 18,691-18,699, 1996.

Christensen, J. H., O. B. Christensen, P. Lopez, van Meijgaarden, E., and Botzet, M., The HIRHAM4 Regional Atmospheric Climate model, *Scientific Report 96-4*, Danish Meteorological Institute, Copenhagen, 1996.

Cionco, R. M., Analysis of canopy index values for various canopy densities, *Boundary Layer Meteorol., 15,* 81-83, 1978.

Clapsaddle, C., and D. Lamb, The sorption behaviour of SO_2 on ice at temperatures between -30°C and –5°C, *Geophys. Res. Lett., 16*, 1173-1176, 1989.

Claussen, M., U. Lohmann, E. Roeckner, and U. Schulzweida, A global data set of land-surface parameters, *Rep. 135*, Max-Planck-Institut für Meteorologie, Hamburg, 1994.

Claussen, M., Estimation of regional heat and moisture fluxes in homogeneous terrain with bluff roughness elements, *J. Hydrol., 166*, 353-369, 1995.

Conklin, M. H., R. A. Sommerfeld, S. K. Laird, and J. E. Villinski, Sulfur dioxide reactions on ice surfaces: Implications for dry deposition to snow, *Atmos. Environ., 27A*, 159-166, 1993.

Davidson, E., and W. Kingerlee, A global inventory of nitric oxide emissions from soils, *Nutrient Cycling in Agroecosystems, 48,* 37-50, 1997.

Davies, T. D., and Mitchell, J. R., Dry deposition of sulphur dioxide onto grass in rural eastern England (with some comparisons with other forms of sulphur deposition), in: *Precipitation scavenging, dry deposition and resuspension*, edited by H. R. Pruppacher, R. G. Semonin and W. G. N. Slinn, 795-806, Elsevier, Amsterdam, 1983.

DeFries, R. S., C. B. Field, I. Fung, C. O. Justice, S. Los, P. A. Matson, E. Matthews, H. A. Mooney, C. S. Potter, K. Prentice, P. S. Sellers, J. R. G. Townshend, C. J. Tucker, S. L. Ustin, and P. M. Viousek, Mapping the land surface for global atmosphere-biosphere models: Toward continuous distributions of vegetation's functional properties, *J. Geophys. Res., 100*, 20,867-20,882, 1995.

Delany, A. C., and T. D. Davies, Dry deposition of NO_x to grass in rural East Anglia, *Atmos. Environ., 17*, 1391-1394, 1983.

Denmead, O. T., and E. F. Bradley, Flux-gradient relationships in a forest canopy, in: *The Forest-Atmosphere Interaction,* edited by B. A. Hutchison and B. B. Hicks, 421-442, 1985.

Dentener, F. J., and P. J. Crutzen, Reaction of N_2O_5 on tropospheric aerosols: Impact on the global distributions of NO_x, O_3, and OH, *J. Geophys. Res.*, *98*, 7149-7163, 1993.

DKRZ, Deutsches Klimarechenzentrum, Modellbetreuungsgruppe, Technical Report No. 6, The ECHAM3 atmospheric general circulation model, Hamburg, 1992.

Dolman, A. J., Estimates of roughness length and zero plane displacement for a foliated and non-foliated oak canopy, *Agric. Forest Meteorol., 36*, 241-248, 1986.

Dovland, H., and A. Eliassen, Dry deposition on a snow surface, *Atmos. Environ., 10*, 783-785, 1976.

Duyzer, J., H. Weststrate, and S. Walton, Exchange of ozone and nitrogen oxides between the atmosphere and coniferous forest, *Water, Air, Soil Pollut., 85*, 2065-2070, 1995.

Erisman, J. W., and G. P. Wyers, Continuous measurements of surface exchange of SO_2 and NH_3: implications for their possible interaction in the deposition process, *Atmos. Environ., 27A*, 1937-1949, 1992.

Erisman, J. W., and D. D. Baldocchi, Modelling dry deposition of SO_2, *Tellus 46B*, 159-171, 1994.

Erisman, J. W., and A. Van Pul, Parameterization of surface resistance for the quantification of atmospheric deposition of acidifying pollutants and ozone, *Atmos. Environ., 28*, 2595-2607, 1994.

Erisman, J. W., and G. P. J. Draaiers, Atmospheric deposition in relation to acidification and eutrophication, Elsevier, New York, 1995.

Erisman, J.W., and W. de Vries, Nitrogen deposition and effects in European forests, *Environ. Reviews, 8*, 65-93. 2000.

Fan, S.-M., S. C. Wofsky, P. S. Bakwin, D. J. Jacob, and D. R. Fitzjarrald, Atmosphere-biosphere exchange of CO_2 and O_3 in the Central Amazon forest, *J. Geophys. Res.*, *95*, 16,851-16,864, 1990.

Farquhar, G. D., P. M. Firth, R. Wetselaar, and B. Weir, On the gaseous exchange of ammonia between leaves and the environment: Determination of the ammonia compensation point, *Plant. Physiol., 66,* 710-714, 1980.

Feichter, J, E. Kjellström, H. Rodhe, F. Dentener, J. Lelieveld, and G. J. Roelofs, Simulation of the troposheric sulfur cycle in a global climate model, *Atmos. Environ., 30*, 1693-1707, 1996.

Fitzgerald, J. W., Approximation formulas for the equilibrium size of an aerosol particle as a function of its dry size and composition and the ambient relative humidity, *J. Appl. Meteorol., 14*, 1044-1049, 1975.

Fitzjarrald, D. R., and D. H. Lenschow, Mean concentration and flux profiles for chemically reactive species in the atmospheric surface layer, *Atmos. Environ., 17,* 2117-2120, 1983.

Fitzjarrald, D. R., K. E. Moore, O. M. R Cabral, J. Scolar, A. O. Manzi, and L. D. De Abreu Sá, Daytime turbulent exchange between the Amazon forest and the atmosphere, *J. Geophys. Res., 95,* 16,825-16,838, 1990a.

Fitzjarrald, D. R., and K. E. Moore, Mechanism of nocturnal exchange between the rain forest and the atmosphere, *J. Geophys. Res., 95,* 16,839-16,850, 1990b.

Fitzjarrald, D. R., and K. E. Moore, Growing season boundary layer climate and surface exchanges in

a subartic lichen woodland, *J. Geophys. Res., 99,* 1899-1917, 1994.

Fowler, D., and M. H. Unsworth, Turbulent transfer of sulfur dioxide to a wheat crop, *Q. J. R. Meteorol. Soc., 105*, 767-783, 1979.

Fuentes, J. D., T. J. Gillespie, G. den Hartog, and H. H. Neumann, Ozone deposition onto a deciduous forest during dry and wet conditions, *Agric. and Forest Meteor., 62*, 1-18, 1992.

Galbally , I. E., and C. R. Roy, Destruction of ozone at the earth's surface, *Q. J. R. Meteorol. Soc., 106*, 599-620, 1980.

Galmarini, S., J. Vilà-Guerau de Arellano, and P. G. Duynkerke, Scaling the turbulent transport of chemical compounds in the surface layer under neutral and stratified conditions, *Q. J. R. Meteorol. Soc., 123,* 223-242, 1997.

Ganzeveld, L., and J. Lelieveld, Dry deposition parameterization in a chemistry general circulation model and its influence on the distribution of reactive trace gases, *J. Geophys. Res., 100*, 20,999-21,012, 1995.

Ganzeveld, L., J. Lelieveld, and G.-J. Roelofs, Dry deposition parameterization of sulfur oxides in a chemistry and general circulation, *J. Geophys. Res.*, *103*, 5679-5694, 1998.

Ganzeveld, L., J. Lelieveld, F. J. Dentener, M. C. Krol , and G.-J. Roelofs, Atmosphere-biosphere trace gas exchanges simulated with a single column model, *submitted to J. Geophys. Res.*, 2000a.

Ganzeveld, L., J. Lelieveld, G.-J. Roelofs, F. J. Dentener, and M. C. Krol, Global soil-biogenic NO_x emissions and the role of canopy processes, *submitted to J. Geophys. Res.*, 2000b.

Gao, W., M. L.Wesely, and I. Y. Lee, A numerical study of the effects of air chemistry on fluxes of NO, NO_2, and O_3 near the surface, *J. Geophys. Res., 96*, 18,761-18,769, 1991.

Gao, W., M. L.Wesely, and P. V. Doskey, Numerical modeling of the turbulent diffusion and chemistry of NO_x, O_3, isoprene and other reactive trace gases in and above a forest canopy, *J. Geophys. Res., 98*, 18,339-18,353, 1993.

Gao, W., and M. L.Wesely, Modelling gaseous dry deposition over regional scales with satellite observations, 1. Model development, *Atmos. Environ., 29*, 727-737, 1995.

Garratt, J. R., and B. B. Hicks, Momentum, heat and water vapour transfer to and from natural and artificial surfaces, *Q. J. R. Meteorol. Soc.*, *99*, 680-687, 1973.

Granat, L., and C. Johansson, Dry deposition of SO_2 and NO_x in winter, *Atmos. Environ.*, *17*, 191-192, 1983.

Guenther, A., C. Nicolas Hewitt, D. Erickson, R. Fall, C. Geron, T. Graedel, P. Harley, L. Klinger, M. Lerdau, W. A. McKay, T. Pierce, B. Scholes, R. Steinbrecher, R. Tallamraju, J. Taylor, and P. Zimmerman, A global model of natural volatile organic compound emissions, *J. Geophys. Res., 100*, 8873-8892, 1995.

Guenther, A. B., and A. J. Hills, Eddy covariance measurement of isoprene fluxes, *J. Geophys. Res.,*

103, 13,145-13,152, 1998.

Guenther, A., B. Baugh, G. Brasseur, J. Greenberg, P. Harley, L. Klinger, S. Serça, and L. Vierling, Isoprene emission estimates and uncertainties for the Central African EXPRESSO study domain, *J. Geophys. Res., 104,* 30,625-30,639, 2000.

Gutman, G., D. Tarpley, A. Ignatov, and S. Olson, The enhanced NOAA Global Land Dataset from the Advanced Very High Resolution Radiometer. *Bull. Am. Meteorol. Soc., 76*, 1141-1156, 1995.

Hameed, S., and J. Dignon, Changes in the geographical distributions of global emissions of NO_x and SO_x from fossil-fuel combustion between 1966 and 1980, *Atmos. Environ., 22,* 441-449, 1988.

Hanson, P. J., and S. E. Lindberg, Dry deposition of reactive nitrogen compounds: a review of leaf, canopy and non-foliar measurements, *Atmos. Environ., 25A*, 1615-1634, 1991.

Harriss, R. C., et al., The Amazon Boundary Layer Experiment (ABLE-2B): wet season 1987, *J. Geophys. Res., 95,*, 16,721-16,736, 1990.

Henderson-Sellers, A., M. F. Wilson. G. Thomas, and R. E. Dickinson, Current global land-surface data sets for use in climate-related studies, *Tech. Note, NCAR/TN-272+STR*, Natl. Cent. For Atmos. Res., Boulder, Co, 1986.

Hicks, B. B., M. L. Wesely, R. L. Coulter, R. L. Hart, J. L. Durham, R. Speer, and D. H. Stedman, An experimental study of sulfur and NO_x fluxes over grassland, *Boundary Layer Meteorol., 34*, 103-121, 1986.

Hicks, B. B., D. D. Baldocchi, T. P. Meyers, R. P. Hosker, Jr., and D. R. Matt, A preliminary multiple resistance routine for deriving dry deposition velocities from measured quantities, *Water, Air, Soil Pollut., 36*, 311-330, 1987.

Hicks, B. B., R. R. Draxler, D. L. Albritton, F. C. Fehsenfeld, J. M. Hales, T. P. Meyers, R. L. Vong, M. Dodge, S. E. Schwartz, R. L. Tanner, C. L. Davidson, S. E. Lindberg, and M. L. Wesely, Atmospheric processes research and process model development, State-of-Science/Technology, *Report 2*, NAPAP, NOAA/ATDD contribution number 89/20, 1989a

Hicks, B. B., D. R. Matt, R. T. McMillen, J. D. Womack, M. L. Wesely, R. L. Hart, D. R. Cook, S. E. Lindberg, R. G. de Pena, and, D. W. Thomson, A field investigation of sulfate fluxes to a deciduous forest, *J. Geophys. Res., 94*, 13,003-13,001, 1989b.

Holland, E. A., B. H. Braswell, J.-F. Lamarque, A. Townsend, J. Sulzman, J.-F. Müller, F. Dentener, G. Brasseur, H. Levy II, J. E. Penner, and G.-J. Roelofs, Variations in the predicted spatial distribution of atmospheric nitrogen deposition and their impact on carbon uptake by terrestrial ecosystems, *J. Geophys. Res., 102,* 15,849-15,866, 1997.

Houweling, S, F. Dentener, and J. Lelieveld, The impact of nonmethane hydrocarbon compounds on troposheric chemistry, *J. Geophys. Res., 103*, 10,673-10,696, 1998.

Huebert, B. J., and C. H. Robert, The dry deposition of nitric acid to grass, *J. Geophys. Res., 90*, 2085-2090, 1985.

Hummelshøj, P., N. O. Jensen, and S. E. Larsen, Particle dry deposition to a sea surface, in: *Precipitation scavenging and atmosphere-surface exchange*, 2, edited by S. E. Schwartz and W. G. N. Slinn, 829-840, Hemisphere Publishing Corporation, Washington, 1992.

Ibrahim, M., L. A. Barrie, and F. Fanaki, An experimental and theoretical investigation of the dry deposition of particles to snow, Pine trees and artificial collectors, *Atmos. Environ., 17*, 781-788, 1983.

IPPC, Climate change: The science of climate change, Contribution of working group 1 to the second assessment report of the Intergovernmental Panel on Climate Change, edited by J. T. Houghton et al., Cambridge University Press, 1995.

Jacob, D. J., and S. C. Wofsy, Budgets of reactive nitrogen, hydrocarbons and ozone over the Amazon forest during the wet season, *J. Geophys. Res., 95*, 16,737-16,754, 1990.

Jacob D. J., and P. S. Bakwin, Cycling of NO_x in tropical forest canopies, In: *Microbial production and consumption of greenhouse gases: methane, nitrogen oxides and halomethanes*, eds.: J. E. Rogers and W. B. Whitman, 237-253, American Society of Microbiology, 1991.

Jacob, D. J., S.-M. Fan, S. C. Wofsy, P. A. Spiro, P. S. Bakwin, J. A. Ritter, E. V. Browell, G. L. Gregory, D. R. Fitzjarrald, and K. E. Moore, Deposition of ozone to tundra, *J. Geophys. Res.*, *97*, 16,473-16,479, 1992.

Jacobs, A. F. G., J. H. van Boxtel, and R. M. M. El-Kilani, Nighttime free convection characteristics within a plant canopy, *Agric. Forest Meteorol., 58,* 247-256, 1992.

Jacobs, A. F. G., J. H. van Boxtel, and R. H. Shaw, The dependence of canopy turbulence on within-canopy thermal stratification, *Boundary Layer Meteorol., 71,* 375-391, 1994.

Johansson, C., and L. Granat, An experimental study of the dry deposition of gaseous nitric acid to snow, *Atmos. Environ., 20,* 1165-1170, 1986

Johansson, C., Pine forest: a negligible sink for atmospheric NO_x in rural Sweden, *Tellus 39B*, 426-438, 1987.

Joss, U., and W. K. Graber, Profiles and simulated exchange of H_2O, O_3, NO_2 between the atmosphere and the HartX Scots Pine Plantation, *Theor. Appl. Climatol., 53*, 157-172, 1996.

Kasibhatla, P. S., H. Levy, II, and W. J. Moxim, Global NO_x, HNO_3, PAN, and NO_y distributions from fossil fuel combustion emissions: A model study, *J. Geophys. Res.*, *98*, 7165-7180, 1993.

Kasibhatla, P., Chameides, W. L., and J. St. John, A three-dimensional global model investigation of seasonal variations in the atmospheric burden of anthropogenic sulfate aerosols, *J. Geophys. Res., 102*, 3737-3759, 1997.

Kerstiens, G., and K. J. Lendzian, Interactions between ozone and plant cuticles, *New Phytol.,* 112, 13-19, 1989.

Kidwell, K. B. (ed.), *Global vegetation index user's guide*, USDOC/NOAA National Climatic Data Center, Satellite Data Services Division, Washington, 45 p, 1990.

Kramm, G., R. Dlugi, and H. Müller, On the determination of dry deposition fluxes of ozone, nitric

oxide and nitric dioxide, *Eurotrac Newsletter, 11*, 2-9, 1993.

Kramm, G., A numerical method for determining the dry deposition of atmospheric trace gases, *Boundary Layer Meteorol., 48,* 157-176, 1989.

Krol, M. C., J. M. Molemaker, and J. Vilà Guerau de Arellano, Effects of turbulence and heterogeneous emissions on photochemically active species in the convective boundary layer, *J. Geophys. Res., 105,* 6871-6884, 2000.

Kruijt, B., Y. Malhi, J. Lloyd, A. D. Nobre, A. C. Miranda, M. G. P. Pereira, A. Gulf, and J. Grace, Turbulence statistics above and within two Amazon rain forest canopies, *Boundary Layer Meteorol., 94,* 297-331, 2000.

Langner, J., and H. Rodhe, A global three-dimensional model of the troposheric sulfur cycle, *J. Atmos. Chem., 13*, 225-263, 1991.

Lee, Y., and S. E. Schwartz, Evaluation of the rate of uptake of nitrogen dioxide by atmospheric and surface liquid water, *J. Geophys. Res., 86,* 11,971-11,983, 1981.

Lelieveld, J., G. J. Roelofs, L. Ganzeveld, J. Feichter, and H. Rodhe, Terrestrial sources and distribution of atmospheric sulfur, *Phil. Trans. Roy. Soc., B, 352*, 149-158, 1997.

Lelieveld, J., and F. J. Dentener, What controls tropospheric ozone? *J. Geophys. Res., 105*, 3531-3551, 2000.

Lenschow, D. H., D. Pearson, Jr., and B. Boba Stankov, Measurements of ozone vertical flux to ocean and forest, *J. Geophys. Res., 87*, 8833-8837, 1982.

Lerdau, M. T., J. W. Munger, and D. J. Jacob, The NO_2 flux conundrum, *Science, 289,* 2291-2293, 2000.

Leuning, R., M. H. Unsworth, H. H. Neumann, and K. M. King, Ozone fluxes to tobacco and soil under field conditions, *Atmos. Environ., 13,* 1155-1163, 1979.

Levy, H, II, and W. J. Moxim, Simulated global distribution and deposition of reactive nitrogen emitted by fossil fuel combustion, *Tellus*, *41B*, 256-271, 1989.

Lieth, H., Modeling the primary productivity of the world, in: *Primary Productivity of the Biosphere,* edited by H. Lieth and R. Whittaker, Springer-Verlag, New York, 1975.

Logan, J. A., Nitrogen oxides in the troposphere: Global and regional budgets, *J. Geophys. Res., 88,* 10,785-10,807, 1983.

Lohmann, U., R. Sausen, L. Bengtsson, U. Cubasch, J. Perlwitz, and E. Roeckner, The Köppen climate classification as a diagnostic tool for general circulation models, in *Clim. Res., 3*, 177-193, 1993.

Massman, W. J., J. Pederson, A. Delany, D. Grantz, G. den Hartog, H. H. Neumann, S. P. Oncley, R. Pearson, Jr., R. H. Shaw, An evaluation of the regional acid deposition model surface module for ozone uptake at three sites in the San Joaquin Valley of California, *J. Geophys. Res., 99*, 8281-8294, 1994.

Matt, D. R., and T. P. Meyers, On the use of the inferential technique to estimate dry deposition of SO_2, *Atmos. Environ., 27A*,, 493-501, 1993.

Matthews, E., Global vegetation and land use: new high resolution data bases for climate studies, *J. Climate and Applied Meteorol., 22,* 474-486, 1983.

McKay, W. A., B. A. Stephens, and G. J. Dollard, Laboratory measurements of ozone deposition to sea water and other saline solutions, *Atmos. Environ.*, *26A*, 3105-3110, 1992.

Mehlmann, A., Grössenverteilung des aerosolnitrats und seine beziehung zur gasförmigen salpetersäure, *Ph.D. Thesis*, Univ. Mainz, 1986.

Metzger, S., Gas/aerosol partitioning: A simplified method for global modeling, *Ph.D. thesis*, Utrecht University, Utrecht, The Netherlands, 2000.

Meyers, T. P., The sensitivity of modeled SO_2 fluxes and profiles to stomatal and boundary layer resistances, *Water, Air, Soil Pollution, 35*, 261-278, 1987.

Meyers, T. P., and K. T. Paw U, Modelling the plant canopy micrometeorology with higher-order closure principles, *Agric. Forest Meteorol., 41,* 143-163, 1987.

Meyers, T. P., and D. D. Baldocchi, The budgets of turbulent kinetic energy and Reynolds stress within and above a deciduous forest, *Agric. Forest. Meteorol., 53,* 207-222, 1991.

Milne, J. W., D. B. Roberts, and D. J. Williams, The dry deposition of sulfur dioxide field measurements with a stirred chamber, *Atmos. Environ., 13*, 373-379, 1979.

Mitra, S. K., S. Barth, and H. R. Pruppacher, A laboratory study on the scavenging of SO_2 by snow crystals, *Atmos. Environ., 24A*, 2307-2312, 1990.

Muhlbaier Dasch, J., and S. H. Cadle, Dry deposition to snow in an urban area, *Water, Air, Soil Pollut., 29*, 297-308, 1986.

Müller, J., Geographical distribution and seasonal variation of surface emissions and deposition velocities of atmospheric trace gases, *J. Geophys. Res.*, 97, 3787-3804, 1992.

Munger, J. W., S. C. Wofsy, P. S. Bakwin, S.-M. Fan, M. L. Goulden, B. C. Daube, and A. H. Goldstein, Atmospheric deposition of reactive nitrogen oxides and ozone in a temperate deciduous forest and a subartic woodland 1. Measurements and mechanism, *J. Geophys. Res., 101,* 12,639-12,657, 1996.

Murphy Jr., C. E., and J. T. Sigmon, Dry deposition of sulfur and nitrogen oxide gases to forest vegetation, in *Acidid precipitation, 3: Sources, deposition and canopy interactions*, edited by S. E. Lindberg, A. L. Page, and S. A. Norton, Springer Verlag, 217-240,1989.

Neubert, A., D. Kley, and J. Wildt, Uptake of NO, NO_2 and O_3 by sunflower (*Helianthus Annuus L.*) and tobacco plants (*Nicotiana Tabacum L.*): dependence on stomatal conductivity, *Atmos. Environ.*, *27A*, 2137-2145, 1993.

Nicholson, K. W., and T. D. Davies, The dry deposition of sulfur dioxide at a rural site, *Atmos.*

Environ., 22, 2885-2889, 1988.

Matthews, E., Global vegetation and land use: new high resolution data bases for climate studies, *J. Climate and Applied Meteorol., 22,* 474-486, 1983.

Norman, J. M., Modeling the complete crop canopy, in *Modification of the aerial environment of crops*, edited by B. J. Barfield and J. F Gerber, 249-280, American Society of Agricultural Engineers, St. Joseph, MI, USA, 538 pp, 1979.

Olson, J., J. A. Watts, and L. J. Allison, *Carbon in live vegetation of major World ecosystems* , ORNL-5862, Oak Ridge National Laboratory, Oak Ridge, Tennessee, 1983.

Olson, J, World ecosystems (WE1.4): Digital raster data on a 10 minute geographic 1080 x 2160 grid square, in *Global Ecosystem Database, Version 1.0: DISC A*, edited by NOAA National Geophysical Data Center, Boulder, CO, 1992.

Padro, J., Seasonal contrasts in modelled and observed dry deposition velocities of O_3, SO_2 and NO_2 over three surfaces, *Atmos. Environ., 27A*, 807-814, 1993a.

Padro, J., H. H. Neumann, and G. Den Hartog, Dry deposition velocity estimates of SO_2, from models and measurements over a decideous forest in winter, *Water, Air, Soil Pollut., 68*, 325-339, 1993b.

Patton, E. G., K. J. Davis, M. C. Barth, P. S. Sullivan, Decaying scalars emitted by a forest canopy: A numerical study, *Boundary Layer Meteorol.*, in press.

Payrissat, M., and S. Beilke, Laboratory measurements of the uptake of sulfur dioxide by different European soils, *Atmos. Environ., 9*, 211-217, 1975.

Penner, J. E., C. S. Atherton, J. Dignon, S. J. Ghan, and J. J. Walton, Tropospheric nitrogen: A three-dimensional study of sources, distributions and deposition, *J. Geophys. Res*, 96, 959-990, 1991.

Petersen, A. C., Convection and chemistry in the atmospheric boundary layer, *Ph.D. thesis*, Utrecht University, Utrecht, The Netherlands, 1999.

Pleim, J. E., A. Venkatram, and R. Yamartino, ADOM/TADAP model development program. The dry deposition module, *Vol. 4,* Ontario Ministry of the Environment, Rexdale, Canada, 1984.

Potter, C. S., P. A. Matson, P. M. Vitousek, and E. Davidson, Process modeling of controls on nitrogen trace gas emissions from soils worldwide, *J. Geophys. Res., 101,* 1361-1377, 1996.

Prahm, L. P., U. Torp, and R. M. Stern, Deposition and transformation rates of sulfur dioxides during atmospheric transport over the Atlantic, *Tellus, 28*, 355-372, 1975.

Raupach, M. R., and A. S. Thom, Turbulence in and above plant canopies, *Ann. Rev. Fluid. Mech., 13,* 97-129, 1981.

Raupach, M. R., A lagrangian analysis of scalar transfer in vegetation canopies, *Q. J. R. Meteorol. Soc., 113,* 107-120, 1987.

Raupach, M. R., Simplified expressions for vegetation roughness length and zero-plane displacement as functions of canopy height and area index, *Boundary Layer Meteorol., 71*, 211-216, 1994.

Rinne, H. J. I., A. C. Delany, J. P. Greenberg, and A. B. Guenther, A true eddy accumulation system for trace gas fluxes using disjunct eddy sampling method, *J. Geophys. Res., 105*, 24,791-24,798, 2000.

Ritter, J. A., J. D. Barrick, C. E. Watson, G. W. Sachse, G. L. Gregory, M. A. Woerner, C. E. Watson, G. F. Hill, and J. E. Collins, Jr, Airborne flux measurements of trace species in an arctic boundary layer, *J. Geophys. Res.*, *97*, 16,601-16,625, 1992.

Ritter, J. A., J. D. Barrick, C. E. Watson, G. W. Sachse, G. L. Gregory, B. E. Anderson, M. A. Woerner, and J. E. Collins, Jr, Airborne boundary layer flux measurements of trace gas species over Canadian boreal forest and northern wetland regions, *J. Geophys. Res.*, *99*, 1671-1685, 1994.

Roberts, J., O. M. R. Cabral, and L. F. De Aguiar, Stomatal and boundary-layer conductance in an Amazonian Terra Firme rain forest, *J. Appl. Ecol., 27,* 336-353, 1990.

Roeckner, E., K. Arpe, L. Bengtsson, S. Brinkop, L. Dümenil, M. Esch, E. Kirk, F. Lunkeit, M. Ponater, B. Rockel, R. Sausen, U. Schlese, S. Schubert, and M. Windelband, Simulations of the present-day climate with the ECHAM model: impact of model physics and resolution, *Report No. 93*, Max-Planck-Institut für Meteorologie, Hamburg, 1992.

Roeckner, E., K. Arpe, L. Bengtsson, M. Christoph, M. Claussen, L. Dümenil, M. Esch, M. Giogetta, U. Schlese, U. Schulzweida, The atmospheric general circulation model ECHAM-4: Model description and simulation of the Present-day Climate, *Report No. 218*, Max-Planck-Institut für Meteorologie, Hamburg, 1996.

Roelofs, G.-J., and J. Lelieveld, Distribution and budget of O_3 in the troposphere calculated with a chemistry-general circulation model, *J. Geophys. Res., 100*, 20,983-20,998, 1995.

Roelofs, G.-J., and J. Lelieveld, Model study of the influence of cross-tropopause O_3 transports on tropospheric O_3 levels, *Tellus, 49B*, 38-55, 1997.

Roelofs, G.-J., and J. Lelieveld, Tropospheric ozone simulation with a chemistry-general circulation model: Influence of higher hydrocarbon chemistry, *J. Geophys. Res., 105*, 22,697-22,712, 2000.

Rondon, A., C. Johansson, and L. Granat, Dry deposition of nitrogen dioxide and ozone to coniferous forest, *J. Geophys. Res., 98*, 5159-5172, 1993.

Schmid, H. P., Source areas for scalars and scalar fluxes, *Boundary Layer Meteorol., 67*, 293-318, 1994.

Schwartz, S. E., Factors governing dry deposition of gases to surface water, in *Precipitation Scavenging and Atmosphere-Surface Exchange*, S. E. Schwartz and W. G. N. Slinn, Coords., 2, 789-801, Hemisphere Publishing Corporation, 1992.

Schwartz, J., Harvesting and long term exposure effects in the relation between air pollution and mortality, *Am. J. Epidemiol., 151*, 440-448, 2000

Sehmel, G. A., Particle and gas dry deposition: a review, *Atmos. Environ.*, *14,* 983-1011, 1980.

Sellers, P. J., Canopy reflectance, photosythesis and transpiration, *Int. J. Remote Sensing, 6*, 1335-1372, 1985.

Sellers, P. J., Y. Mintz, Y. C. Sud, and A. Dalcher,, A simple biosphere model (SiB) for use within general circulation models, *J. Atmos. Sci., 43*, 505-531, 1986.

Sellers, P. J., W. J. Shuttleworth, J. L. Dorman, A. Dalcher, and J. M. Roberts, Calibrating the Simple Biosphere model for Amazonian tropical forest using field and remote sensing data. Part I: Average calibration with field data, *J. Appl. Meteorol., 28*, 727-759, 1989.

Sharkey, T. D., F. Loreto, D. Baldocchi, and A. Guenther, The BEMA project – A North American prospective, *Atmos. Environ., 31,* 251-255, 1997.

Shuttleworth, W. J., et al., Observations of radiation exchange above and below Amazonian forest, *Q. J. R. Meteorol. Soc., 110,* 1163-1169, 1984.

Sievering, H., J. Boatman, E. Gorman, Y. Kim, L. Anderson, G. Ennis, M. Luria, and S. Pandis, Removal of sulfur from the marine boundary layer by ozone oxidation in sea-salt aerosols, *Nature, 360*, 571-573, 1992.

Slinn, W. G. N., Dry deposition and resuspension of aerosol particles - a new look at some old problems, in *Atmosphere-surface exchange of particulate and gaseous pollutants*, edited by R. J. Engelmann and G. A. Sehmel, 1-40, U. S. DOE Tech. Info. Center, Oak Ridge, TN, 1976.

Slinn, S. A., and W. G. N. Slinn, Predictions for particle deposition on natural waters, *Atmos. Environ., 14*, 1013-1016, 1980.

Slinn, W. G. N., Predictions for particle deposition to vegetative canopies, *Atmos. Environ., 16*, 1785-1794, 1982.

Sommerfeld, R. A., and D. Lamb, Preliminary measurements of SO_2 absorbed on ice, *Geophys. Res. Lett., 13*, 349-351, 1986.

Spedding, D. J., Sulfur dioxide absorption by sea water, *Atmos. Environ., 6*, 583-586, 1972.

Spiro, P. A., D. J. Jacob, and J. A. Logan, Global inventory of sulfur emissions with 1°x 1° resolution, *J. Geophys. Res., 97*, 6023-6036, 1992.

Stocker, D. W., D. H. Stedman, K. F. Zeller, W. J. Massman, and D. G. Fox, Fluxes of nitrogen oxides and ozone measured by Eddy correlation over a shortgrass prairie, *J. Geophys. Res., 98*, 12,619-12,630, 1993.

Thoene, B., P. Schröder, H. Papen, A. Egger, and H. Rennenberg, Absorption of atmospheric NO_2 by spruce (*Picea abies* L. Karst.) trees. I. NO_2 influx and its correlation with nitrate reduction, *New Phytol., 117*, 575-585, 1991.

Trumbore, S. E., M. Keller, S. S. Wofsy, and J. M. Da Costa, Measurements of soil and canopy exchange rates in the Amazon rain forest using ^{222}Rn, *J. Geophys. Res., 95,* 16,865-16,873, 1990.

Valdez, M. P., R. C. Bales, D. A. Stanley, and G. A. Dawson, Gaseous deposition to snow, 1. Experimental study of SO_2 and NO_2 deposition, *J. Geophys. Res., 92*, 9779-9787, 1987.

Van Pul, W. A. J., The flux of ozone to a maize crop and the underlying soil during a growing season, *Ph.D. thesis*, Wageningen Agricultural University, The Netherlands, 1992.

Vermetten, A. W. M., P. Hofschreuder, J. H. Duyzer, H. S. M. A. Diederen, F. C. Bosveld, and W. Bouten, Dry deposition of SO_2 onto a stand of Douglas Fir: The influence of canopy wetness, *Rep. R-508*, Depart. Of Air Quality, Agricultural University Wageningen, 1991.

Verver, G., Interactions of mixing and chemistry in the atmospheric boundary layer, *Ph.D. thesis*, Utrecht University, Utrecht, The Netherlands, 1999.

Vilà-Guerau de Arellano, J., and P. G. Duynkerke, Atmospheric surface layer similarity theory applied to chemically reactive species, *J. Geophys. Res., 100,* 1397-1408, 1995.

Walcek, C. J., R. A. Brost, J. S. Chang, and M. L. Wesely, SO_2, sulfate and HNO_3 deposition velocities computed using regional landuse and meteorological data, *Atmos. Environ.*, *20*, 949-964, 1986.

Walton, S., M. W. Gallagher, and J. H. Duyzer, Use of a detailed model to study the exchange of NO_x and O_3 above and below a deciduous canopy, *Atmos. Environ., 31*, 2915-2931, 1997.

Wang, Y., J. A. Logan, and D. J. Jacob, Global simulation of tropospheric O_3-NO_x-hydrocarbon chemistry. I. Model formulation, *J. Geophys. Res., 103,* 10,713-10,725, 1998.

Warneck, P., Chemistry of the natural atmosphere, Academic Press, San Diego, 1988.

Weiss, A. and J. M. Norman, Partioning solar radiation into direct and diffuse, visible and near-infrared components, *Agric. Forest Meteorol., 32*, 205-213, 1985.

Weitz, A. M., M. Keller, E. Linder, and P. M. Crill, Spatial and temporal variability of nitrogen oxide and methane fluxes from a fertilized tree plantation in Costa Rica, *J. Geophys. Res., 104,* 30,097-30,107, 1999.

Wesely, M. L., D. R. Cook, and R. M. Williams, Field measurements of small ozone fluxes to snow, wet bare soil, and lake water, *Boundary Layer Meteor.*, *20*, 459-471, 1981.

Wesely, M. L., J. A. Eastman, and E. D. Yalvac, An Eddy correlation measurement of NO_2 flux to vegetation and comparison to O_3, *Atmos. Environ.*, *16*, 815-820, 1982.

Wesely, M. L., D. R. Cook, and R. L. Hart, Fluxes of gases and particles above a deciduous forest in wintertime, *Boundary Layer Meteorol., 27*, 237-255, 1983.

Wesely, M. L., D. R. Cook, and R. L. Hart, Measurements and parameterization of particulate sulfur dry deposition over grass, *J. Geophys. Res., 90*, 2131-2143, 1985.

Wesely, M. L., Parameterization of surface resistances to gaseous dry deposition in regional-scale numerical models, *Atmos. Environ.*, *23*, 1293-1304, 1989.

Wesely, M. L., D. L. Sisteron, and J. D. Jastrow, Observations of the chemical properties of dew on vegetation that affect the dry deposition of SO_2, *J. Geophys. Res., 95*, 7501-7514, 1990.

Wesely, M. L., and B. B. Hicks, A review of the current status of knowledge on dry deposition, *Atmos. Environ., 34,* 2261-2282, 2000.

Whitby, K. T., The physical characterisitcs of sulfur aerosols, *Atmos. Environ., 12*, 135-159, 1978.

Wieringa, J., Updating the Davenport roughness classification, *J. Wind Engin. Industr. Aerodyn., 41-44*, 357-368, 1991.

Williams, R. M., A model of the dry deposition of particles to natural water surfaces, *Atmos. Environ., 16*, 1933-1938, 1982.

Wilson, M. F., and A. A. Henderson-Sellers, A global archive of land cover and soils data for use in general circulation climate models, *J. Climatology., 5*, 119-143, 1985.

Yienger, J. J., and H. Levy, II, Global inventory of soil-biogenic NO_x emissions, *J. Geophys. Res., 100*, 11,447-11,464, 1995.

Samenvatting

De uitwisseling van gassen zoals ozon, zwavel en stikstof oxiden, en fijne stofdeeltjes (aerosolen) tussen de atmosfeer en het aardoppervlak bepaalt in belangrijke mate de gas en aerosol concentraties waaraan mensen en de biosfeer worden blootgesteld. Wetenschappelijk onderzoek heeft aangetoond dat blootstelling aan te hoge concentraties van bepaalde gassen en aerosolen schadelijk is voor de gezondheid. Bovendien is in de jaren zeventig het besef gegroeid dat de achteruitgang van de vitaliteit van bossen voornamelijk het gevolg was van de verzuring van het milieu door de opname van verzurende stoffen uit de atmosfeer door de vegetatie en bodems. Door emissiereducties van stoffen die bijdragen aan de verzuring, is de verzuringsproblematiek in Europa en Noord-Amerika, waar dit probleem zich het eerst openbaarde, teruggedrongen. Echter, de toenemende verzuringsproblematiek in zich snel ontwikkelende landen, bijvoorbeeld China, zorgt ervoor dat verzuringsonderzoek een actueel onderwerp blijft.

Het onderzoek van de atmosferisch chemie heeft zich de laatste jaren vooral geconcentreerd op het broeikaseffect. De toename in de concentraties van broeikasgassen en de potentiële veranderingen van het klimaat worden bestudeerd door gebruik te maken van metingen en modellen. Atmosferische chemiemodellen worden gekoppeld aan transport- of klimaatmodellen om de atmosferische chemie en de relatie met het klimaat te onderzoeken. Eén van de relevante processen van de atmosferische chemie is de uitwisseling van gassen en stofdeeltjes aan het aardoppervlak. Hierin wordt onderscheid gemaakt tussen verwijderingsprocessen van gassen en aerosolen uit de atmosfeer -de zogenaamde natte en droge depositie- en processen die een bron zijn voor gassen en aerosolen -de antropogene emissies en de biogene emissies. De studie die in deze thesis beschreven is, is voornamelijk gericht op de beschrijving van het droge depositieproces in een mondiaal chemie en klimaatmodel. Echter, de droge depositie van enkele gassen is gerelateerd is aan de biogene emissies en daarom is dit proces ook in deze studie betrokken.

Droge depositie is de verwijdering aan het aardoppervlak door de opname, bijvoorbeeld door de vegetatie, de bodem en de oceaan. De verwijdering door dit proces wordt uitgedrukt in een droge depositieflux, die wordt berekend als het product van de gasconcentratie dichtbij het aardoppervlak en de droge depositiesnelheid. De droge depositiesnelheid weerspiegelt de opnamesnelheid van alle betrokken processen, zoals het transport door turbulentie naar het aardoppervlak en de opname door de vegetatie. Door de seizoens en dagelijkse variatie in de opnameprocessen, bijvoorbeeld de toename in de opname door de huidmondjes van de vegetatie door een toename in zonlicht, vertoont de droge depositiesnelheid een duidelijke dagelijkse en seizoensgang. Bovendien is de absolute orde van grootte van de droge depositiesnelheid afhankelijk van het soort oppervlak, aangezien elk oppervlak een andere

affiniteit heeft voor gassen en stofdeeltjes door verschillen in de biologische, chemische en fysische eigenschappen. Zo is bijvoorbeeld de droge depositiesnelheid van ozon boven een droog tropisch regenwoud veel groter dan de droge depositiesnelheid boven een nat tropisch bos doordat ozon niet goed oplost. Anderzijds, de droge depositiesnelheid van ozon boven een toendra is veel kleiner dan die boven een tropisch bos doordat het tropisch bos een veel grotere hoeveelheid biomassa, en daarmee een grotere opnamecapaciteit heeft, in vergelijking met de toendra.

In de eerste generatie chemie-transport/klimaatmodellen is het droge depositieproces zeer eenvoudig beschreven door gebruik te maken van constante droge depositiesnelheden. Het voornaamste doel van deze studie is de implementatie van een meer realistische beschrijving van het droge depositieproces in een chemie-klimaatmodel, door expliciet de dagelijkse en seizoensgang in de droge depositiesnelheid te berekenen als functie van het soort oppervlak. Dit is mede ingegeven door het belang van het droge depositieproces voor de mondiale budgetten van gassen, zoals ozon en zwaveldioxide, in de troposfeer (de onderste 10-15 km van de atmosfeer). Zo verwijdert droge depositie ongeveer 40% van alle zwavel die in de atmosfeer geëmitteerd wordt. Een tweede belangrijke motivatie voor het introduceren van een realistische beschrijving van het droge depositieproces heeft te maken met de evaluatie van chemie-transport/klimaatmodellen door de vergelijking van berekende concentraties en fluxen met metingen. Aangezien de meeste metingen aan het oppervlak uitgevoerd worden, en dus de bijdrage van het droge depositieproces weerspiegelen, moet dit proces realistisch worden beschreven in het model om een eerlijke vergelijking te garanderen. Bovendien bevat het chemie-klimaat model dat in deze studie gebruikt is, het ECHAM model (European Center Model, Hamburg version), een zodanig gedetailleerde beschrijving van het oppervlak dat dit model uitermate geschikt is om een expliciete en consistente beschrijving van het droge depositieproces te ontwikkelen. In de oppervlaktelaag van het ECHAM model, die ongeveer 70 m diep is, wordt de land- en zeefractie onderscheiden binnen elk gridbox. De landfractie is opgedeeld in vier oppervlaktefracties: de vegetatiefractie waarvoor de opname door de vegetatie word berekend als functie van de hoeveelheid biomassa, de instraling en het bodemvocht, de fractie kale bodem, een fractie die bedekt is met sneeuw of landijs, en als laatste de fractie vegetatie en kale bodem die nat is door neerslag of dauwvorming.

In hoofdstuk 2 is de ontwikkeling van een eerste versie van een droge depositieschema in ECHAM voor de gassen ozon (O_3), stikstof oxide (NO) en dioxide (NO_2) en salpeterzuur (HNO_3) beschreven. Het droge depositieschema berekent de droge depositiesnelheid als een functie van het turbulent transport en moleculaire diffusie naar het oppervlak en de opname door het oppervlak, gebruik makend van de weerstands-analogie. Hiermee wordt de droge depositiesnelheid berekend als de inverse waarde van een selectie van parallelle en in serie geschakelde weerstanden tegen het transport náár en opname dóór het oppervlak
Er zijn relatieve verschillen van ongeveer 35% tussen de O_3 depositiefloxen en concentraties -berekend door het nieuwe droge depositieschema -en de berekening met constante depositiesnelheden. Een vergelijking van de berekende en gemeten O_3 depositiesnelheden geeft aan dat het model over het algemeen de metingen redelijk kan reproduceren. Echter, voor sommige ecosystemen, zoals toendra en tropisch bos, zijn er belangrijke verschillen. Dit heeft te maken hebben met de representatie van de vegetatie in de versie van het ECHAM model dat voor deze studie gebruikt is. De hoeveelheid biomassa wordt weergegeven door een constante hoeveelheid bladoppervlak van 4 m^2 per m^2 bodem, ongeacht het soort

vegetatie. In werkelijkheid varieert deze parameter tussen een waarde van ongeveer 1 voor gras en 7 tot 8 voor bossen.

In hoofdstuk 3 is de introductie van een meer realistische mondiale verdeling van de vegetatie beschreven. Tevens wordt in dit hoofdstuk de uitbreiding van het droge depositieschema naar zwavel dioxide (SO_2) en het sulfaat aerosol (SO_4^{2-}) beschreven. De droge depositiesnelheid van het sulfaat aerosol wordt berekend als functie van de massaverdeling omdat er grote verschillen zijn in de aerosol droge depositiesnelheid als functie van de deeltjesgrootte. De droge depositiesnelheid van sulfaat boven land wordt berekend door te integreren over een continentale massaverdeling van het sulfaat aerosol, terwijl boven de oceanen een massaverdeling van sulfaat wordt gebruikt die representatief is voor maritieme condities. Boven zee wordt tevens rekening gehouden met de toename van de sulfaat depositiesnelheid door de aanwezigheid van schuimkoppen bij hoge windsnelheden, het invangen van sulfaat aerosol door zeezout en de groei van het aerosol voor een hoge luchtvochtigheid. De maximale relatieve verschillen in de SO_2 en SO_4^{2-} concentraties die berekend zijn met het nieuwe droge depositie schema en een schema dat gebruik maakt van constante depositiesnelheden, zijn ongeveer 50%.

Het uitwisselingsproces van de reactieve stikstof (di)oxides (NO_x) is gecompliceerd: de tijdsschaal van de chemische reacties is namelijk vergelijkbaar met de tijdsschaal van het turbulent transport. Daardoor is het gebruik van de vergelijkingen voor turbulent transport van een inert gas voor de berekening van de droge depositiesnelheid niet altijd gerechtvaardigd. Dit is afhankelijk van de verhouding tussen de chemische en turbulente tijdsschaal. Bovendien is de richting van de uitwisselingsflux niet eenduidig gedefinieerd omdat NO_x wordt verwijderd door droge depositie, maar tevens wordt geëmitteerd door de bodem. De uiteindelijke richting van de flux boven vegetatie is afhankelijk van de emissie en depositieflux en van de turbulente menging tussen de atmosfeer en de vegetatie. De turbulente menging bepaalt de verblijftijd van NO_x in de vegetatie. De chemische reacties in de vegetatie zijn bovendien verschillend van die boven de vegetatie omdat de fotochemische reacties beïnvloed worden door de uitdoving van straling in de vegetatie. Door deze interacties tussen de emissies, droge depositie, turbulentie en chemie kan het voorkomen dat er een neerwaartse (depositie) flux van NO_x tussen de atmosfeer en de vegetatie is ondanks dat er een opwaartse (emissie) flux van NO_x uit de bodem is. Om het belang van deze fluxdivergentie in de vegetatie voor de mondiale uitwisseling van NO_x te onderzoeken, is een meerlaags vegetatiemodel voor de atmosfeer-biosfeer uitwisseling van gassen ontwikkeld. Het model berekent expliciet de fluxdivergentie als functie van de emissies door de bodem en planten, droge depositie, chemische omzettingen, en de turbulente menging tussen de vegetatie en de atmosfeer. Voor de ontwikkeling en de evaluatie van het meerlaags vegetatiemodel is een kolomversie van het ECHAM model gebruikt. Het gebruik van een 1-D model vereenvoudigt de modelontwikkeling en evaluatie doordat modelparameters, zoals de vegetatiestructuur, voorgeschreven kunnen worden.
De modelevaluatie in hoofdstuk 4 laat zien dat het model de gemeten concentraties en fluxen in en boven een tropisch regenwoud, loofbos en een arctische taiga redelijk kan reproduceren. De nachtelijke fluxen en concentraties zijn zeer gevoelig voor de beschrijving van de turbulente uitwisseling. Een vergelijking van het meerlaags vegetatiemodel en het oorspronkelijke model ("big leaf" model), waarin de interacties tussen de emissies en droge depositie niet worden meegenomen, laat zien dat er voor verontreinigde gebieden geen grote

verschillen zijn in de berekende NO_x fluxen. Echter, voor relatief schone locaties, zoals het tropische bos en de taiga, zijn er belangrijke verschillen tussen de NO_x fluxen berekend met het vegetatiemodel en het "big leaf" model. Deze verschillen benadrukken het belang van het berekenen van de fluxdivergentie voor dit soort ecosystemen met behulp van het meerlaags vegetatiemodel.

Het meerlaags vegetatiemodel is geïmplementeerd in het chemie-klimaat model ECHAM om de NO_x fluxdivergentie op mondiale schaal te onderzoeken. Dit werk is gepresenteerd in hoofdstuk 5. De gevoeligheid van de berekende fluxen en concentraties van NO_x en O_3 voor de biogene emissies van NO_x door de bodem, is onderzocht door twee verschillende emissieschattingen te gebruiken. Ondanks de grote verschillen in de mondiale jaarlijkse NO_x emissieflux voor de twee emissieschattingen, is de gevoeligheid van de NO_x en O_3 concentraties en fluxen verrassend laag. Dit komt door terugkoppelingen in de droge depositie, chemie en transport processen. Overeenkomstig met de resultaten van hoofdstuk 4, worden de grootste verschillen tussen de NO_x fluxen en concentraties van het meerlaags vegetatiemodel en het "big leaf" model, berekend voor ecosystemen in relatief schone gebieden. Voor ecosystemen in de nabijheid van antropogene bronnen, voornamelijk op het Noordelijk Halfrond, zijn de verschillen relatief klein. De studie van de fluxdivergentie van reactieve gassen zal worden voortgezet in de toekomst, waarbij gebruik zal worden gemaakt van het kolommodel voor procesgerichte studies, en ECHAM voor de mondiale schaal studies.

De expliciete representatie van uitwisselingsprocessen van gassen en aerosol als functie van landbedekking en landgebruik, biedt de mogelijkheid om ECHAM te gebruiken voor scenariostudies. Het doel van deze studies is om de invloed van veranderingen in landgebruik en landbedekking op de atmosferische chemie en het klimaat te onderzoeken.
Echter, een essentieel onderdeel van de modelstudies is de continue verbetering van de procesbeschrijving en evaluatie van de modellen door vergelijking met metingen. Daarom is de samenwerking met wetenschappers die betrokken zijn bij het meten van uitwisselingsprocessen essentieel. Deze meetresultaten zullen hopelijk bijdragen aan het reduceren van de grootste onzekerheden in het modelleren van de uitwisseling van gassen en aerosolen tussen de atmosfeer en het aardoppervlak op de mondiale schaal.

Curriculum Vitae

Laurens Ganzeveld is geboren op 6 November 1966 te Elburg. In 1986 behaalde hij zijn VWO diploma aan het Lambert Franckens College in Elburg. Nadat al spoedig bleek dat de gewenste voorkeur voor de vliegopleiding er niet in zat, is hij begonnen met de studie Milieuhygiëne aan de Landbouw Universiteit te Wageningen. In 1992 heeft hij het doctoraal examen Milieuhygiëne behaald. De vrije oriëntatie van de studie Milieuhygiëne bood de mogelijkheid om de vele aspecten van de milieu problematiek beter te bestuderen maar de studie is vooral gericht geweest op de luchtkwaliteit en de meteorologie. Hierna heeft hij, in het kader van de vervangende dienstplicht, een jaar lang door de gangen van de vakgroep Luchtkwaliteit van de Landbouw Universiteit getijgerd, waarna hij op een aantal tijdelijke contracten gewerkt heeft bij deze vakgroep als wetenschappelijk medewerker. In 1997 is hij naar de Universiteit van Utrecht verhuisd waar, op dezelfde basis als in Wageningen, een tijdelijke contract de mogelijkheid heeft geboden om het werk dat in dit proefschrift is beschreven, af te ronden.